INCLUSION COMPOUNDS OF CHOLIC ACID AND METHYL CHOLATE

by

JANET LESLEY SCOTT

Thesis presented to the

UNIVERSITY OF CAPE TOWN

for the degree of

DOCTOR OF PHILOSOPHY

Department of Chemistry
University of Cape Town
Rondebosch
7700
South Africa

February 1995

ACKNOWLEDGEMENTS

I would like to express my heartfelt gratitude to the following:

Professor Luigi Nassimbeni and Associate Professor Mino Caira for expert guidance and constructive criticism.

Various members of the Crystallography Research Group, particularly Dr Susan Bourne and Dr Leonard Barbour, for fruitful discussion. Anita Coetzee for kinetic debates.

My parents for their support.

PUBLICATIONS AND CONFERENCES

PARTS OF THIS THESIS HAVE BEEN PUBLISHED:

1. Mino R. Caira, Luigi R. Nassimbeni* and Janet L. Scott, 'Selective Inclusion by Cholic Acid', *J. Chem. Soc., Chem. Commun.*, 1993, p 612-614.

2. Mino R. Caira, Luigi R. Nassimbeni* and Janet L. 1. Scott, 'Inclusion Compounds of Cholic Acid with Aliphatic Esters', *J. Chem. Soc. Perkin Transactions 2*, 1993, p 623-628.

3. Mino R. Caira, Luigi R. Nassimbeni and Janet L. Scott*, 'Crystal Structure and Multiphase Decomposition of a Novel Cholic Acid Inclusion Compound with Mixed Guests', *J. Chem. Soc. Perkin Transactions 2*, 1994, p 1403-1405.

4. Mino R. Caira, Luigi R. Nassimbeni and Janet L. Scott*, 'Cholic Acid Inclusion Compounds with Ketone Guests', *J. Chem. Crystallogr.*, 1994, **24**, 12, p 783 - 791.

5. Janet L. Scott*, 'Solid-vapour Reactions of Cholic Acid and Methyl Cholate with Acetonitrile: Structures and Reaction Kinetics', *J. Chem. Soc. Perkin Transactions 2*, 1994, in press.

PARTS OF THIS THESIS HAVE BEEN PRESENTED AT THE FOLLOWING CONFERENCES:

'The 10th International Conference on the Chemistry of the Organic Solid State.' University of British Columbia, Vancouver, Canada, 1991.

'Molecular Recognition and Synthetic Design.', University of Cape Town, Cape Town, South Africa, 1992

'The 11th International Conference on the Chemistry of the Organic Solid State.' Jerusalem, Israel, 1993.

'Molecular Recognition and Synthetic Design.', University of Cape Town, Cape Town, South Africa, 1994

ABSTRACT

The inclusion capacities of Cholic Acid (CA) and its O(28) methyl ester, Methyl Cholate (MC) have been investigated.

The crystal structures of the inclusion compounds of CA with:

Aliphatic ketones:
- Acetone
- Methyl ethyl ketone
- Diethyl ketone

Aliphatic esters:
- Methyl acetate
- Ethyl acetate
- Ethyl propionate
- *n*-Propyl acetate
- *i*-Propyl acetate

Mixed guests:
- Methyl acetate / *i*-Propyl acetate
- 1,2-Dichlorobenzene / Acetone
- Acetone / Water

Vinyl esters:
- Vinyl acetate
- Methyl Methacrylate

Aromatic guests:
- Benzonitrile
- Aniline
- Nitrobenzene
- Propiophenone
- *p*-Toluidine
- *p*-Nitro-toluene
- *m*-Nitro-toluene

as well as those of CA and MC with acetonitrile and MC alone are presented and analysed with respect to host conformation (both of the steroid backbone and side chain), hydrogen bonding patterns and host-guest and guest-guest interactions. Subtle guest responsive changes in bilayer packing and host conformation resulting in channels with differing cross sectional shapes and areas are noted.

Data derived from the crystal structures of unsolvated cholic acid (CA(α))[1] and the inclusion compound CA•acetophenone[2] from published accounts are included for comparative purposes.

Decomposition behaviour of all of the aforementioned inclusion compounds as well as that of a number of related compounds were investigated by both rising temperature thermogravimetry (TG) and differential scanning calorimetry (DSC). Decomposition pathways involving solid-solid phase changes both with and without guest loss were identified and features seen in DSC traces related by use of a modified Weissenberg camera which allows continuous recording of the X-ray powder pattern under heating. Alternatively, X-ray powder diffraction (XRD) was used to identify phases occurring during decomposition.

Isothermal TG was employed to measure desorption isotherms for a number of the stable aromatic guest and acetonitrile inclusion compounds. Rate laws describing the desorption mechanisms are ascribed and values for the parameters E_a (activation energy) and A (the pre-exponential factor) derived. The compounds with aromatic ketone guests (CAPR and CAACET) show complex decomposition pathways involving a number of steps which are described by the use of separate but overlapping rate law functions.

The solid-vapour and solid-solid reactivity of the host molecules CA and MC was investigated. The relative rates of reaction and rate laws pertaining to guest absorption and solid-solid reactions of CA with benzonitrile, aniline, nitrobenzene, *p*-toluidine and *p*-Br-phenol were investigated as were the rates of absorption of acetonitrile by CA and MC hosts. An attempt was made to compute the 'strength' of hydrogen bonding interactions in the structures of CA(α), MC(α), CACN and MCCN and to relate these to the measured values of the kinetic parameters of both the forward and reverse reactions:

$$HOST_{(s,\alpha)} + CH_3CN_{(g)} = HOST{\bullet}CH_3CN_{(s,\beta)}$$

Preliminary investigations into the selective inclusion by CA of certain guests are presented. Such selectivity is discussed with reference to the formation of crystallographically mixed guest compounds. Atom-atom potentials are used to evaluate the potential energy (PE) of the guest molecules in their crystalline molecular environment and thereby account for the selective behaviour.

1 K. Miki, N. Kasai, M. Shibakami, S. Chirachanchai, K. Takemoto and M. Miyata, *Acta Crystallogr. Sect. C*, 1990, **46**, p 2442.

2 K. Miki, A. Masui, K. Kasai, M. Miyata, M. Shibakami and K. Takemoto, *J. Am. Chem. Soc.*, 1988, **110**, p 6594.

ABBREVIATIONS AND SYMBOLS

Most of the abbreviations and symbols used in this dissertation are widely accepted and in common use in the chemical literature. The mnemonics used to describe each compound are detailed on the inserted bookmark and in the fold-out table at the end of the document.

A	Arrhenius pre-exponential factor
b.p.	normal boiling point
CA	cholic acid
CFOM	combined figure of merit
CSD	Cambridge Structural Database
DCA	deoxycholic acid
DSC	differential scanning calorimetry
E	normalised structure factor
E_a	activation energy
G	guest
H	host
k	rate constant
MC	methyl cholate
M_r	molecular mass
m.p.	melting point
NMR	nuclear magnetic spectroscopy
TG	thermogravimetry
V	cell volume
XRD	X-ray powder diffraction
Z	number of structural units per cell
α	angle between b and c unit cell axes, **or** extent of reaction, **or** host compound phase with no included guest
β	angle between a and c unit cell axes, **or** known inclusion compound phase
γ	angle between a and c unit cell axes, **or** unknown (intermediate) inclusion compound phase
τ	torsion angle
•••	non-bonded contact such as a hydrogen bond

TABLE OF CONTENTS

CHAPTER 1: INTRODUCTION

INCLUSION CHEMISTRY

The concepts of inclusion chemistry are well established and have been summarised by Gokel: "The field encompasses the study of non-covalent interactions that occur between hosts and guests or substrates and receptors of many different types."[1] This is extremely broad and includes discussion of host-guest chemistry, supramolecular chemistry and molecular recognition. The importance of this burgeoning field of study was recognised by the award of the Nobel prize in Chemistry to Charles J. Pedersen[2], Donald J. Cram[3] and Jean-Marie Lehn[4] in 1987.

So many examples of inclusion compounds exist that any attempt at even the shallowest of complete overviews would be doomed to failure; instead, a few of the more interesting examples will be presented and the reader is referred to a number of excellent monographs and reviews on the subject for further detail.[5,6,7]

A number of important discoveries in inclusion chemistry have followed since Davy's recognition of a chlorine clathrate hydrate last century[8] but it is only recently that the compositions and structures of large numbers of such compounds have been elucidated leading to a greater depth of understanding of the underlying principles of inclusion. Understanding of the factors affecting inclusion and the types of intermolecular interactions occurring in turn provide the information for rational, directed host design for the enclathration of specific guest molecules.

This sudden proliferation in the field has led to some confusion in nomenclature and attempts to systematise classification of inclusion compounds have been suggested by Herbstein[9] and Weber.[10] In each case the type of intermolecular interactions that predominates is considered, Herbstein including considerations of the type of packing while Weber details host-host and host-guest interactions and topologies as summarised in Figures 1.1 and 1.2.

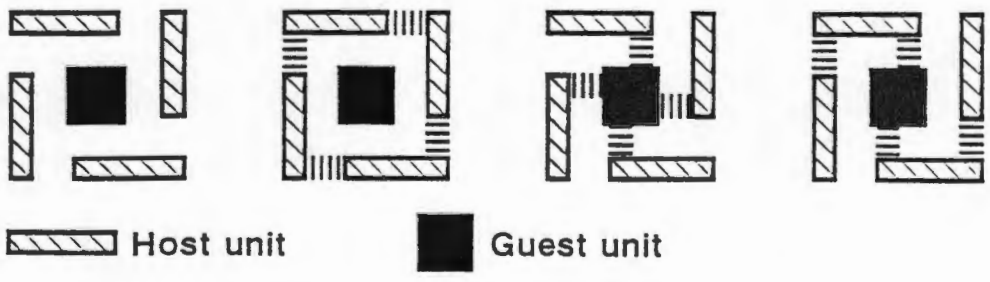

Figure 1.1: Schematic representation of the types of interactions occurring in inclusion compounds. From left to right: no short range interactions, host-host interactions, host-guest interactions, host-host and host-guest interactions. (Redrawn from Weber[10])

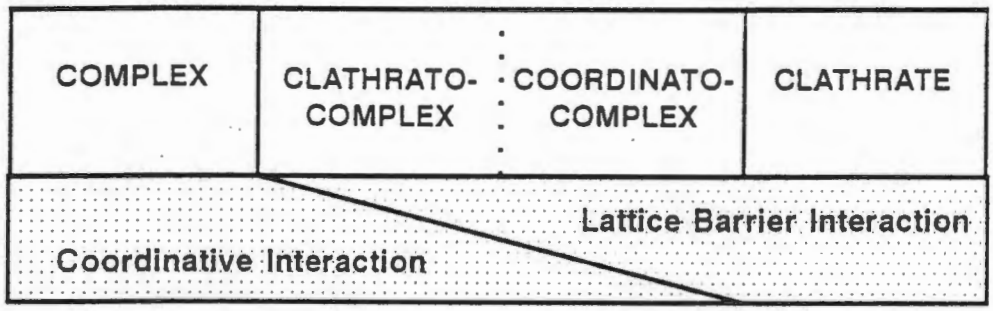

Figure 1.2: Classification of inclusion compounds according to their topology. (After Weber[10])

Given the broad definition mentioned above, inclusion compounds might be considered to include solid solutions or dispersions and polymeric matrices as well as compounds formed with inorganic host compounds such as zeolites[11,12] and in solution, the so-called 'liquid clathrates'.[13-16] We shall concentrate on the study of *crystalline* inclusion compounds with *organic* hosts. These may be broadly divided into two main groups:

i) compounds formed by host molecules which, by dint of their connectivity, have a cavity inherent in their structure into which guest molecules may fit

ii) multimolecular host assemblages which produce cavities or holes upon association into a crystal in which guest molecules are trapped.

There are, of course, no clear distinctions between these as even compounds with large intramolecular cavities may, upon crystallisation, wholly or partly entrap guests in cavities formed between hosts. Similarly host molecules without cavities may show distinct association with guest molecules in solution.

Group i: Hosts with intramolecular cavities.

Calixarenes:

Calixarenes are named for their shape which is similar to that of a calix or vase, being cup-shaped with a crater in the middle.[17] These hosts are synthesized by the base catalysed condensation of phenol with formaldehyde and consist of a cyclic collection of substituted aromatic rings, the basic building block of which is illustrated in Figure 1.3. The molecules may be variously functionalised at either top or bottom lip producing a vast range of host molecules with different cavity sizes and lip functionality for the inclusion of diverse guest molecules. The different shapes and functionalities of two calixarene hosts are illustrated in Figure 1.4.

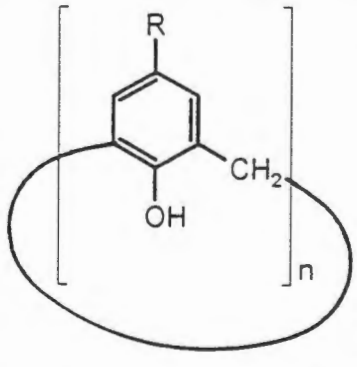

Figure 1.3: Basic unit of which calixarenes are constructed. Molecules with n in the range 4 to 8 have been synthesized.

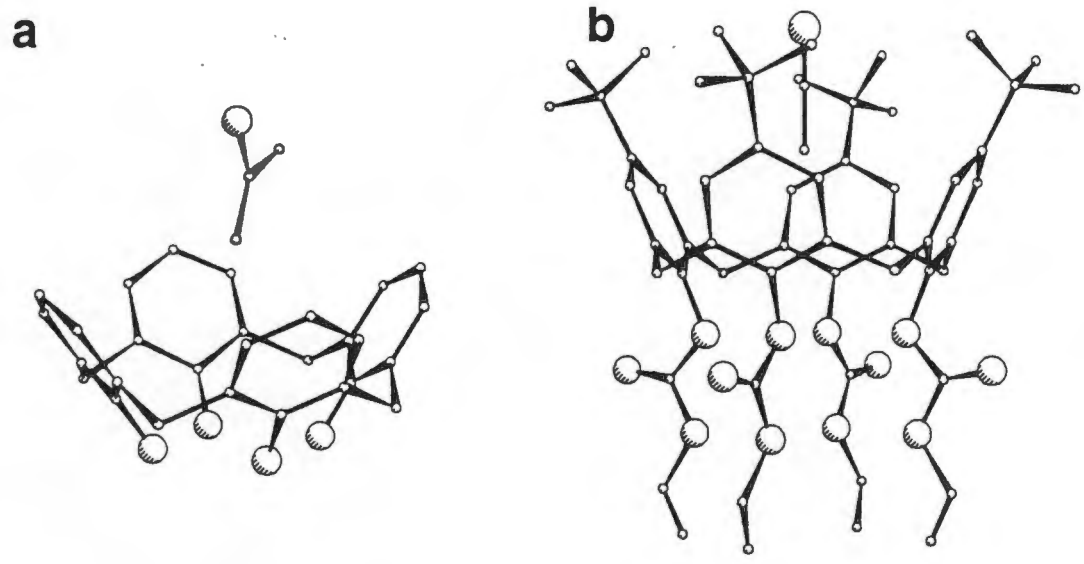

Figure 1.4: Two calixarene host molecules with different groups at each lip.
a) Calix[4]arene•acetone[18]
b) Tetraethyl *p*-t-butylcalix[4]arene-tetracarbonate•acetonitrile.[19]

Crown Ethers and Related compounds:

Cyclic ethers with a huge variety of sizes and shapes have been synthesised[2,20] and converted by further functionalisation and reaction into cryptands[21,22] or spherands[23] capable of more completely enclosing guest molecules. A further refinement was the synthesis of lariat ethers designed as crown ethers with 'arms' which close off the cavity on one side as in the interesting example of a crown ether with steroid 'arm' presented in Figure 1.5 .

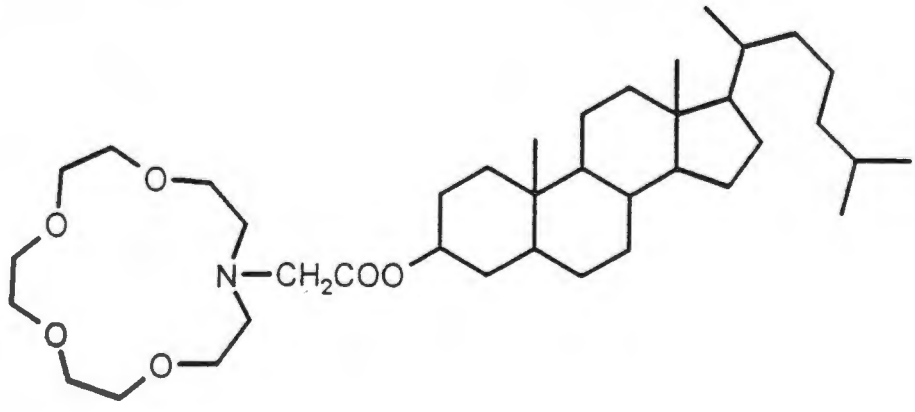

Figure 1.5: Lariat ether with steroid 'arm'.[24]

Cyclodextrins:

Cyclodextrins are cyclic oligosaccharides consisting of α-1,4-linked D-glucose units. These are large cyclic molecules which have cylindrical cavities of varying sizes. Hydroxy groups line the rims of both ends of the cavity and these may be used for further reaction to produce cyclodextrins with specific

properties. The interior of the cavity is hydrophobic and is shown to include many different types of guest molecules.[25] Although the shape of this molecule would lead one to expect that all inclusion compounds formed would exist with the guest accommodated in the cavity, this is not always the case. For example in the 1:1 inclusion compound of heptakis(2,6-di-O-methyl)-β-cyclodextrin (DM-β-CDx) with *p*-nitrophenol the host cavity includes two water molecules and one methoxy group of an *adjacent host* molecule while the guest is found in cavities *between* the hosts[26] as illustrated in Figure 1.6.

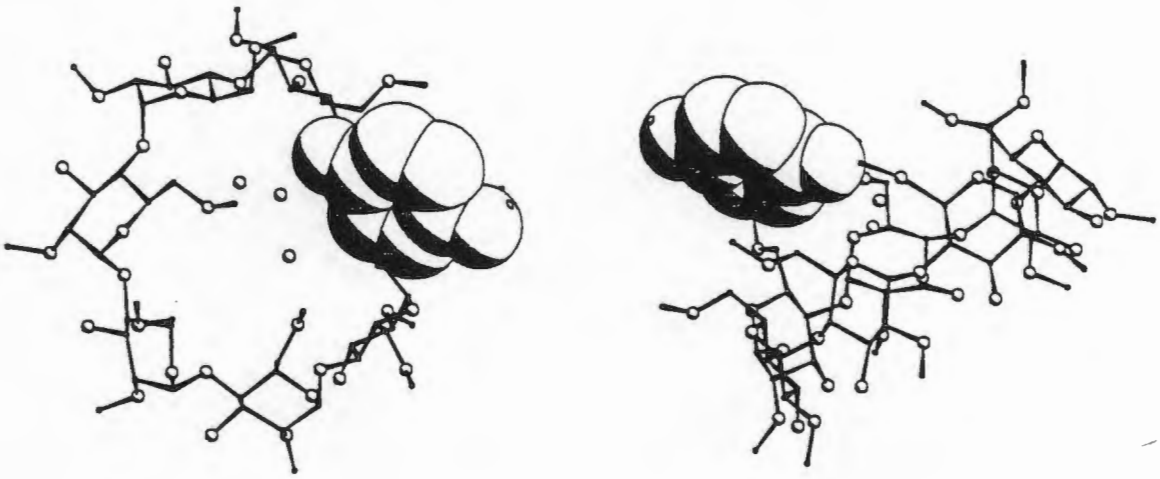

Figure 1.6: Two views of (DM-β-CDx)•*p*-nitrophenol 1:1 inclusion complex. Guest atoms are drawn with van der Waals radii.

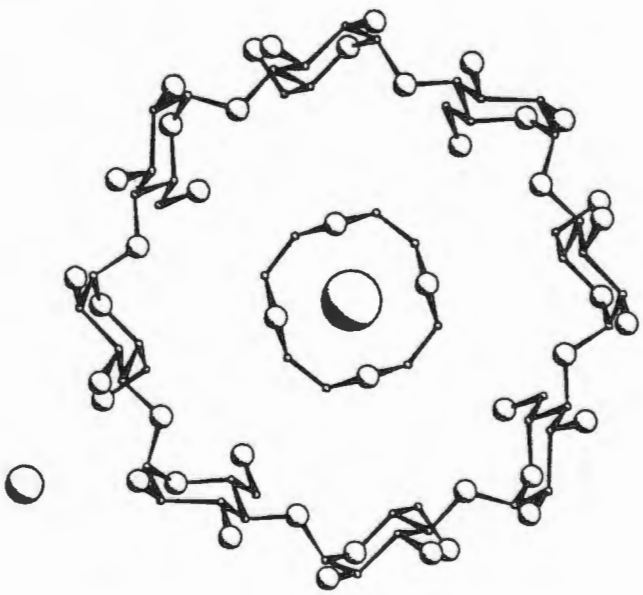

Figure 1.7: Double macrocycle inclusion compound 2(γ-CD)•2(12-crown-4)•Na^+Cl^-. Na^+ ions are included within the crown ether which is in turn included by the cyclodextrin. Defining host and guest in such a complex becomes complicated.

Cyclodextrin molecules have been used in the formation of 'double macrocycles' where a macrocyclic compound such as a crown ether is included by γ-cyclodextrin. The crown ether may, in turn, include various anions[27,28] in the ratio 2:2:1 as in the compound 2(γ-CD)•2(12-crown-4)•Na^+Cl^- illustrated in Figure 1.7.

Group ii: Multimolecular host assemblages.

While most of the earlier host molecules employed for the preparation of inclusion compounds were discovered by accident a greater degree of understanding of the structural principles leading to the formation of host:guest compounds has led to the development of rational directed host design. The shape and geometry of the potential host molecule is recognised as important[29] and in particular, the ability of the host to co-ordinate or bind to other molecules[30,31] (host or guest) and the inability to achieve efficient close packing are identified as useful design features.[32,33]

The host compounds of the second group are so numerous that no attempt will be made to describe separate classes of host compounds; instead, examples of interesting and useful phenomena will be detailed.

Separation:

Host-guest complexation can be a very effective method for separation of close isomers which, due to similarity in boiling points, are not effectively separated by conventional fractional distillation methods. One of the earlier reports of such an application was in the separation of isomers of nitro-toluene using a clathrate chromatographic system with a Werner type host compound (a nickel co-ordination compound).[34]

Toda and co-workers have described systems which afford, upon decomposition of the inclusion compound, close to one hundred percent isomericaly pure material.

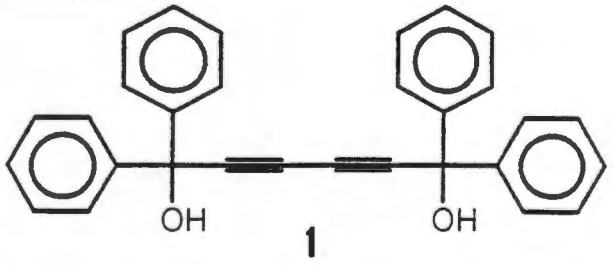

1

p-Methylbenzaldehyde was obtained from the inclusion crystals with the 'dogbone, diol host' 1 while the *o*-isomer remained in solution[35].

Numerous other such examples in which one isomer is regained from the inclusion crystals by distillation under reduced pressure while another remains in solution have been described.[36,37]

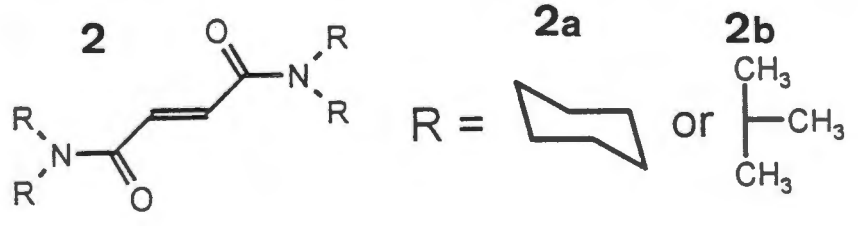

Separation of isomers of cresol by complexation with amide host molecules[38,39] **2a** and **b** has been accounted for in terms of stability of the inclusion compounds formed.[40,41]

Not all examples of separation involve guests which are hydrogen bonded to the host molecules upon inclusion. Hydrocarbons have also been selectively enclathrated by judicious choice of host.[42]

A very interesting application of separation by inclusion results in the case of tautomeric compounds. It often occurs that a compound which exhibits significant dynamic tautomerism in solution is stabilised in one or other form upon inclusion.

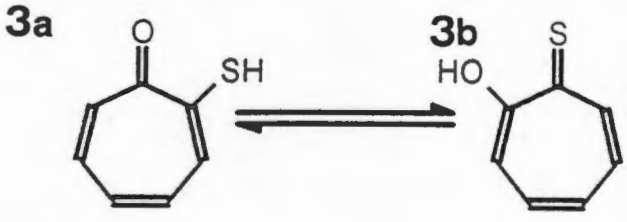

This may even result in stabilisation of the *minor isomer* as occurs when the 2-mercapto substituted tropone **3** (which occurs predominantly as the 2-hydroxytropothione **3b** in solution) is enclathrated as the 2-mercaptotropone **3a** with the 'dogbone host' **1a** mentioned before.[43]

Isolation of natural products such as cholesterol, brucine, strychnine, caffeine[44] and nicotine[45] may be achieved somewhat more easily by complexation and crystallisation than by chromatographic methods.

One of the most important forms of separation facilitated by inclusion compound formation is the separation of optical isomers and here natural products such as brucine (mentioned above), which are chiral and already resolved by virtue of the existence of only one enantiomer in nature, are employed as *hosts* for the selective inclusion of chiral, optically active guest isomers.[46]

Regio- and stereo-selective reaction control:

The environment of an inclusion compound may provide a perfect 'reaction vessel'. Guest molecules are often tightly bound with little freedom to rotate or undergo conformational change. The positions of host and guest are fixed and (except at crystal defects) the environment of all molecules is constant.

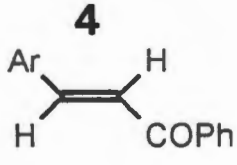

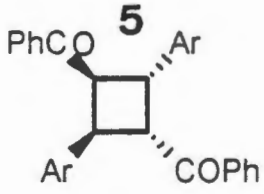

Thus reactions like the irradiation of **4** as an inclusion compound guest results in formation of the *syn* head to tail dimer **5** in good yield[47]. Similar reaction in solution yields a mixture of products.

Analysis of the crystal structure of the inclusion compound indicates that the

reacting centres are held in the correct orientation for reaction at a distance of <4.0 Å which is shorter than the reactive limit described by Schmidt.[48] This reaction does not occur in crystals of the pure reactant as the reactant centres are unfavourably placed.[49]

Stereocontrol of intramolecular reactions may also be dramatically improved by inclusion.[50] The reactant species is restrained from certain modes of molecular movement or rearrangement and thus one reaction pathway is favoured leading to the formation of one product in excess. In some cases an otherwise symmetrical molecule may be constrained to a chiral unsymmetrical conformation upon inclusion[51] such that reaction leads to the optically active product as occurs in the example detailed in Figure 1.8.

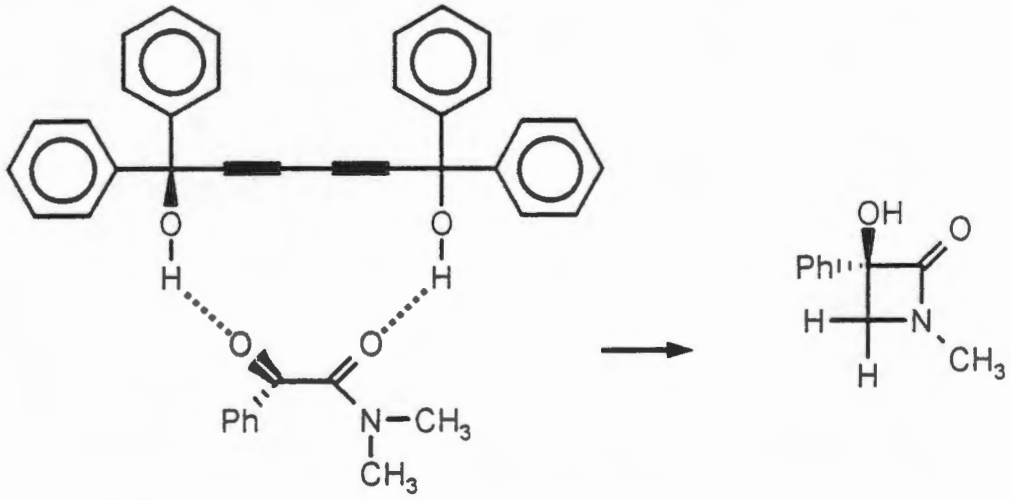

Figure 1.8: Imposition of chirality by inclusion. The achiral guest molecule is constrained to adopt a chiral conformation in the inclusion compound crystal and, upon irradiation, a chiral product results.

Storage of labile compounds:

Highly labile compounds may be stabilised by formation of inclusion compounds. This is of course similar to the separation of tautomeric compounds described above where the minor tautomer in solution may be significantly stabilised by inclusion. Many chiral selenoxides (which are potentially useful synthons) have a short half-life for racemisation[52] yet when included by a chiral host compound may be maintained in an optically pure, stable state.[53] The compounds are declathrated when required for synthesis.

Related to the storage of otherwise unstable compounds is the controlled release of compounds such as bacteriocides[54] or pheromones.[55] The valuable substance is slowly released as the inclusion compound decays over time.

Chemical Sensors:

Inclusion compounds may be useful as agents for chemical sensors. The inclusion of a guest molecule may change a detectable physical characteristic of the host such as colour[56,57] or fluorescence or may have a secondary effect such as in piezoelectric devices which detect weight gain as the inclusion compound is formed.[58] The rate and selectivity of inclusion (and therefore of response) are important in such applications.

INCLUSION COMPOUNDS OF STEROID HOSTS:

History:

The steroidal bile acids are derived, as the name suggests, from bile secreted from the livers of vertebrates. In the natural state these occur in the conjugated form with peptide linkages via the side chain to amino acids, most commonly glycine or taurine.

Deoxycholic (DCA) and cholic acids (CA), I and II in Figure 1.9, are the most commonly occurring bile acids. Other related acids such as chenodeoxycholic (CDCA) and apocholic acid (AC), III and IV, constitute far smaller proportions of bile. Being readily available natural compounds (relatively large amounts are extracted from the bile of domestic sheep, cattle and pigs) the chemistry of the bile acids was extensively investigated in the late 19th and early 20th century. A review by Sobotka[59] in 1934 detailed the collected knowledge of the bile acids to that date.

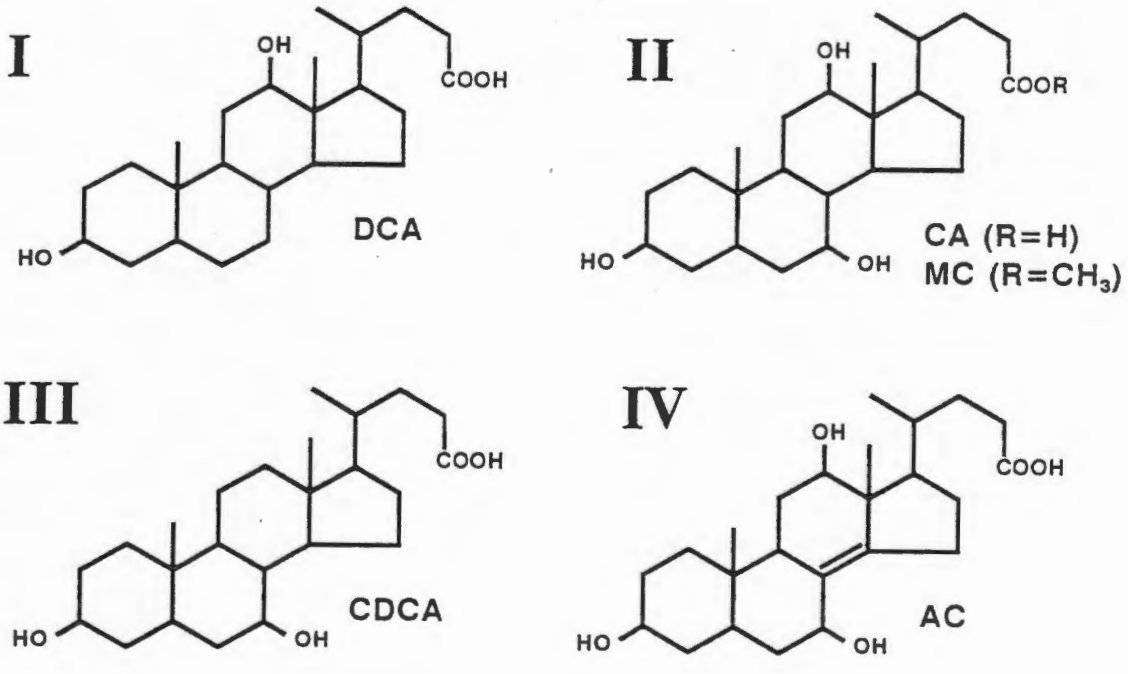

Figure 1.9: Molecular structures of some of the common bile acids.

The capacity of steroidal acids to form inclusion compounds was first remarked upon in 1833[60] the term "Cholansaure" (Choleic acids) being used to describe a wide range of bile acid adducts of varying composition. The transformation of cholic acid into deoxycholic acid containing "crystal acetic acid" was recorded by Mylius.[61] It is now clear that this compound was, in fact, an inclusion compound of DCA with acetic acid, the crystal structure of which is now known.[87]

High vacuum distillation applied by Wieland and Sorge[62] to the choleic acids revealed the presence of a number of fatty acids such as palmitic acid, stearic acid and oleic acids in the distillate. The remaining non-volatile component was identified as pure DCA. These authors developed the "choleic acid

principle" in which they elucidated the concept of complexation or co-ordination of DCA and fatty acids.

The realisation that the fatty acid components could be replaced by acetic acid, acetone, alcohols or ether and that compounds such as butyric acid, phenol and naphthalene could be induced to crystallise with DCA in *specific* proportions followed. It was widely believed (and only recently challenged) that of all the bile acids only DCA showed significant inclusion capability. Mylius recognised the formation of choleic acids by CA with alcohols and mercaptans[63] and the formation of a choleic acid of AC was commented upon by Boedecker and Volk;[64,65] yet in 1934 Sobotka comments in his review[59]: "... if we compare deoxycholic acid and apocholic acid on the one side and cholic acid, lithocholic acid and cholanic acid on the other side, all of which have no pronounced co-ordinative power ...". (Cholanic acid is a steroidal acid similar to CA or DCA but lacking hydroxy groups at positions 3, 7 and 12).

The question of co-ordination number (or host:guest ratio) was investigated by Wieland and Sorge[62] and Rheinboldt showed that only co-ordination numbers allowing for "symmetrical arrangement" i.e. 4, 6 and 8 and less commonly 2 or 3 occurred. While physical properties may be shown to change in a regular fashion in any homologous series, the H:G ratio (co-ordinative valence) is a periodic function dependent on molecular size, or even more simply, in the case of the fatty acids, on the length of the longest molecular chain.[66] This dependence of H:G ratio on chain length is depicted in Figure 1.10.

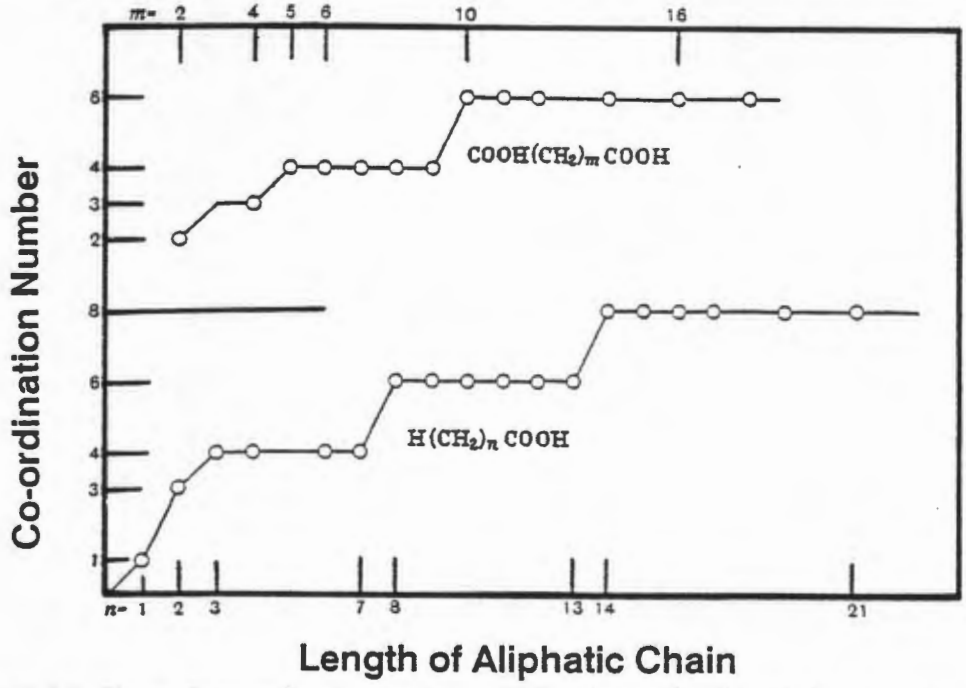

Figure 1.10: Change in co-ordination number or H:G ratio as a function of chain length.

Interestingly Sobotka and Goldberg used DCA inclusion compound formation to separate *l*- isomers of camphor, phenyl ethyl ethanol, dipentene and methyl ethyl acetic acid from racemic mixtures of the guests.[67,68] While the concept of separation of enantiomers is now well established this was a startling result at the time and it is surprising that it has been little further pursued.

The stabilisation of certain tautomeric forms was recognised in the study of choleic acids with various tautomeric ketones.[69,70] An example of such behaviour is exemplified in the inclusion compound formed by DCA and ethyl acetoacetate. In the inclusion compound this ketone exists exclusively in the enol form.

The bile acids are thought to act as transport mediators in the gut rendering insoluble compounds such as cholesterol soluble by the formation of mixed micelles of bile salt and lecithin.[71] Much work has been directed towards discerning the behaviour of aqueous solutions of bile salts with respect to micelle formation and consequent solubilisation of insoluble compounds, such as cholesterol, in the gut.[72,73,74]

Crystal Structures:

DCA, CA, CDCA and AC are steroids with ABCD fused ring systems exhibiting *cis/trans/trans* ring junctions and a 17β side chain. The molecules are curved by dint of the ring fusion restraints and only the side chain and to a lesser extent the D-ring conformations can vary. They are chiral natural products occurring in only one enantiomeric form.

While a number of early crystallographic studies were carried out,[75-86] it is only recently that large enough numbers of crystal structures of inclusion compounds of steroidal bile acids have been elucidated to allow the discernment of similarities and differences in structure and to attempt to relate these to the properties of the compounds.

Reports of a wide range of crystal structures of α-phases and inclusion compounds of DCA, CDCA, AC, CA and MC are presented in Table 1.1. Host:guest ratios, cell parameters and pertinant referances are detailed while any related studies or interesting structural features are mentioned as 'comments'.

Table 1.1: Selected Crystal Structure Data for Inclusion Compounds of Steroidal Bile Acids.

DEOXYCHOLIC ACID CRYSTAL STRUCTURES

	H:G	Space Group	Cell Parameters			Refs	Comments
Acetic Acid	1:1	$P2_12_12_1$	25.55 90	13.81 90	7.11 90	87	Guest molecules form hydrogen bonded chains in host channels.
Acetone	2:1	$P2_12_12_1$	25.81 90	13.61 90	7.23 90	88, 89	Solid state addition by photolysis results in stereospecific and regiospecific addition to C(6).
Ethyl Methyl Ketone	2:1	$P2_12_12_1$	25.81 90	13.59 90	7.23 90	89	
Diethyl Ketone	2:1	$P2_12_12_1$	25.83 90	13.56 90	7.24 90	89	
Pinacolone	2:1	$P2_12_12$	27.132 90	13.814 90	7.233 90	90,91	
Methyl pentyl ketone	3:1	$P2_12_12_1$	25.529 90	13.440 90	7.214 90	89	
(*S*)-3-methyl-cyclohexanone	2:1	$P2_12_12_1$	26.90 90	13.52 90	14.16 90	89	

(*R*)-3-methyl-cyclohexanone	2:1	$P2_12_12_1$	26.90 90	13.52 90	14.16 90	89	
Ethyl Acetate	2:1	$P2_12_12_1$	25.438 90	13.457 90	7.243 90	92,93	
Acetophenone	2:1	$P2_12_12_1$	25.243 90	13.606 90	7.198 90	93,94	Includes structure of trideuterated acetophenone
p-F-acetophenone	1:0.375	$P2_12_12_1$	25.270 90	13.579 90	7.198 90	95	Photoaddition of guest to host results in *S*- product at C(5) i.e. the same product as achieved with acetophenone.
p-F-acetophenone/ Acetophenone	5:1:1	$P2_12_12_1$	25.262 90	13.611 90	7.208 90	96	Photolysis results in addition by hydrogen abstraction at C(5) to produce the *S*- product.
m-Cl-acetophenone	3:1	$P2_12_12_1$	25.283 90	13.639 90	7.198 90	93	Photoaddition at C(5) results in formation of *S*-product i.e. the same product as is formed with acetophenone.
Propiophenone	3:1	$P2_12_12_1$	25.343 90	13.634 90	7.229 90	96	UV irradiation results in formation of diastereomeric photoproducts of addition at C(5) and C(6)
p-F-propiophenone	3:1	$P2_12_12_1$	25.432 90	13.582 90	7.201 90	96	
p-Cl-Propiophenone	3:1	$P2_12_12_1$	25.432 90	13.582 90	7.201 90	96	
p-di-Iodo-benzene	2:1	$P2_12_12_1$	26.59 90	13.58 90	7.17 90	97	

Phenyl acetylene	2:1	$P2_12_12_1$	25.542 90	13.662 90	7.227 90	99	γ-irradiation did not result in polyphenylacetylene formation as the distance between double bonds in the crystal is too large.
Phenanthrene	3:1	$P2_12_12_1$	26.81 90	13.60 90	21.66 90	100	Stability study[101]
Styrene	2:1	$P2_12_12_1$	26.59 90	13.59 90	7.28 90	102	Vaporisation behaviour measured by torsion/effusion method. Enthalpy values for formation of clathrate estimated.
Naphthalene	2:1	$P2_12_12_1$	26.50 90	13.72 90	7.38 90	102	Vaporisation behaviour measured by torsion/effusion method. Enthalpy values for formation of clathrate estimated.
1,2-Benzanthracene	3:1	$P2_12_12_1$	26.89 90	13.69 90	7.29 90	100	Stability study employing torsion/effusion method.
Quadricyclane	2:1	$P2_12_12_1$	27.150 90	13.359 90	14.161 90	103	Investigation into feasibility of norbornadiene ⇌ quadricyclane conversiomn for energy storage and retrieval.
Norbornadiene	2:1	$P2_12_12_1$	27.13 90	13.46 90	14.21 90	103	Comparison of guest cavity size with that of quadricyclane - see above.
Thiocamphenilone	2:1	$P2_12_12$	13.738 90	27.203 90	7.189 90	104	Does not undergo photoaddition with H-abstraction - unidentified polymeric products obtained.
Ferrocene	3:1	$P2_12_12_1$	27.288 90	13.679 90	7.072 90	105	Guest ordered - unlike other ferrocene inclusion compounds.
Di-tert-Butyl-thioketone	2:1	$P2_12_12$	13.933 90	27.294 90	7.285 90	106	No photolysis addition product to host steroid on irradiation.

d-Camphor	2:1	$P2_12_12$	27.353 90	13.814 90	7.233 90	107	Guest is spherically disordered. Potential energy calculations indicate 4 possible guest positions.
(E)-*p*-Dimethyl-aminoazobenzene	4:1	$P2_12_12$	25.676	13.731 90	7.160 90	108 90	Short contacts between Host and Guest indicate C-H•••π interactions.
di-tert-butyl-diperoxycarbonate	4:1	$P2_12_12_1$	27.16	13.48 90	14.17 90	109 90	Thermolysis or photolysis results in stereospecific and regiospecific hydroxylation at position C(5).
Palmitic acid/ Ethanol	8:1:1	$P2_12_12_1$	26.02 90	13.54 90	7.27 90	110	Vaporisation studies by torsion effusion method.[111]
Water	2:3	$P4_12_12$	14.00 90	14.00 90	48.90 90	112	Water molecules form continuous H-bonded chains and are also H-bonded to the host molecules.
Ethanol/ water	2:1:1	$P4_12_12$	14.07 90	14.07 90	49.33 90	114	Host-guest H-bonding result in 'bilayer' formation with guest molecules included in the bilayer structure.
Ethanol/ water	3:2:1	$P6_5$	15.12 90	15.12 90	18.68 120	115	Spiral H-bonded structure.
Dimethyl sulphoxide/ Water	2:1:1	$P6_5$	15.117 90	15.117 90	18.695 90	113	

APOCHOLIC ACID							
Acetone	1:1	$P2_12_12_1$	24.47 90	14.26 90	7.50 90	88	
CHENODEOXYCHOLIC ACID							
no guest	-	$P2_12_12_1$	18.785 90	8.120 90	14.889 90	116	
Ethyl Acetate	1:1	$P6_5$	22.169 90	22.169 90	10.226 120	117	
Br-benzene	1:?	$P6_5$	22.250 90	22.250 90	10.225 120	118	Synchrotron radiation determination. Host:guest ratio not determined - guest highly disordered.
CHOLIC ACID							
No guest	-	$P2_12_12_1$	16.477 90	8.394 90	16.993 90	119	
Water	2:1	$P6_522$	13.736 90	13.736 90	8.506 120	120, 121	Water molecules are extensively disordered and arrayed over a number of possible sites.
Water	1:1	$P2_1$	12.794 90	8.157 117.60	12.885 90	122	Tetrahedrally hydrogen-bonded water molecules form an integral part of the hydrogen-bonded layer.
Methanol	1:1	$P2_12_12_1$	15.198 90	11.625 90	14.560 90	123	H:G ratio may be higher than indicated by crystal structure analysis.

Ethanol	1:1	$P2_12_12_1$	14.661 90	11.759 90	15.066 90	124, 123	
1-Propanol	1:1	$P2_12_12_1$	15.026 90	11.864 90	14.951 90	125	Guest molecules fit almost perfectly into cavities.
(*S*)-γ-Valerolactone	1:1	$P2_1$	13.010 90	8.003 104.76	14.049 90	126	Separation of optical isomers[150]. ^{13}C NMR study[151].
Acetophenone	1:1	$P2_1$	13.719 90	8.093 113.69	14.229 90	127	
3-Fluoro-aniline	1:2	$P2_1$	14.326 90	7.847 106.58	16.125 90	128	Unusual H:G ratio resulting from formation of channels perpendicular to *b* ascribed to guest-guest repulsion.
Benzene	1:1	$P2_1$	13.627 90	8.033 114.25	14.076 90	129	
METHYL CHOLATE							
Methanol	1:1	C_2	25.184 90	7.797 121.05	15.174 90	130, 131	
2-Propanol	1:1	C_2	25.835 90	8.137 121.08	15.553 90	131	

DCA Inclusion Compounds:

The inclusion compounds of DCA comprise the largest group of steroid bile acid host inclusion compounds studied to date. The structures of these compounds may be divided into three types which are described by Giglio[132] as follows:

i) Orthorhombic structures: by far the largest group of DCA inclusion compounds crystallise in the orthorhombic space groups $P2_12_12_1$ and $P2_12_12$ have similar host conformations. The side chain exhibits the *gauche* conformation and the D-ring approaches the half-chair form. Host bilayers bound together by host-host hydrogen bonding such that the exposed sides of the bilayers are hydrophobic and the hydrophilic groups are 'hidden' within occur parallel to the *bc* direction. Adjacent host bilayers are related by 2_1 symmetry. The host bilayers are puckered and guest molecules accommodated in the channels formed between these. The group may be divided into two subgroups according to the bilayer translation distance which is reflected in the length of the *c*-axis. These are designated:

α: bilayer translation *ca* 7.2 Å,

β: bilayer translation *ca* 14.2 Å.

and occur upon inclusion of threadlike guest molecules and spherical guest molecules respectively. Examples of the packing diagrams typical to this type are presented in Figure 1.11a. The differences in packing give rise to shifts in the relative positions of facing monolayers. In the β type structures these are at approximately the same height in *a* while in the α type structures the facing monolayers are shifted by about 3.6 Å along *c*.

ii) Tetragonal structures: host conformations are similar to those found in the orthorhombic structures with bilayers related to each other by a 4_1-axis such that the bilayer extends in the *ab* plane. Adjacent monolayer rows occur at approximately the same height but the channels formed are not hydrophobic in nature and the guest molecules participate in the hydrogen bonding schemes. An example of the type of packing exhibited in crystals belonging to this group is presented as Figure 1.11b.

iii) Hexagonal structures: host molecules in structures belonging to the hexagonal space groups exhibit conformations different from those found in structures belonging to either of the above groups: the side chain adopts the *trans* conformation and the D-ring the β envelope form. Hydrogen bonding schemes too differ from those described above with helices of DCA molecules hydrogen bonded to each other and to the guest molecules packed in spirals about the 6_5-axis as illustrated in Figure 1.11c. The hydrophilic cavity thus formed has a diameter of only *ca* 4 Å and can accommodate only small polar guest molecules.

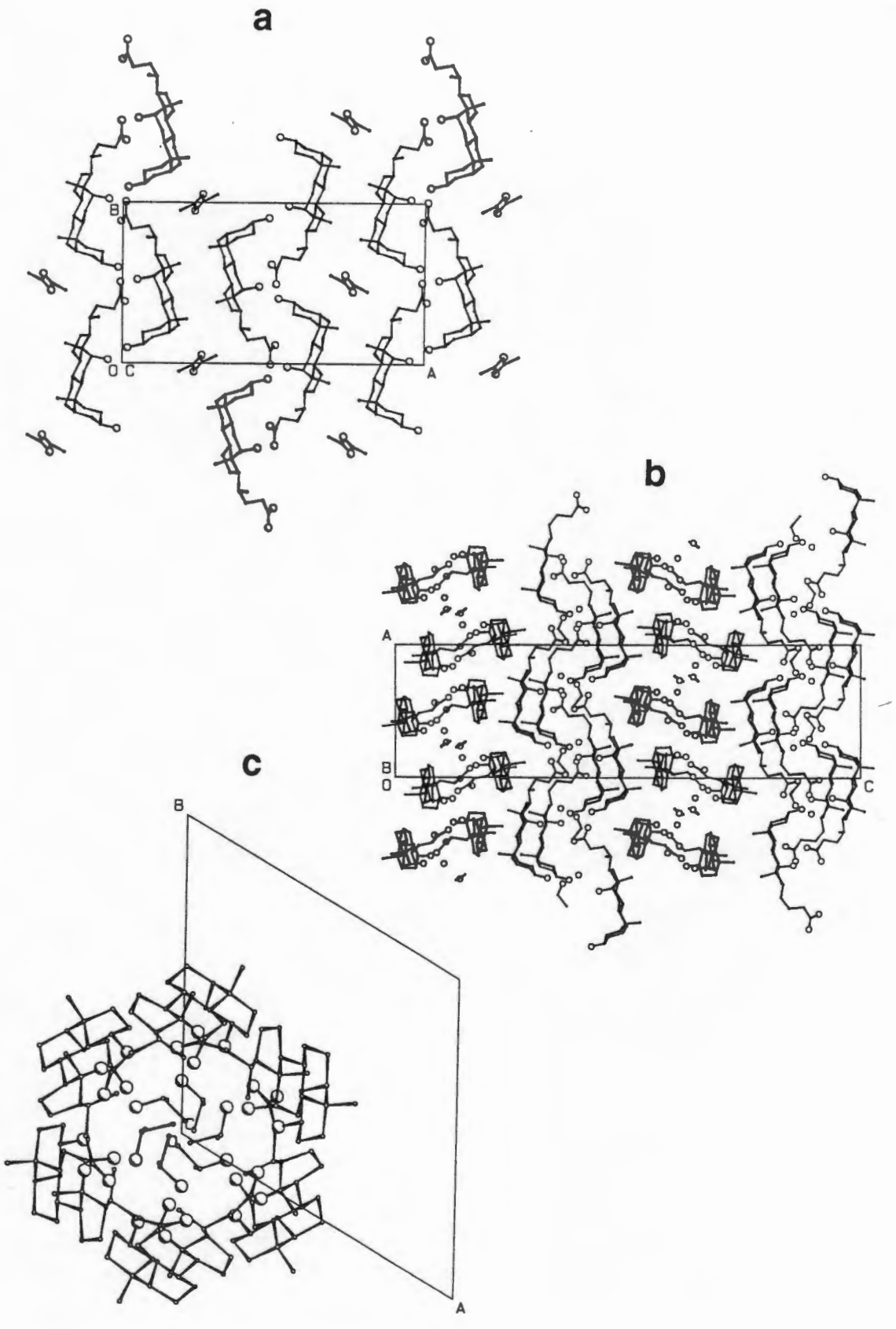

Figure 1.11: Packing diagrams representing the three types of structures found in DCA inclusion compounds.

a) 5DCA•2acetone crystallises in the orthorhombic system. (Guest molecules are disordered.)

b) 2DCA•3.H_2O crystallises in the tetragonal system.

c) 3DCA•2ethanol•H_2O crystallises in the hexagonal system.

Stability and Decomposition Studies:

The stability of DCA inclusion compounds and thus the strength of host:guest interactions has been investigated by the torsion effusion method[101,102] allowing determination of the vapour pressure of gaseous guest in equilibrium with its choleic acid as a function of temperature. Since DCA is non-volatile and does not contribute to the vapour pressure, the enthalpy change associated with the release of guest from the crystal of the choleic acid inclusion compound, (ΔH_r) and the corresponding heat of formation (ΔH_f) could be derived once guest vaporisation enthalpies were known.

Table 1.2 drawn from reference 132 details the results of such experiments on a small group of DCA inclusion compounds.

Table 1.2: Experimental results for the values of ΔH_r and ΔH_f for a number of DCA inclusion compounds.

Guest	H:G ratio	T range (K)	ΔH_r (kJ)	ΔH_f (kJ)
Styrene	2:1	353-414	56.9(5.4)	15.1(5.4)
Naphthalene	2:1	361-419	72.0(5.4)	23.8(5.4)
Phenanthrene	3:1	403-441	128.9(5.9)	50.2(7.1)
1,2-benzanthracene	3:1	405-429	126.4(7.5)	21.8(9.2)
11,12-benzofluoranthene	3:1	414-454	124.3(3.8)	4.6(5.0)

Variation in these values is ascribed to differences in host:guest interactions. The primary such interaction is that between the C(18) methyl groups and the π-cloud of the guest aromatic rings described as 'polarisation bonding'.[103] This type of interaction will be stronger the greater the guest polarisability and the overall host:guest interaction will depend on the total number of such interactions per guest. Thus the inclusion compound with phenanthrene exhibits two such 'hooks' while that with styrene has only one. Although the number of condensed rings increases for the last two compounds in the Table there are only two C(18)•••π interactions and the ΔH values for guest release are similar.

Photoaddition of Guest to DCA:

A number of inclusion compounds of DCA undergo regio- and stereo-specific photolysis or thermolysis to produce modified steroids.[88,93,95,96,109] Reaction with included di-*t*-butyl diperoxycarbonate results in the formation of two major products designated **6** and **7** below,[109] while photoaddition of included acetone to DCA yields three major products designated **8** , **9** and **10** below. These results are explained in terms of the packing of the complexes and in the second case the geometry of interaction of the carbonyl group of the guest and the abstractable hydrogen atoms of the host. To test their assertions about the topochemical nature of the reactions the authors consider the structure of a related compound namely the inclusion compounds of AC with acetone[88] which does not undergo such reaction.

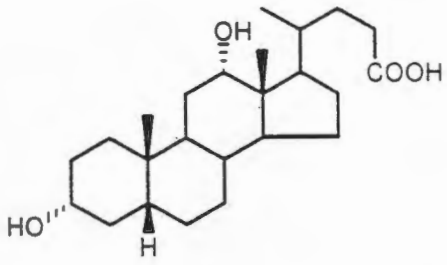

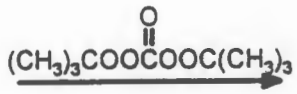

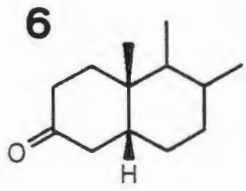

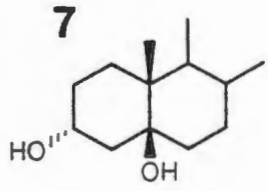

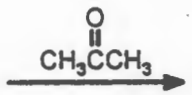

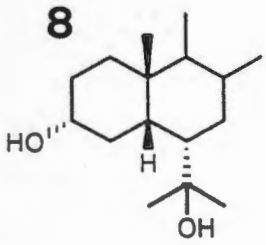

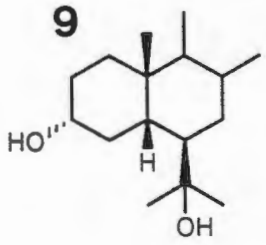

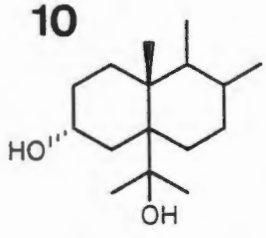

Reaction with included acetophenone leads to formation of a single diastereomeric reaction product with absolute configuration *S* at C(5) **11** below. This is opposite to the configuration expected from consideration of the host:guest packing at the reaction site[133] and initiated a comprehensive study of such reactions with acetophenone and related molecules. A number of the reactions occur without disruption of the crystal structure (a single crystal to single crystal transformation) and the reaction may be followed by single crystal X-ray diffractometry.

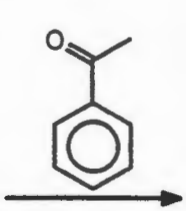

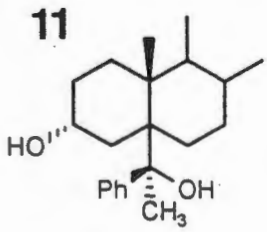

Reaction is shown to proceed by 180 ° rotation of the acetyl group of the guest.[89,96] The crystal structures of both the partially reacted compounds and the photoproducts were achieved.

Polymerisation in DCA channels:

The channels of DCA represent chiral environments in which guest molecules may interact with those above and below but are well separated from guests in other channels (at least in defect free regions of the crystals). The type of polymerisation reaction that would be expected is depicted schematically in Figure 1.12. Miyata and Takemoto reported radiation-induced polymerisation of 2,3-substituted butadienes[134] and of vinyl monomers[135] in the DCA channels while Audisio and Silvani achieved reaction of penta-1,3-diene monomers.[136] A list of polymerisation reactions using guest monomers included in DCA is presented in Table 1.3.

Table 1.3: Polymerisation in DCA Inclusion Compound Channels.

Monomer	m.p. (°C)	Tacticity	References	Comments
2,3-Dimethyl-butadiene	240-250	1,4-trans	137,142 138,139	Effects of postirradiation polymerisation temperature and additives.[142] Preparation by replacement.[139]
2,3-Dichloro-butadiene	>300	1,4-trans	142	Highly isotactic polymer.
cis-penta-1,3-diene		largely 1,4-trans	140	Isotactic and optically active, $[\alpha]_D = -21^o$
trans-penta-1,3,-diene		largely 1,4-trans	140	Polymer is *not* isotactic as is that resulting from the *cis* monomer. $[\alpha]_D = 0.3^o$
trans-2-methyl penta-1,3-diene	250		141	Polymer shows high degree of optical activity. $[\alpha]_{577} = 290^o$, $[\alpha]_{546} = 350^o$, $[\alpha]_{435} = 560^o$, $[\alpha]_{365} = 940^o$
Butadiene	unstable	atactic	142, 142	Prepared by replacement of acetone in channels.

2- and 3-methyl-pentadiene and isoprene result in viscous gel-like low molecular weight polymers in low yield. Acrylonitrile, methacrylonitrile, β-propiolactone, diketene and dioxane form inclusion compounds with DCA but no polymerisation occurs upon irradiation.[142]

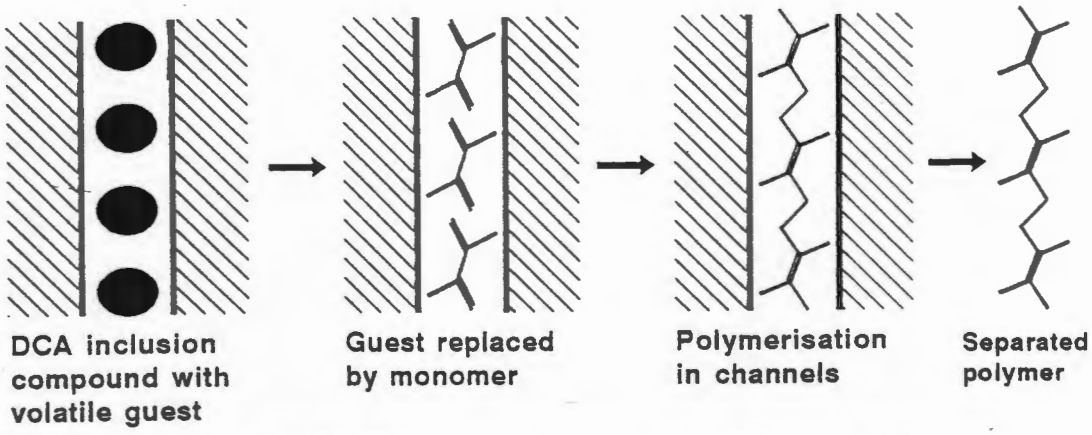

Figure 1.12: Schematic of the polymerisation occurring in the channels of DCA inclusion compounds. Guests are constrained to particular positions relative to each other and a high degree of topotactic control is achieved.

The inclusion compound used were produced by two different methods: crystallisation of the inclusion compound from solutions of DCA either directly dissolved in guest monomer or from solutions made by dissolution of both host and guest in a co-solvent *OR* by replacement of volatile guests such as acetone in the inclusion compound crystals with the monomer guest.[143] The replacement of one guest with another appears not to have been confirmed in all cases, often being inferred from the retention of the gross shape of the crystals and the lack of significant solubility of host in guest monomer (e.g. butadiene[143]). Polymers thus obtained often contain high proportions of 1,2-addition products which would appear to indicate that polymerisation might occur *outside* the channels of the DCA inclusion compounds so that the regio-control due to the highly constrained relative positions of the guest molecules is lost. This possibility is surely reinforced by the reported low stability of the DCA butadiene complex which is readily replaced by other guests, introduced into the reaction vessel to test that effect of additives on the rate and products of polymerisation.[143] Addition of species that readily form stable DCA inclusion compounds significantly increases the relative amounts of 1,2-addition products presumably obtained by ousting significant quantities of the butadiene monomers from their places in the channels. This seems to reinforce the suggestion that the polymerisation of such monomers may proceed (at least in part) outside the channels of DCA and represent therefore the polymerisation of butadiene *in the presence of* DCA rather than *inclusion polymerisation.* It is surprising that, in spite of the experimental evidence, the authors appear not to consider this possibility, specifically stating that this represents an example of a regio- and stereo-specifically controlled polymerisation reaction within clathrate channels.

In other cases such as the polymerisation of 2,3-dimethylbutadiene the addition of the homologous saturated molecule (2,3-dimethyl butane) greatly decreased polymer yield, presumably by replacement of monomer units within the channel disrupting the chain reaction.[135,144] This, combined with an interesting solid state NMR study of this polymerisation reaction in the channels of the DCA inclusion compound channels,[145] provide clear evidence that this reaction, at least, is an example of in-channel polymerisation.

CA Inclusion Compounds:

Until recently CA was thought to have limited inclusion capacity forming inclusion compounds with water, either in a 2:1[120,121] or 1:1[122] host:guest ratio, or with small aliphatic alcohols (methanol, ethanol and 1-propanol).[123,124] Recently a report of a channel type inclusion compound with acetophenone guest has appeared.[127] Shortly thereafter the same authors presented a surprising finding: upon soaking crystals of CA(α) in acetophenone for a period of time the inclusion compound was formed without loss of crystallinity. A single crystal to single crystal transformation is claimed for the reaction:[146]

$$CA_{(s,\alpha)} + \text{acetophenone}_{(l)} = CA\bullet\text{acetophenone}_{(s,\beta)}.$$

It was this finding that initiated the present study.

During the time period over which the work presented in this thesis was carried out, a number of reports of CA inclusion compounds have appeared and a summary of the structures reported to date is presented in Table 1.1.

CA host alone:

Unlike DCA the structure of CA without included guest molecules (CA(α)) is known.[119] The packing diagram of this structure is presented as Figure 1.13 . The CA molecules pack together so that all hydroxyl and carboxylic acid oxygen atoms are involved in hydrogen bonds. The hydrogen bonding system is quite different to that noted in the majority of CA inclusion compounds as will be discussed in detail later.

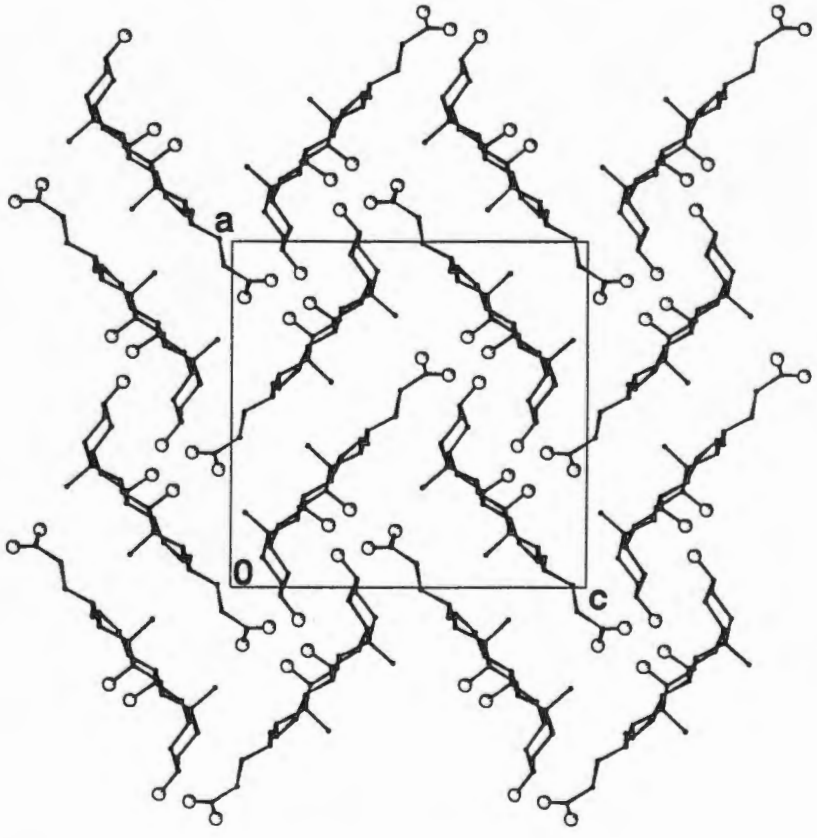

Figure 1.13: Packing diagram of CA(α) viewed down [010]. Drawn from data derived from the structure by Miyata *et al.*[119]

Packing:

Inclusion of water results in the formation of either hexagonal crystals belonging to the space group $P6_522$ (H:G, 2:1) or in crystals belonging to the space group $P2_1$ (H:G, 1:1). The former are similar in packing to the ethanol/water inclusion compound of DCA while the latters packing bears a resemblance to that seen in DCA inclusion compounds crystallising in the tetragonal system. The packing diagrams of both compounds are presented in Figures 1.14a and b. In both cases extensive hydrogen bonding between host and guest and host and host occurs.

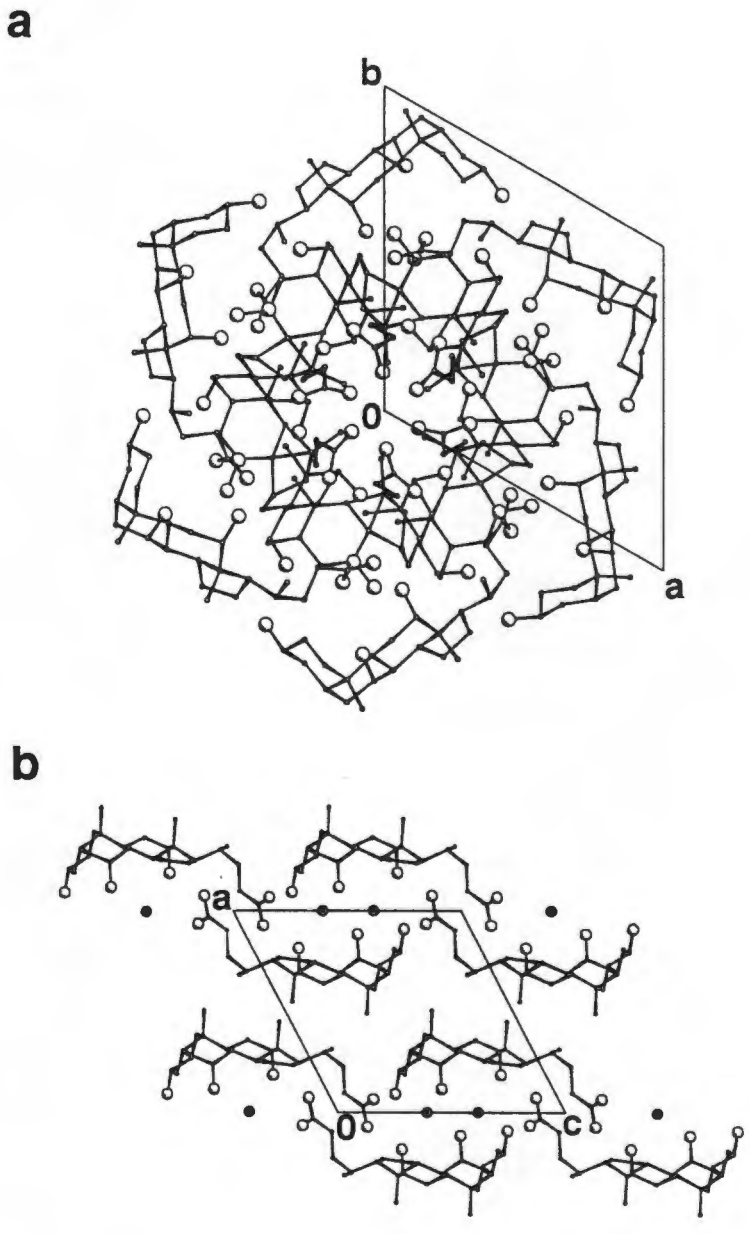

Figure 1.14: Packing diagrams of
a) CA•½H_2O (disordered water molecule omitted)
b) CA•H_2O (filled circles - water oxygen atoms)
redrawn from data derived from the structure by Lessinger and Low[121] and Lessinger[122].

The crystal structures of the inclusion compounds with alcohol guests exhibit no bilayer formation and the host molecules are hydrogen bonded in a three dimensional array both to other host molecules as well as to the guest alcohols.[123] Guest molecules are contained in cavities and it is reported by Jones and Nassimbeni[123] that the dimensions of the cavities are such that the 1-propanol molecule provides a nearly 'perfect fit' while that of the methanol guest appears to occupy only 50% of the available space allowing for inclusion of other non-hydrogen bonded methanol molecules in the cavities. They suggest that the guest cavities are incompletely isolated and that these non-hydrogen bonded molecules may diffuse out of the crystal via the small interconnecting channels thereby accounting for the poor stability of this compound.

Miyata *et al* report the existence of CA inclusion compounds containing a diverse range of included guests.[147] Although host:guest ratios are reportedly determined by TG and ^{1}H-NMR analysis as well as uv-vis spectroscopy it appears that some of the guest identities are incorrectly assigned. No further reports of a number of the supposedly included compounds appear and we have found certain of the experiments impossible to duplicate. Specifically: the thermal analysis results of the CA•benzoic acid compound are very similar to those of the complex formed by CA•acetone•3H_2O while benzoic acid has not been shown to be included and no further reports of the inclusion of a molecule as large as benzophenone have appeared. The benzophenone adduct is reported to melt at 170 °C with no appearance of a host melt (at *ca* 200 °C). While a number of CA inclusion compounds with solid guests do exhibit this sort of behaviour the melting point is remarkably close to that of CA•½H_2O, the only crystals ever achieved from solutions containing benzophenone in this study. The inclusion of butanol is reported with the unusual H:G ratio of 1:2 yet in a later paper the same authors report using butanol as a solvent to facilitate inclusion of hydrocarbon guests on the basis that butanol is *not* included by CA.[148]

While the structures of the inclusion compounds with alcohols and water show host:guest hydrogen bonding it so transpires that, although many guest molecules included by CA bear polar groups capable of participating in hydrogen bonding, the most common type of inclusion compound is that of the tubulate clathrate with no short range host guest interactions. One of the first tubulate clathrate inclusion compounds reported was that of CA with acetophenone.[127] The structure is similar to those of the DCA compounds crystallising in orthorhombic space groups; the host steroids are aggregated into puckered bilayers bound together by intermolecular host-host hydrogen bonds and packed together leaving channels parallel to *b* (in these structures) into which the guest molecules are packed as may be seen in Figure 1.15. Unlike the 5DCA•2Acetophenone complex the host:guest ratio is 1:1 and the guests are stacked one above the other in the channel with the aromatic rings almost parallel to each other.

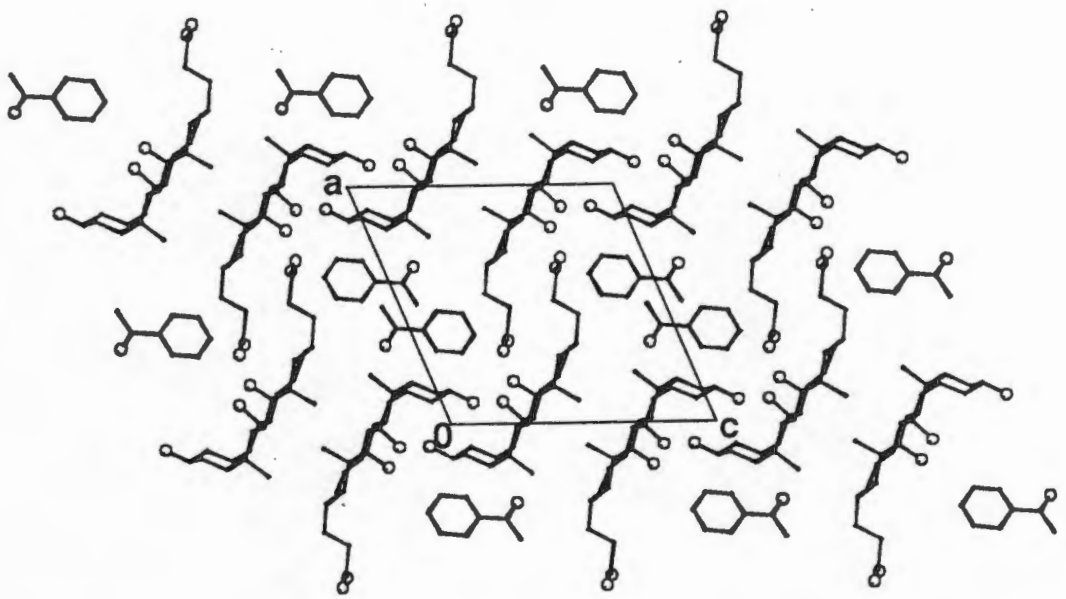

Figure 1.15: packing diagram of CA•acetophenone redrawn from data derived from the structure by Miki *et al.*[127]

Guest Intercalation:

A later report in *Nature*[146] describes the absorption of acetophenone by CA crystals to form the inclusion compound. While this in itself is not unusual the authors claim that the transformation occurs with no loss of crystal integrity: a single crystal to single crystal transformation. Further they suggest that the crystals so obtained are of a quality to allow single crystal X-ray analysis. This is a startling result as, although such guest intercalation is not unknown, most compounds so formed do not require significant rearrangement (including reorientation) of the constituent molecules and are true intercalation compounds. In the CA(α) = CA•Acetophenone transformation it is required that host:host hydrogen bonds are broken and that concerted rotation of the host molecule pairs occurs while the acetophenone molecule diffuses into the crystal; all without significant fracturing or fragmentation. Added to this, CA is significantly soluble in acetophenone yet the authors did not find it necessary to presaturate the acetophenone with CA.[149] It would be interesting to follow this intercalation reaction by single crystal X-ray diffractometry could such a change be induced to occur under constant observation such that one could be sure that the resultant crystals were not the result of dissolution and recrystallisation processes. We have tried this experiment under different conditions but always failed to achieve a single crystal to crystal transformation.

A similar phenomenon of guest exchange where γ-valerolactone is replaced by acetyl acetone is also reported.[150] Again the evidence for the occurrence of a single crystal to single crystal transformation is indirect being inferred from the gross appearance of the crystals viewed by electron microscopy.

Separation of Isomers by Inclusion:

CA inclusion compound formation has been used to achieve separation of optical isomers with significant enantiomeric excesses of (*S*)-(-)-γ-valerolactone and (*S*)-(-)-butyrolactone in the crystals when prepared from racemic mixtures of guest[150]. The crystal structure of the (*S*)-(-)-γ-valerotaclone inclusion compound is reported[126] and a solid state ^{13}C NMR study investigating the relative populations of R and S enantiomers and their conformations and molecular motions provides interesting data about the reasons for selectivity.[151] The results of the solid state NMR study suggest that the (*S*)-isomer is preferred because it may adopt the lower energy conformation yet still fit in the channel and have a lower barrier to molecular rotation than the (*R*)- isomer.

Unusual Host:Guest ratios:

Very recently two papers have appeared detailing inclusion compounds with CA with unusual H:G ratios. The crystal structure of CA with 3-fluoro-aniline describes a compound with two guest molecules per host resulting in an unusual packing arrangement.[128] The packing diagram of this compound is presented as Figure 1.16. Guest molecules are accommodated in channels between the host bilayers and a second channel has opened up between the host bilayers into which a second guest molecule fits. The authors suggest that this is a result of steric repulsions between the fluorine atoms of the guests in the channels designated A.

Nakano *et al* detail the inclusion of a number of hydrocarbon guests by CA.[148] While the only crystal structure reported (that with benzene included) exhibits the usual 1:1 H:G ratio they report inclusion of various guests in larger H:G ratios. A number of examples are listed in Table 1.4.

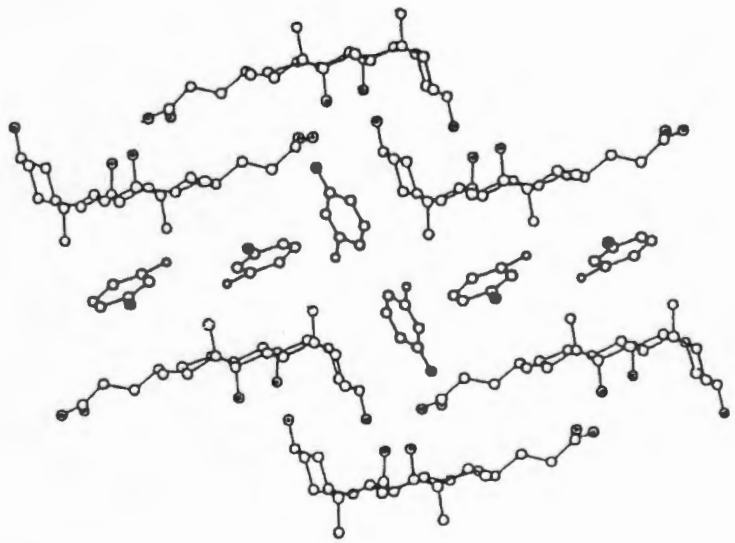

Figure 1.16: Packing diagram of the CA•3-F-aniline inclusion compound[128]. Note the second channel between the host bilayers.

Table 1.4: Inclusion compounds of CA with unusual host:guest stoichiometries. Drawn from Nakano *et al.*[148]

Guests	Guest Release T (° C)	Molar ratio H:G
Tetralin	89, 113	3:2
Myrcene	117	2:1
Cyclohexane	Not clear	3:2
Ethylcyclohexane	110	2:1
Dibutyl ether	109	2:1
β-Ionone	142	2:1
Methyl decanoate	118	2:1

Derivatives of Cholic Acid:

In addition to the inclusion compounds with CA the inclusion capacity of a number of derivatives of CA have been examined. A particularly notable example is that of the amide derivative, cholanamide (V). This compound forms inclusion compounds with a large number of different guest molecules particularly those bearing hydrogen bond acceptor groups.[152]

V

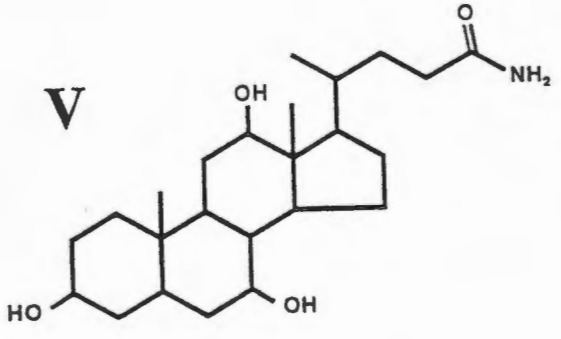

The reported crystal structures of the inclusion compounds are very similar to those of CA except that conversion of the carboxylic end group of the side chain allows for formation of an extra hydrogen bond without disruption of the host-host hydrogen bonding necessary for bilayer formation. For example in the 1,4-dioxane inclusion compound the guest molecules are accommodated in channels but interact with the host bilayers via a hydrogen bond from the $-NH_2$ group of the host side chain to one of the dioxane oxygen atoms.[153]

OBJECTIVES OF THIS STUDY

This study is concerned with the structure/reactivity relationships of the inclusion compounds of the steroid host cholic acid (and to a lesser degree methyl cholate).

The approach adopted is to elucidate the crystal structures of the inclusion compounds of CA with a range of guest molecules of varying size and shape, and bearing different functional groups. A large enough selection of such inclusion compounds would allow comparison of packing modes, host conformation and manner of guest inclusion with a view to predicting future structures.

The solid state reactivity of CA is of particular interest as the inclusion compounds may be formed by reaction of the solid host with guest vapours or with solid guest. The possibility of achieving topotactic control of guest reaction (e.g. polymerisation) within the crystals of the inclusion compound as well as the kinetics of decomposition and absorption are investigated.

1 G.W. Gokel, in 'Inclusion Compounds, Vol 4', Eds. J.L. Atwood, J.E.D. Davies and D.D. MacNicol, Oxford University Press, Oxford-New York-Tokyo, 1991.

2 C.J. Pederson, *Angew. Chem., Int. Ed. Engl.*, 1988, **27**, p 1021.

3 D.J. Cram, *Angew. Chem., Int. Ed. Engl.*, 1988, **27**, p 1009.

4 J.-M. Lehn, *Angew. Chem., Int. Ed. Engl.*, 1988, **27**, p 89.

5 Molecular Inclusion and Molecular Recognition - Clathrates I , *Topics in Current Chemistry*, Vols. 140 , Ed. E. Weber, Springer Verlag, Berlin-Heidelberg, 1987.

6 Molecular Inclusion and Molecular Recognition - Clathrates II , *Topics in Current Chemistry*, Vols. 149, Ed. E. Weber, Springer Verlag, Berlin-Heidelberg, 1988.

7 Inclusion Compounds Vol. 1-3, eds. J.L. Atwood, J.E. Davies and D.D. MacNicol, Academic Press, London, 1984.

8 H. Davy, *Philos. Trans. R. Soc. London,* 1811, **101**, p1.

9 F.H. Herbstein , *Acta Chim. Hung.*, 1993, **130**, p 377.

10 E. Weber, in ref 5 above.

11 D. W. Breck, *J. Chem. Ed.*, 1964, **41**, p 678.

12 R.M. Barrer, Zeolites and Clay Minerals as Sorbents and Molecular Sieves, Academic Press, London-New York-San Francisco, 1978.

13 J.L. Atwood in ref 5 above.

14 M.V. Gaudet, D.C. Peterson and M.J. Zaworotko, *J. Incl. Phenom.*, 1988, **6**, p 425.

15 J.L. Atwood, S.G. Bott, A.W. Coleman, K.D. Robinson, S.B. Whetstone and C.M. Means, *J. Am. Chem. Soc.*, 1987, **109**, p 8100.

16 D.R. Bond, G.E. Jackson, H.C. Joao, M.N. Hofmeyr, T.A. Modro and L.R. Nassimbeni, *J. Chem. Soc., Chem. Commun.*, 1989, p 1910.

17 C.D. Gutsche and R. Muthukrishnan, *J. Org. Chem.*, 1982, **43**, p 4905.

18 R. Ungaro, A. Pochini, G.D. Andreetti, V. Sangermano, *J. Chem. Soc., Perkin Trans. 2*, 1984 , p 1979.

19 M.A. McKervey, E.M. Seward, G. Ferguson, B.L. Ruhl, *J. Org. Chem.*, 1986, **51**, p 3581.

20 G.W. Gokel, "Crown Ethers and Cryptands" in Monographs in Supramolecular Chemistry", Ed. J.F. Stoddart, The Royal Soc. of Chemistry, Cambridge, 1991.

21 J.-M. Lehn and J.-P. Sauvage, *J. Chem. Soc., Chem. Commun.*, 1971, p440.

22 B. Dietrich, J.-M. Lehn and J.-P. Sauvage, *Tetrahedron Lett.*, 1969, p 2885.

23 D.J. Cram, *J. Incl. Phenom.*, 1988, p 397.

24 G.W. Gokel, J.C. Hernandez, A.M. Viscariello, K.A. Arnold, C.F. Campana, L. Echegoyen, F.R. Fronczek, R.D. Gandour, C.R. Morgan, J.E. Trafton, S.R. Miller, C. Minganti, D. Eiband, R.A. Schultz and M. Tamminen, *J. Org. Chem.*, 1987, **52**, p 2932.

25 W. Saenger in Vol. 2 ref 7 above.

26 K. Harata, *Bull. Chem. Soc. Jpn.*, 1975, **48**, p 2409.

27 F. Vögtle and W.M. Muller, *Angew. Chemie, Int. Ed. Engl.*, 1979, **18**, p 623.

28 S. Kamitori, K. Hrotsu and T. Higuchi, *J. Am. Chem. Soc.* 1987, **109**, p 2409.

29 E. Weber in ref 5.

30 E. Weber, I. Csöregh, B. Stensland and M. Czugler, *J. Am. Chem. Soc.*, 1984, **106**, p 3297.

31 H. Hart, L.-T.W. Lin and I. Goldberg, *Mol. Cryst. Liq. Cryst.*, 1986, **137**, p 277.

32 F. Toda, K. Agaki, *Tetrahedron. Lett.*, 1968, p 3695.

33 E.G. Kyba, G.W. Gokel, F. de Jong, K. Koga, L.R. Sousa, M.G. Siegel, L. Kaplan, G.D.Y. Sogal and D.J. Cram, *J. Org. Chem.*, 1977, **42**, p 4173.

34 D. Sybilska and E. Smolkova-Keulemansova in Vol 3 ref 0.

35 F. Toda in ref 5 above.

36 K. Tanaka and F. Toda, *Nippon Kagaku Kaishi*, 1986, p 932.

37 F. Toda, in Inclusion Compounds, Volume 4, 1991, Eds. J.L Atwood, J.E.D. MacNicol, Oxford University Press, Oxford-New York-Tokyo, p 126.

38 F. Toda, Y. Tagami, T.C.W. Mak, *Chem. Lett*, 1986, p 113.

39 F. Toda, Y. Tagami, T.C.W. Mak, *Chem. Lett*, 1986, p 1909.

40 M.R. Caira, L.R. Nassimbeni, J.L. Scott and F. Toda, *J. Chem. Cryst.*, **24**, p 495.

41 M.R. Caira, L.R. Nassimbeni, J.L. Scott and F. Toda, *J. Chem. Cryst.*, **24**, p 545.

42 E. Weber, J. Ahrendt, M. Czuglerand I. Csöregh, *Angew. Chemie., Int. Ed. Engl.*, 1986, **98**, p 719.

43 F. Toda, K. Tanaka, T. Asao, Y. Ikegami, N. Tanaka, K. Hamada and T.

Fujiwara, *Chem. Lett.*, 1988, p 509.

44 M. Segawa, K. Mori and F. Toda, *Chem. Lett.*, 1988, p 1755.

45 K. Fukawa, S. Harada, N. Kasai, M. Toda, K. Mori and F. Toda, *Bull. Chem. Soc. Jpn.*, 1989, **62**, p 2714.

46 F. Toda, K. Tanaka and H. Ueda, *Tetrahedron Lett.*, 1981, **22**, p 4669.

47 F. Toda and K. Tanaka, *J. Chem. Soc. Chem. Commun.*, 1983, p 593.

48 G. M. J. schmidt, *Pure Appl. Chem*. 1971, **27**, p 647.

49 D. Rabinovich, *J. Chem. Soc. (B)*, 1970, p 11.

50 F.Toda in ref 6 above.

51 M. Kaftory, M. Yagi, K. Tanaka and F. Toda, *J. Org. Chem.*, 1988, **53**, p 4391.

52 F.A. Davies, J. M. Billmers and O.D. Stringer, *Tetrahedron Lett.*, 1983, **24**, p 3191.

53 F. Toda and K. Mori, *J. Chem. Soc., Chem. Commun.*, 1986, p 1357.

54 A. Sekikawa, T. Kawamura, S. Hirano, Y. Wakamatsu, M. Yamamoto and F. Amano, Japanese patent JP 63,175,068, 1988.

55 A. Botski, K. Yannakopoulou and E. Hadjoudis, *Carbohydrate Res.*, 1993. **241**, p 37.

56 D.J. Cram, R.A. Carmack and R.G. Helgesen, *J. Am. Chem. Soc.*, 1988, **110**, p 571.

57 R.C. Hlgeson, B.P. Czech, E. Chapoteau, C.G. Gebauer, A. Kumar and D.J. Cram, J. Am. Soc., 1989, **111**, p 6339.

58 A. Ehlen, C. Wimmer, E. Weber and J. Bargon, *Angew. Chem., Int. Ed. Engl.*, 1993, **32**, p 110.

59 H. Sobotka, *Chemical Reviews*, 1934, **15**, p 311.

60 H. Demarcay, *Ann.*, 1833, **27**, p 220.

61 F. Mylius, *Ber.*, 1886, **19**, p 369.

62 H. Wieland and H. Sorge, *Z. Physiol. Chem.*, 1916, **96**(1), paper no. 2.

63 F. Mylius, *Ber.*, 1887, **20**, p1968.

64 F. Boedecker and H. Volk, *Ber.*, 1920, **53**, p 1852.

65 F. Boedecker and H. Volk, *Ber.*, 1921, **54**, p2302.

66 H. Sobotka and A. Goldberg, *Biochem. J.*, 1933, **26**, p555.

67 H. Sobotka, *Naturwissenschaften*, 1931, **19**, p 595.

68 H. Sobotka and A. Coldberg, *Biochem. J.*, 1932, **26**, p 905.

69 H. Sobotka and J. Kahn, *Biochem. J.*, 1932, **26**, p 898.

70 H. Sobotka and J. Kahn, *Ber.*, 1932, **65**, p 227.

71 K. Jumiper, *Am. J. Med.*, 1965, **39**, p 98.

72 A.R. Campanelli, S.C. de Sanctis, E. Giglio, N.V. Pavel and C. Quagliata, *J. Inc. Phenomen. and Mol. Recog. in Chem.*, 1989, **7**, p 391.

73 A.R. Campanelli, S.C. de Sanctis, L. Galantine and E. Giglio, *J. Inc. Phenomen. and Mol. Recog. in Chem.*, **10**, 1991, p 367.

74 J. Gyimesi, L. Barcza, *J. Inc. Phenomen. and Mol. Recog. in Chem.*, 1993, **15**, p 153.

75 G. Giacomello and E. Bianchi, *Ric. Sci.*, 1942, **12**, p 345.

76 R.O. Hertzog, O. Kratky and S. Kuriyama, *Naturwiss.*, 1931, **19**, p 524.

77 Y. Go and O. Kratky, *Z. Phys. Chem.*, 1934, **B26**, p 439.

78 Y. Go and O. Kratky, *Z. Kristallogr.*,1935, **A92**, p 310.

79 G. Giacomello and O. Kratky, *Z. Kristallogr.*, 1936, **A95**, p 459.

80 O. Kratky and G. Giacomello, *Monatsh. Chem.*, 1936, **69**, p 427.

81 V. Caglioti and G. Giacomello, *Gazz. Chim. Ital.*, 1939, **69**, p 245.

82 G. Giacomello, *Gazz. Chim. Ital.*, 1939, **69**, p 790.

83 G. Giacomello and E. Bianchi, *Gazz. Chim. Ital.*, 1943, **73**, p 3.

84 G. Giacomello and E. Bianchi, *Gazz. Chim. Ital.*, 1943, **73**, p 285.

85 H. Fischmeister, *Monatsh. Chem*, 1954, **85**, p 182.

86 M. Bonamico and G. Giacomello, *Gazz. Chim. Ital.*, 1962, **92**, p 647.

87 B.M. Craven, G.T. DeTitta, *J. Chem. Soc., Chem. Comm.*, 1972, p 530.

88 M. Lahav, L. Leiserowitz, R. Popovitz-Biro, C.-P. Tang, *J. Am. Chem. Soc.*, 1978, **100**, p 2542.

89 R. Popovitz-Biro, C.P. Tang, H.C. Chang, M. Lahav, L. Leiserowitz, *J. Am. Chem. Soc.*, 1985, **107**, p 4043.

90 V.M. Coiro, F. Mazza, G. Pochetti, E. Giglio, N.V. Pavel, *Acta Cryst., C (Cr. Str. Comm.)*, 1985, **41**, 229.

91 V.M. Coiro, F. Mazza, G. Pochetti, E. Giglio, *Acta Cryst., A (Fnd. Cryst.)*, 1984, **40**, p C273.

92 L.R. Nassimbeni, M.L. Niven, D.A. Stuart, K.J. Zemke, *J. Cryst. Spectrosc.*, 1986, **16**, p 557.

93 C.P. Tang, H.C. Chang, R. Popovitz-Biro, F. Frolow, M. Lahav, L. Leiserowitz, R.K. McMullan, *J. Am. Chem. Soc.*, 1985, **107**, p 4058.

94 H.C. Chang, C.P. Tang, R. Popovitz-Biro, M. Lahav, L. Leiserowitz, *New J. Chem. (Nouv. J. Chim.)*, 1981, **5**, p 475.

95 H.C. Chang, R. Popovitz-Biro, M. Lahav, L. Leiserowitz, *J. Am. Chem. Soc.*, 1982, **104**, p 614.

96 Y. Weisinger-Lewin, M. Vaida, R. Popovitz-Biro, H.C. Chang, F. Mannig, F. Frolow, M. Lahav, L. Leiserowitz, *Tetrahedron*, 1987, **43**, p 1449.

97 S.C. de Sanctis, E. Giglio, V. Pavel, C. Quagliata, *Acta Crystallogr., Sect. B*, 1972, **28**, p 3656.

98 J.P. Schaefer, L.L. Reed, *Acta Crystallogr., Sect. B*, 1972, **28**, p 1743.

99 E. Giglio, F. Mazza, L. Scaramuzza, J.*Inclusion Phenomena*, 1985, **3**, p 437.

100 S.C. de Sanctis, E. Giglio, V. Pavel, C.Q uagliata, *Acta Crystallogr., Sect. B*, 1972, **28**, p 3656.

101 D. Ferro, P. Imperatori and C. Quagliata, *J. Chem. Eng. Data.*, 1983, **28**, p 242.

102 D. Ferro, C. Quagliata, E. Giglio and V. Piacente, *J. Chem. Eng. Data*, 1981, **26**, p 192.

103 V.M. Coiro, E. Giglio, F. Mazza, N.V. Pavel, *J.Inclusion Phenomena*, 1984, **1**, p 329.

104 K. Padmanabhan, V. Ramamurthy, K. Venkatesan, *J. Inclusion Phenomena*, 1987, **5**, p 315.

105 K. Miki, N. Kasai, H. Tsutsumi, M. Miyata, K. Takemoto, *J. Chem. Soc., Chem. Comm.*, 1987, p 545.

106 K. Padmanabhan, K. Venkatesan, V. Ramamurthy, *Can. J. Chem.*, 1984, **62**, p 2025.

107 J.G. Jones, S. Schwarzbaum, L. Lessinger, B.W. Low, *Acta Crystallogr., Sect. B*, 1982, **38**, p 1207.

108 V.M. Coiro, E. Giglio, F. Mazza, N.V. Pavel, G. Pochetti, *Acta Crystallogr., Sect. B*, 1982, **38**, p 2615.

109 N. Friedman, M. Lahav, L. Leiserowitz, R. Popovitz-Biro, C.-P. Tang, Z. Zaretskii, *J. Chem. Soc., Chem. Comm.*, 1975, p 864.

110 V.M. Coiro, A. D'Andrea, E. Giglio, *Acta Crystallogr., Sect. B*, 1980, **36**, p 848.

111 P. Imperatori and L. Quagliata, *Thermochim. Acta*, 1986, **98**, p 277.

112 C.P. Tang, R. Popovitz-Biro, M. Lahav, L. Leiserowitz, *Isr. J. Chem.*, 1979, **18**, p 385.

113 S.C. de Sanctis, E. Giglio, F. Petri, C. Quagliata, *Acta Crystallogr., Sect. B*, 1979, **35**, p 226.

114 V.M.Coiro,A.D'Andrea,E.Giglio, *Acta Crystallogr., Sect. B*, 1979, **35**, p 2941.

115 S. Candeloro De Sanctis, V.M. Coiro, E. Giglio, S. Pagliuca, N.V. Pavel, C. Quagliata, *Acta Crystallogr., Sect. B*, 1978, **34**, p 1928.

116 P.F. Lindley, M.M. Mahmoud, F.E. Watson, W.A. Jones, *Acta Crystallogr., Sect. B*, 1980, **36**, p 1893.

117 P. Van der Sluis, A. Schouten, J.A. Kanters, *Acta Cryst., C (Cr. Str. Comm.)*, 1990, **46**, p 2165.

118 P.J. Rizkallah, M.M. Harding, P.F. Lindley, A.A. Aigner, A. Bauer, *Acta Cryst., B (Str. Sci.)*, 1990, **46**, p 262.

119 K. Miki, N. Kasai, M. Shibakami, S. Chirachanchai, K. Takemoto, M. Miyata, *Acta Cryst., C (Cr. Str. Comm.)*, 1990, **46**, p 2442.

120 L. Lessinger, *Eur. Cryst. Meeting*, 1985, **9**, p 417.

121 L. Lessinger, B.W. Low, *J. Cryst. Spectrosc.*, 1993, **23**, p 85.

122 L. Lessinger, *Cryst. Struct. Commun.*, 1982, **11**, p 1787.

123 E.L. Jones, L.R. Nassimbeni, *Acta Cryst.,B (Str. Sci.)*, 1990, **46**, p 399.

124 P.L. Johnson, J.P. Schaefer, *Acta Crystallogr., Sect. B*, 1972, **28**, p 3083.

125 E.L. Jones, L.R. Nassimbeni, *Acta Cryst., B (Str. Sci.)*, 1990, **46**, p 399.

126 K. Miki, N. Kasai, M. Shibakami, K. Takemoto, M. Miyata, *J. Chem. Soc., Chem. Comm.*, 1991, p 1757.

127 K. Miki, A. Masui, N. Kasai, M. Miyata, M. Shibakami, K. Takemoto, *J.Am.Chem.Soc.*, 1988, **110**, p 6594.

128 M. Shibakami and A. Sekiya, *J. Chem. Soc., Chem. Commun.*, 1994, p 429.

129 K. Nakano, K. Sada and M. Miyata, *Chem. Lett.*, 1994, p 137.

130 M. Miyata, W. Goonewardena, M. Shibakami, K. Takemoto, A. Masui, K. Miki, N. Kasai, *J. Chem. Soc., Chem. Comm.*, 1987, p 1140.

131 K. Miki, A.Masui, N. Kasai, W. Goonewardena, M. Shibakami, K. Takemoto, M. Miyata, *Acta Cryst., C (Cr. Str. Comm.)*, 1992, **48**, p 503.

132 E. Giglio, in Vol 2, 7 above.

133 R. Popovitz-Biro, H.C. Chang, C.P. Tang, N.R. Shochet, M. Lahav and L. Leiserowitz, *Pure Appl. Chem.*, 1980, **52**, p 2693.

134 M. Miyata and K. Takemoto, *Polymer Letters Edition*, 1975, **13**, p 221.

135 M. Miyata and K. Takemoto, *J. Polymer Sci.*, 1976, **55**, p 279.

136 G. Audisio and A. Silvani, *J.C.S. Chem. Comm.*, 1976, p 481.

137 M. Miyata and K. Takemoto, *Polymer Letters*, 1975, **13**, p221.

138 M. Miyata, K. Morioka and K. Takemoto, *J. Polymer Sci.*, 1977, **15**, p 2987.

139 M. Miyata, K. Morioka and K. Takemoto, *J. Polymer Sci.*, 1977, **15**, p 2987.

140 G. Audisio and A. Silvani, *J.C.S. Chem. Comm.*, 1976, p 481.

141 M. Miyata and K. Takemoto, *Polymer J.*, 1977, **9**(1), p111.

142 M. Miyata and K. Takemoto, *J. Macromol. Sci. - Chem.*, 1978, **A12**(5), p 637.

143 M. Miyata and K. Takemoto, *J. Macromol. Sci. - Chem.*, 1978, **A12**(5), p 637.

144 M. Miyata, K. Morioka and K. Takemoto, *J. Polymer. Sci.*, 1977, **15**, p 2987.

145 S.J. Heyes and C. M. Dobson, Macromolecules, 1992, **25**, p 3617.

146 M. Miyata, M. Shibakami, S. Chiranchai, K. Takemoto, N. Kasai and N. Miki, *Nature*, 1990, **343**, p 446.

147 K. Miki, A. Masui, N. Kasai, M. Miyata, M. Shibakami and K. Takemoto, *J. Am. Chem. Soc.*, 1988, **110**, p 6594.

148 K. Nakano, K. Sada and M. Miyata, *Chem. Lett.*, 1994, p 137.

149 M. Miyata, personal communication, 1992.

150 M. Miyata, M. Shibakami and K. Takemoto, *J. Chem. Soc., Chem. Commun.*, 1988, p 655.

151 F. Imashiro, D. Kwahara and T. Terao, *J. Chem. Soc., Perkin Trans. 2*, 1993, p 1759.

152 K. Sada, T. Kondo and M. Miyata, *Chem. Mater.*, 1994, **6**, p 1103-1105.

153 K. Sada, T. Kondo, M. Miyata, T. Tada and K. Miki, *J. Chem. Soc., Chem. Commun.*, 1993, p 753.

CHAPTER 2: EXPERIMENTAL.

HOST COMPOUNDS:

Cholic acid, (CA), and Methyl cholate, (MC), purchased from Sigma Chemical Company, Dorset UK were recrystallised once from a mixture of acetone and ethyl acetate and in some cases a second time from either methanol or ethanol. The crystals thus obtained were dried *in vacuo* at 120 °C for a minimum of three hours to remove any enclathrated solvent. Purity was checked by DSC analysis and deemed acceptable when the melt was indicated by a single, sharp endotherm in the range 199-202 °C.

GUEST COMPOUNDS:

The various guest compounds were dried in the fashion appropriate to the compound. For example, aliphatic ketones were stirred with anhydrous $MgSO_4$ and stored over dried molecular sieves while high boiling compounds such as Nitrobenzene and Aniline were redistilled and stored over dried molecular sieves and protected from light if necessary.

CRYSTAL GROWTH:

Crystals of the inclusion compounds formed from solutions of dried CA or MC either dissolved directly in the liquid guest or with host and guest dissolved in a co-solvent such as acetone or methyl ethyl ketone (MEK). It proved imperative that all compounds be rigorously dried (particularly in CA crystallisations), to prevent formation of either CA hydrate or CA hemihydrate, both of which crystallise readily from solutions containing trace amounts of water.

Solutions of host and guest and/or co-solvent were forced through 0.50 μm Millex LCR disposable filters to remove dust and other debris to reduce the number of nucleation sites thereby preventing proliferation of small crystals. Solutions were cooled in glass vials and maintained at room temperature with crystals forming during the cooling process if supersaturated solutions were used, or else by slow evaporation of solvent at room temperature. Crystals of CA without included guest (required for some experiments) were grown from acetone solutions at temperatures above 30 °C while MC (α) crystals were grown serendipitously from a solution of MC with *t*-butyl alcohol in acetone after many unsuccessful attempts to grow good single crystals from acetone and a number of other solvents.

NUCLEAR MAGNETIC RESONANCE SPECTROSCOPY:

Samples for ^{1}H-NMR analysis were dissolved in d_6-DMSO and their spectra recorded at 200 MHz on a Varian VXR-200 spectrometer or at 400 MHz on a Unity-400 spectrometer.

OPTICAL MICROSCOPY:

Melting points, temperatures of guest release events and other thermal events

were measured visually on a Linkam TH600 hot stage mounted on a Nikon microscope equipped with both polarising filters and overhead lighting. The temperature was controlled by a Linkam CO600 temperature controller and the hot stage calibrated using the melting points of azobenzene (68 °C), benzil (95 °C), benzanilide (163 °C) and dicyanodiamide (210 °C). Events occurring during heating could be recorded using a camera mounted on the microscope. To simulate the conditions under which TG or DSC experiments were carried out, the sample mounted on the hot stage could be maintained in a flow of nitrogen purge gas which served to flush away any guest vapours evolved.

COMPETITION EXPERIMENTS:

Hot solutions of CA in acetone were combined with mixtures of guests in mole fractions of 0 to 1 and allowed to crystallise by slow cooling and controlled evaporation. Guest ratios in the mother liquour were checked by gas chromatography (GC) to ensure that no significant evaporation of the lower boiling component had occurred. Volumes were chosen such that an excess of the lesser guest with respect to CA concentration was maintained. Crystals of the inclusion compounds so formed were subjected to TG and DSC analysis to determine total mass of enclathrated guest and guest release temperatures. Where these were different from those of either guest alone the mole fraction of each guest in the crystals was determined by GC analysis. Small quantities of the crystals were placed in a glass vial with septum cap and rapidly heated. The mixture of gaseous guests evolved was injected onto a suitable column chosen for adequate separation of the guests under analysis. Alternatively the evolved guests were allowed to condense, dissolved in acetone and injected onto the column. Similar results were obtained by each method.

KINETICS OF INCLUSION:

Both host molecules under study react with guest molecules to form inclusion compounds in phases other than solution. Analyses of the kinetics of reaction of solid host with guest vapours and with solid guests were undertaken. CA was recrystallised either from acetonitrile, acetone or ethyl acetate or mixtures of these and MC from a mixture of acetone and acetonitrile and dried *in vacuo* as before. The dried host material was then crushed (agate mortar and pestle) and sieved with various fractions (notably 212-250 μm and 63-125 μm) retained for reaction.

Solid / Vapour Reactions

The rates of reaction of gaseous guests with solid host to form the inclusion compounds were measured using an apparatus similar to a McBain balance. Instead of measurement of extension of a silica spring as a monitor of weight gain, the reactions were followed using an electronic balance interfaced to a microcomputer. The apparatus is illustrated in Figures 2.1 and 2.3 and described in detail by Barbour *et al*[1]. The sample pan is held suspended in the reaction vessel by means of a permanent magnet coupled to an electromagnet attached to the balance. The sealed reaction vessel containing the sample is

maintained under reduced pressure and the liquid guest introduced. Vapourisation is almost immediate and a pool of liquid guest is maintained in the base of the vessel to ensure constant vapour pressure of guest. A thermocouple and pressure tranducer allow measurement of the temperature and pressure within the reaction chamber.

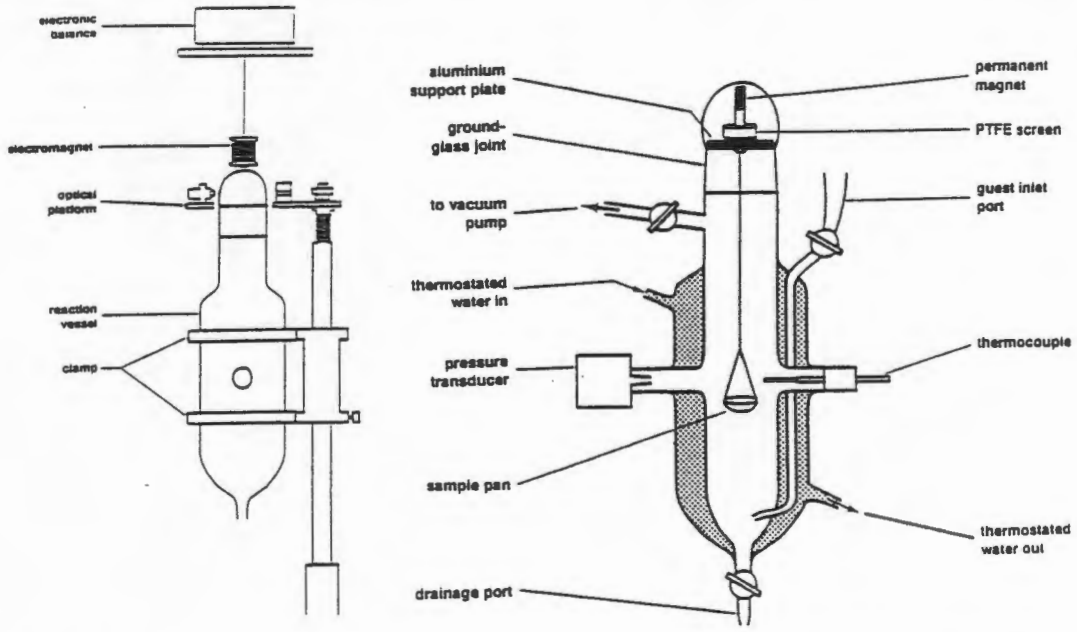

Figure 2. 1: Levitating balance equipment used to monitor weight gain (or loss) in reactions of solid host with guest vapours under isothermal conditions.

Alternatively, where the reaction:

$$H_{(s,\alpha)} + G_{(g)} = HG_{(s,\beta)}$$

proceeded very slowly, the experimental arrangement illustrated in Figure 2.2a was employed. A quantity of dried, sieved host was placed in a glass vial which was in turn fitted inside a larger vial which contained either guest liquid immobilised on an inert substrate, or powdered solid guest and the whole immersed in a thermostated water bath. Samples were periodically removed and the extent of reaction determined from weight loss on TG analysis.

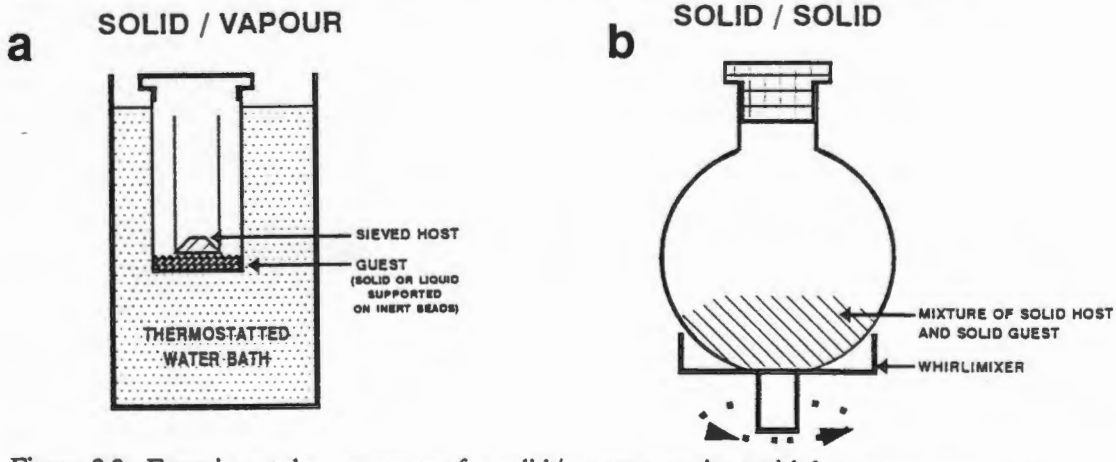

Figure 2.2: Experimental arrangement for solid/vapour reactions with low vapour pressure guests and for solid/solid reactions.

Solid / Solid Reactions

Preliminary tests of solid/solid reactivity were carried out by grinding mixtures of the solid, dried host and guest in an agate mortar and pestle and then allowing the ground mixture to stand, with occasional grinding, for a number of days. The mixtures were then washed in a sintered glass funnel to remove all unreacted guest and the resultant powder tested for weight loss on TG analysis. If the solid state formation of an inclusion compound was noted, then a controlled solid/solid experiment was carried out as follows: Host material prepared as for solid/vapour experiments was placed with a tenfold molar excess of powdered, solid guest in a small round-bottomed flask which was affixed to the top of a 'whirlimixer' to achieve continuous, efficient mixing of the reaction components as illustrated in Figure 2.2b. Samples were removed periodically and washed with copious amounts of diethyl ether to remove all unreacted guest. Neither CA nor the inclusion complexes were soluble in diethyl ether while all guests employed were highly soluble in diethyl ether, affording easy separation. Extent of reaction was subsequently determined by weight loss as measured by TG.

X-RAY POWDER DIFFRACTION (XRD):

Isothermal XRD

Crystals were crushed to a fine powder (under mother liquour in the case of highly labile compounds), but usually not sieved to ensure uniform particle size as the rate of desorption of guest increases rapidly with decreasing particle size. Preferred orientation effects were not, therefore, precluded but good agreement obtained upon comparison of experimental XRD traces with calculated patterns implies that these were not severe. In some cases it proved impossible to obtain accurate XRD traces due to guest desorption during sample preparation and scanning.

Powder diffraction patterns were measured using a Philips PW1050/80 vertical goniometer with PW1394 motor control unit and PW1390 channel control unit mounted on a PW1130/90 X-ray generator operating at 50 kV and 30 mA. Nickel-filtered copper K_α radiation (λ = 1.5418 Å) was passed through ½° receiving slits and a 1° anti-scatter slit. Samples were scanned over the range 6-36° 2θ in steps of 0.1° at a rate of 2° $(2\theta).min^{-1}$.

Ramped Temperature XRD:

XRD patterns of the inclusion compounds at different temperatures were recorded using a modified Weissenberg camera after Boeyens *et al*[2]. Sample and film movement were decoupled to allow continuous recording of the powder pattern of the sample while temperature was raised at a set rate. A diagram of the apparatus is indicated as Figure 2.3.

Crushed samples were mounted in Lindemann capillary tubes with mother liquour. Tubes were not completely sealed to allow escape of guest vapour and prevent pressure buildup. Screens were placed so that the diffracted beam

passed through a narrow slit, (*ca.* 4 mm), before impinging on the film, resulting in a series of lines corresponding to a segment of the diffraction pattern. Phase changes were clearly visible as shown diagrammatically below. Traces of relative intensity vs 2θ were produced by scanning the powder patterns photometrically.

Experimental XRD patterns were compared with calculated patterns produced using the program LAZY PULVERIX[3] modified to produce Gaussian curves instead of lines (described under the section entitled computation).

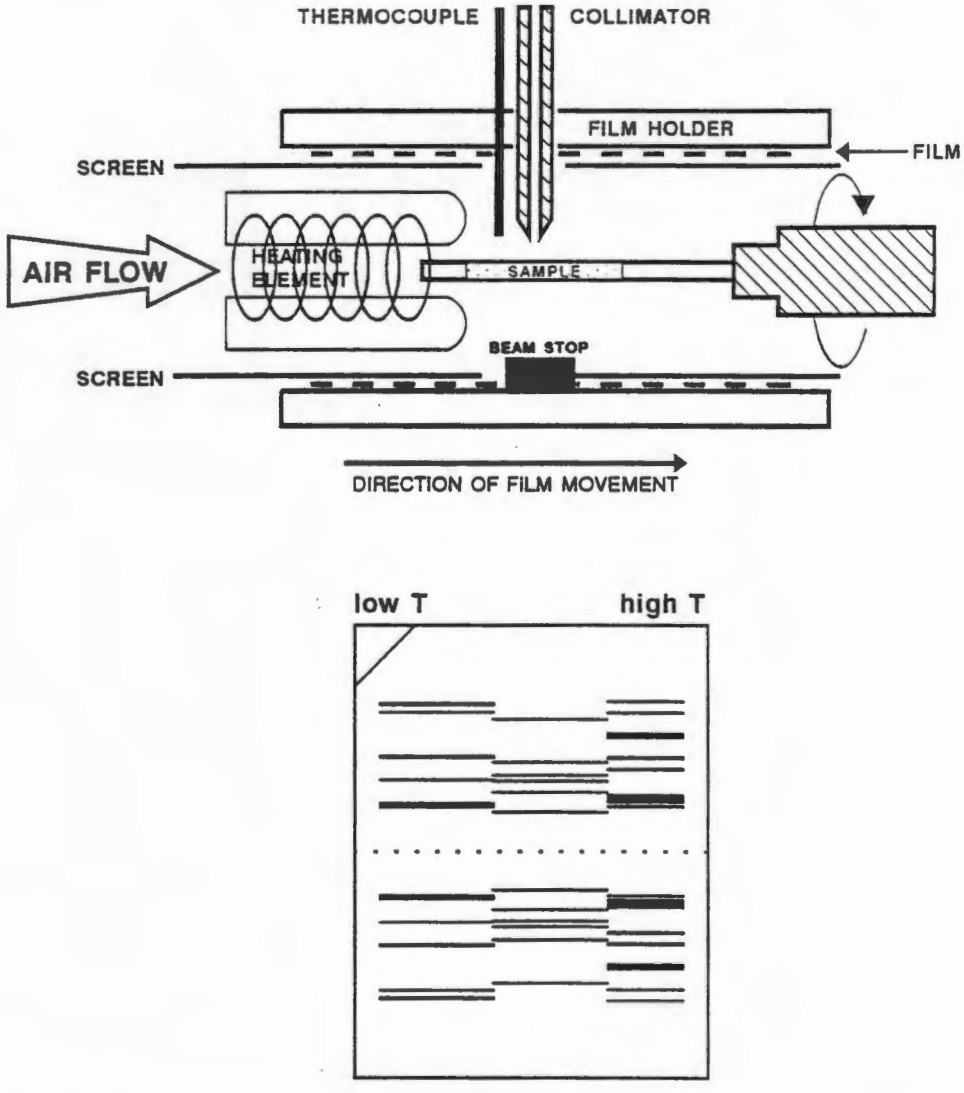

Figure 2.3: Modified Weissenberg camera for recording of powder patterns under heating.

THERMAL ANALYSIS:

TG and DSC analyses were performed using a Perkin Elmer PC7 system. The TG thermocouple and balance were calibrated using built-in procedures for furnace and weight calibration. Two-point standard temperature calibration was performed by measuring the apparent Curie points of Alumel and Nickel and correcting to the known values of 163 °C and 354 °C.

The DSC analyser was calibrated by measuring the apparent melt points of Indium and Zinc and correcting to the known values of 156.4 °C and 419.5 °C. Calibration of heat flow was achieved using the enthalpy of melting for Indium (28.5 Jg^{-1}).

Programmed Thermal Analysis:

Rising temperature TG and DSC analyses were carried out at heating rates of 20 °C.min^{-1} (unless otherwise stated) and using dry nitrogen purge gas at a flow rate of 40 ml.min^{-1}. Samples of mass 1-10 mg were blotted dry on filter paper and lightly crushed before analysis in the range 30-230 °C. DSC curves were normalised to a sample mass of 1.000 mg for comparison and baseline correction applied in each case.

As the geometries and sample environments of the TG and DSC analysers are appreciably different the curves do not always correspond exactly, the DSC peak relating to a weight loss event frequently appearing at a temperature slightly higher than might be predicted by consideration of the first derivative of the weight loss curve. The differing geometries of the instruments are indicated in Figure 2.4.

Samples for TG analysis were placed in an open platinum pan with no barrier to diffusion of the guest vapours away from the sample, while samples for DSC analysis were placed in lidded, vented pans (crimped closed), in turn fitted into the platinum furnace crucible and covered with a holed platinum lid. This leads to retardation of DSC peaks, particularly those associated with an event leading to evolution of gas (such as a guest release event), presumably due to the slower rate of removal of the guest vapour from the vicinity of the sample.

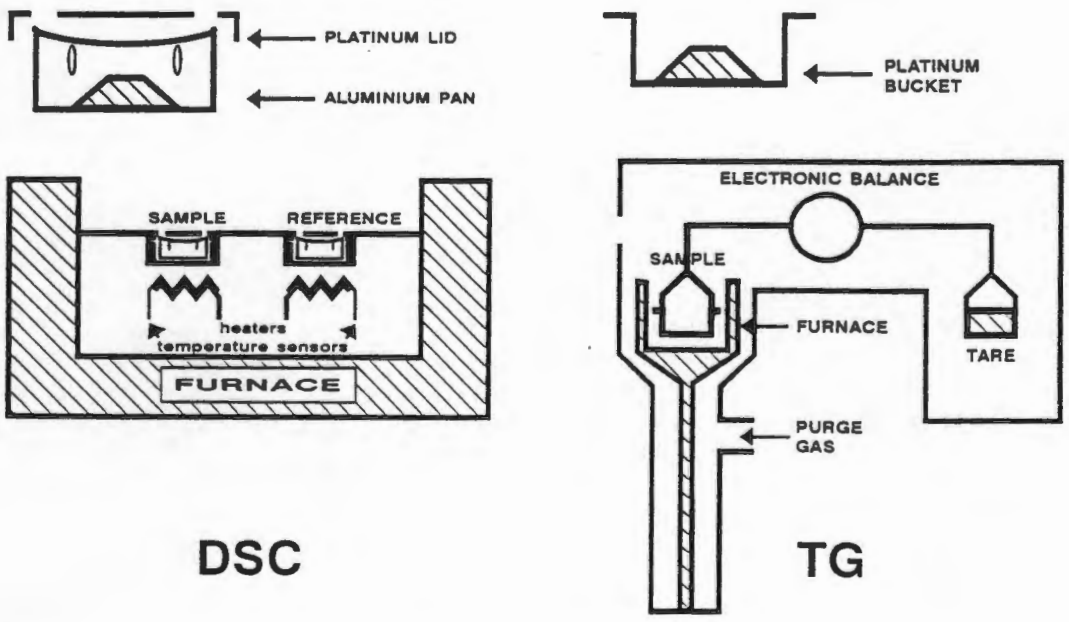

Figure 2.4: Comparison of TG and DSC analyser geometries.

Isothermal Thermogravimetry:

Isothermal decomposition curves for use in analysis of kinetic data were produced under the same conditions of purge gas flow etc. as programmed TG. Sieved samples of similar mass, (within 1 mg) were heated rapidly to a specific temperature and then the temperature was maintained constant until the guest release reaction was complete. These data were used to generate extent of reaction (α) vs time curves for analysis of decomposition kinetics.

CRYSTAL STRUCTURE ANALYSIS:

Single crystals for diffractometry were cut from large crystals which, upon rotation, extinguished plane polarised light uniformly. Fragments of suitable size were cut from larger crystals as the crystals of the inclusion compounds were either flat plates or needles and as such rather smaller in at least one dimension. All crystals were mounted in 0.3 mm or 0.5 mm Lindemann capillary tubes and flame-sealed top and bottom. In cases where desorption of guest was deemed likely, a small quantity of mother liquour was included in the tube; however, even crystals that proved stable to guest desorption over relatively long periods of time were mounted in this way as compounds contained in the commonly used glues attacked the crystals. This sealed capillary tube was then mounted in a brass pin before insertion into either the camera or diffractometer goniometer head as illustrated in Figure 3.6.

Preliminary cell parameters and space group symmetry were measured from oscillation and Weissenberg photographs taken on a Stoë goniometer using Ni-filtered Cu-K_α radiation, (λ = 1.5418 Å).

Accurate cell parameters were obtained by least-squares analysis of the setting angles of 24 reflections collected in the θ range 16 - 17° and centred on the diffractometer. Data were collected on an Enraf-Nonius CAD4 diffractometer at 294 K using graphite-monochromated Mo-K_α radiation, (λ = 0.7107 Å) and the ω-2θ scan mode with a final acceptance limit of 20 σ at 20 °min^{-1} and a maximum recording time of 40 s. The vertical aperture length was fixed at 4 mm, the aperture width at (1.12 + 1.05 tan θ) mm and the scan width at (x + 0.35 tan θ, x = 0.80 or 0.85)° in ω. During each data collection three reference reflections were monitored periodically to check crystal stability. Data were corrected for Lorentz-polarisation effects. Crystal data and other experimental parameters are given in table 2.1 Absorption corrections were not applied as values of μR_{min} and μR_{max} (where R_{max} and R_{min} are one-half the largest and smallest crystal dimensions respectively) were between 0 and 0.1 for all crystal fragments used and thus values of A^* indicated are 1.00[4].

COMPUTATION:

Computation of calculated powder XRD patterns was achieved using a modified version of the program LAZYPULVERIX[3] performed on a personal computer running the DOS operating system. Input includes details of cell parameters, space group symmetry and atomic co-ordinates, and Debye-Waller factors. Output is in the form of bar graphs of relative intensity versus degrees 2θ. The "lines" are then transformed to Gaussian curves and joined to provide a trace for comparison with experimental data.

Structure solution and refinement computations were performed on a remote VAX mainframe computer running the VMS 5.4 operating system or on a MicroVAX 3100-900 running the VMS 5.5 operating system.

All structures were solved by direct methods using the program SHELX-86[5] and refined by full-matrix or blocked-matrix least-squares refinement using the

programs SHELX-76[6] and SHELXL-93[7]. In SHELX-76 complex neutral atom scattering factors for non-hydrogen atoms after Cromer and Mann[8] and for hydrogen atoms after Stewart *et al*[9] were employed while in SHELXL-93 neutral atom scattering factors as contained in the International Tables for X-Ray Crystallography, Vol. C, 1992[10] were employed.

Structures refined using the program SHELX-76 were refined against F minimising $\Sigma w(|F_o|-|kF_c|)^2$ for those reflections with $F > 4\sigma(F)$ (or $F > 3\sigma(F)$ where deemed appropriate) while those refined using SHELXL-93 were refined against F^2 using all data.

Agreement between observed (F_o) and calculated structure factors is expressed by the residual index, R, defined as:

$$R = \frac{\Sigma \, ||F_o| - |F_c||}{\Sigma \, |F_o|}$$

Since refinement against F^2 leads to R indices larger than those based on F the "conventional" R factor, (R_1), is always presented for comparison. R_2, the residual factor resulting from refinement on F^2 is presented for structures refined in this fashion and is defined as:

$$R_2 = \left(\frac{\Sigma \, (F_o^2 - F_c^2)^2}{\Sigma \, (F_o^2)^2} \right)^{1/2}$$

Agreement may also be expressed in terms of the weighted residual factors, R_w or wR_2:

SHELX-76:

$$R_w = \frac{\Sigma \, w^{1/2} \, |\Delta F|}{\Sigma \, w^{1/2} \, |F_o|} \qquad \text{where } w = \frac{1}{\sigma^2(F_o) + gF_o^2}$$

Values of g were chosen to ensure constant distributions of $<w(|F_o| - |F_c|)^2>$ with respect to $\sin\theta$ and $(F_o/F_{max})^{1/2}$.

SHELXL-93:

$$wR_2 = \left(\frac{\Sigma \, [w(F_o^2 - F_c^2)^2]}{\Sigma \, [w(F_o^2)^2]} \right)^{1/2}$$

where

$$w = 1/[\sigma^2(F_o^2) + (aP)^2 + bP]$$

$$P = [\text{Max}(0, F_o^2) + 2F_c^2]/3$$

Values of a and b were chosen to minimise trends in the analysis of variance in terms of F_c^2.

Refining against F^2 leads to greater deviations of the "Goodness of Fit", (S), from unity than refinement against F. These values are thus also not directly comparable for structures refined against F^2 and F. S is defined as:

SHELX-76:

$$S = \left(\frac{\Sigma \, w \, (|F_o| - |F_c|)^2}{(N - n_p)} \right)^{1/2}$$

SHELXL-93:

$$S = \left(\frac{\Sigma \, w \, (|F_o^2| - |F_c^2|)^2}{(N - n_p)} \right)^{1/2}$$

Where N is the number of reflections and n_p the number of parameters.

Geometrical molecular structure parameters were calculated using the program

PARST[11] in the case of structures refined using SHELX-76. Channel shapes and void volumes were investigated using the programs OPEC[12] and MOLMAP[13]. In both cases a packing analysis routine is applied in which all host atoms are assigned spherical radii equal to their van der Waals radii. Guest atoms are removed in the calculation and the channel is thus represented as unoccupied volume in packing density maps.

The Cambridge Structural Database (CSD)[14] was used to retrieve and analyse published crystal data while molecular and packing diagrams were produced using either the IBM PC version of PLUTO[15] or ORTEP[16].

STRUCTURE SOLUTION AND REFINEMENT:

Most structures were solved by direct methods using the program SHELX-86 which is based on a random start multisolution philosophy[4]. Equivalent reflections, (including Friedel opposites) were merged and those with $F_o < 4\sigma(F_o)$ are flagged as "unobserved" and suppressed. A figure of merit, R_{int}, for the refection data set was calculated:

$$R_{int} = \frac{\Sigma|F_o^2-(F_o^2)_{mean}|}{\Sigma F_o^2} \qquad R_{sigma} = \frac{\Sigma\sigma(F_o)^2}{\Sigma F_o^2}$$

Mean $|E^2-1|$ values (where E is the normalised structure factor), for the zonal reflections i.e. *0kl*, *h0l*, *hk0* and the remainder are checked for consistency with space group symmetry. CA and MC are chiral natural products which occur as one enantiomer; thus, neither the question of space group centrosymmetry nor that of absolute configuration arises.

Many structures solved simply by tangent refinement (with no fixed phases), of a subset of reflections with high estimated α values and with priority given to those reflections that take part in the largest number of negative quartets. The best 10% of subset phase permutations were subjected to multisolution tangent refinement and two figures of merit calculated for all refined permutations:

$$R_\alpha = \frac{\Sigma w(\alpha-\alpha_{est})^2}{\Sigma w(\alpha_{est})^2} \qquad w = \frac{1}{(\alpha_{est}+5)}$$

and

$$NQUAL = \frac{\Sigma[\Sigma(E_1E_2)\Sigma(E_3E_4E_5)]}{\Sigma[|(E_1E_2)||(E_3E_4E_5)|]}$$

where the outer summations are performed over all refined reflections and the inner summations over triplets and negative quartet relations involving a given reflection.

Some structures proved impervious to this treatment and were solved using the subset of reflections with highest estimated α values or with the subset of reflections chosen such that all three indices were even and had the highest α values. This last strategy proved particularly useful in solving some of the structures belonging to the space group *P*1.

The "correct" solution as judged by the value of the combined figure of merit, CFOM:

$$CFOM = R_{\alpha} + [0 \text{ or } (NQUAL\text{-}wn)]^2$$

where wn is a structure dependent constant which should be about 0.1 more negative than the anticipated value of NQUAL. CFOM should be a minimum for the "best" solution which is retained for calculation and synthesis of an E-map after extension by further tangent expansion. One cycle of E-Fourier recycling is carried out before evaluation of the point-atom R-factor based on E-values, R_E, is evaluated. If $R_E < 0.3$ the solution was judged "correct" provided that it was also chemically reasonable. By variation of input parameters all structures but one were solved in this way. Most host atoms were located in E-maps and coordinates input into SHELX-76 or SHELXL-93 for refinement. Atoms of the steroid side chain and of guest molecules (particularly more volatile guest molecules), were located in difference electron density maps after a few full-matrix least-squares refinement cycles.

As all the structures solved occurred in polar space groups, devices for defining the origins were applied: appropriate coordinates of one atom of the steroid nucleus were fixed for refinement in SHELX-76 and polar origin restraints after Flack and Schwarzenbach[17] applied for refinement in SHELXL-93.

Details of restraints, constraints and other factors peculiar to individual structure solutions or refinement are discussed in chapter 3. Final atomic coordinates, temperature factors, tables of bond lengths, angles and torsion angles are contained in appendix A and tables of observed and calculated structure factors in appendix B.

Experimental and refinement details are provided in table 2.1.

Table 2.1: Crystal data, experimental and refinement parameters. Structures refined on F^2 using SHELXL.

		CAMA	CAET	CAEP	CAPAC	CAIP
Crystal data						
Guest		Methyl Acetate	Ethyl Acetate	Ethyl Propionate	*n*-Propyl Acetate	*i*-Propyl Acetate
Molecular formula		$C_{24}H_{40}O_5$ $\bullet C_3H_6O_2$	$C_{24}H_{40}O_5$ $\bullet C_4H_8O_2$	$C_{24}H_{40}O_5$ $\bullet C_5H_{10}O_2$	$C_{24}H_{40}O_5$ $\bullet C_5H_{10}O_2$	$C_{24}H_{40}O_5$ $\bullet C_5H_{12}O_2$
Molecular weight ($gmol^{-1}$)		482.658	496.685	510.712	510.712	510.712
Space group		$P1$	$P2_1$	$P2_1$	$P2_1$	$P2_1$
a(Å)		12.223(2)	13.668(3)	13.571(1)	16.802(5)	16.604(3)
b(Å)		8.189(1)	7.824(4)	7.969(1)	7.882(1)	7.979(3)
c(Å)		14.204(2)	14.095(2)	14.237(1)	12.107(4)	12.141(2)
$\alpha(^\cdot)$		90.18(1)	90.0	90.0	90.0	90.0
$\beta(^\cdot)$		105.72(2)	113.53(1)	113.53(1)	118.06(3)	117.76(2)
$\gamma(^\cdot)$		94.03(1)	90.0	90.0	90.0	90.0
V(Å^3)		1364.8(6)	1385.2(8)	1411.7(3)	1415(7)	1423.4(7)
Z		2	2	2	2	2
$D_c(gcm^{-3})$		1.174	1.194	1.201	1.199	1.192
μ(MoKα) (cm^{-1})		0.48	0.48	0.48	0.48	0.48
F(000)		528	544	560	560	560
Data collection						
Crystal dimensions (mm)		0.3 x 0.4 x 0.4	0.2 x 0.3 x 0.5	0.3 x 0.3 x 0.4	0.5 x 0.5 x 0.5	0.4 x 0.3 x 0.3
Range	h	-14 13	-16 14	-16 14	-14 14	-14 14
	k	-9 9	0 9	0 9	0 9	0 9
	l	0 16	0 16	0 16	0 19	0 18
Total exposure time (h)		38.5	21.3	21.5	23.0	22.1
Intensity Variation (%)		-8	-3.6	-6.4	-3.4	-6.9
Number of reflections collected		4997	4885	2736	2699	2792
Final refinement						
No. of reflections(independent)		4879	2625	2705	2688	2705
No. of restraints		11	9	2	3	6
No. of parameters		584	284	283	340	340
Goodness of fit on F^2		1.050	1.036	1.034	1.027	1.029
R indices:						
$I>2\sigma(I)$	R_1	0.0668	0.0732	0.0680	0.0700	0.0656
	wR_2	0.1807	0.2042	0.1709	0.1880	0.1699
All data	R_1	0.1265	0.1198	0.1175	0.1605	0.1306
	wR_2	0.2195	0.2473	0.2044	0.2430	0.2061
Weights:	a	0.1330	0.1387	0.0906	0.1477	0.1016
	b	0.5735	1.1575	1.6257	0.3721	1.2909
$\Delta\rho$max (eA^{-3})		0.48	0.58	0.61	0.44	0.43
$\Delta\rho$min (eA^{-3})		-0.32	-0.39	-0.40	-0.35	-0.42

Table 2.1: Crystal data, experimental and refinement parameters. Structures refined on F^2 using SHELXL.

		CAMEK	CAPTOL	CAPNOT	MC(alpha)
Crystal data					
Guest		Methyl Ethyl Ketone	*p*-Toluidine	*p*-Nitrotoluene	none
Molecular formula		$C_{24}H_{40}O_5$ •C_4H_8O	$C_{24}H_{40}O_5$ •C_7H_9N	$C_{24}H_{40}O_5$ •$C_7H_7NO_2$	$C_{25}H_{42}O_5$
Molecular weight ($gmol^{-1}$)		480.686	515.735	545.717	422.606
Space group		$P2_1$	$P2_1$	$P2_1$	$P2_12_12$
a(Å)		12.597(3)	13.577(4)	13.495(1)	42.387(2)
b(Å)		8.191(5)	8.078(2)	8.266(4)	14.563(3)
c(Å)		27.954(4)	14.182(6)	14.398(2)	7.660(1)
α(˚)		90.0	90.0	90.0	90.0
β(˚)		105.40(1)	114.42(3)	114.61(1)	90.0
γ(˚)		90.0	90.0	90.0	90.0
V($Å^3$)		2780.8(9)	1416.3(8)	1451.1(7)	4728.4(1)
Z		4	2	2	8
D_c(gcm^{-3})		1.148	1.209	1.249	1.187
μ(MoKα) (cm^{-1})		0.48	0.45	0.51	0.46
F(000)		1056	564	592	928
Data collection					
Crystal dimensions (mm)		0.35 x 0.45 x 0.40	0.3 x 0.35 x 0.3	0.2 x 0.2 x 0.25	0.1 x 0.2 x 0.25
Range	h	0 15	16 14	0 16	0 50
	k	0 9	0 9	0 9	-17 0
	l	-32 32	0 16	-16 15	0 9
Total exposure time (h)		40.0	22.9	22.4	34.4
Intensity Variation (%)		-4	0.6	1.7	-3.9
Number of reflections collected		5510	2794	2860	4715
Final refinement					
No. of reflections(independent)		5249	2680	2738	4714
No. of restraints		6	1	6	8
No. of parameters		557	306	364	541
Goodness of fit on F^2		0.987	1.036	1.033	1.018
R indices:					
$I>2\sigma(I)$	R_1	0.0895	0.0612	0.0608	0.0667
	wR_2	0.2426	0.1667	0.1489	0.1629
All data	R_1	0.2062	0.1338	0.1714	0.2394
	wR_2	0.3829	0.2054	0.1882	0.2343
Weights:	a	0.2015	0.1263	0.0955	0.1085
	b	0.5591	0.1860	0.1906	1.2858
Extinction coefficient		-	-	-	-
$\Delta\rho$max (eA^{-3})		-0.34	0.25	0.36	0.45
$\Delta\rho$min (eA^{-3})		-0.34	-0.25	-0.36	-0.33

Table 2.1: Crystal data, experimental and refinement parameters. Structures refined on F using SHELX-76.

	CAMI	CAVA	CAMM	CACN	MCCN
Crystal data					
Guest	Methyl Acetate•*i*-Propyl Acetate	Vinyl Acetate	Methyl Methacrylate	acetonitrile	acetonitrile
Molecular formula	$2C_{24}H_{40}O_5$ $\bullet C_3H_6O_2\bullet.\backslash C_5H_{10}O_2$	$C_{24}H_{40}O_5$ $\bullet C_4H_6O_2$	$C_{24}H_{40}O_5$ $\bullet C_5H_8O_2$	$C_{24}H_{40}O_5$ $\bullet C_2H_3N$	$C_{25}H_{42}O_5$ $\bullet C_2H_3N$
Molecular weight ($gmol^{-1}$)	993.370	494.669	508.696	449.632	463.656
Space group	*P*1	*P*1	$P2_1$	$P2_1$	$P2_1$
a(Å)	12.289(2)	12.284(2)	12.960(2)	9.645(2)	9.891(3)
b(Å)	8.238(4)	8.237(2)	8.060(2)	8.401(1)	8.390(2)
c(Å)	14.246(3)	14.286(4)	14.642(3)	15.747(4)	16.024(4)
α(˚)	90.39(3)	89.57(1)	90.0	90.0	90.0
β(˚)	105.83(1)	105.91(2)	114.00(1)	101.01(2)	99.10(2)
γ(˚)	94.97(2)	85.70(1)	90.0	90.0	90.0
V($Å^3$)	1381.6(8)	1385.6(6)	1397.2(5)	1252.5(5)	1313.0(6)
Z	1	2	2	2	2
$D_c(gcm^{-3})$	1.194	1.186	1.209	1.192	1.173
μ(MoKα) (cm^{-1})	0.48	0.48	0.48	0.46	0.45
F(000)	544	540	556	492	508
Data collection					
Crystal dimensions (mm)	0.3 x 0.35 x .25	0.4 x 0.4 x 0.5	0.3 x 0.3 x 0.35	0.4 x 0.4 x 0.35	0.5 x 0.5 x 0.4
Range *h, k, l*	±9, ±14, 17	±9, ±14, 17	±15, 9, 17	±11, 10, 18	±11, 9, 19
Total exposure time (h)	40	38.5	21.8	18.6	19.8
Intensity Variation (%)	-17.8	-9	-0.6	0.4	-1.8
No. of reflections collected	5076	5067	2753	2449	2561
No. of Reflections $I_{rel} > 2\sigma I_{rel}$	3226	3786	2324	1804	1894
Final refinement					
No. of reflections(independent)	3224	3784	1930	1774	1894
No. of parameters	325	274	367	320	310
R indices:					
R	0.0674	0.0649	0.0381	0.0409	0.0489
wR	0.0729	0.0709	0.0367	0.0395	0.0520
g	0.0075	0.001591	0.000120	0.0001	0
S	0.749	2.123	1.593	1.75	3.27
$\Delta\rho$max (eA^{-3})	0.31	0.40	0.15	0.22	0.43
$\Delta\rho$min (eA^{-3})	-0.31	-0.26	-0.16	-0.36	-0.31

Table 2.1: Crystal data, experimental and refinement parameters. Structures refined on F using SHELX-76.

	CAACD	CADEK	CAPR	CABN	CAAN
Crystal data					
Guest	Acetone	Diethyl Ketone	Propiophenone	Benzonitrile	Aniline
Molecular formula	$2C_{24}H_{40}O_5$ $\bullet 3C_3H_6O$	$C_{24}H_{40}O_5$ $\bullet C_5H_{10}O$	$C_{24}H_{40}O_5$ $\bullet C_9H_{10}O$	$C_{24}H_{40}O_5$ $\bullet C_7H_5N$	$C_{24}H_{40}O_5$ $\bullet C_6H_7N$
Molecular weight ($gmol^{-1}$)	991.398	494.713	542.757	511.703	501.708
Space group	$P1$	$P2_1$	$P2_1$	$P2_1$	$P2_1$
a(Å)	12.655(3)	12.787(2)	16.790(1)	13.642(3)	13.742(2)
b(Å)	8.354(3)	8.117(1)	7.928(5)	8.133(2)	8.049(1)
c(Å)	14.125(3)	13.960(2)	12.262(3)	14.055(3)	14.095(2)
$\alpha(^\circ)$	91.93(3)	90.0	90.0	90.0	90.0
$\beta(^\circ)$	106.02(2)	103.82(1)	114.25(2)	114.12(2)	115.20(2)
$\gamma(^\circ)$	94.68(3)	90.0	90.0	90.0	90.0
V(Å^3)	1428.1(7)	1407.1(4)	1488.2(10)	1423.3(6)	1410.7(4)
Z	2	1	2	2	2
$D_c(gcm^{-3})$	1.153	1.168	1.211	1.194	1.181
μ(MoKα) (cm^{-1})	0.46	0.45	0.46	0.45	0.44
F(000)	544	544	592	556	548
Data collection					
Crystal dimensions (mm)	0.45 x 0.45 x 0.45	0.45 x 0.45 x 0.35	0.3 x 0.3 x 0.25	0.35 x 0.3 x 0.35	0.4 x 0.5 x 0.5
Range h, k, l	±9, ±15, 16	±13, 20, 17	±14, 9, 19	±16, 9, 16	±16, 9, 16
Total exposure time (h)	38.2	42.1	22.9	23.3	20.5
Intensity Variation (%)	-17.9	-2.1	-0.7	-9.7	-1.8
No. of reflections collected	5368	5168	2942	2821	2784
No. of reflections $I_{rel} > 2\sigma I_{rel}$	3144	3631	2172	1932	2097
Final refinement					
No. of reflections (independent)	3026	3470	2145	1853	2010
No. of parameters	307	320	338	306	302
R indices:					
R	0.0575	0.0747	0.0515	0.0781	0.0642
wR	0.0856	0.0798	0.0575	0.0876	0.0752
g	0.010	0.000558	0.0013	0.0075	0.003174
S	4.20	5.22	1.59	1.38	1.53
$\Delta\rho$max (eA^{-3})	0.49	0.34	0.32	0.31	0.41
$\Delta\rho$min (eA^{-3})	-0.24	-0.44	-0.27	-0.16	-0.24

Table 2.1: Crystal data, experimental and refinement parameters. Structures refined on F using SHELX-76.

	CANI	CAMN	CADC	CAAC
Crystal data				
Guest	Nitrobenzene	*m*-Nitro-toluene	Acetone•1,2-Dichlorobenzene	Acetone•3water
Molecular formula	$C_{24}H_{40}O_5$ •$C_6H_5NO_2$	$C_{24}H_{40}O_5$ •$C_7H_7NO_2$	$2C_{24}H_{40}O_5$ •C_3H_6O•$C_6H_4Cl_2$	$C_{24}H_{40}O_5$ •C_3H_6O•$3H_2O$
Molecular weight ($gmol^{-1}$)	531.69	545.717	1022.24	520.702
Space group	$P2_1$	$P2_1$	$P1$	$P2_1$
a(Å)	13.579(2)	12.442(3)	12.474(3)	13.111(3)
b(Å)	8.106(3)	8.066(1)	8.252(2)	7.759(2)
c(Å)	14.048(1)	14.519(2)	14.214(8)	14.893(3)
$\alpha(^{\cdot})$	90.0	90.0	91.09(3)	90.0
$\beta(^{\cdot})$	113.52(1)	102.63(1)	106.31(3)	105.70(2)
$\gamma(^{\cdot})$	90.0	90.0	94.43(2)	90.0
$V(Å^3)$	1417.8(6)	1421.8(4)	1398.8(10)	1458.5(6)
Z	2	2	1	2
$D_c(gcm^{-3})$	1.245	1.275	1.119	1.186
μ(MoKα) (cm^{-1})	0.51	0.52	1.34	0.51
F(000)	576	592	514	572
Data collection				
Crystal dimensions (mm)	0.25 x 0.25 x 0.5	0.3 x 0.3 x 0.35	0.5 x 0.5 x 0.5	0.45 x 0.45 x 0.35
Range h, k, l	±16, 9, 16	±14, 9, 17	±14, ±9, 16	±15, 9, 17
Total exposure time (h)	20.3	20.4	42.7	20.2
Intensity Variation (%)	1	-1.2	6	-1.8
No. of reflections collected	2876	2810	5117	2885
No. of reflections $I_{rel} > 2\sigma I_{rel}$	2054	2324	3023	2327
Final Refinement				
No. of reflections (independent)	2034	2183	3021	2263
No. of parameters	311	383	310	374
R indices:				
R	0.0651	0.0389	0.0940	0.0480
wR	0.0756	0.0359	0.0981	0.0576
g	0.001056	0	0.007	0.004139
S	3.13	2.34	1.00	1.05
$\Delta\rho$max (eA^{-3})	0.56	0.25	0.38	0.41
$\Delta\rho$min (eA^{-3})	-0.39	-0.30	-0.31	-0.24

1 L.J. Barbour, K. Achleitner and J.R. Greene, *Thermochimica Acta*, 1992, **205**, p 171.

2 Jan C.A. Boeyens, Ernst Ferg, Demetrius C. Levendis and F.R. Ludwig Schöning , *S. Afr. J. Chem.*, 1991, **44**, p 42.

3 K. Yvon, W. Jeitschko and E. Parthé, *J. Appl. Cryst.*, 1977, **10**, p 73.

4 International Tables for Crystallography, Vol. C, ed. A.J.C. Wilson, Kluwer Academic Publishers, Dordrecht, Boston, London, 1992, p 523.

5 G.M. Sheldrick, SHELX-86, *Crystallographic Computing 3*, eds. G.M. Sheldrick, C. Kruger and R. Goddard, Oxford University Press, 1985.

6 G. M. Sheldrick, *Computing in Crystallography*, eds. H. Schenk, Olthof-Hazenkamp, J. von Konigsveld and G.C. Bassi, Delft University Press, 34, 1978.

7 G.M. Sheldrick, SHELXL-93: A Program for Crystal Structure Determination, *J. Appl. Crystallogr.*, in preparation, 1993.

8 D.T. Cromer and J.B. Mann, *Acta Crystallogr.*, 1986, **A24**, p 321.

9 R.F. Stewart, E.R. Davidson and W. T. Simpson, *J. Chem. Phys.*, 1965, **42**, p 3175.

10 *International Tables for Crystallography, Volume C,* ed. A.J.C. Wilson, Kluwer Academic Publishers, Dordrecht, 1992.

11 M. Nardelli, *Comput. Chem.*, 1983, **7**, p 95.

12 A. Gavezzotti, *J. Am. Chem. Soc.*, 1983, **105**, p 5220.

13 L. J. Barbour, PhD Thesis - University of Cape Town, 1994.

14 Cambridge Structural Database and Cambridge Structural Database System, Version 4.4 (January 1991) to Version 5.07 (April 1994), Cambridge Crystallographic Data Centre, University Chemical Laboratory, Cambridge, England

15 W.D.S. Motherwell in "PLUTO and PLUTOX - programs for plotting molecular and crystal structures.", Cambridge University, England, unpublished,
Modified by E.J. Dodson and G.D. Smith, further modified by M. Webster and E.J. Gabe, NRC, Canada, 1985.

16 C.K. Johnson, ORTEP: A Fortran Thermal Ellipsoid Program for Crystal Structure Illustrations.

17 H.D. Flack and D. Schwarzenbach, *Acta Crystallogr. Sect. A*, 1988, **44**, p 499.

CHAPTER 3: CRYSTAL STRUCTURE ANALYSIS.

Structure solution and refinement are described in the experimental section (chapter 2) and may be summarised:

i) Structure solution by direct methods using the program SHELX-86[1] - in most cases the non-hydrogen atoms of the host steroid nucleus were located and in the structures with non-volatile guest molecules the steroid side chain *and* guest non-hydrogen atoms were frequently also found.

ii) Refinement by full- or blocked-matrix least-squares refinement using the programs SHELX-76[2] or SHELXL-93[3] with location of any missing non-hydrogen atoms from difference electron density maps. Origin fixing in the space groups $P2_1$ and $P1$ was achieved by appropriate fixing of atomic co-ordinates where structures were refined using SHELX-76 and by the use of polar axis restraints after Flack and Schwarzenbach[4] in structures refined using SHELXL-93.

iii) Host non-hydrogen atoms were refined anisotropically except where this led to unreasonably high temperature factors and in some cases it proved possible to extend this to guest atoms as well; however, in many cases guest non-hydrogen atoms required bond length restraints to ensure sensible molecular geometry and these will be detailed individually.

iv) Most host hydrogen atoms were placed in calculated positions with positional parameters riding on the host atoms and tied to a common temperature factor for each type: methyl, methylene and methine. The resultant refined U values are explicitly quoted for each structure. All were within the range deemed acceptable for refinement using data collected at 294 K. Guest hydrogen atoms were included in calculated positions only if the guest non-hydrogen atoms exhibited no disorder and reasonable temperature factors. In some structures hydroxyl hydrogen atoms were found from difference electron density maps and were refined with bond length constraints; O-H bond lengths dependent on O•••O distances after Olovson and Jönson[5] were assigned. In some cases attempts to refine hydroxyl hydrogen atoms in this manner led to unreasonable values for the isotropic displacement parameters and in such cases these atoms were omitted from the final models.

v) Weighting schemes were chosen as detailed in chapter 2 and tables of atomic co-ordinates, bond lengths and angles are contained in appendix A while structure factors are presented in appendix B.

vi) In all cases cell choices were made and data transformed (if necessary) such that all structures are directly comparable.

CHOLIC ACID INCLUSION COMPOUNDS.

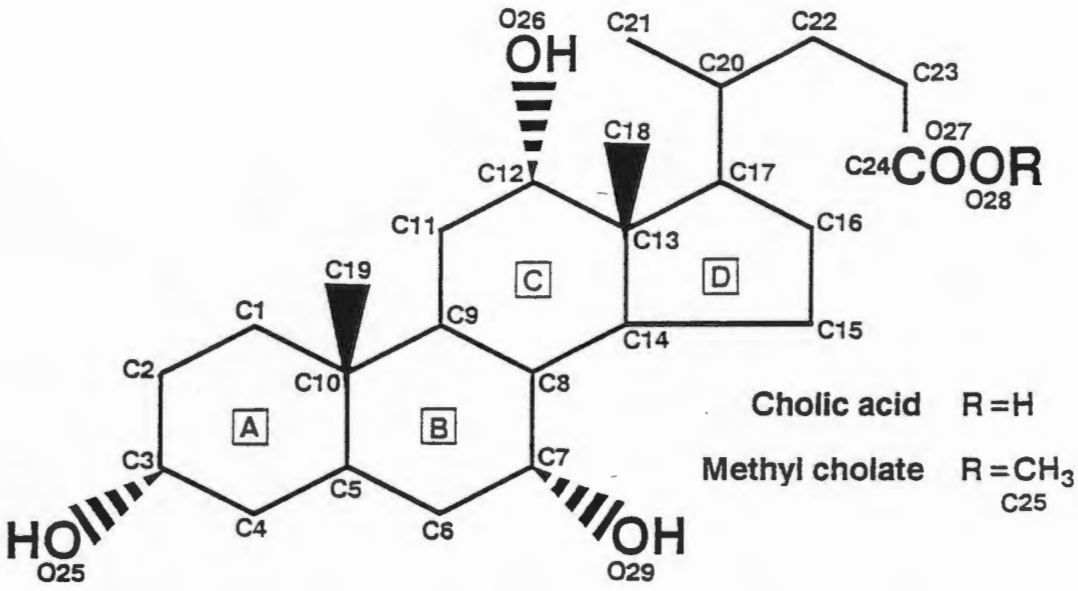

Figure 3.1: Molecular numbering of Cholic Acid and Methyl Cholate.

Most of the inclusion compounds of cholic acid crystallise to form structures which are very similar, as might be inferred from the similarity in cell parameters. Cholic acid is a steroid occurring in only one enantiomeric form in nature and the space groups represented by crystalline cholic acid inclusion compounds are thus always chiral; all of the inclusion compounds studied crystallise in one of two polar space groups: $P2_1$ or $P1$.

Molecules of cholic acid (and methyl cholate) are curved due to the *cis* A-B ring junction. The hydroxyl groups attached to the steroid nucleus protrude from the α-face so that the molecule exhibits a concave hydrophilic face and a convex hydrophobic face as is illustrated in Figure 3.2a. These molecules associate via host-host hydrogen bonding resulting in the formation of lipid bilayers which are puckered due to the curved shape of the molecules, (see Figure 3.2b). The hydrophilic α-face of the steroid is thus buried in the centre of the bilayer while the hydrophobic β face, out of which the C(18) and C(19) atoms protrude, remains exposed. These bilayers pack together to form crystals such that channels, in which guests are accommodated, remain between them as shown in Figure 3.2c. These channels are bounded by the host A-ring and side chain.

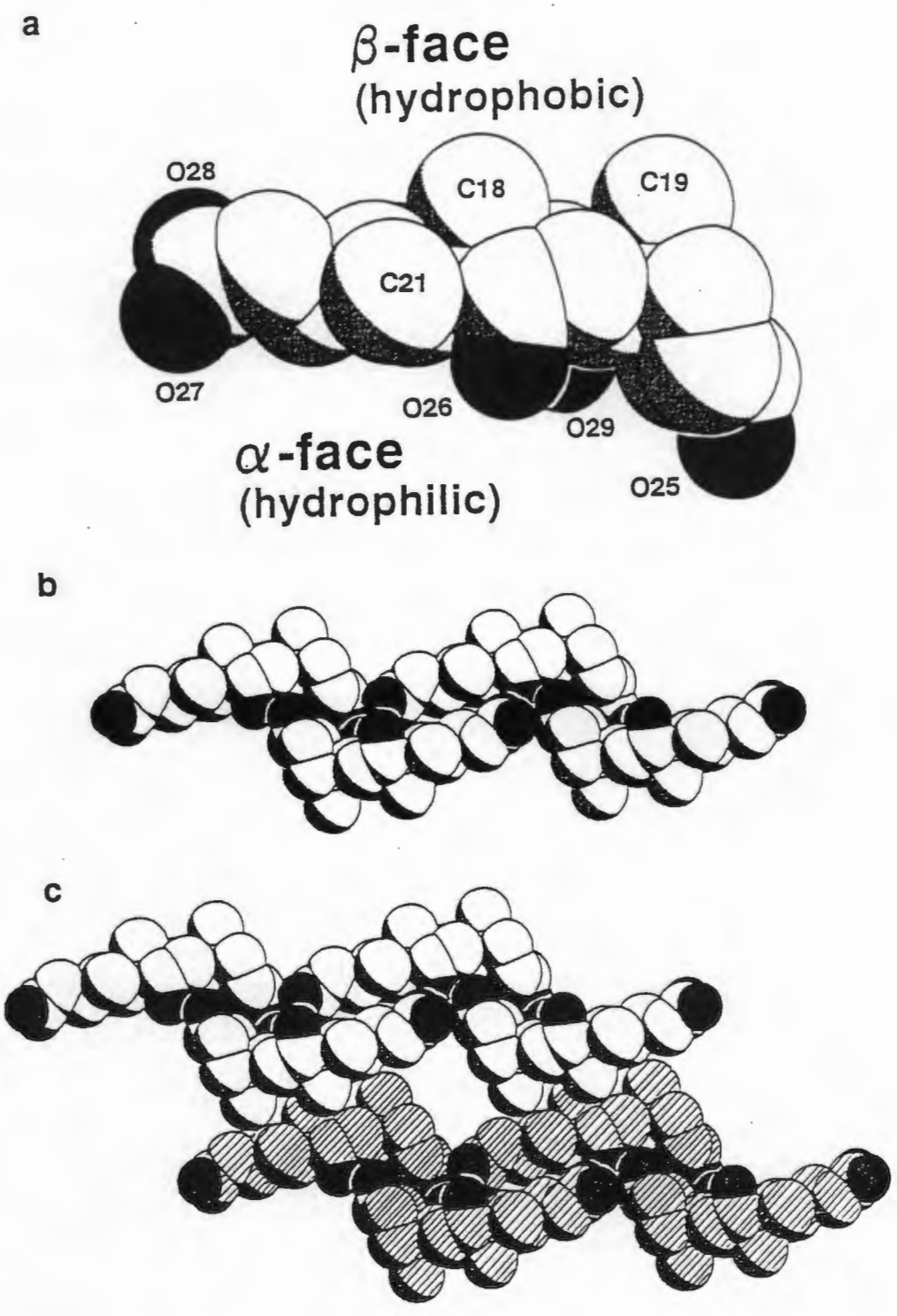

Figure 3.2: a) Space-filling diagram of cholic acid viewed side-on to the steroid nucleus showing the concave hydrophilic and convex hydrophobic sides. (Oxygen atoms are shaded) b) Association of CA host molecules into puckered bilayers bound together by hydrogen bonding. c) Association of bilayers as in the tubulate clathrate inclusion compounds of CA. Note channels resulting from the puckered nature of the bilayers.

There are usually no short range host-guest interactions and the general packing motif may be represented as in Figure 3.3. In all cases cell choices are such that the *b* direction is the direction of bilayer propagation. Thus in the structures crystallising in the space group $P2_1$ the guests are arrayed in channels perpendicular to (101) along a 2_1-axis so that columns of guest molecules spiral through the structure. Structures crystallising in the space group *P*1 result when the angle of the bilayer sheets is not perpendicular to (101) and the 2_1 diad is lost. The channel no longer represents a smooth spiral and guest molecules adopt different positions relative to each other.

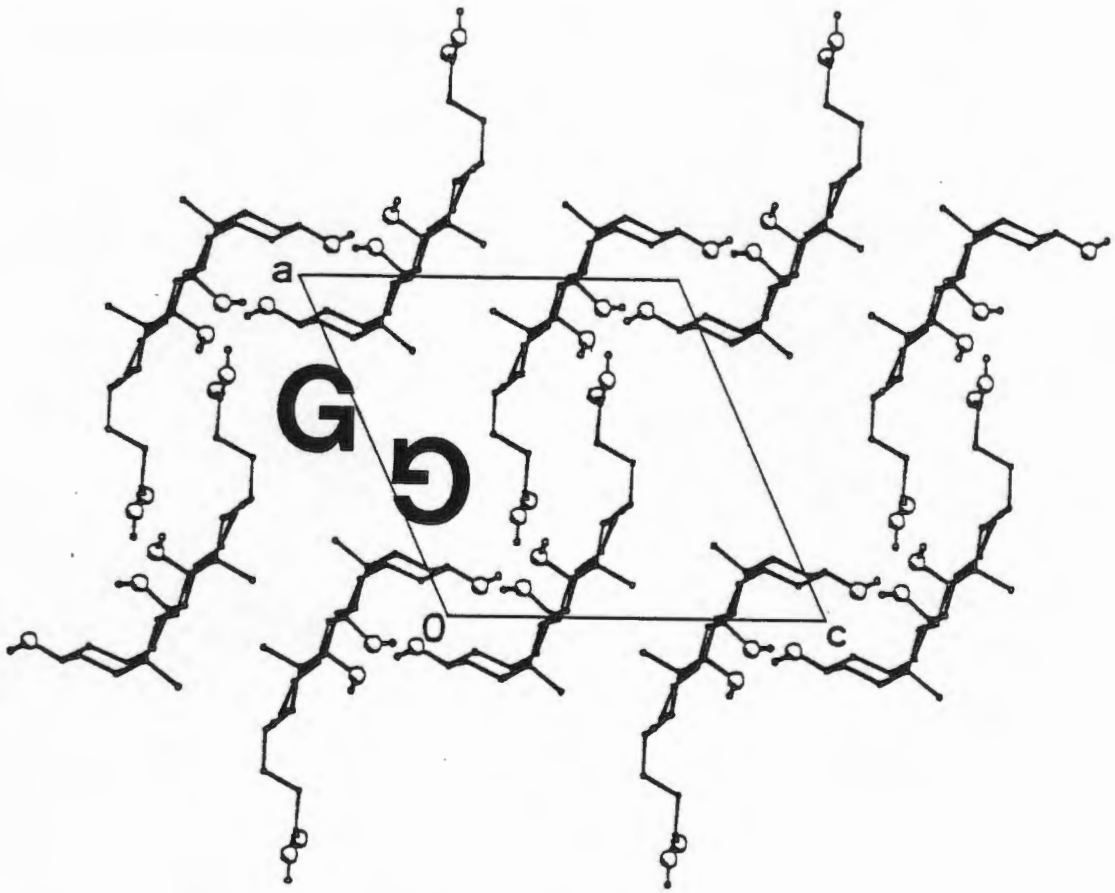

Figure 3.3: Packing motif exhibited by the tubulate clathrate CA inclusion compounds. Oxygen atoms are indicated as larger spheres.

The host-host hydrogen bonding pattern is similar for each structure although free rotation about the C(23)-C(24) bond allows the oxygen atoms of the carboxylic acid group to adopt two possible positions in the hydrogen bonding network. This effect is transmitted throughout the hydrogen-bond network resulting in reversal of the directions of donor and acceptor interactions since O(27) (the carbonyl oxygen) must always act as an acceptor atom. This is illustrated schematically in Figure 3.4 where scheme 1 represents the O(28)-H(28O)•••O(29)-H(29O)•••O(25)-H(25O)•••O(26)-H(26O)•••O(27) interaction and scheme 2 the O(28)-H(28O)•••O(26)-H(26O)•••O(25)-H(25O)•••O(29)-H(29O)•••O(27) interaction.

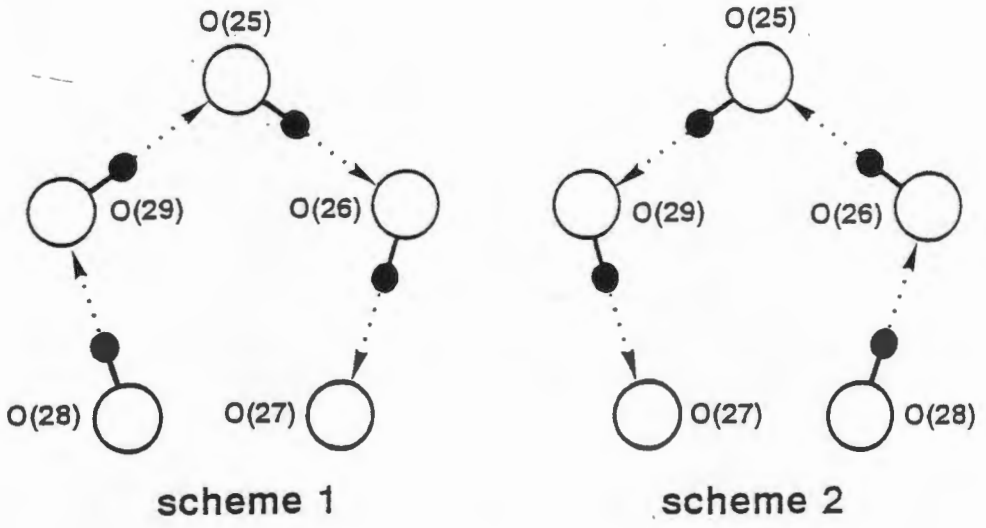

Figure 3.4: Schematic representation of the two hydrogen bonding schemes expressed in the crystals of CA inclusion compounds.

This appears to have no effect on the packing or strength of host guest interactions and this feature may be seen to occur in otherwise isostructural compounds. Indeed, some structures appear to show disorder of the COOH group as indicated by averaged C-O bond lengths and peaks (in electron density difference maps) at both possible hydrogen atom positions. The host-host hydrogen bond network is illustrated in Figure 3.5. The bilayers, held together by strong and extensive hydrogen bonding interactions propagate infinitely in the *b* direction but are only associated with each other by dint of weak van der Waals interactions.

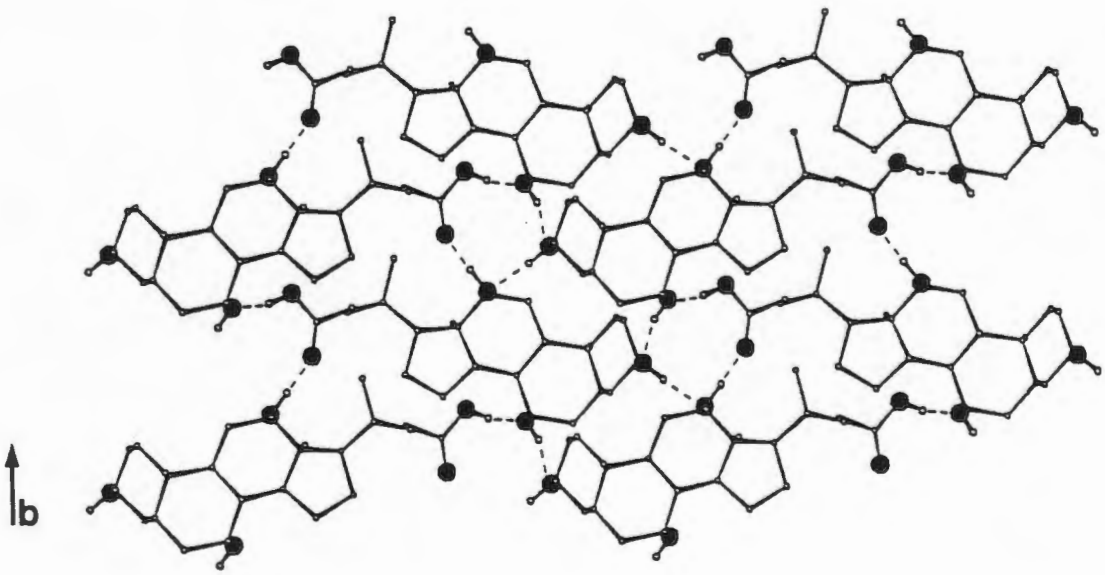

Figure 3.5: A single CA bilayer viewed as a projection onto the bilayer plane which corresponds to a projection onto (101). Oxygen atoms are shaded and hydrogen bonds indicated as dotted lines.

The rigid ABCD fused ring steroid nucleus has very little conformational freedom and thus only changes in the conformation of the flexible side chain (and to a small extent the D-ring) allow modification of the molecular shape. Subtle changes in side chain conformation lead to modification of the channel shape and size allowing different guests to be accommodated. The relative positions of the host bilayers also affect the channel shape and this too may vary depending on the spatial and conformational demands of the included guests.

The crystal structures studied will be grouped according to the type of guest molecule included. Description of specific details relating to refinement as well as any unusual features will be dealt with in the same sections while a general discussion of similarities and differences of the large group of similar structures which the Cholic acid inclusion compounds comprise will follow.

Conventional numbering of the steroid acid and its ester derivative was used and the numbering scheme of the host molecules is presented in scheme 3.1 and Figure 3.6 which shows the molecular structure of the cholic acid and methyl cholate hosts. Guest numbering will be indicated in each section. Where there is more than one host molecule per asymmetric unit, as in the structures crystallising in the space group *P*1, these are designated A and B. There is a bookmark at the beginning and a fold-out table at the end of this thesis, to aid the reader in remembering the mnemonics chosen as the names of each structure. The first two letters represent the host, either Cholic acid (CA) or Methyl cholate (MC) while the remaining letters are chosen to indicate the name of the guest molecules included.

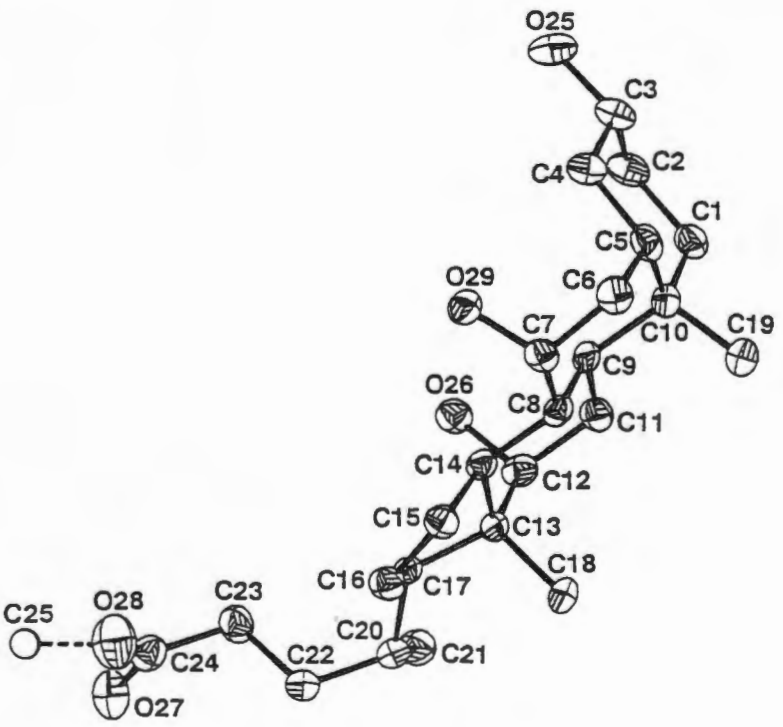

Figure 3.6: ORTEP molecular diagram of CA at 30 % enclosure ellipsoids indicating atomic numbering.

Group 1: Aliphatic ketones: CAACD, CAMEK, CADEK.

	CAACD	CAMEK	CADEK
Space Group	$P1$	$P2_1$	$P2_1$
H:G	2:3	1:1	1:1
Z	1	4	2
a / Å	12.655(3)	12.597(3)	12.787(2)
b / Å	8.354(3)	8.191(5)	8.117(1)
c / Å	14.125(3)	27.954(4)	13.960(2)
α / ^{o}	91.93(3)	90	90
β / ^{o}	106.02(2)	105.40(1)	103.82(1)
γ / ^{o}	94.68(3)	90	90

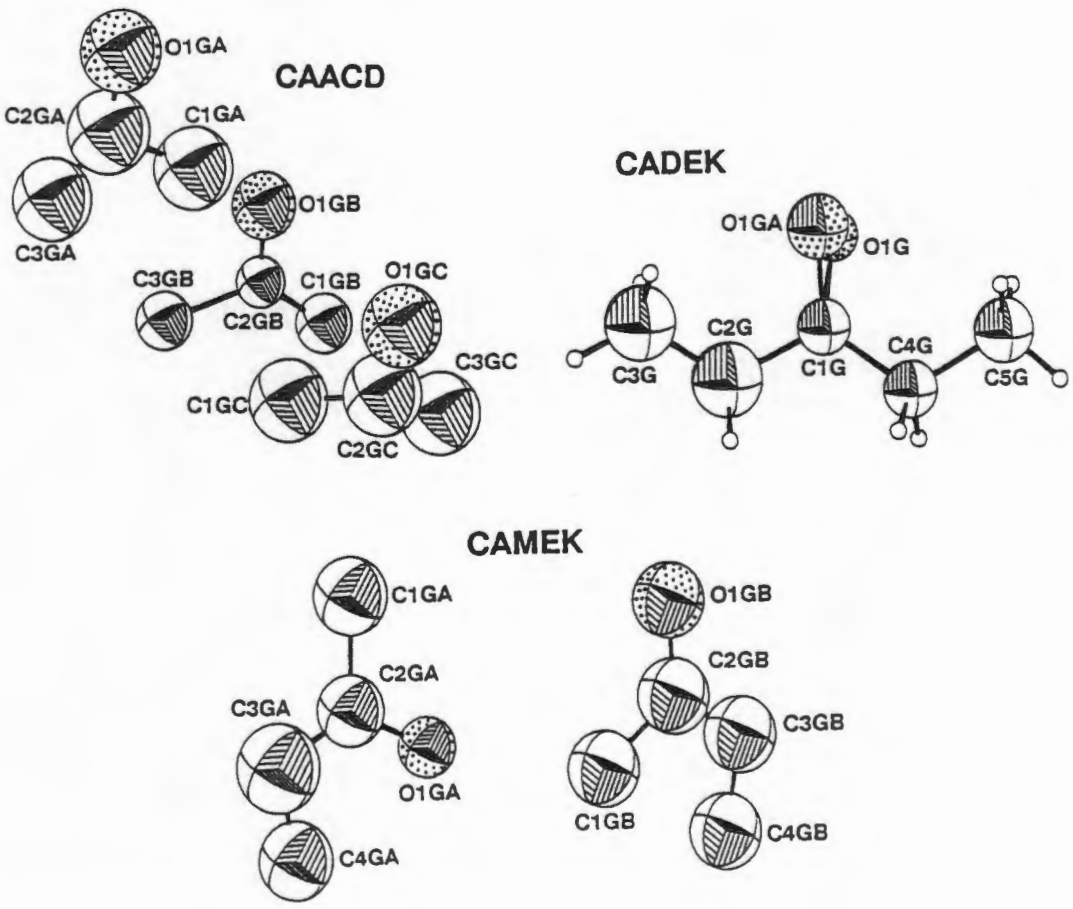

Refinement

Host non-hydrogen atoms were refined anisotropically in CAMEK and CADEK but in CAACD only host hydroxyl oxygen atoms, methyl group carbon atoms and atoms of the steroid side chain were refined anisotropically. Guest atoms were refined isotropically in all cases and bond length and distance

restraints applied to retain reasonable molecular geometry. Guest molecules showed a high degree of thermal motion and temperature factors of guest B of CAMEK were fixed at U=0.25 Å^2 while the A and C molecules of CAACD were extensively restrained. Assignment of guest oxygen atom positions for CAACD was difficult as the geometry of the acetone guest does not allow unambiguous assignment on the basis of connectivity. The highest peak in the electron density difference map of the three surrounding the sp^2 centre was assigned to be that of the oxygen atom in each case. The guest oxygen atom of CADEK was refined over two sites with s.o.f.s constrained to total unity. These refined to 0.50 for each position and the resultant bond lengths are the same: C(1G)-O(1G) 1.29(2) Å, C(1G)-O(1GA) 1.29(3) Å.

U values for geometrically generated hydrogen atoms refined to:

CAACD	CH_3	0.077(13) Å^2	CH_2	0.033(5) Å^2	CH	0.029(7) Å^2
CAMEK	CH_3	0.084(9) Å^2	CH_2	0.061(5) Å^2	CH	0.034(5) Å^2
CADEK	CH_3	0.074(7) Å^2	CH_2	0.064(4) Å^2	CH	0.034(4) Å^2

Hydroxyl hydrogen atoms were only included in the final model of CADEK as, although those of the other host molecules could often be located in electron density difference maps, these proved impossible to refine.

Results

Packing diagrams of the three structures are presented as Figures 3.7a, b and c.

The unusual stoichiometry of the CA complex with acetone is confirmed by weight loss % on TG analysis as is discussed in detail in chapter 4: experimental 17.5%, calculated 17.6%. The bilayers of this complex are tilted from the normal to the (101) plane resulting in the space group $P1$. There are subtle differences in the side chain conformations of the two independent host molecules as indicated in Figure 3.8a and there are three molecules of included acetone per two molecules of host which pack to maximise space filling in the channel.

The structure of the inclusion compound with methyl ethyl ketone (Figure 3.7b) exhibits a unique doubling of the *c*-axis not seen in any of the other CA inclusion compounds studied. There are two independent host molecules per asymmetric unit (Z=4) and these exhibit differences in side chain conformation (Figure 3.8b) as well as switching of the relative positions of O(27) and O(28) with the result that both hydrogen bond schemes mentioned before occur in the same crystal. The relationship of the two independent host molecules is indicated in the packing diagram, Figure 3.7b. These are not related by symmetry; instead subsequent bilayers are related by the 2_1-axes at ½,y,0 and ½,y,½. The bilayers are thus shifted ½ along *b* relative to each other and there are two crystallographically distinct channels with slightly differing cross sectional shape yet accommodating the same guest in each.

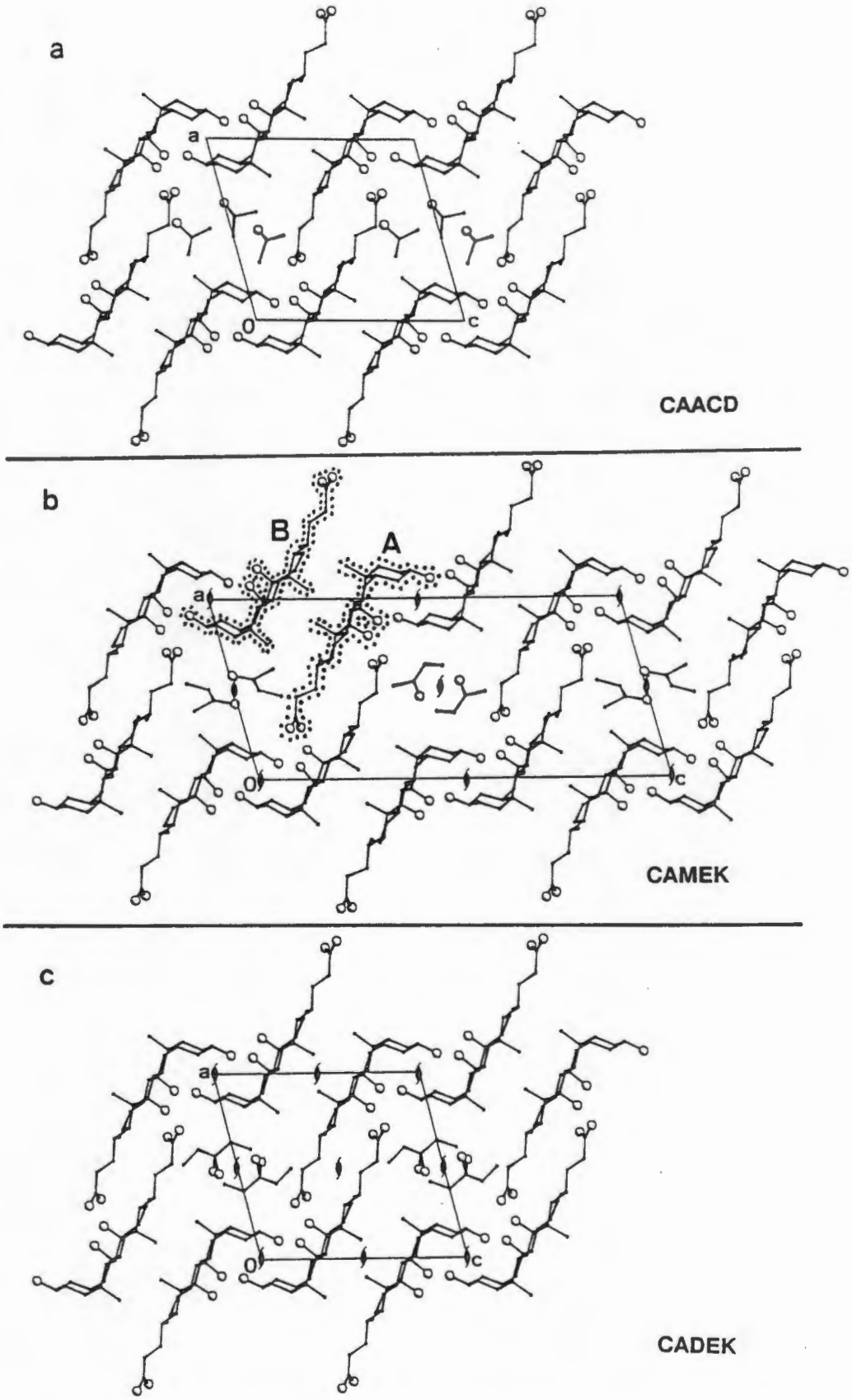

Figure 3.7: Packing diagrams viewed as projections of (010) of a) CAACD, b) CAMEK and c) CADEK. Note the 2:3 host:guest stoichiometry of CAACD and the doubled *c* axis of CAMEK.

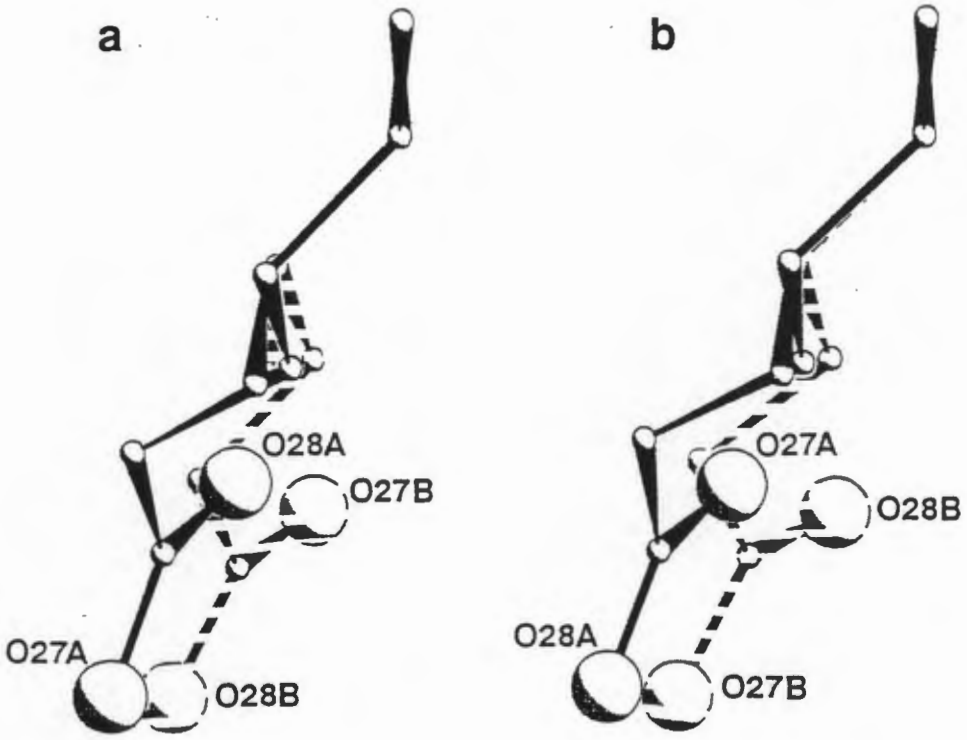

Figure 3.8: Side chain conformations of a) CAACD and b) CAMEK hosts. The 'B' molecule is indicated by broken lines. Note the opposite orientations of the COOH groups in each pair of hosts.

Guest molecules adopt different positions and conformations in the differently shaped channels but are related to other guests in the same channel by 2_1 symmetry as required by the space group. Thus there are spirals of each guest conformation alternating through the crystal. The packing of the guests in the channels is illustrated in Figure 3.9b. In both cases the carbonyl oxygen atom of the guest points away from the channel walls and no short range host:guest interactions occur.

CADEK represents the most commonly seen type of cholic acid inclusion compound: the host guest ratio is 1:1 and Z=2 in the space group $P2_1$. Guests are regularly spaced in the channel as required by the 2_1-axis normal to (010). Only one type of channel occurs and the guests stack in a spiral fashion with their long molecular axes tilted with respect to each other as illustrated in Figure 3.9c.

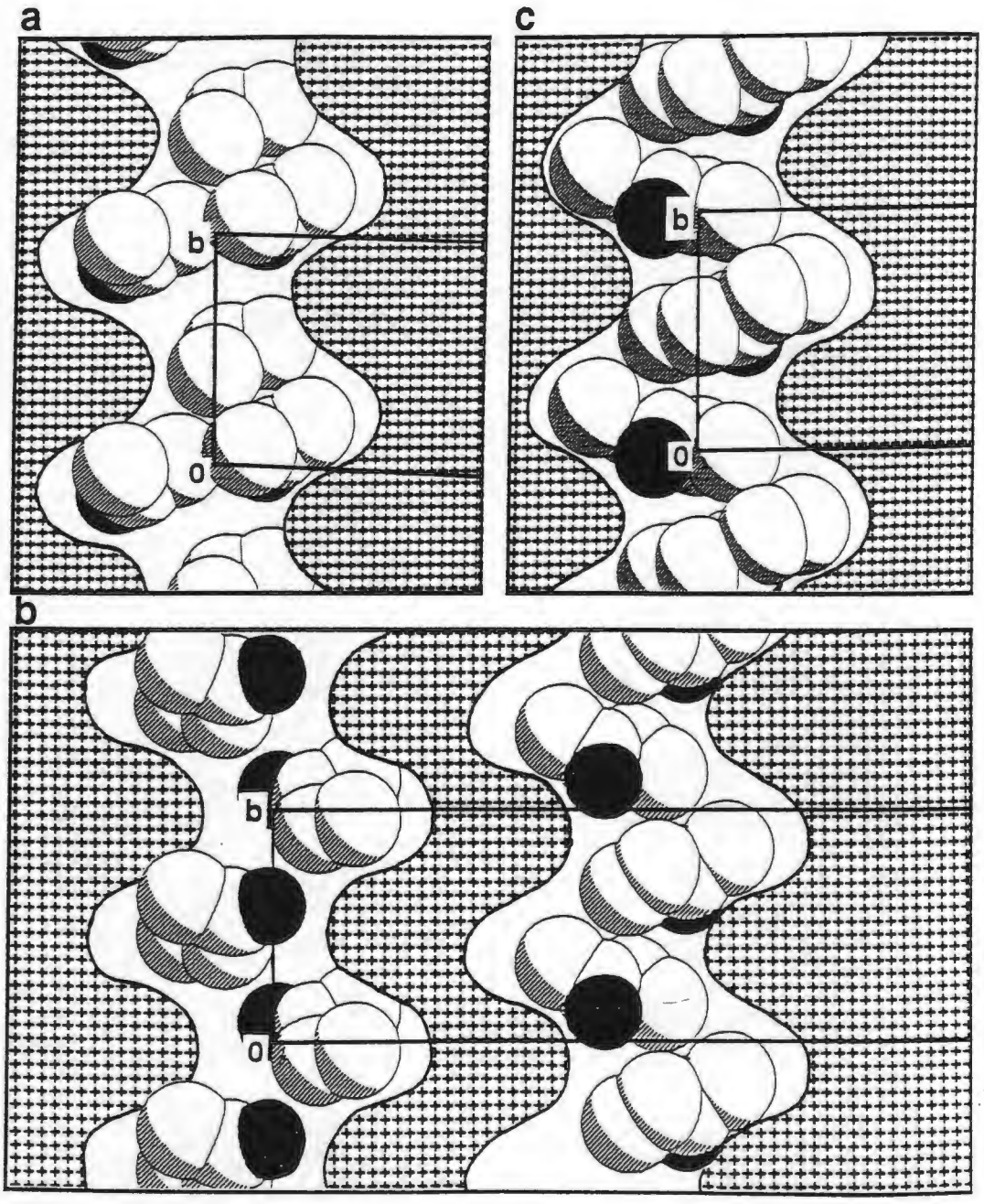

Figure 3.9: Space filling plots of the guests indicating their orientation in the channels viewed down [100]. a) CAACD, b) CAMEK and c) CADEK. Oxygen atoms of the guest molecules are shaded and hydrogen atoms are omitted.

Group 2: Aliphatic esters: CAMA, CAET, CAEP, CAPAC, CAIP.

	CAMA	CAET	CAEP	CAPAC	CAIP
Space Group	$P1$	$P2_1$	$P2_1$	$P2_1$	$P2_1$
H:G	1:1	1:1	1:1	1:1	1:1
Z	2	2	2	2	2
a / Å	12.223(2)	13.668(3)	13.571(1)	16.802(5)	16.604(3)
b / Å	8.189(1)	7.824(4)	7.969(1)	7.882(1)	7.979(3)
c / Å	14.204(2)	14.095(2)	14.237(1)	12.107(4)	12.141(2)
α / °	90.18(1)	90	90	90	90
β / °	105.72(2)	113.53(1)	113.53(1)	118.06(3)	117.76(2)
γ / °	94.03(1)	90	90	90	90

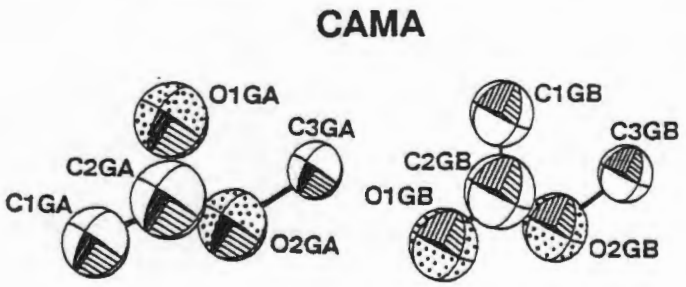

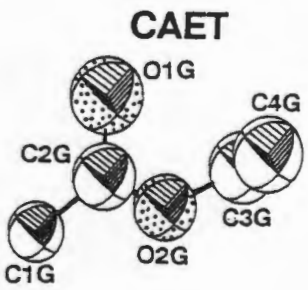

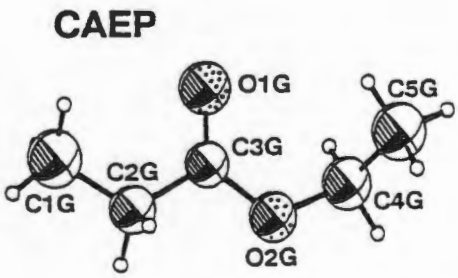

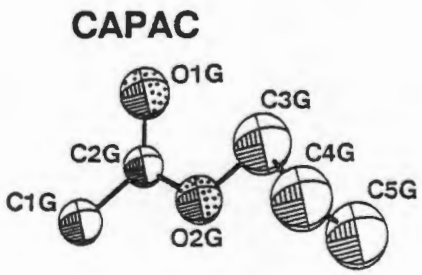

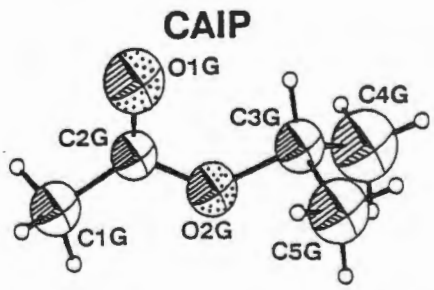

Refinement

Host non-hydrogen atoms were refined anisotropically except for those of the carboxylic group oxygen atoms of CAEP and CAET which exhibited unreasonably high anisotropic displacement parameters. Disorder of the host carboxylic acid group was indicated in CAEP and CAPAC although only in the latter was O(27) refined as disordered over two positions with s.o.f.s of 0.76 and 0.24. The C-O bonds lengths of CAEP are C(24)-O(27) 1.242(11) Å and C(24)-O(28) 1.267(9) Å suggesting disorder of the COOH group such that neither of

the two possible hydrogen bond schemes predominates and the bond lengths measured are averaged values.

All guest atoms were located unambiguously in electron density difference maps but required bond length and "anti-bumping" restraints[3] for sensible refinement. In CAMA, CAET and CAEP the atoms surrounding the sp^2 centre of the guests were restrained to planar geometry. Host hydroxyl hydrogen atoms were refined for CAET and CAIP only.

U values for geometrically generated hydrogen atoms refined to:

CAMA	CH_3	0.068(6) Å^2	CH_2	0.052(3) Å^2	CH	0.039(4) Å^2
CAET	CH_3	0.086(9) Å^2	CH_2	0.049(4) Å^2	CH	0.032(5) Å^2
CAEP	CH_3	0.070(7) Å^2	CH_2	0.046(4) Å^2	CH	0.038(5) Å^2
CAPAC	CH_3	0.049(7) Å^2	CH_2	0.054(5) Å^2	CH	0.038(6) Å^2
CAIP	CH_3	0.061(7) Å^2	CH_2	0.042(4) Å^2	CH	0.039(5) Å^2

Results

These five structures of CA with aliphatic esters may be divided into two distinct groups designated A and B. Group A comprises the structures CAMA, CAET and CAEP which have similar unit cell parameters, with CAMA slightly distorted from monoclinic geometry by the tilt of the bilayers. The second group, B, comprises CAPAC and CAIP with unit cell parameters significantly different to group A. The difference between these two groups results from the occurrence of two different stacking modes of the CA bilayers. This is illustrated in Figures 3.10a and b, which display projections of CAEP and CAIP down [010]. In CAEP the C(18) methyl groups pack in close proximity about the screw diad at 0,y,½ while in CAIP the C(19) groups are in close contact. This indicates a shift in the relative positions of the host bilayers and results in channels with different cross sectional shape as illustrated in Figure 3.12. Abbreviated packing diagrams of the other structures are presented as Figures 3.10c, d and e for comparison.

The stacking mode of these similar guests in their respective channels is also found to differ as is illustrated in Figures 3.11a and b. The guests of type A structures pack with their long molecular axes approximately perpendicular to the screw diads while those of group B adopt a herringbone pattern with the long molecular axis at 45° to *b* shown in Figure 3.11.

The side chain conformations of the host steroid are similar in all structures except that of CAMA. The more extended conformation of CAMA results in less puckered bilayers and hence a channel with smaller cross sectional area accommodating the smaller guest.

A comparison of the extended and puckered side chain conformations is presented as Figure 3.13a and the differences in side chain conformation of the side chain of CAMA as Figure 3.13b.

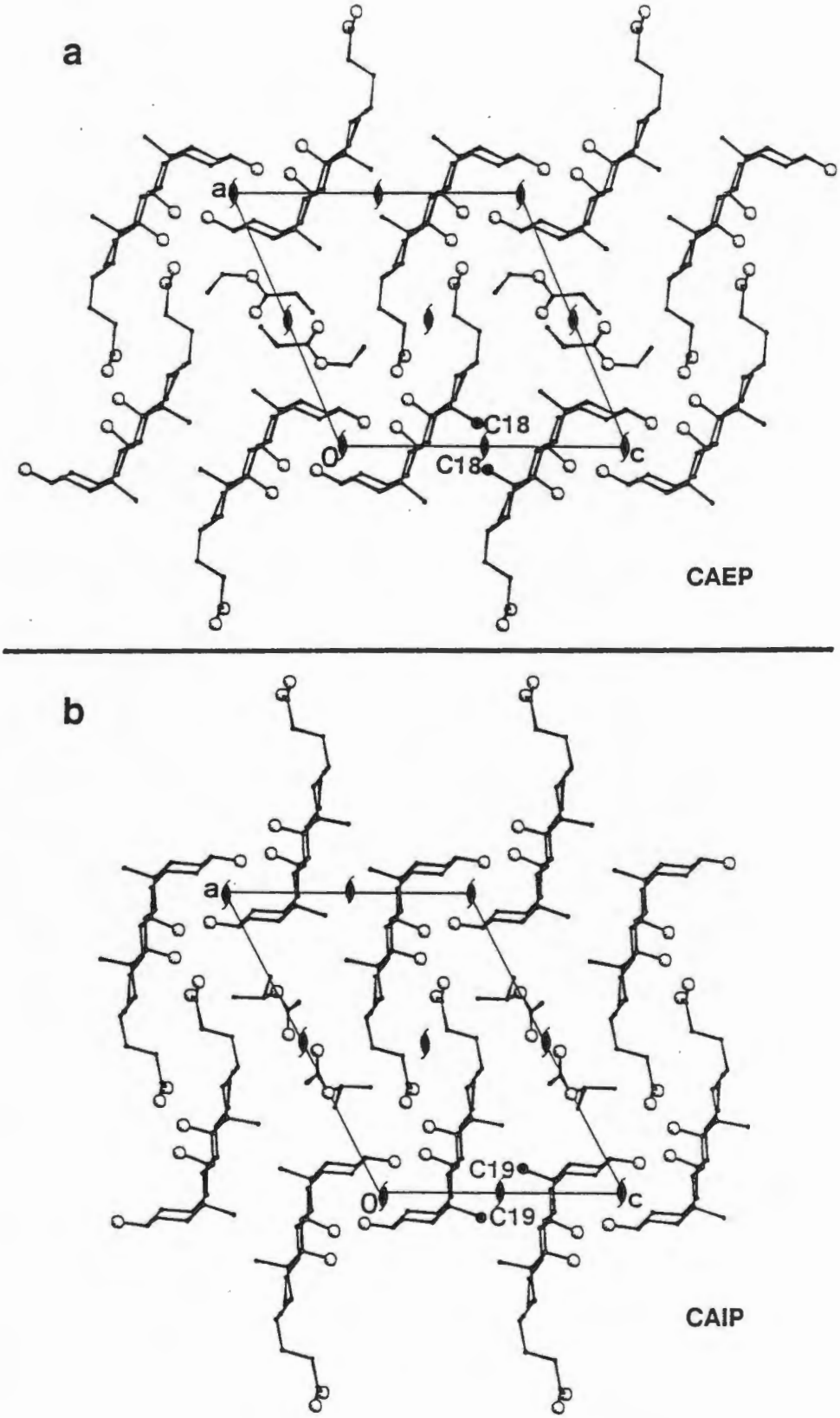

Figure 3.10: Packing diagrams of a) CAEP (A-type) and b) CAIP (B-type) viewed down [010] showing the two different packing modes adopted by CA inclusion compounds. One pair of methyl groups in close proximity about a 2_1 axis are shaded for clarity.

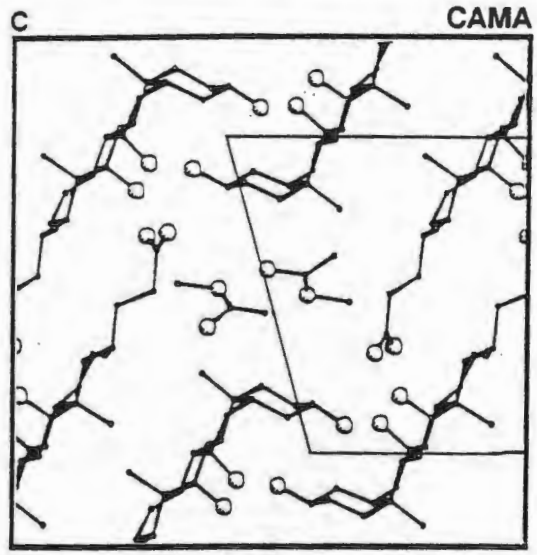

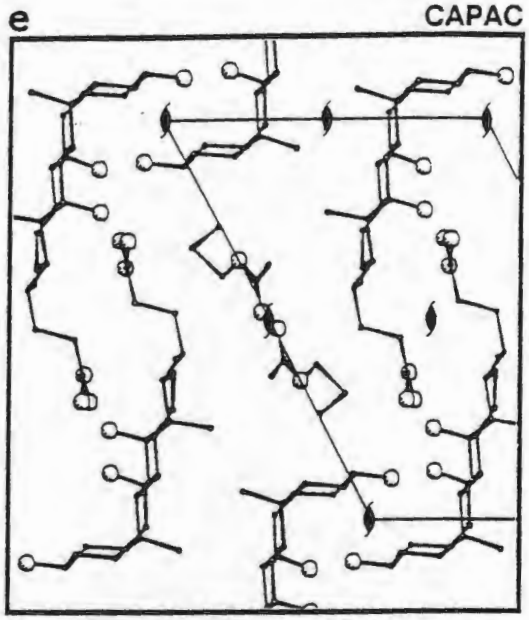

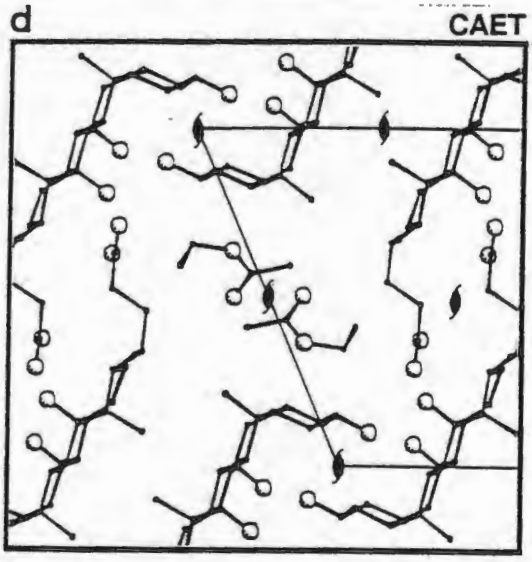

Figure 3.10 continued:
abbreviated packing diagrams of:
c) CAMA
d) CAET
e) CAPAC

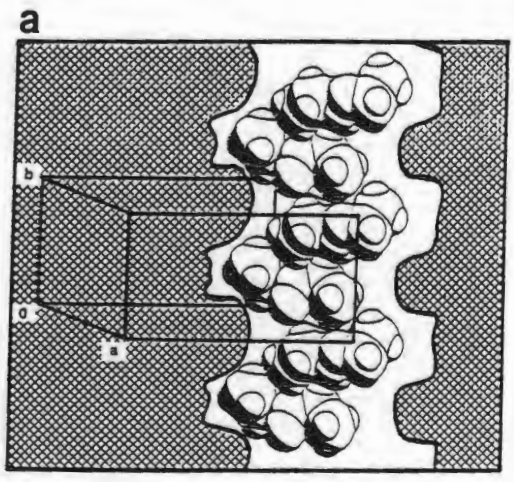

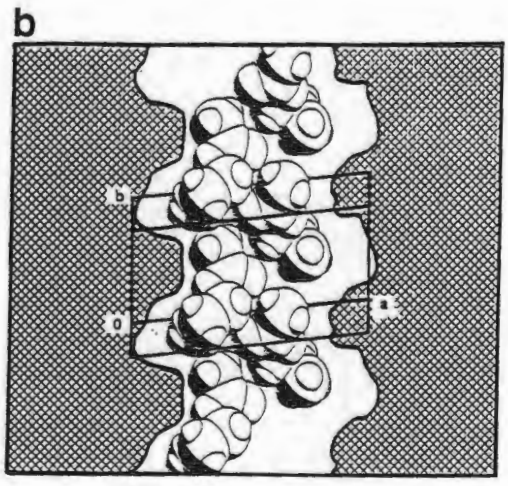

Figure 3.11: Space filling diagrams of the guests packed in the channels of A-type a) CAEP and B-type b) CAPAC structures.

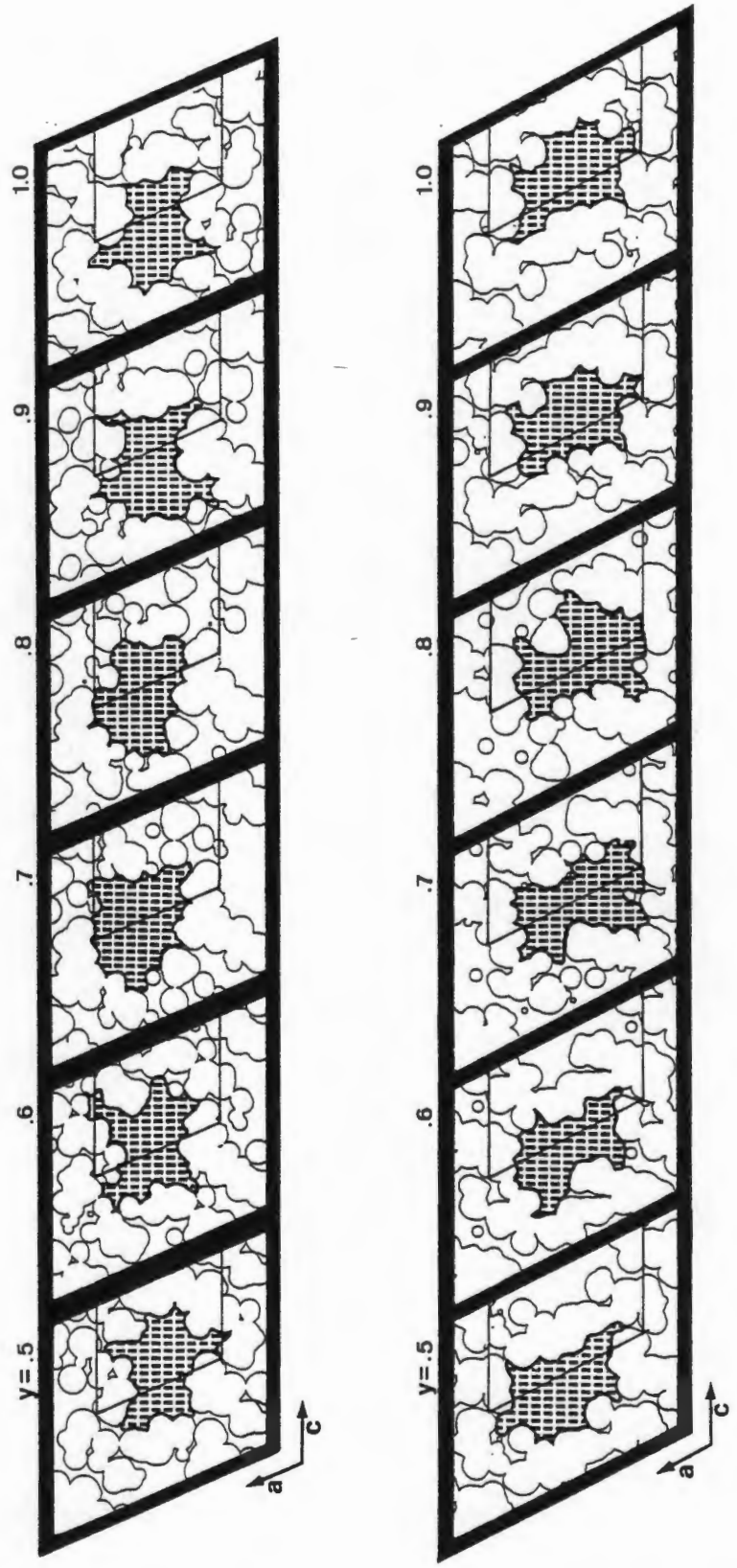

Figure 3.12: Slices perpendicular to [010] at y = 0.1 intervals showing the cross sectional shapes of the channels formed compounds adopting the A- and B-type packing modes. a) CAEP and b) CAIP.

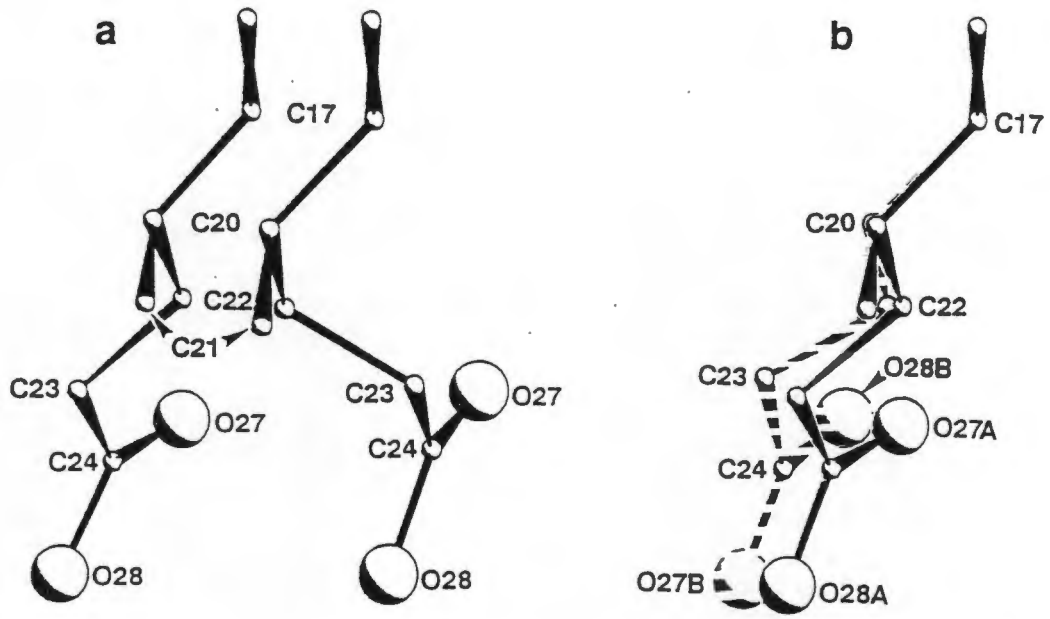

Figure 3.13: Differences in side-chain conformations: a) CAMA and CAIP, extended and puckered conformations respectively and b) CAMA hosts A and B.

Since it appears that the B packing mode is favoured in crystals containing larger guest molecules, crystallisations with n-butyl acetate and a number of its structural isomers were attempted. Crystals of the 1:1 inclusion compounds of *n*-butyl acetate, ethyl butyrate and sec-butyl acetate are readily grown from solutions of the host in liquid guest at temperatures below 21 °C. These crystals proved extremely labile, fracturing upon removal from mother liquour or when exposed to even marginally raised temperatures while still immersed in liquour. Attempts to mount crystals of the inclusion compounds with such guests proved unsuccessful except when the crystals were grown and mounted in temperature controlled rooms and transferred directly from mother liquour into a Lindemann capillary containing mother liquour. Refined cell data for crystals of CA•*n*-butyl acetate (CANBU) are as follows: Space group $P2_1$, a = 16.416(6) Å, b = 7.880(1) Å, c = 12.150(2) Å, β = 111.05(3), V = 1467(1), Z = 2. Note that the cell parameters exhibit the longer a axis length seen in CAPAC and CAIP, compounds which exhibit the B-type packing mode.

Attempts at room-temperature data collections resulted in rapid decay of the crystals even when sealed in Lindemann capillary tubes above mother liquour. In most cases the capillaries containing the damaged crystals still contained quantities of mother liquour and it appears that the crystals were damaged by exposure to the X-ray beam. None of the data sets obtained resulted in crystal structures of publishable quality, however one of the data sets collected contained enough observed reflections to allow direct methods solution and location of the host non-hydrogen atoms. Although guest atoms could not be unambiguously located and no further results (bond lengths etc.) are to be presented here it is nonetheless clear that the packing mode of CANBU is the B type as illustrated in the host packing diagram, Figure 3.14.

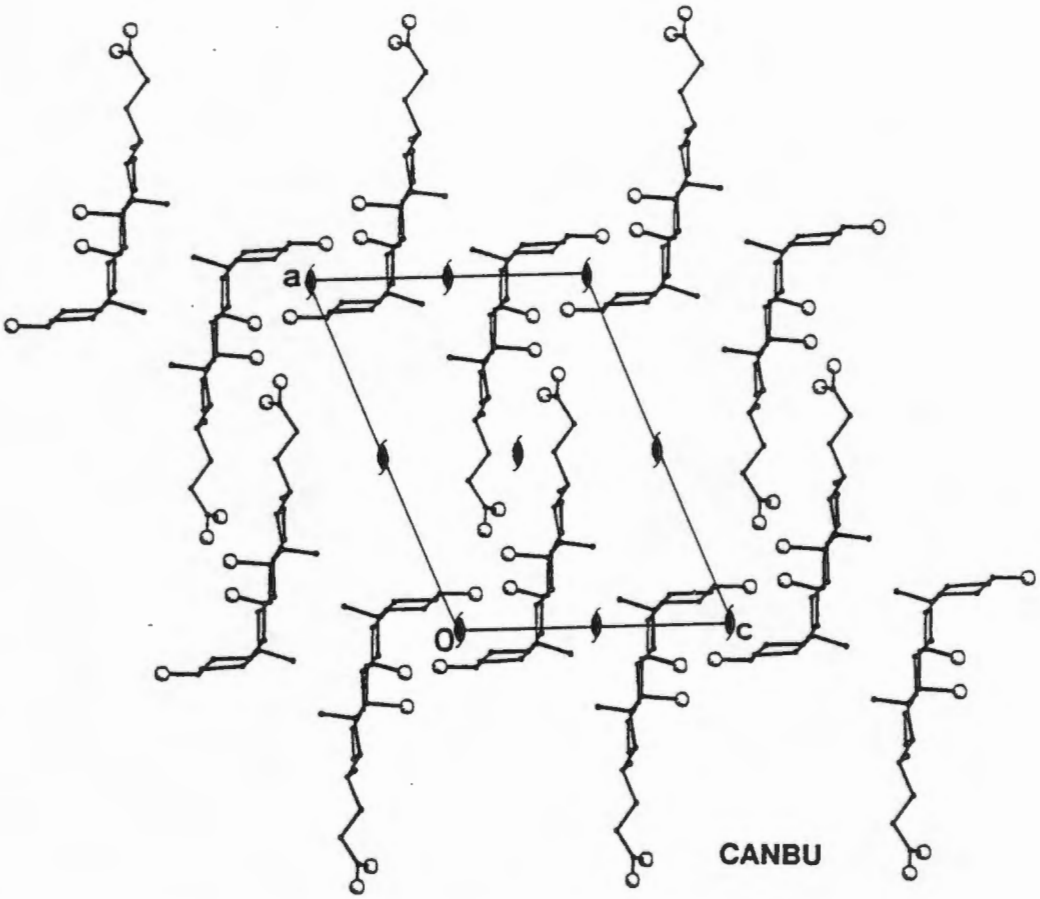

Figure 3.14: Packing diagram of CA•*n*-Butyl acetate with guest removed.

Group 3: Vinyl esters: CAVA, CAMM.

	CAVA	CAMM
Space Group	$P1$	$P2_1$
H:G	1:1	1:1
Z	2	2
a / Å	12.284(2)	12.960(2)
b / Å	8.237(2)	8.060
c / Å	14.286(4)	14.642(3)
α / °	89.57(1)	90
β / °	105.91(2)	114.00(1)
γ / °	85.70(1)	90

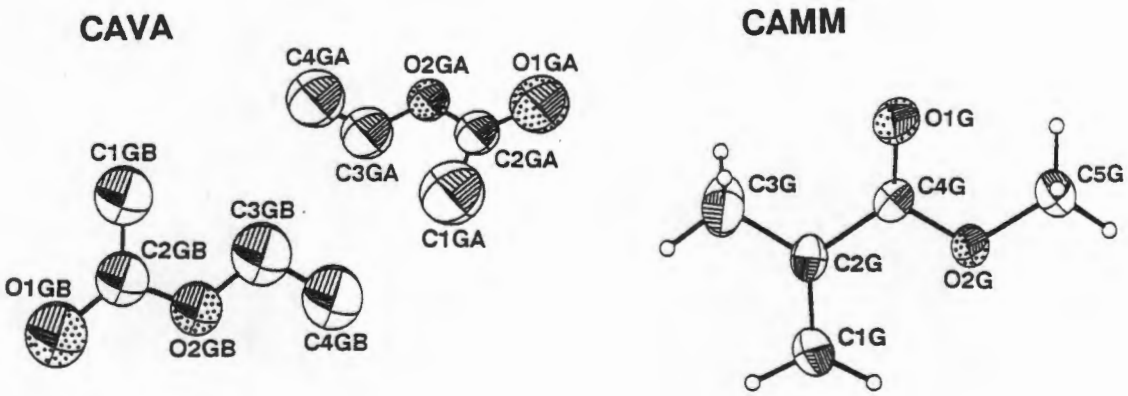

Refinement

All non-hydrogen atoms of the host and those of the methyl methacrylate guest were refined anisotropically while the guest atoms of CAVA were refined isotropically. Host hydroxyl and guest hydrogen atoms were included in the final model of CAMM but not of CAVA.

U values for geometrically generated hydrogen atoms refined to:

CAVA	CH_3 0.094(9) Å^2	CH_2 0.047(4) Å^2	CH 0.030(4) Å^2
CAMM	CH_3 0.055(4) Å^2	CH_2 0.044(2) Å^2	CH 0.029(3) Å^2

Results

Abbreviated packing diagrams of CAVA and CAMM showing the orientation of the guests in the channels are presented as Figures 3.15a and b respectively. CAMM crystallises in the space group $P2_1$ and CAVA in the space group $P1$. The loss of the 2_1 axis in CAVA is reflected in the positions of the guests relative to each other and as with CAMA results in a channel of smaller cross section, irregular spacing of the guest molecules and differences in the side

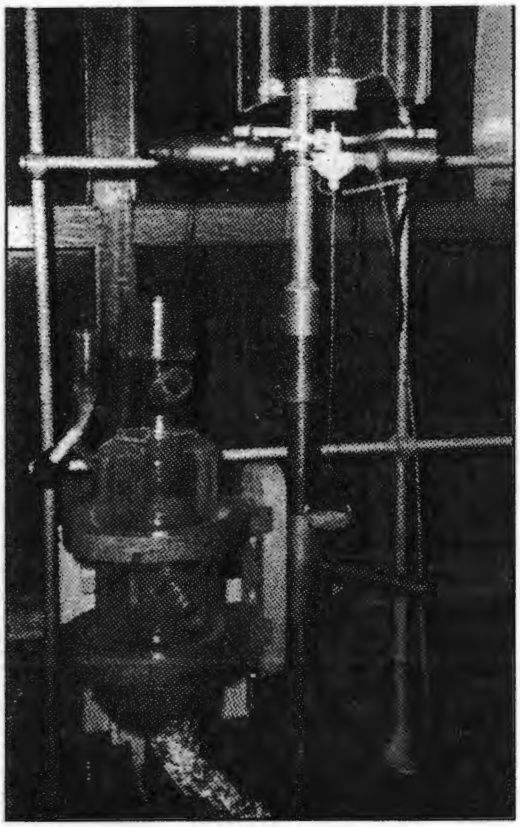

Figure 2.5: Levitating balance aparutus. The reaction chamber is lowered and swung to one side to allow a clear view of the levitating sample holder.

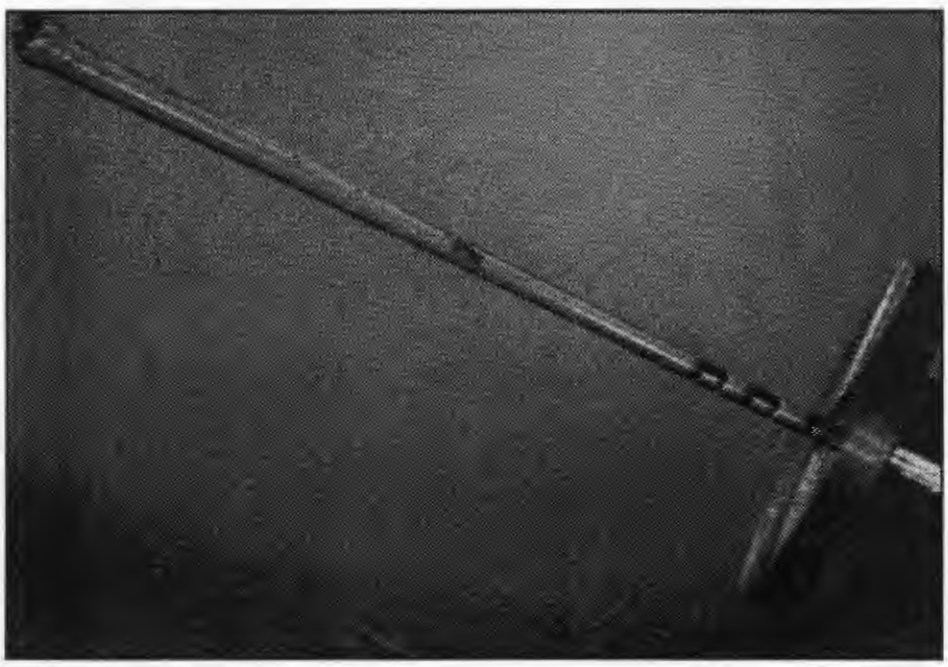

Figure 2.6: Crystal mounted in flame sealed Lindemann tube with mother liquor.

chain conformations of the two crystallographically independent host molecules.

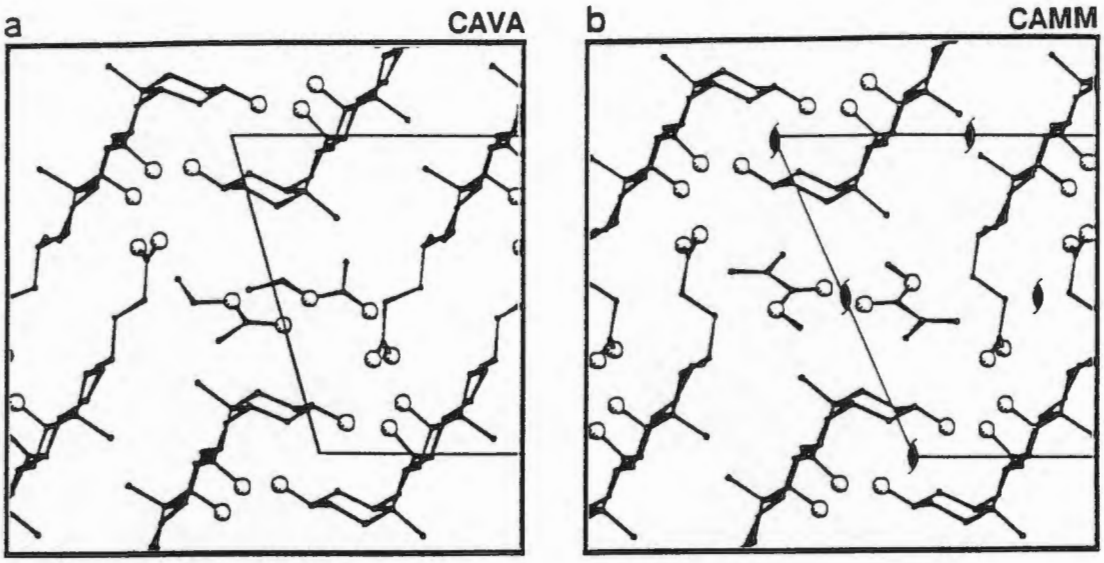

Figure 3.15: Abbreviated packing diagrams of a) CAVA and b) CAMM.

Both of these guests were chosen because of their use as monomers for polymerisation reactions. It was hoped that the stacking of the guests would be such that the double bonds would be in a favourable position for reaction allowing topotactic control of the polymerisation reaction. This expectation was based on the guest's centre to centre distance of *ca* 4 Å in most of the CA inclusion compounds studied, which is within the outer boundary of reactivity as described by Kearsley[6]. Such polymerisation reactions have for example been achieved in the channels of inclusion compounds of perhydrotriphenylene[7] and deoxycholic acid[8] with trans 1,3 pentadiene guest.

The stacking of the guests is shown in Figure 3.16a (CAVA) and b (CAMM). Because of the loss of the 2_1-axis the guests of CAVA are not spaced regularly in the channel and the unsaturated groups of pairs of guests appear to be within reactive distance; nonetheless the compound appears inert to polymerisation either by exposure to *uv* radiation or the initiator *n*-Butyl Lithium. Guests are lost as monomers upon heating. Examination of the stereogram Figure 3.16 reveals that although pairs of guests are in close proximity the double bonds are not in favourable orientation with respect to each other and considerable rotation is necessary before the geometry of the unsaturated groups is suitable for reaction to occur. Similarly the double bonds of the methyl methacrylate monomer are oriented towards the channel walls with *ca* 8 Å between nearest neighbour unsaturated groups. No polymerisation of guests within the channels occurs: indeed the incorporation of these monomers into the channels of the inclusion compounds serves to stabilise them and prevent reaction, an effect usually achieved in solution by the addition of inhibitors.

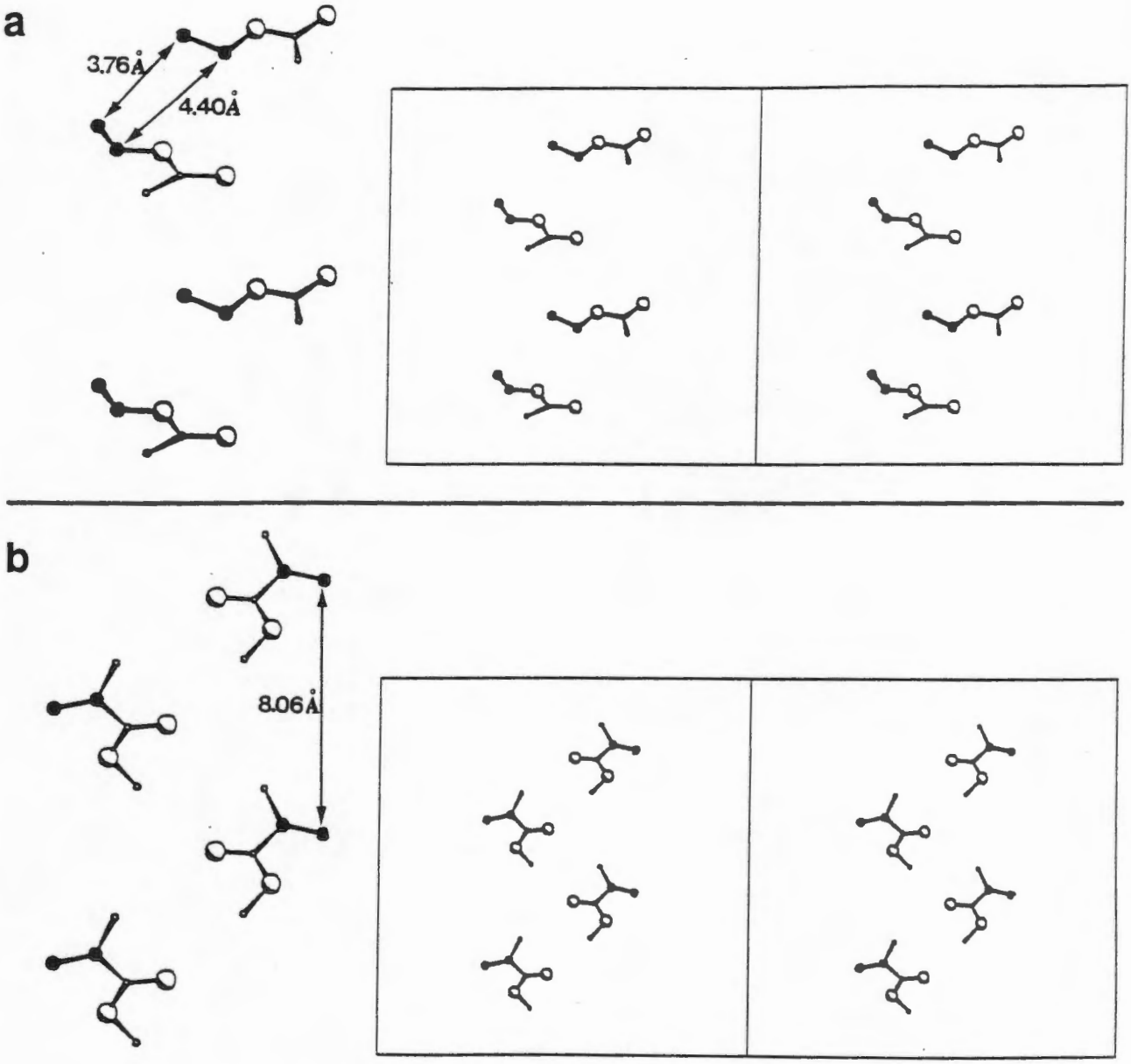

Figure 3.16: Packing of the monomer guests in the channels of the inclusion compounds a) CAVA and b) CAMM. Carbon atoms of the ethene group are shaded for clarity.

Group 4: Aromatic guests: CABN, CAAN, CANI, CAPR, CAPTOL, CAPNOT, CAMN.

	CABN	CAAN	CANI	CAPR
Space Group	$P2_1$	$P2_1$	$P2_1$	$P2_1$
H:G	1:1	1:1	1:1	1:1
Z	2	2	2	2
a / Å	13.642(3)	13.742(2)	13.579(2)	16.790(1)
b / Å	8.133(2)	8.049(1)	8.106(3)	7.928(5)
c / Å	14.055(3)	14.095(2)	14.048(1)	12.262(3)
α / °	90	90	90	90
β / °	114.12(2)	115.20(2)	113.52(1)	114.25(2)
γ / °	90	90	90	90

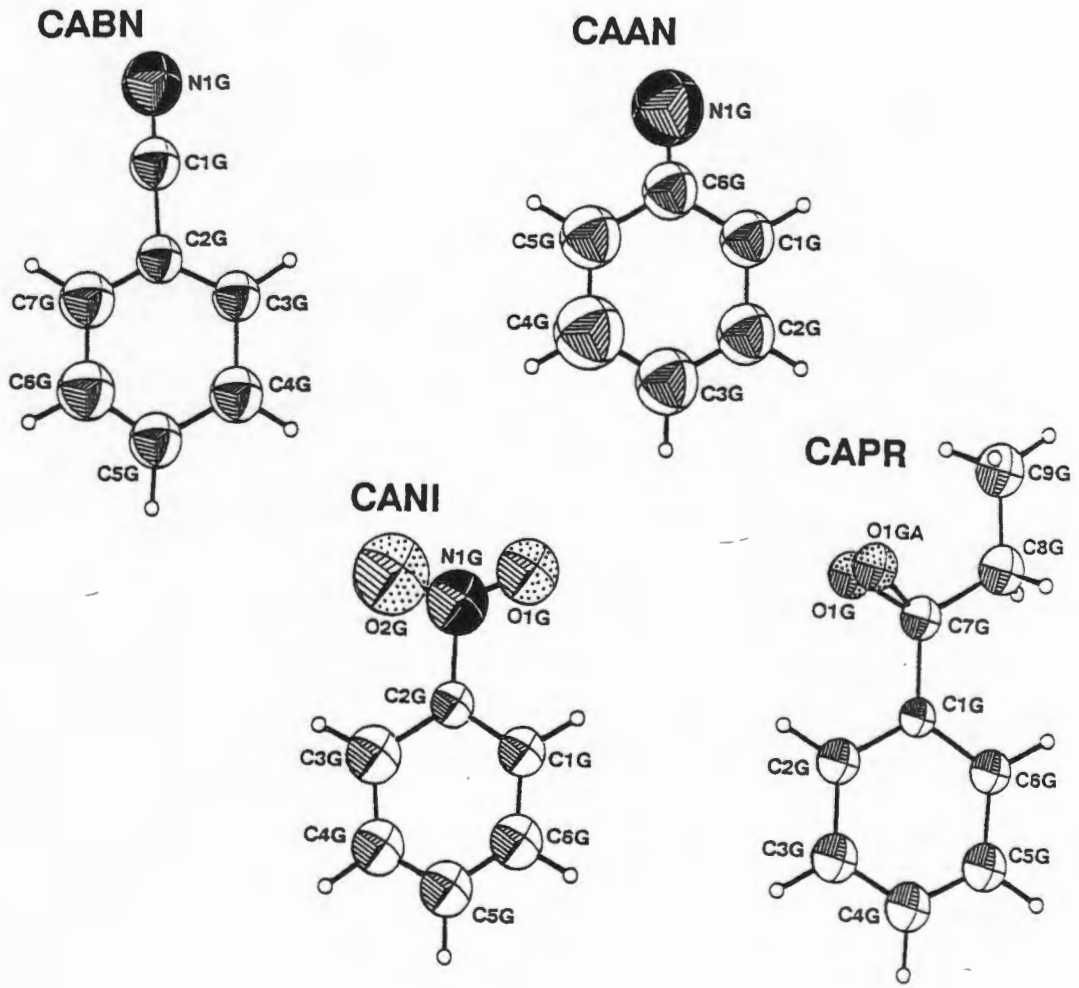

	CAPTOL	CAPNOT	CAMN
Space Group	$P2_1$	$P2_1$	$P2_1$
H:G	1:1	1:1	1:1
Z	2	2	2
a / Å	13.577(4)	13.495(1)	12.442(3)
b / Å	8.078(2)	8.266(4)	8.066(1)
c / Å	14.182(6)	14.398(2)	14.519(2)
α / ^{o}	90	90	90
β / ^{o}	114.42(3)	114.61(1)	102.63(1)
γ / ^{o}	90	90	90

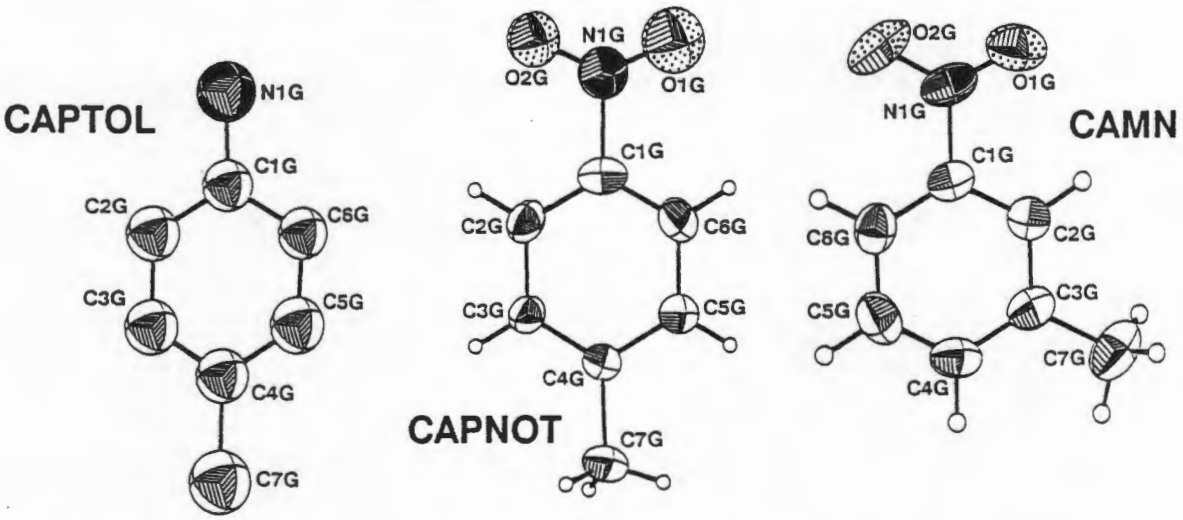

Refinement

All aromatic guest inclusion compounds of CA studied crystallise in the space group $P2_1$ with 1:1 host:guest stoichiometry. In each case the non-hydrogen atoms of the host were refined anisotropically as were the guest atoms of CAMN and CAPNOT (nitro group atoms refined isotropically). Host hydroxyl hydrogen atoms were located and refined with bond length restraints in the cases of CAAN, CANI, CAPR, CAPNOT and CAMN. The oxygen atom of the propiophenone guest molecule of CAPR was modelled as disordered over two sites with the sum of the s.o.f.s constrained to unity which resulted in s.o.f.s of 0.65 for O(1G) and 0.35 for O(1GA).

U values for geometrically generated hydrogen atoms refined to:

CABN	CH_3 0.069(9) Å^2	CH_2 0.056(5) Å^2	CH 0.047(7) Å^2
CAAN	CH_3 0.090(8) Å^2	CH_2 0.060(4) Å^2	CH 0.038(4) Å^2
CANI	CH_3 0.057(6) Å^2	CH_2 0.047(4) Å^2	CH 0.035(5) Å^2
CAPR	CH_3 0.084(4) Å^2	CH_2 0.056(4) Å^2	CH 0.044(4) Å^2
CAPTOL	CH_3 0.070(7) Å^2	CH_2 0.059(4) Å^2	CH 0.045(5) Å^2
CAPNOT	CH_3 0.060(8) Å^2	CH_2 0.053(5) Å^2	CH 0.034(6) Å^2
CAMN	CH_3 0.069(4) Å^2	CH_2 0.038(2) Å^2	CH 0.038(2) Å^2

Results

All of these compounds pack in the "A" motif, i.e. with C(18) methyl groups in close proximity about the screw diad, except for CAPR which forms the "B" type with elongated channel cross section as illustrated in Figure 3.17a and b.

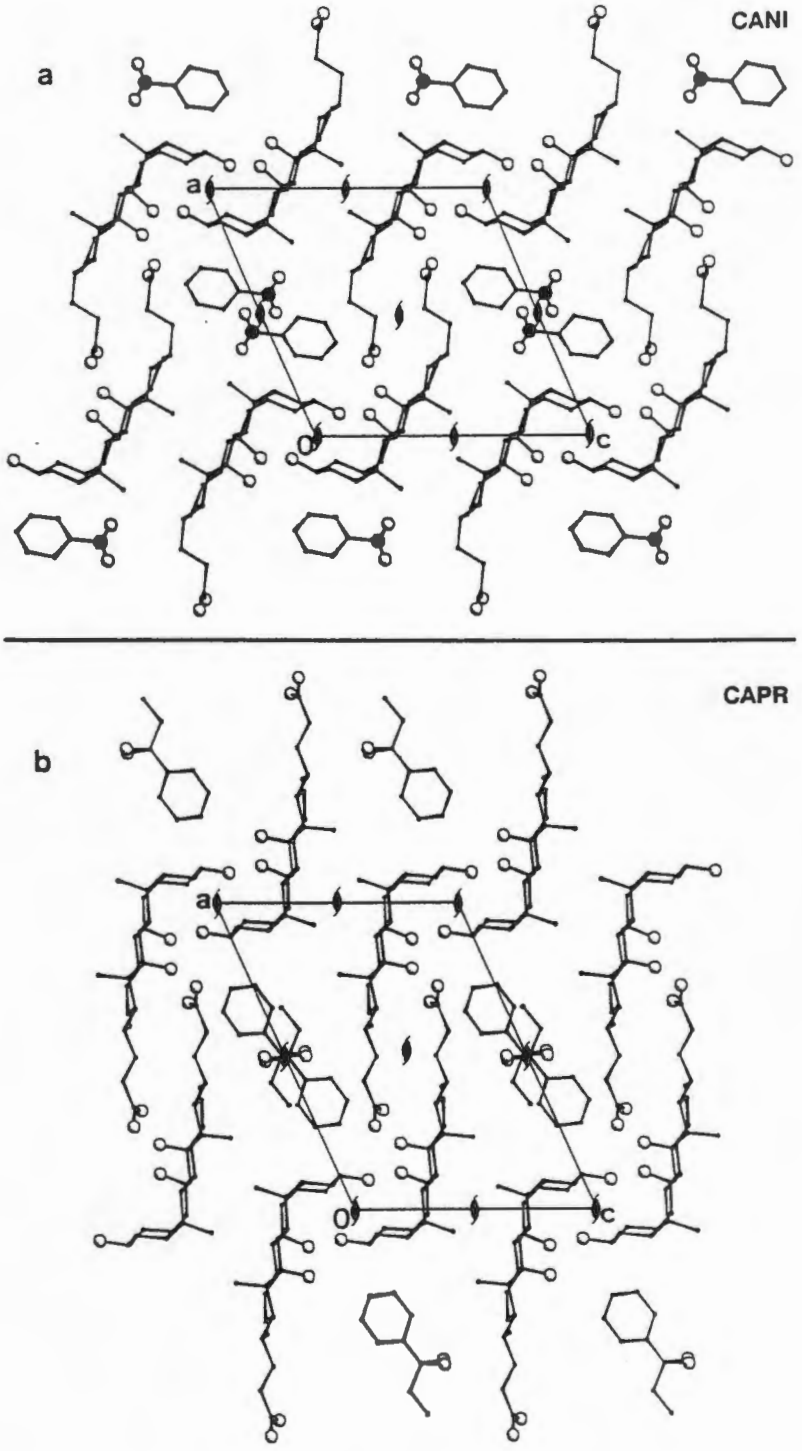

Figure 3.17: Packing diagrams of a) CANI and b) CAPR viewed down [010]. These represent A- and B-type structures respectively.

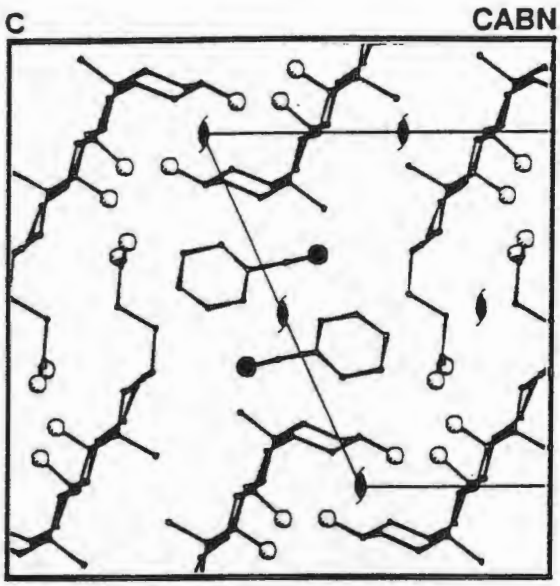

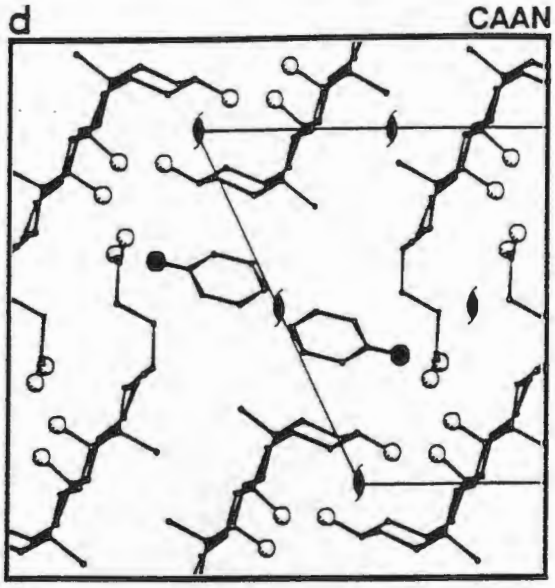

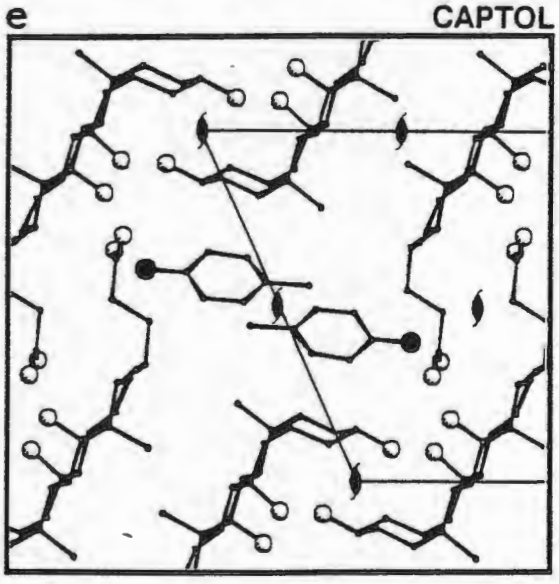

Figure 3.17 continued: Abbreviated packing diagrams of:
c) CABN
d) CAAN
e) CAPTOL
f) CAPNOT
g) CAMN.
Nitrogen atoms are indicated as shaded atoms while oxygen atoms are large open circles as before and both oxygen atoms of the disordered carbonyl group of CAPR are shown.

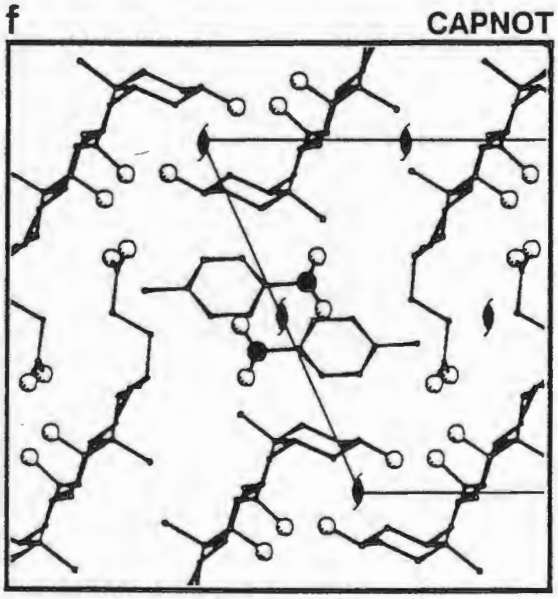

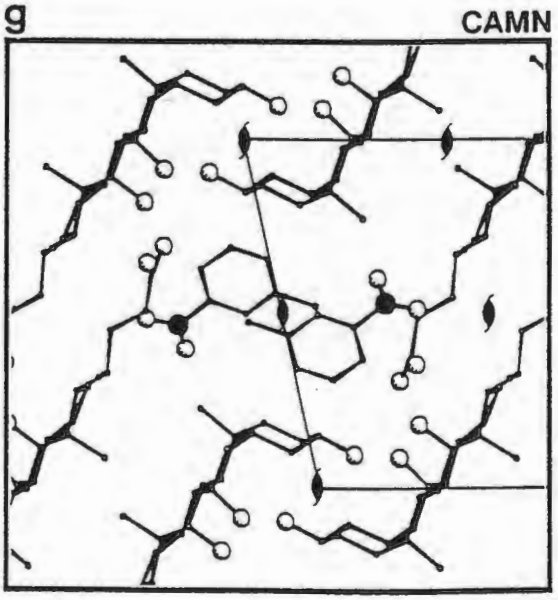

Abbreviated packing diagrams of all of the other inclusion compounds with aromatic guests are presented as Figures 3.17c, d, e, f and g. Although a number of the guest molecules have hydrogen-bonding donor or acceptor groups, all, except the amino group, are orientated away from the channel walls thus precluding any host-guest hydrogen-bonded interactions as may be seen in the packing diagrams.

The amino groups of aniline and *p*-amino-toluene are directed towards the hydrophilic pocket formed where O(28), O(27) and O(26) are partially exposed in the channel wall. The N•••O distances are however rather longer than might be expected in the case of hydrogen bonded groups being 3.17(2) Å for N1G•••O26 and 3.37(2) Å for N1G•••O27 in CAAN and 3.31(1) Å for N1G•••O28 and 3.23(1) Å for N1G•••O26 in CAPTOL. Assuming the amino hydrogen atoms to be coplanar with the aromatic ring (these could not be located in electron density difference maps) reveals that the geometry of the N-H•••O interaction is poor, indicating at best a very weak interaction. Figures 3.18a and b are stereograms indicating the positions of guest amino groups relative to the exposed host oxygen atoms.

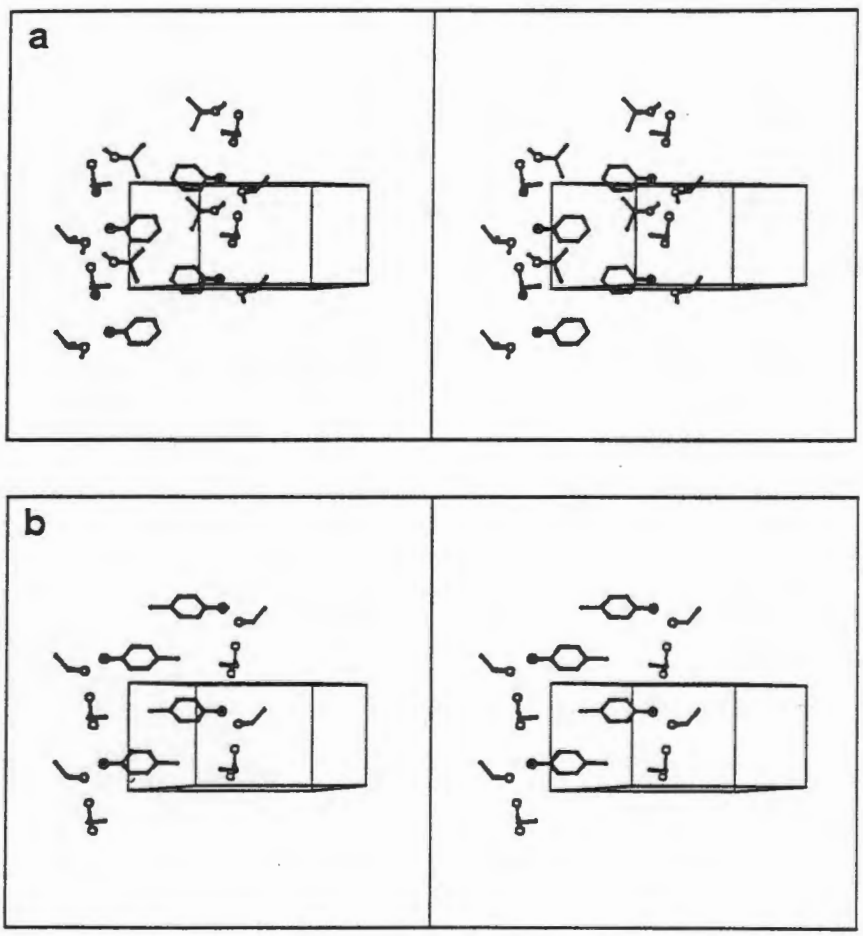

Figure 3.18: Stereograms of amino guests and host oxygen atom exposed in the channel walls. All other host atoms are removed for clarity and the guest nitrogen atoms shaded.

All of the aromatic guests included have polar groups attached to the central aromatic ring. The electron donating or withdrawing nature of each substituent group and thus the polarity of each guest is indicated in Figure 3.19. Comparison of these schematics with the packing diagrams indicated in Figure 3.17 reveals that the negative end of the guest dipole is, almost without exception, orientated towards the centre of the channel, hidden in the guest stack and far removed from any interaction with the channel walls. Even in the case of *p*-amino toluene, where both the amino and methyl groups are electron donating, the overall dipolar direction (the degree of donating character of CH_3 is less than that of NH_2) reflects that of the rest of the group. The only guest molecule which appears to partially violate this trend is *m*-nitro toluene where the NO_2 group is oriented towards the outside of the guest stack as may be seen in Figure 3.20b.

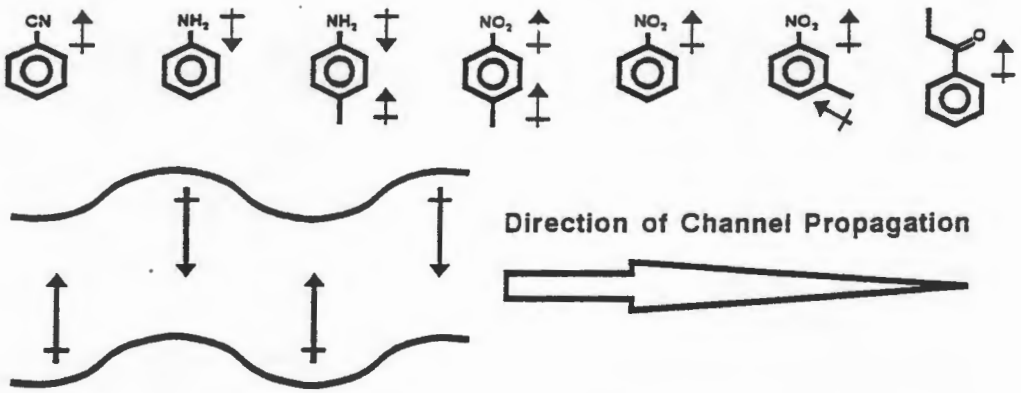

Figure 3.19: Schematic diagrams indicating electron withdrawing or donating nature of guest substituent groups as well as the relative orientation of the dipoles in the channels of the inclusion compounds.

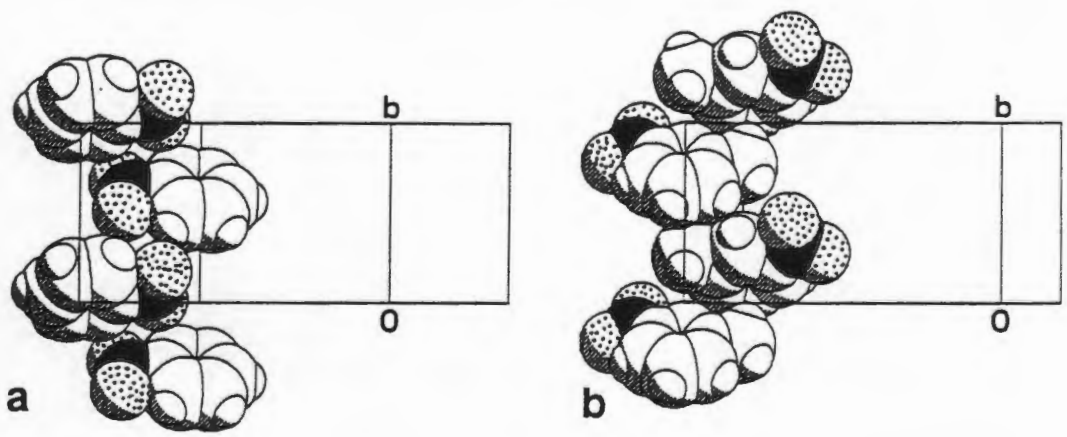

Figure 3.20: Space filling diagrams of the guests with host atoms removed viewed perpendicular to the channel direction which coincides with [010] a) CANI and b) CAMN. Oxygen atoms are speckled and nitrogen atoms shaded.

Group 5: Mixed guests: CAMI, CADC, CAAC.

	CAMI
Space Group	$P1$
H:G	1:½G_1:½G_2
Z	2
a / Å	12.289(2)
b / Å	8.238(4)
c / Å	14.246(3)
α / °	90.39(3)
β / °	105.83(1)
γ / °	94.97(2)

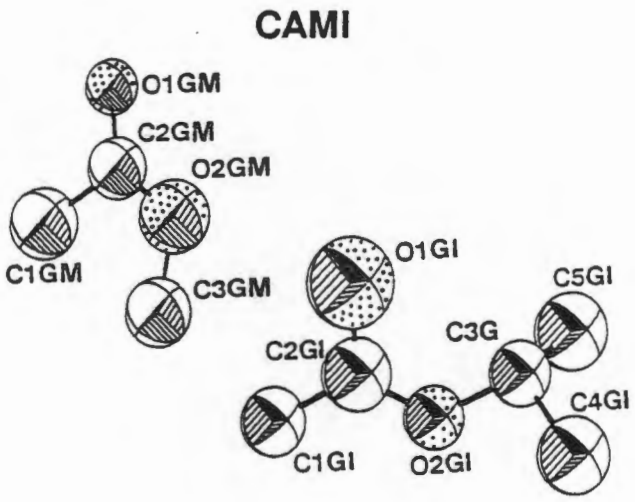

Crystals of CA inclusion compounds were grown from 1:1 solutions of mixtures of aliphatic esters. The resultant crystals appear to contain both guests in the same ratio as in solution. CAMI is an example of such a compound.

Refinement

There are, as in the case of all structures crystallising in the space group $P1$, two independent host molecules with slightly differing side chain conformations. Most non-hydrogen atoms of the host and guest were refined isotropically with the exception of the host oxygen atoms and side chain which were subjected to anisotropic refinement.

U values for geometrically generated hydrogen atoms refined to:

CAMI	CH_3	0.064(9) Å^2	CH_2	0.058(6) Å^2	CH	0.035(6) Å^2

Results

The packing diagram of CAMI is presented as Figure 3.21. The different guests pack alternately in the channel in a regular fashion as indicated in Figure 3.22. The 1:½:½ (H:G_1:G_2) stoichiometry is confirmed by weight loss % on TG analysis.

Crystals grown from 1:1 mixtures of other aliphatic esters also appeared to include both guests and the refined unit cell dimensions of the resultant crystals are presented in Table 3.1 along with those of the pure esters for comparison.

Weight loss percent on TG analysis (chapter 4) supports the assertion that these represent inclusion compounds containing mixed guests as does the change from $P2_1$ to $P1$ symmetry. Space group symmetry requires that alternate guests be identical in crystals of CA inclusion compounds with a 2_1-axis coincident with b. It would be reasonable to suppose that the crystals grown from methyl/ethyl or methyl/*n*-propyl acetate solutions would exhibit similar structures to CAMI with alternating guests packed into the channels formed between host bilayers.

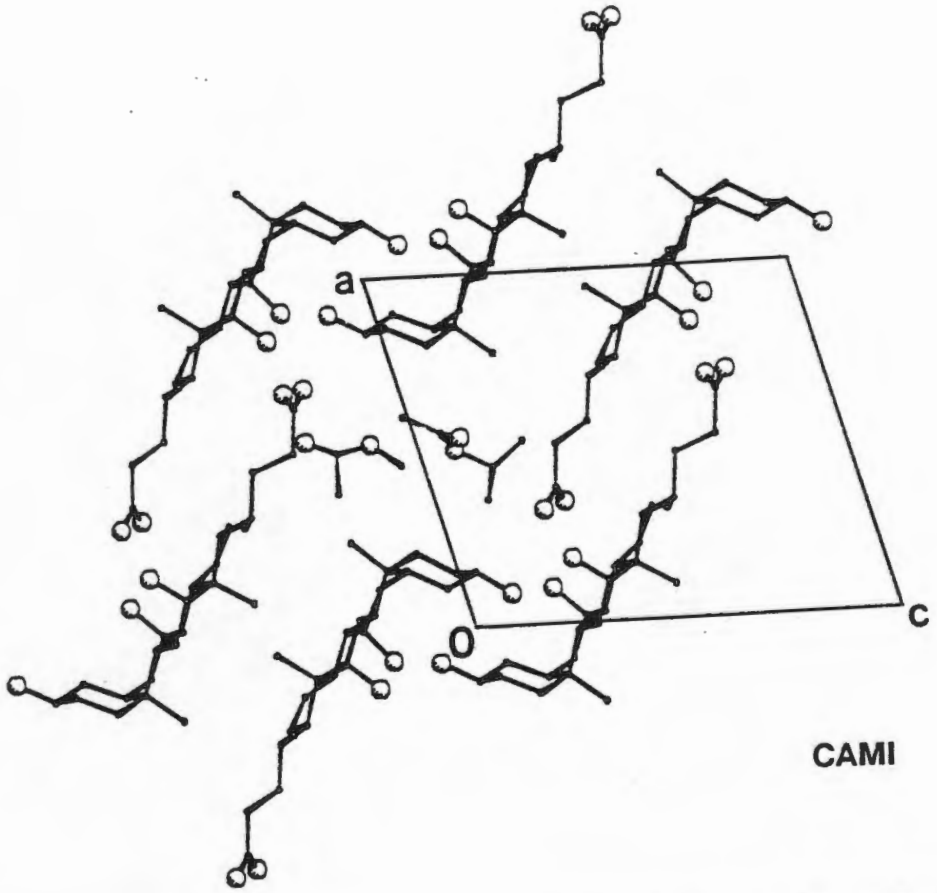

Figure 3.21: Packing diagram of the mixed guest compound CAMI viewed as a projection of (010). Both guests are visible in the same channel.

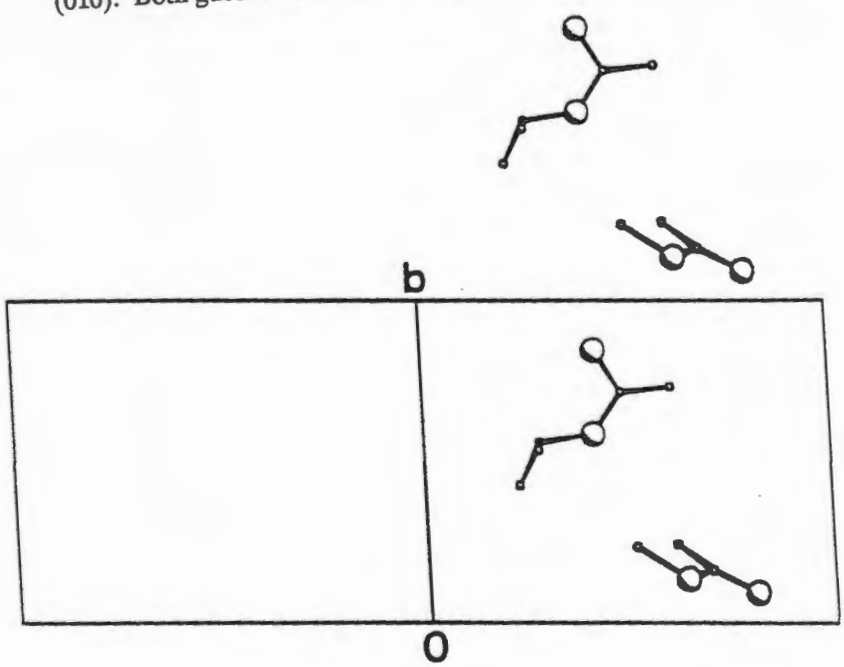

Figure 3.22: Methyl acetate and *i*-propyl acetate guests alternating in the channel of CAMI as viewed down [101].

Table 3.1 : Refined Unit Cell Parameters for CA Inclusion Compounds with Pure and Mixed Ester Guests.

	Methyl Acetate	Methyl Acetate/ Ethyl Acetate	Ethyl Acetate	Methyl Acetate/ n-Propyl Acetate	*n*-Propyl Acetate
Space Group	$P1$	$P1$	$P2_1$	$P1$	$P2_1$
a / Å	12.223(2)	12.283(2)	13.668(3)	12.325(3)	16.802(5)
b / Å	8.189(1)	8.229(2)	7.824(4)	8.262(2)	7.882(1)
c / Å	14.204(2)	14.236(2)	14.095(2)	14.249(2)	12.107(2)
α / ^{o}	90.18(1)	90.45(2)	90	90.77(1)	90
β / ^{o}	105.72(2)	106.04(1)	113.53(1)	106.30(2)	117.76(2)
γ / ^{o}	94.03(1)	94.30(2)	90	94.67(2)	90
V / Å^3	1364(5)	1378(4)	1382(8)	1387(7)	1415(7)

The volumes of the unit cells of the crystals grown from mixed guest solutions are intermediate between those of the pure guest crystals in each case.

	CADC
Space Group	*P*1
H:G	1:½G_1:½G_2
Z	2
a / Å	12.474(3)
b / Å	8.252(2)
c / Å	14.214(8)
α / °	91.09(3)
β / °	106.31(3)
γ / °	94.43(2)

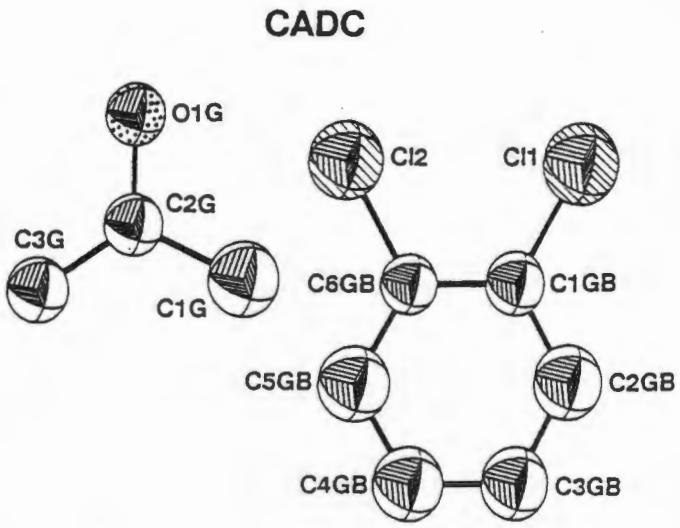

Refinement

All host non-hydrogen atoms were refined anisotropically and all guest non-hydrogen atoms isotropically. No guest or host hydroxyl group hydrogen atoms were included. The carbon atoms of the 1,2-dichlorobenzene guest were constrained to the geometry of a regular hexagon during refinement.

U values for geometrically generated hydrogen atoms refined to:

CADC | CH_3 0.052(11) Å^2 CH_2 0.029(6) Å^2 CH 0.035(8) Å^2

Results

The packing diagram of CADC is presented as Figure 3.23. 1,2-Dichlorobenzene and acetone guest molecules are contained in the same channels and this, together with the bilayer tilt angle relative to the normal to (101) results in loss of 2_1 symmetry.

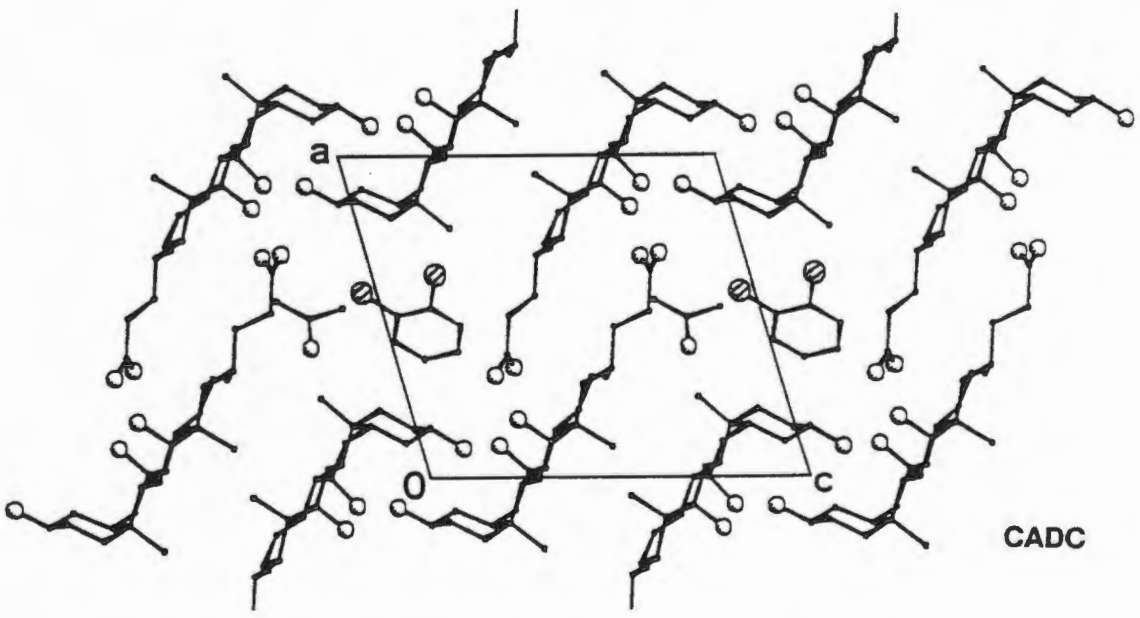

Figure 3.23: Packing diagram of CADC viewed as a projection of (101). Chlorine atoms are striped.

As with the mixed guest structure of CAMI the guests are found to pack alternately in the channel tilted at an angle of approximately 45° to the channel axis as illustrated in Figure 3.24. As is the case in most of the CA inclusion compounds there are no short range guest-guest or host-guest interactions.

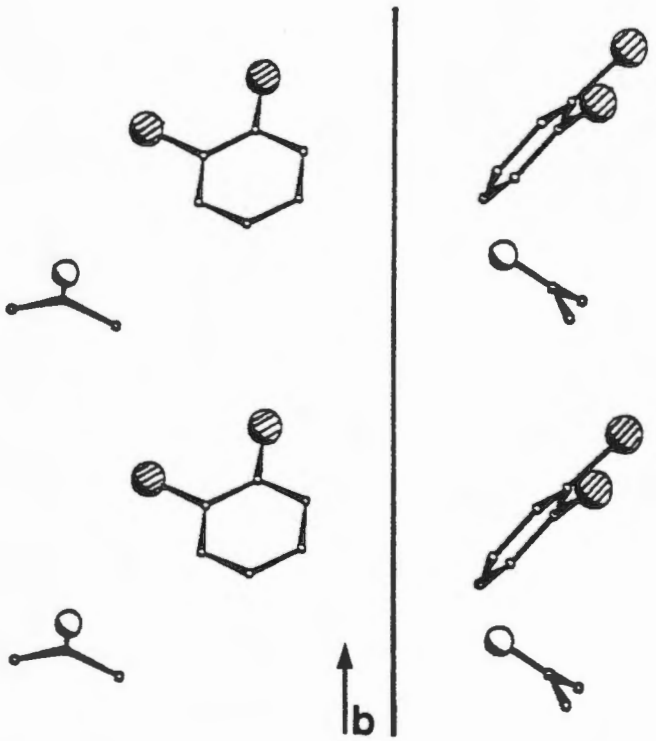

Figure 3.24: Acetone and 1,2-dichlorobenzene guests stacked alternately in the channel viewed perpendicular to the channel direction which is coincident with [010].

	CAAC
Space Group	$P2_1$
H:G	1:1:3
Z	2
a / Å	13.111(3)
b / Å	7.759(2)
c / Å	14.893(3)
α / °	90
β / °	105.70(2)
γ / °	90

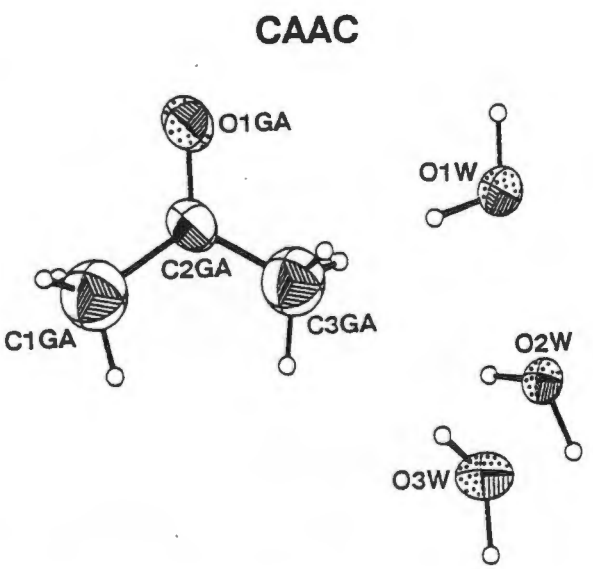

Refinement

All non-hydrogen atoms including oxygen atoms of the water molecules but excluding the acetone methyl carbon atoms were refined anisotropically. The hydroxyl group hydrogen atoms and those of the water molecules were located in electron density difference maps and refined with bond length restraints.

U values for geometrically generated hydrogen atoms refined to:

CAAC | CH_3 0.041(3) Å^2 CH_2 0.060(3) Å^2 CH 0.068(5) Å^2

Results

This structure is unusual amongst CA inclusion compound structures as the host-host hydrogen bonding system which is responsible for the formation of bilayers with largely hydrophobic exteriors is disrupted. There is instead extensive host-host and guest-guest as well as host-guest hydrogen bonding. Bilayers are formed but these are of a completely different composition from those seen in other structures in that the acetone and water molecules are an integral part of such layers as is illustrated in Figure 3.25.

There are ten unique hydrogen bonds in the asymmetric unit involving all potentially hydrogen bonded groups. These are illustrated in Figure 3.27. O•••O Distances, bond lengths and hydrogen bond angles are listed in Table 3.2. These ten unique hydrogen bonds translated along the screw axis at ½,y,½ form infinitely propagating hydrogen bonded spirals through the crystal in the *b* directions as illustrated in Figure 3.26. All host hydroxy oxygen atoms except O(28) act as hydrogen bond acceptors. O(1W) and O(2W) act as donors and acceptors for two hydrogen bonds each whilst O(3W) accepts only one hydrogen bond from O(1W) but donates two. The acetone guest molecule is held in the hydrogen bond network by a hydrogen bond from O(25) of the host.

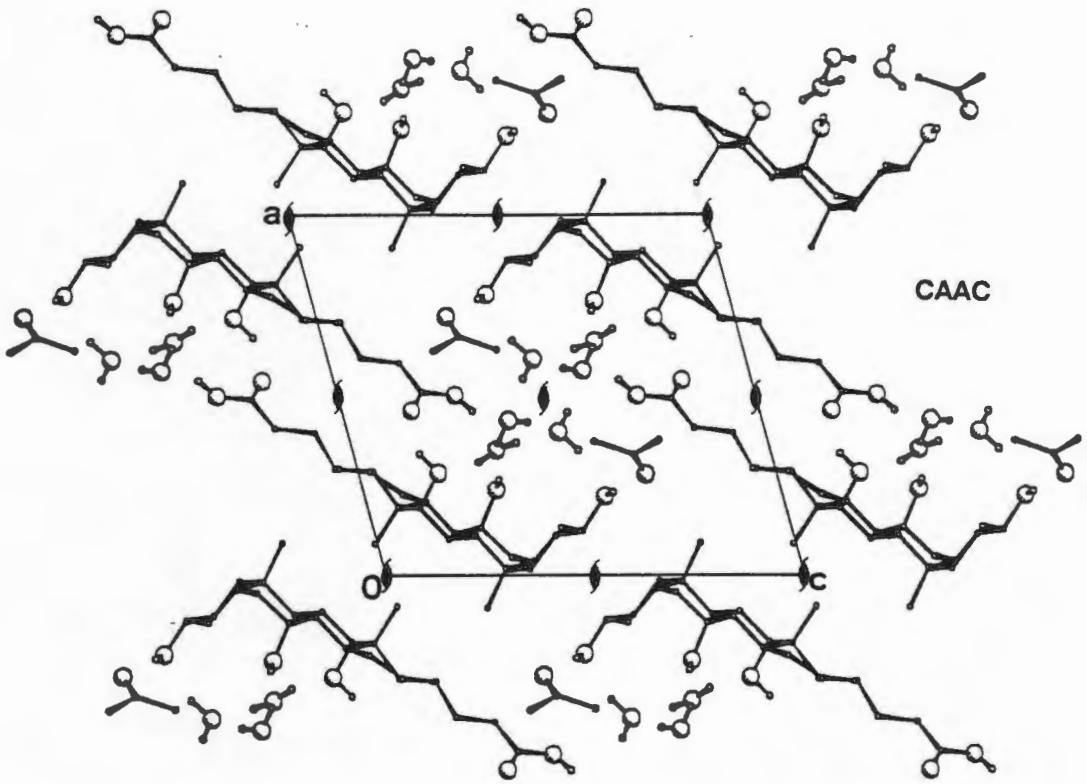

Figure 3.25: Packing diagram of CAAC viewed down [010]. All host and guest oxygen atoms are represented as large open circles.

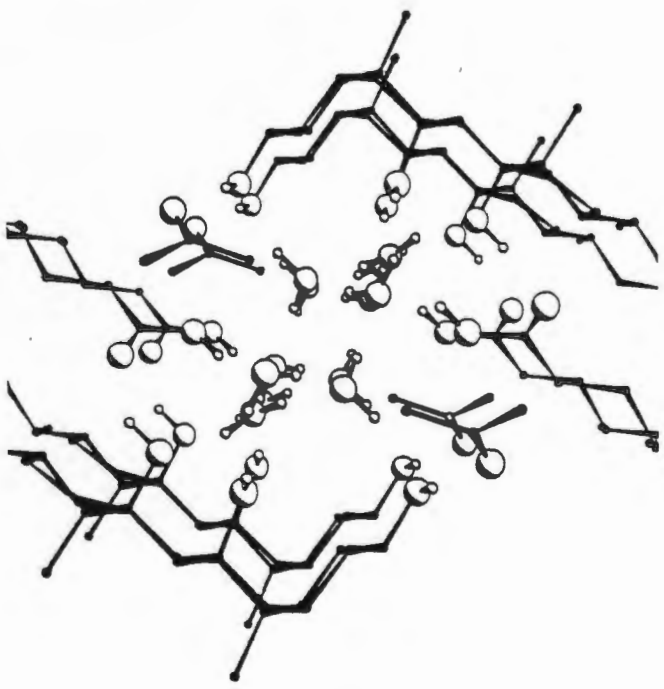

Figure 3.26: A perspective view of the infinitely propagating spiral hydrogen-bonded network. Two unit cell depths in y are indicated.

Table 3.2: Hydrogen Bonding Distances and Angles for CAAC.

		O•••O (Å)	O-H (Å)	H•••O (Å)	O-H•••O (°)
1	O(25)-H(25)•••O(1GA)	2.925(8)	0.95(3)	2.01(3)	159(2)
2	O(1W)-H(11W)•••O(25)	2.894(6)	0.96(6)	2.00(6)	154(5)
3	O(3W)-H(23W)•••O(1W)	2.931(8)	0.96(5)	1.99(5)	168(4)
4	O(26)-H(26)•••O(27)^{2}	2.733(6)	0.97(7)	1.93(8)	139(6)
5	O(2W)-H(12W)•••O(26)	2.676(6)	0.98)5)	1.73(5)	161(6)
6	O(28)^{1}-H(28)•••O(2W)^{3}	2.740(6)	0.97(10)	1.79(9)	165(8)
7	O(1W)-H(21W)•••O(3W)	2.792(6)	0.96(4)	1.84(4)	173(4)
8	O(3W)-H(13W)•••O(29)	2.844(6)	0.96(5)	1.93(6)	160(5)
9	O(29)^{2}-H(29)^{2}•••O(2W)^{3}	2.761(7)	0.96(3)	1.83(3)	163(3)
10	O(2W)-H(22W)•••O(1W)	2.772(6)	0.96(5)	1.82(5)	172(5)

1 x, y, z+1 2 -x+1, y-½, -z+1 3 -x+1, y+½, -z+1

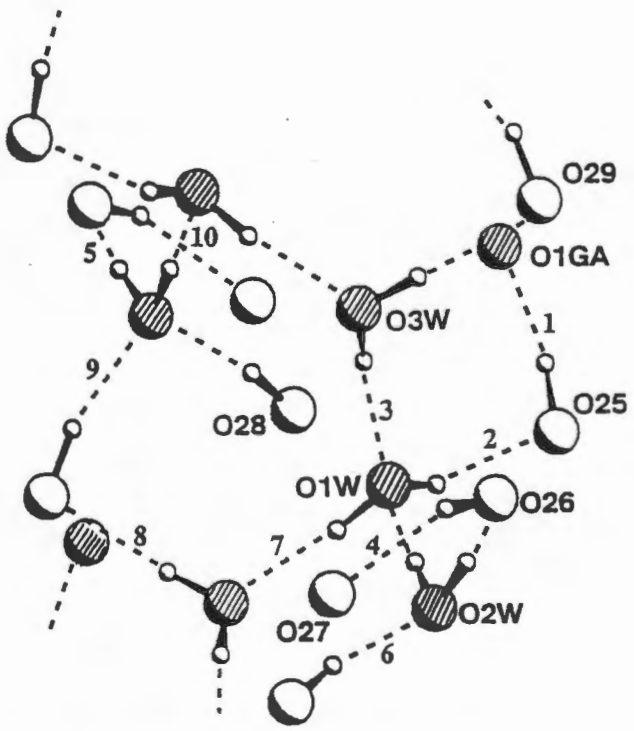

Figure 3.27: Hydrogen bonding network of CAAC viewed perpendicular to [010]. Guest acetone and water oxygen atoms are striped and all 10 unique hydrogen bonds indicated.

Group 6: Acetonitrile Structures: CACN, MCCN.

	CACN	MCCN
Space Group	$P2_1$	$P2_1$
H:G	1:1	1:1
Z	2	2
a / Å	9.645(2)	9.891(3)
b / Å	8.401(1)	8.390(2)
c / Å	15.747(4)	16.024(4)
α / °	90	90
β / °	101.01(2)	99.10(2)
γ / °	90	90

Both CA and MC form inclusion compounds with acetonitrile.

Refinement

All host non-hydrogen atoms were refined anisotropically. Hydroxyl hydrogen atoms were found in electron density difference maps and refined with bond length restraints for both host molecules. Guest non-hydrogen atoms of CACN were refined anisotropically and hydrogen atoms of the methyl group generated geometrically while those of MCCN were refined isotropically and no guest hydrogen atoms were included.

U values for geometrically generated hydrogen atoms refined to:

CACN	CH_3	0.060(5) Å^2	CH_2	0.048(3) Å^2	CH	0.025(3) Å^2
MCCN	CH_3	0.074(6) Å^2	CH_2	0.048(4) Å^2	CH	0.043(5) Å^2

Results

The structures of the inclusion compounds of CA and its methyl ester with acetonitrile are very similar as is obvious from the packing diagrams presented as Figures 3.28a and b. Unlike most of the inclusion compounds of CA the guest molecules are not accommodated in channels but in cavities completely isolated from neighbouring guest molecules as illustrated in Figure 3.29a and b.

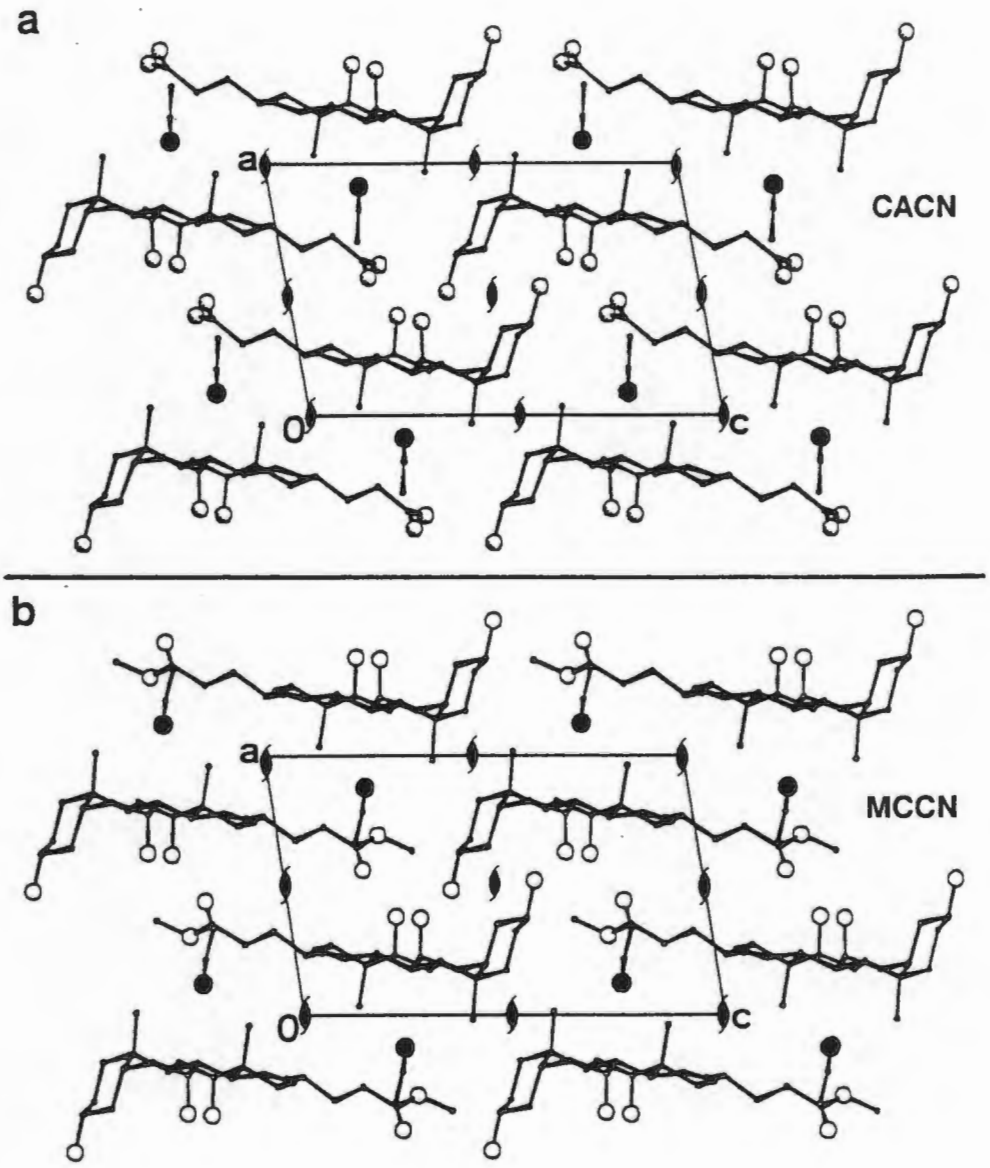

Figure 3.28: Packing diagrams of a) CACN and b) MCCN viewed down [010]. Guest nitrogen atoms are shaded.

The host-host hydrogen bonding system which facilitates formation of bilayers is disrupted in the compound with the methyl ester host as O(28) no longer participates in the hydrogen bonding scheme. The acid host bilayer structure is stabilised by the hydrogen bonding system: O(28)-H(28O)•••O(29)-H(29O)•••O(25)-H(25O)•••O(26)-H(26O)•••O(27) while the scheme of the ester host hydrogen bonding is O(26)-H(26O)•••O(25)-H(25O)•••O(29)-H(29O)•••O(27). The difference in the hydrogen bonding order is not necessarily due to the intervention of the ester group as similar behaviour has been noticed in otherwise isostructural compounds such as CAEP and CAIP as discussed before.

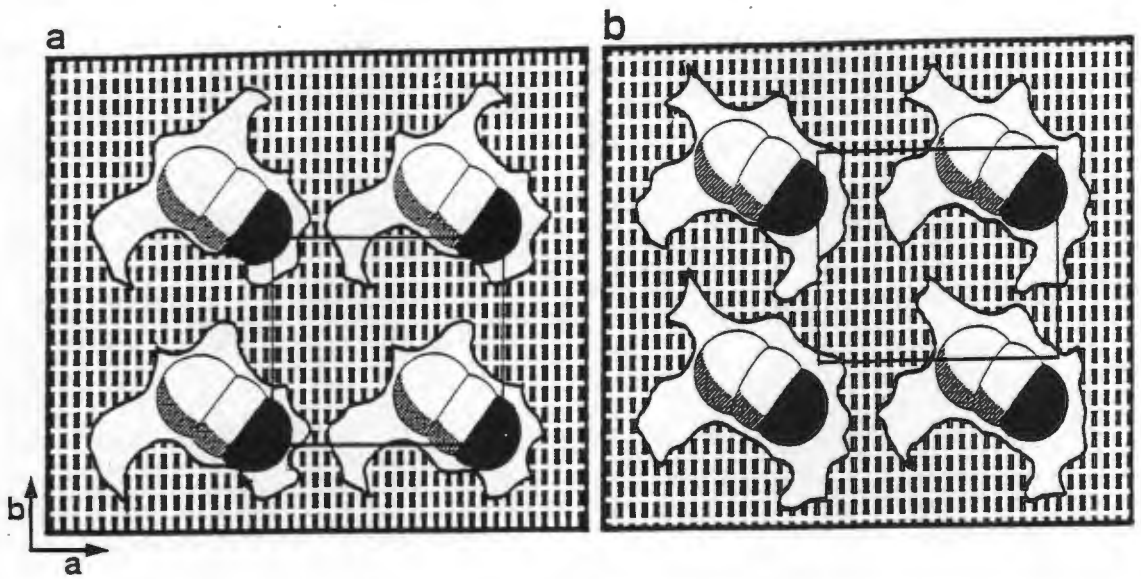

Figure 3.29: Slices perpendicular to the *c*-direction at z = 0.25 of a) CACN and b) MCCN indicating the cavities in which guest molecules are accommodated.

Side chain conformations of both the free acid and its methyl ester are similar, differing most in the orientation of the COOH and $COOCH_3$ groups as illustrated in Figure 3.30.

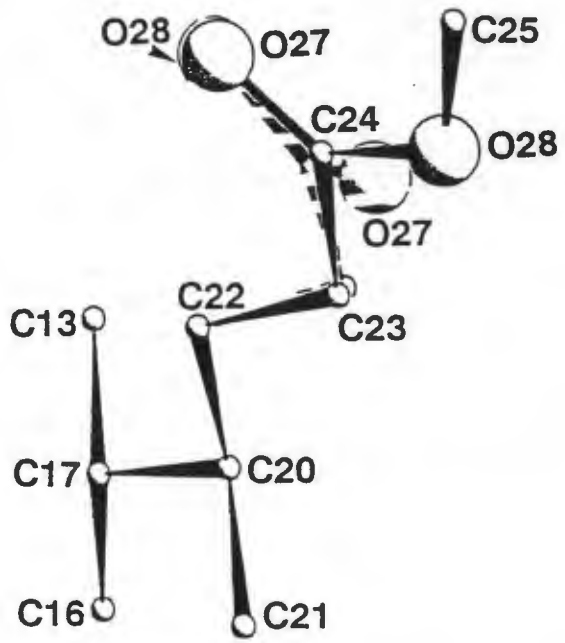

Figure 3.30: Comparison of the side chain conformations of the host molecules in CACN (broken line) and MCCN (solid line). Note the changes in orientation of the COOR group.

Group 7: α-Phase structures: MC(α)

	MC(α)	CA(α)[9]
Space Group	$P2_12_12$	$P2_12_12_1$
Z	8	4
a / Å	42.387(2)	16.477(4)
b / Å	14.563(3)	8.394(3)
c / Å	7.660(1)	16.993(3)
α / °	90	90
β / °	90	90
γ / °	90	90

Data for CA(α) from the structure by Miki *et al*[9] are included for comparison.

Refinement

All host non-hydrogen atoms except the oxygen and methyl carbon atoms of the terminal ester group were refined anisotropically. Host hydroxyl hydrogen atoms were located in electron density difference maps and refined with O-H bond lengths restraints.

Results

There are two independent MC molecules in the asymmetric unit of the MC(α) structure and these are labelled molecules A and B in the packing diagram, Figure 3.32. These exhibit very different side chain conformations, molecule B having the extended conformation while molecule A exhibits a puckered side chain conformation resulting in increased curvature of the steroid molecule as illustrated in Figure 3.31.

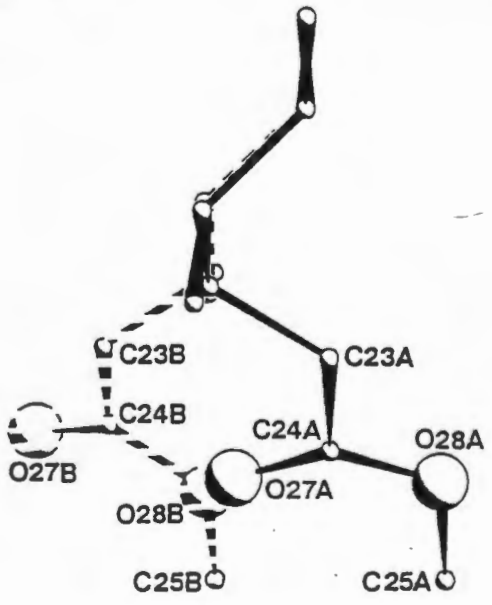

Figure 3.31: Comparison of the side chain conformations of hosts A and B of MC(α). These adopt puckered and extended conformations respectively.

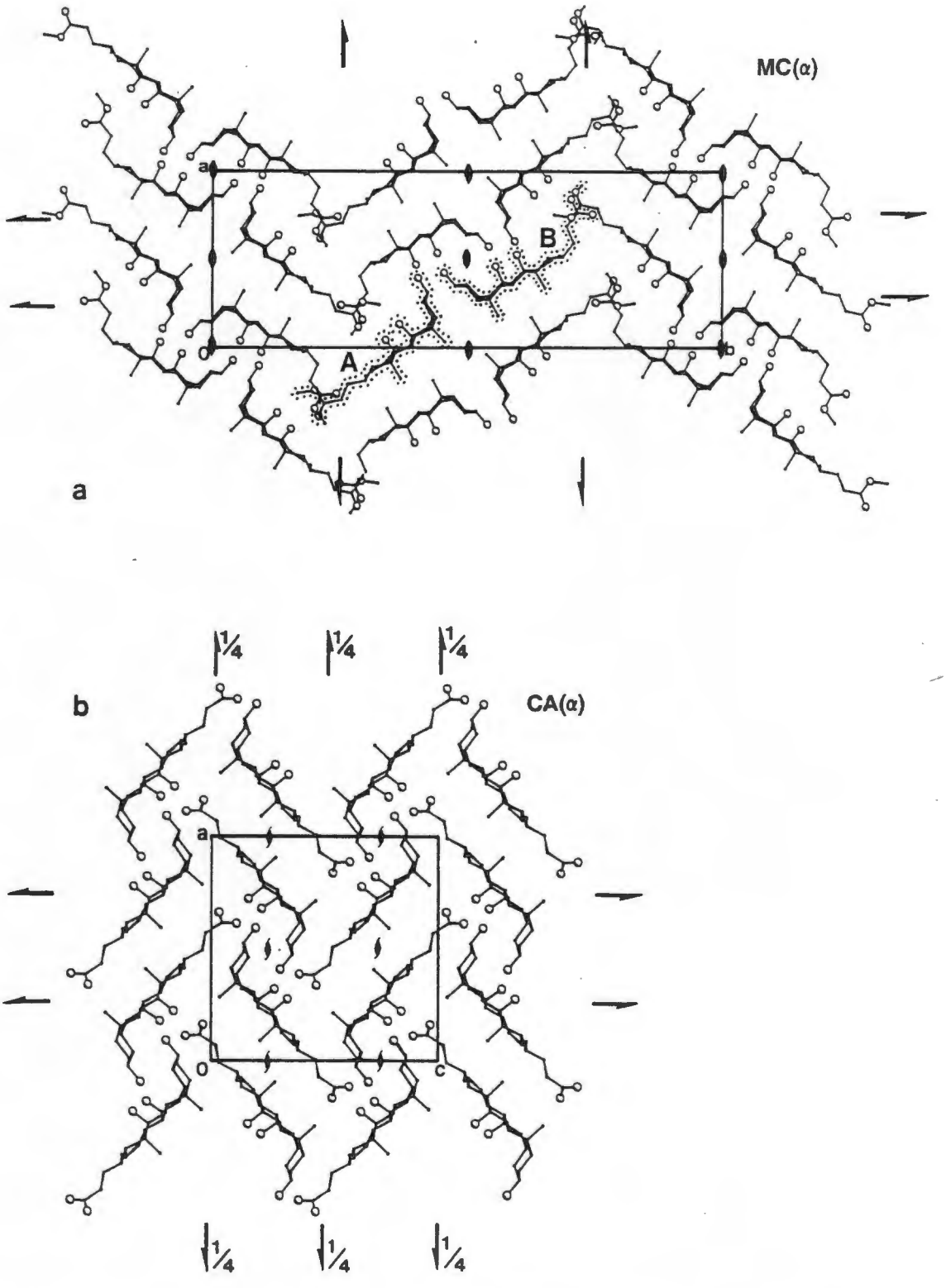

Figure 3.32: a) Packing diagram of MC(α) viewed down [001]. The crystallographically unique host molecules are indicated by dotted lines and labelled A and B. b) Packing diagram of CA(α) viewed down [010] produced from data derived from the structure by Miki *et al*[9].

The independent host molecules of the MC(α) phase with their significantly different conformations show very different hydrogen bonding schemes. Distances and angles defining the hydrogen bond schemes are detailed in Table 3.3 and the differences for MC hosts A and B are illustrated in Figure 3.33. A number of O-H•••O interactions which may appear possible from this diagram, (such as that between O(29B) and O(26B)), are at best very weak interactions with poor O-H•••O geometry and long O•••O distances. This contrasts strongly with the CA(α)[9] structure in which there is a single host molecule in the asymmetric unit and a very different hydrogen bonding scheme as illustrated in Figure 3.32b. It is of particular interest that the hydrogen bonding potential of the CA molecule is fully realised in the α-phase while that of the MC host molecule is not, a number of potentially hydrogen bonded groups being involved in only very weak interactions.

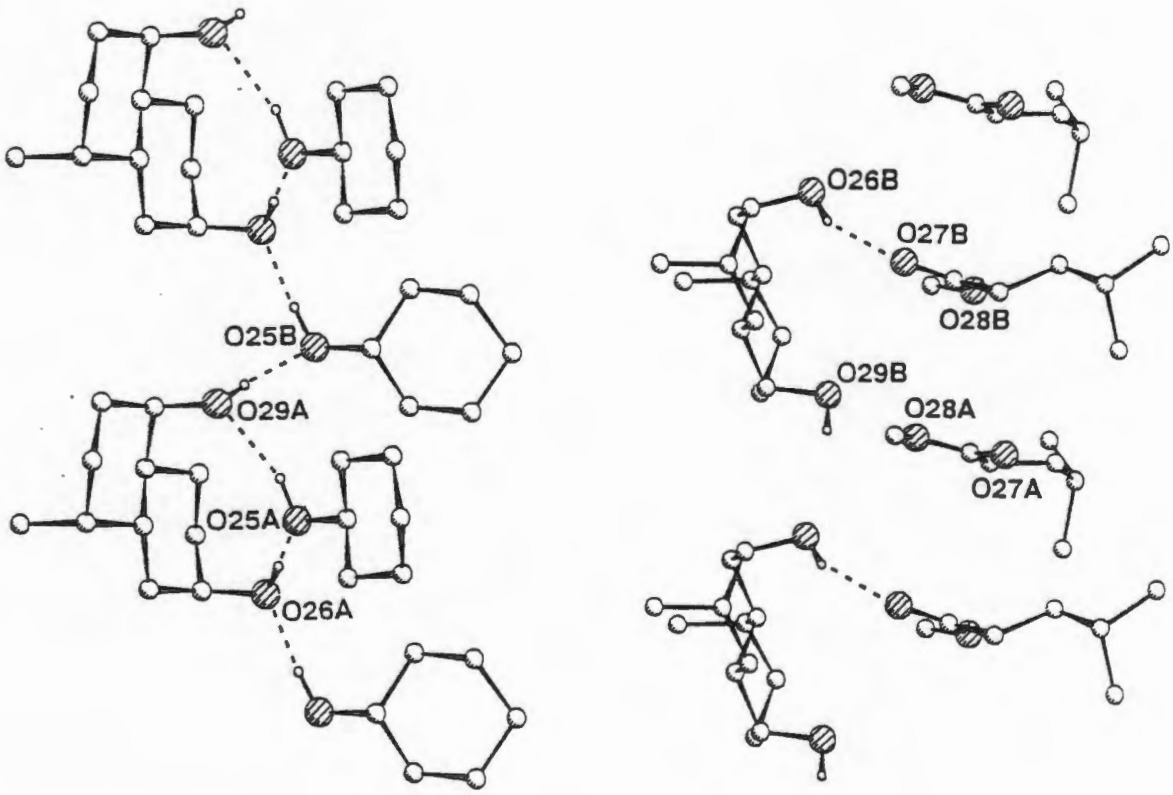

Figure 3.33: Illustration of the different hydrogen-bonding networks expressed in the structure of MC(α). Some oxygen atoms are not involved in hydrogen bonds either as donor or acceptor atoms.

Table 3.3: Hydrogen Bonding Schemes for MC(α).

	O•••O (Å)	H•••O (Å)	O-H•••O (°)
MC(α)			
O(25A)-H(5AO)•••O(29A)[a]	3.028(10)	2.10(4)	160(9)
O(29A)-H(9AO)•••O(25B)[b]	2.830(9)	1.90(2)	160(4)
O(25B)-H(5BO)•••O(26A)[a]	2.730(9)	1.78(3)	174(10)
O(26A)-H(6AO)•••O(25A)[a]	2.884(9)	1.93(2)	178(9)
O(26B)-H(6BO)•••O(27B)[c]	2.945(11)	2.05(5)	155(9)
O(29B)-H(9BO)•••O(26B)[d]	3.254(10)	2.82(7)	141(8)
O(29B)-H(9BO)•••O(28A)[e]	3.612(10)	2.50(8)	136(8)
CA(α) (Miki *et al.*[9])			
O(28)-H(28)•••O(26)	2.634	1.68	173
O(26)-H(26)•••O(25)	2.723	1.80	174
O(25)-H(25)•••O(29)	2.774	1.88	171
O(29)-H(29)•••O(27)	2.857	1.98	169

a -x+2, -y, z b -x-2, -y, z+1 c -x+1½, y-½, -z+1
d -x+2, -y, z-1 e x, y, -1+z

DISCUSSION

Given the similarities in most of the inclusion compounds of CA, it is instructive to examine the group as a whole.

A- and B- type structures

The A-type structure appears to be formed more frequently than the B-type. Of the nineteen structures of tubulate clathrate inclusion compounds formed by CA studied, only three exhibit the B-type packing motif: CAIP, CAPAC and CAPR. Analysis of the hydrogen bond patterns and distances as well as consideration of any other close contacts (both favourable and unfavourable) do not reveal the reason for this predominance of the A-type packing mode. Hydrogen bonding potential of the host molecules is completely fulfilled in either case and the O•••O lengths and O-H•••O angles are comparable.

It is probable that the appearance of the B-type packing mode is related to the fit of the guests in the differently shaped channel so produced. Since it appears that the guest is oriented with the electron-withdrawing end of the dipole away from the channel walls it might be possible to choose guests similar to propiophenone where the electron withdrawing substituent is not situated at an 'end' of the molecule and thereby force the formation of the B mode with its more elongated channel cross section.

Steroid Backbone Conformation

The fused ABCD steroid backbone has little conformational freedom and little difference is noted in the ring conformations in all of the structures studied.

Conformational analysis of each ring is achieved using the quantitative basis for analysis developed by Cremer and Pople[10] which allows expression of the geometry of puckering relative to a unique mean plane in terms of amplitude and phase. For six membered cyclohexyl type rings there are three puckering degrees of freedom which may be described by a 'spherical polar set'[10]: Q, θ and ϕ. The nomenclature of Boeyens[11] is used to describe the conformations of the six membered rings. For five membered cyclopentyl type rings there exist only two puckering degrees of freedom and these may be uniquely described in terms of Q and ϕ.

Values for the spherical polar coordinates describing the A, B and C rings of the steroid backbone of all structures studied are presented as Tables 3.4 and Q and ϕ for the D-rings as Table 3.5. The puckering amplitudes for each ring occur in a narrow range implying that the ring conformations are very similar.

All the six membered rings exhibit nearly perfect chair conformations as indicated by θ *ca* 180 ° or 0 ° corresponding to $^4C_1$ and $^1C_4$ conformations respectively. Translating these to the correspond to the numbering of the steroid backbone the conformations are $^4C_1$, $^8C_5$ and $^9C_{13}$ respectively. Examples of each are illustrated as Figures 3.34a, b and c.

Table 3.4: Parameters defining the conformations of the A, B and C rings.

		A-ring			B-ring			C-ring		
		Q	ϕ (°)	θ (°)	Q	ϕ (°)	θ (°)	Q	ϕ (°)	θ (°)
CAACD	A	0.533(18)	-95(10)	179(2)	0.548(20)	174(31)	176(2)	0.547(9)	-162(32)	4.0(20)
	B	0.570(21)	-83(21)	174(2)	0.595(21)	138(12)	170(2)	0.563(21)	164(37)	3.2(22)
CAMEK	A	0.554(10)	-172(14)	176.0(10)	0.547(9)	118(10)	174(9)	0.587(10)	164(5)	11.2(9)
	B	0.548(10)	-138(14)	176.0(10)	0.555(9)	148(7)	172(10)	0.543(9)	-153(10)	5.3(10)
CADEK		0.556(6)	-97(8)	175.6(6)	0.546(6)	123(6)	174.4(6)	0.567(6)	158(6)	5.4(6)
CAMA	A	0.550(10)	-128(12)	175.1(10)	0.561(10)	141(6)	170.6(10)	0.545(10)	-170(9)	6.2(10)
	B	0.547(9)	-93(14)	175.1(11)	0.551(8)	160(12)	175.4(10)	0.574(9)	152(10)	5.5(9)
CAET		0.563(7)	-96(13)	175.7(11)	0.542(7)	130(10)	176.3(7)	0.578(6)	145(6)	5.5(6)
CAEP		0.553(8)	-86(10)	176.3(7)	0.546(7)	155(9)	175.8(7)	0.565(6)	145(8)	4.3(6)
CAPAC		0.546(8)	-89(10)	175.1(9)	0.545(8)	139(11)	176.1(8)	0.581(7)	167(8)	4.5(7)
CAIP		0.553(7)	-73(10)	175.9(7)	0.543(6)	133(9)	175.8(7)	0.558(7)	156(9)	3.9(6)
CAVA	A	0.550(6)	-134(7)	175.3(6)	0.564(7)	133(5)	172.7(7)	0.548(6)	-174(7)	5.5(6)
	B	0.546(6)	-101(10)	176.1(7)	0.541(5)	152(7)	175.1(6)	0.565(6)	151(7)	4.9(6)
CAMM		0.550(4)	-104(6)	175.3(5)	0.550(4)	140(5)	175.0(5)	0.569(4)	151(6)	4.3(4)
CABN		0.542(8)	-92(19)	177.3(8)	0.557(8)	158(7)	173.9(8)	0.575(8)	146(11)	3.7(8)
CAAN		0.552(6)	-93(8)	175.6(7)	0.541(6)	152(6)	173.7(6)	0.555(5)	117(12)	2.8(5)
CANI		0.564(6)	-111(11)	176.9(6)	0.539(6)	142(6)	173.8(6)	0.572(6)	167(8)	4.1(6)
CAPR		0.556(5)	-83(9)	176.2(5)	0.541(5)	144(7)	176.0(5)	0.580(5)	107(19)	1.4(4)
CAPTOL		0.552(7)	-102(13)	176.8(7)	0.545(6)	148(6)	173.6(7)	0.567(7)	156(8)	4.1(6)
CAPNOT		0.558(8)	-91(10)	175.5(9)	0.546(7)	122(9)	175.0(8)	0.565(7)	147(11)	4.3(7)
CAMN		0.567(3)	-71(5)	175.1(4)	0.546(3)	141(2)	175.3(4)	0.563(3)	151(6)	3.4(3)
CAMI	A	0.552(11)	-106(18)	175.7(11)	0.549(12)	149(13)	175.3(11)	0.581(11)	146(14)	4.3(10)
	B	0.539(11)	-125(14)	175.2(13)	0.569(11)	154(8)	172.2(11)	0.544(11)	179(13)	5.0(11)
CADC	A	0.564(11)	-135(20)	176.4(11)	0.563(12)	156.2(10)	174(1)	0.547(11)	-158(10)	6.5(11)
	B	0.549(11)	-146(23)	176.8(12)	0.525(9)	165(14)	175(1)	0.543(11)	138(12)	4.9(11)
CAAC		0.543(5)	-116(9)	176.6(5)	0.564(4)	153(5)	174.8(5)	0.564(4)	158(6)	3.8(4)
CACN		0.555(4)	-1332(5)	175.4(4)	0.572(4)	140(2)	169.7(4)	0.551(4)	-170(3)	7.6(4)
MCCN		0.558(6)	-133(10)	176.5(5)	0.565(5)	158(4)	171.7(5)	0.548(5)	166(6)	5.6(5)
MC(α)	A	0.552(9)	-106(8)	172.7(9)	0.569(8)	107(6)	172.3(9)	0.539(9)	176(5)	10.8(9)
	B	0.563(8)	-117(8)	174.1(8)	0.554(8)	178(7)	172.2(9)	0.559(9)	106(6)	1.9(7)

The relationship of these rings to each other in the fused system is illustrated in Figure 3.35.

The strained five membered D-ring exhibits slightly greater conformational flexibility as evidenced by the greater spread of ϕ values noted in the different structures as listed in Table 3.5.

Table 3.5: Conformational Parameters defining D-ring conformation.

		Q	ϕ (°)
CAACD	A	0.452(19)	-160.6(29)
	B	0.484(21)	-174.1(24)
CAMEK	A	0.478(9)	-162.0(12)
	B	0.467(8)	-175.3(12)
CADEK		0.469(5)	-169.4(6)
CAMA	A	0.470(10)	-173.1(12)
	B	0.464(9)	-165.7(13)
CAET		0.470(6)	-164.9(8)
CAEP		0.460(6)	-165.9(8)
CAPAC		0.468(7)	-166.7(9)
CAIP		0.462(6)	-166.9(8)
CAVA	A	0.474(6)	-173.1(7)
	B	0.458(6)	-163.6(8)
CAMM		0.465(4)	-167.0(5)
CABN		0.481(8)	-171.1(13)
CAAN		0.459(6)	-167.8(7)
CANI		0.474(5)	-167.2(6)
CAPR		0.480(5)	-168.4(6)
CAPTOL		0.467(6)	-169.5(7)
CAPNOT		0.489(7)	-168.2(8)
CAMN		0.467(3)	-166.8(5)
CAMI	A	0.464(9)	-164.0(14)
	B	0.463(10)	-170.6(13)
CADC	A	0.481(11)	-171.1(13)
	B	0.464(10)	-164.3(16)
CAAC		0.465(4)	-169.9(5)
CACN		0.464(4)	-169.6(5)
MCCN		0.456(5)	-178.9(8)
MC(α)	A	0.448(9)	-171.6(12)
	B	0.450(8)	-175.4(11)

These correspond to conformations between $^{14}H_{13}$ and E_{13} or in other words a half-chair conformation with C(14) (α) and C(13) (β) or an envelope conformation with C(13) (β). An examination of the endocyclic torsion angles (presented in Table 3.6) defining the ring conformation confirms the E_{13} / $^{14}H_{13}$ character of this ring. The angle τ_{D3} is significantly smaller than all other

angles yet significantly greater than zero as required for a perfect envelope conformation with C(13) below the plane. Figure 3.36 illustrates the relationship between these angles and those expected in the two conformational forms between which all the D-ring conformations fall.

Table 3.6: Endocyclic Torsion Angles Defining the D-ring conformations.
τ_{D1} = C(17)-C(13)-C(14)-C(15), τ_{D2} = C(13)-C(14)-C(15)-C(16),
τ_{D3} = C(14)-C(15)-C(16)-C(17), τ_{D4} = C(15)-C(16)-C(17)-C(13),
τ_{D5} = C(16)-C(17)-C(13)-C(14)

		τ_{D1} (°)	τ_{D2} (°)	τ_{D3} (°)	τ_{D4} (°)	τ_{D5} (°)
CAACD	A	46.6(19)	-38.4(19)	14.5(21)	13.1(21)	-37.0(20)
	B	47.8(18)	-33.6(20)	5.2(21)	24.2(20)	-42.9(18)
CAMEK	A	48.5(8)	-39.3(9)	15.3(10)	14.6(10)	-38.1(8)
	B	46.6(9)	-31.9(9)	4.2(10)	24.2(9)	-41.9(8)
CADEK		47.6(6)	-35.6(6)	9.1(7)	20.0(6)	-40.2(6)
CAMA	A	46.5(8)	-32.8(9)	5.7(15)	23.3(9)	-42.3(8)
	B	46.9(8)	-36.9(9)	12.0(10)	16.7(9)	-38.2(8)
CAET		47.8(9)	-37.9(10)	12.7(10)	16.6(10)	-38.3(9)
CAEP		46.7(5)	-36.7(6)	11.5(7)	17.3(6)	-38.4(6)
CAPAC		47.5(7)	-36.4(7)	10.7(8)	18.2(8)	-39.5(7)
CAIP		47.1(6)	-36.5(7)	10.9(7)	18.1(7)	-39.1(6)
CAVA	A	47.6(5)	-34.0(5)	5.6(6)	23.3(6)	-42.4(5)
	B	46.4(5)	-37.3(5)	13.1(6)	15.5(6)	-37.5(5)
CAMM		48.1(9)	-35.8(10)	8.1(11)	22.3(10)	-41.7(9)
CABN		49.0(8)	-37.4(8)	11.1(9)	18.9(9)	-40.6(8)
CAAN		47.0(6)	-36.0(7)	10.1(7)	18.6(7)	-39.7(6)
CANI		48.0(6)	-36.8(6)	10.7(7)	18.9(7)	-40.1(6)
CAPR		48.6(5)	-36.7(6)	10.0(6)	19.8(6)	-40.7(5)
CAPTOL		46.9(5)	-34.8(6)	8.8(7)	20.4(6)	-40.4(5)
CAPNOT		49.8(6)	-37.1(7)	9.9(7)	20.5(7)	-42.2(6)
CAMN		47.6(4)	-37.0(4)	11.0(4)	18.1(4)	-32.2(4)
CAMI	A	47.8(9)	-38.2(10)	13.3(11)	15.5(11)	-38.0(9)
	B	46.6(9)	-34.1(10)	7.7(10)	21.1(9)	-41.1(8)
CADC	A	48.1(9)	-35.8(10)	8.1(11)	22.3(10)	-41.7(9)
	B	47.3(9)	-37.2(10)	13.3(12)	16.5(12)	-38.3(10)
CAAC		47.2(4)	-34.6(5)	8.3(5)	20.3(5)	-40.6(4)
CACN		47.4(4)	-35.0(4)	8.8(5)	20.2(5)	-40.5(4)
MCCN		46.6(6)	-33.7(6)	7.4(7)	20.9(7)	-40.3(6)
MC(a)	A	45.9(8)	-32.9(9)	6.7(10)	21.1(9)	-40.3(8)
	B	47.1(8)	-32.6(9)	4.3(10)	24.5(9)	-43.6(8)

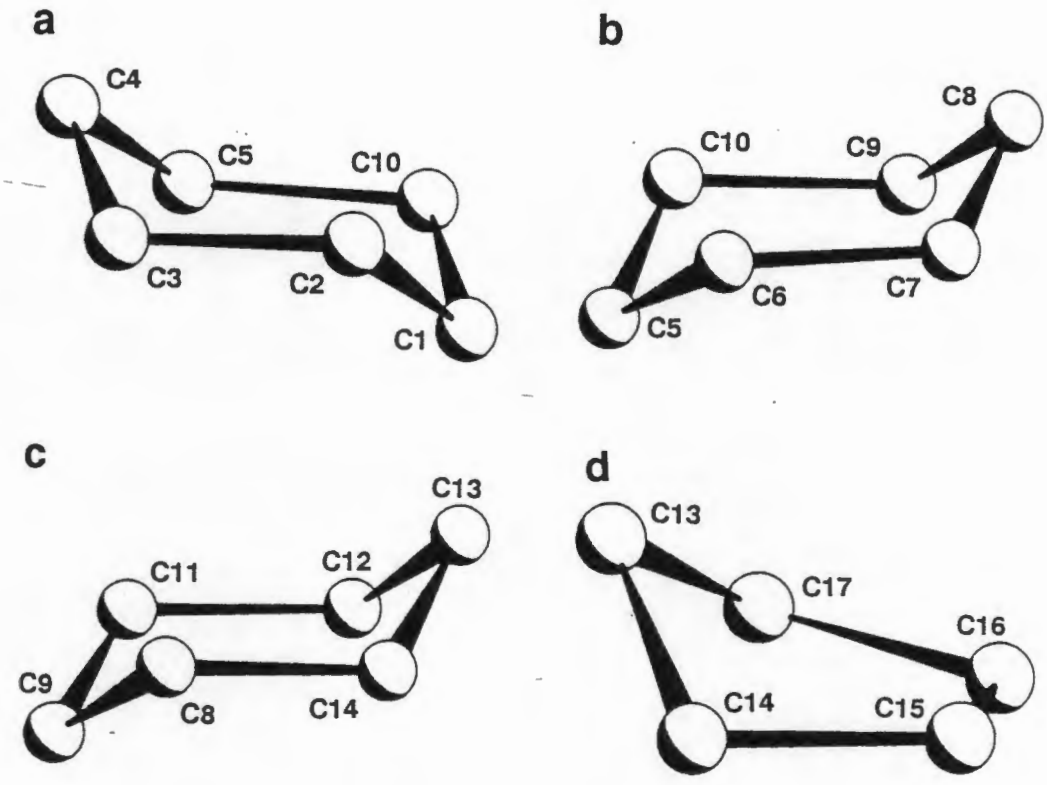

Figure 3.34: Conformations of the steroid backbone rings.

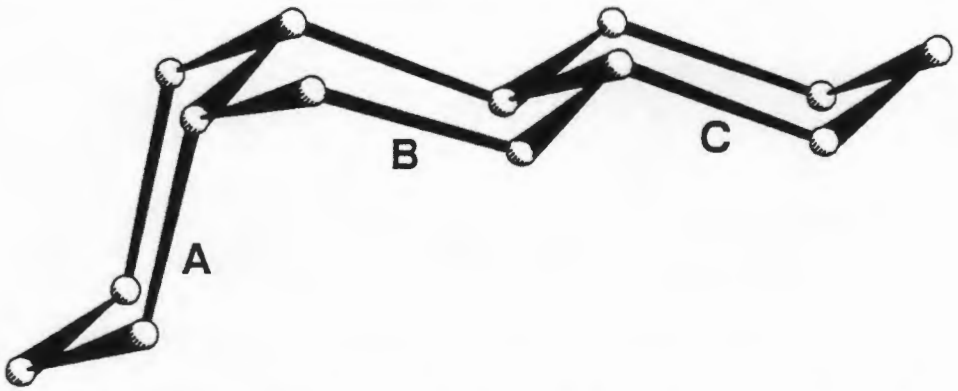

Figure 3.35: Conformation of the ABCD rings in the fused ring system that constitutes the steroid backbone.

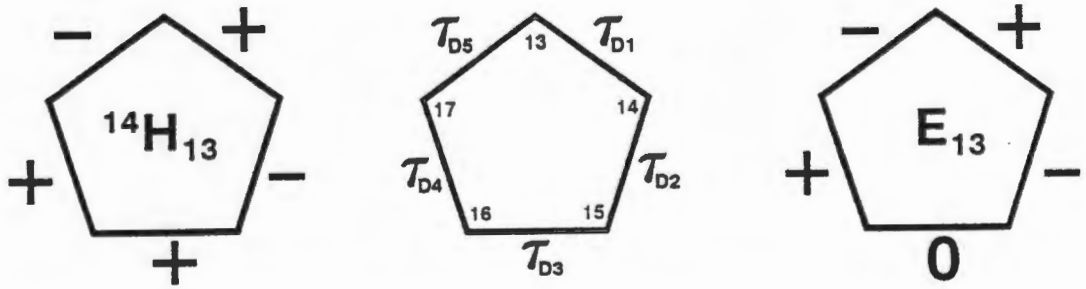

Figure 3.36: Signs for the endocyclic torsion angles of the steroid D-ring for the pure half-chair conformation with C(14) up and C(13) down (left) and that of the pure envelope conformation with C(13) out of the plane (right). The numbering of the torsion angles is illustrated at centre.

The conformations noted for the D-ring are within the range defined by Thomas[12] for similar steroid structures where the C/D ring fusion is trans and the substituent at position 17 is acyclic and other than a keto group.

Twist of the steroid backbone may be measured by consideration of the non-bonded- or pseudo-torsion angle C(19)-C(10)•••C(13)-C(18) as described by Duax and Norton[13]. In all of the structures studied this angle approaches 0 ^{o} indicating no twist along the steroid backbone. An example is illustrated in Figure 3.37.

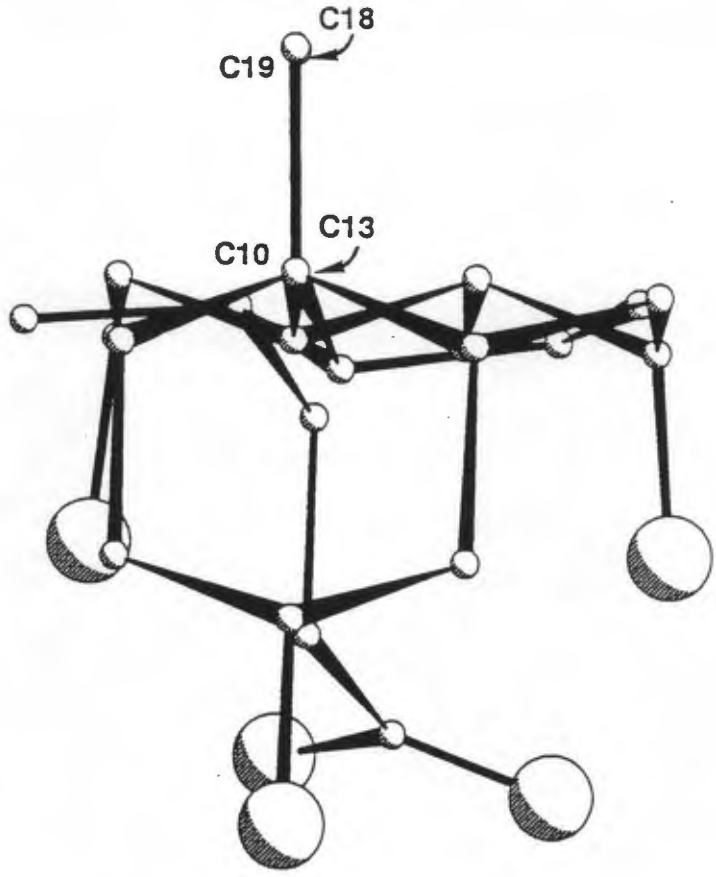

Figure 3.37: View along the steroid backbone from C(10) to C(13) illustrating the coincidence of C(19) and C(18) indicative of a value close to 0 ^{o} for the pseudo-torsion angle C(19)-C(10)•••C(13)-C(18).

Side Chain Conformation

Table 3.7 lists the torsion angles which uniquely define the side chain conformation of all structures studied and Figure 3.38 indicates the choice of torsion angles used. The MC structures as well as those of CACN and CAAC are separated from the rest as these differ from the typical tubulate clathrate structures exhibited by the majority of CA inclusion compounds. Clearly τ_1 and τ_3 are almost invariant being in the range -170 to 170^{o} i.e. adopting a trans conformation. This allows for the least intramolecular interaction but according to calculations of van der Waals energy of the side chain of cholanic acids does not, in fact represent the minimum energy conformation for these bonds[14]. τ_2 and τ_4 (and thus τ_5) are not invariant and define the differences in

side chain conformation as exhibited by these structures. These are indicated in the bar charts Figure 3.39a and b. τ_4 and τ_5 are not independent of each other defining, as they do, the orientation of the carboxylic acid group relative to the C(23)-C(24) bond. C(23), C(24), O(27) and O(28) are constrained to planarity by the sp^2 hybridisation of C(24), thus $\tau_5 = (180 - |\tau_4|)$.

Values for the torsion angle τ_2 are plotted as Figure 3.39a. Clearly there exist two groups of structures with τ_2 in the range 55 to 65° or -155 to -180°. These values are similar to those corresponding to minima in the van der Waals energy as calculated by Giglio and Quagliata[14] (τ_2 = 60 or -170°). Only host A of CAMI exhibits the angle τ_3 corresponding to the value calculated to represent the minimum energy conformation (τ_3 = -50°). This phenomenon is noted by the abovementioned authors: "..it seems probable that the higher van der Waals energy of the more extended conformations is largely counterbalanced by the energy gain due to the formation of more hydrogen bonds,..." to which might be added: and the gain in energy due to the inclusion of a guest species in the host framework.

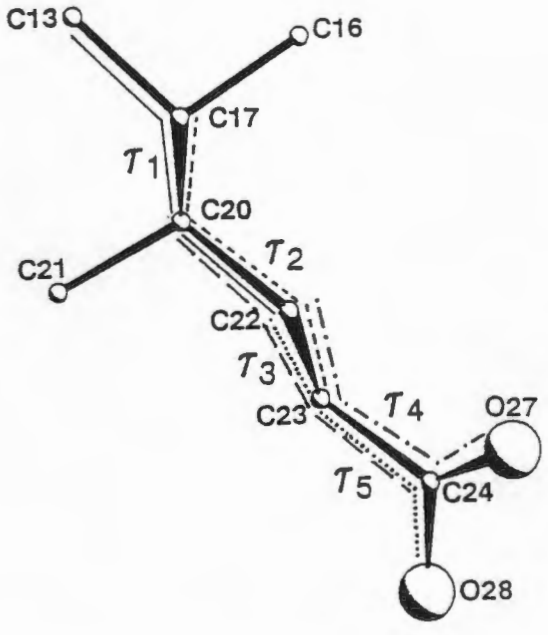

Figure 3.38: Torsion angles uniquely defining the CA side chain.

These two ranges for τ_3 represent, respectively, the puckered and extended side chain conformations and result in a difference in the overall "length" of the host molecule as illustrated in Figure 3.40. As mentioned before this in turn affects the dimensions and cross-sectional shape of the channel and is also reflected in the angle of intersection of a and c. The β angle for the structures in which the host is puckered are in the range 113.5 - 115.2 ° while those with an extended host conformation are in the range 102.6 - 106.3° for the A-type structures as illustrated in Figure 3.41. While there are only three structures of the B-type these too appear to exhibit the same trend: CAIP, CAPAC exhibit the puckered host conformation and β = 117.76° and 118.06° respectively while the CAPR

host exhibits the extended conformation and has β = 114.25 °.

As mentioned in the discussion of individual structures above, there is no preferred orientation of the COOH group and it may adopt one of two possible conformations without consequence to the host-host hydrogen bonding schemes (except a change of direction of donor and acceptor interactions). To maintain the correct geometry for hydrogen bond formation in spite of variation in τ_3 the angle τ_4 (and hence τ_5) must vary. This is reflected in Figures 3.39a and b which illustrates that $\tau_{4/5}$ is below a threshold value of 99.0 ° for the structures with puckered host and above 125 ° for those with extended host conformation.

Table 3.7: Torsion Angles Defining Side-chain configuration.
τ_1 = C(13)-C(17)-C(20)-C(22), τ_2 = C(17)-C(20)-C(22)-C(23),
τ_3 = C(20)-C(22)-C(23)-C(24), τ_4 = C(22)-C(23)-C(24)-O(28),
τ_5 = C(22)-C(23)-C(24)-O(27)

		τ_1 (°)	τ_2 (°)	τ_3 (°)	τ_4 (°)	τ_5 (°)
CAACD	A	-176.7(18)	-155.9(17)	-176.2(18)	131.2(22)	-52.6(27)
	B	-177.8(16)	-174.3(17)	178.4(17)	-24.4(30)	157.5(19)
CAMEK	A	177.8(8)	-156.4(9)	-174.4(10)	128.7(11)	-52.0(13)
	B	-178.0(8)	-165.2(10)	-178.3(10)	-33.6(19)	146.9(11)
CADEK		178.9(5)	-166.2(6)	177.7(6)	-32.7(11)	146.0(7)
CAMA	A	-177.5(6)	-166.5(6)	179.0(6)	-28.9(11)	156.5(9)
	B	179.2(5)	-159.4(6)	-174.7(6)	132.6(8)	-50.0(9)
CAET		178.0(5)	65.2(8)	-168.7(7)	-107.0(10)	71.7(9)
CAEP		179.1(5)	65.7(7)	-172.5(6)	78.5(9)	-100.9(8)
CAPAC		176.5(6)	65.6(9)	-169.0(8)	-111.4(19)	73.1(11)
CAIP		176.7(5)	62.9(8)	-174.7(9)	86.3(10)	-92.6(8)
CAVA	A	-176.2(5)	-167.0(5)	177.5(5)	-27.7(9)	150.2(5)
	B	-179.8(5)	-158.3(5)	-175.4(5)	-49.7(8)	130.5(7)
CAMM		176.7(4)	59.5(5)	-173.5(4)	91.3(6)	-88.1(5)
CABN		177.7(7)	59.0(10)	-173.6(8)	85.5(13)	-94.1(11)
CAAN		-179.8(6)	60.3(8)	173.2(6)	84.6(10)	-95.0(8)
CANI		177.5(6)	59.98(8)	-175.0(6)	85.8(10)	-94.1(9)
CAPR		-178.7(5)	-169.7(5)	177.0(5)	-31.2(9)	147.4(6)
CAPTOL		178.4(5)	61.2(7)	-174.5(6)	82.5(9)	-94.6(7)
CAPNOT		177.3(6)	54.7(9)	-177.1(7)	99.0(9)	-83.9(8)
CAMN		178.7(3)	-166.6(4)	170.0(4)	-39.7(6)	141.7(4)
CADC	A	-175.5(9)	-171.8(9)	174.3(10)	-25.0(18)	155.6(10)
	B	-179.4(9)	-155.5(9)	-172.5(9)	125.1(13)	-54.6(13)
CAMI	A	179.7(9)	-157.9(9)	-56.1(9)	127.3(12)	-52.6(13)
	B	-176.4(7)	-165.8(8)	120.0(9)	-30.8(16)	148.7(10)
CAAC		177.1(4)	-177.3(4)	166.5(4)	0.7(8)	177.6(5)
CACN		-177.2(4)	-164.1(4)	-172.3(4)	142.6(5)	-37.7(6)
MCCN		-178.4(5)	169.8(6)	-175.0(6)	-6.1(12)	174.8(6)
MC(α)	A	-178.4(5)	60.0(10)	170.7(10)	-14.4(18)	163.8(12)
	B	174.7(7)	-165.4(8)	-175.1(9)	-133.9(13)	48.4(14)

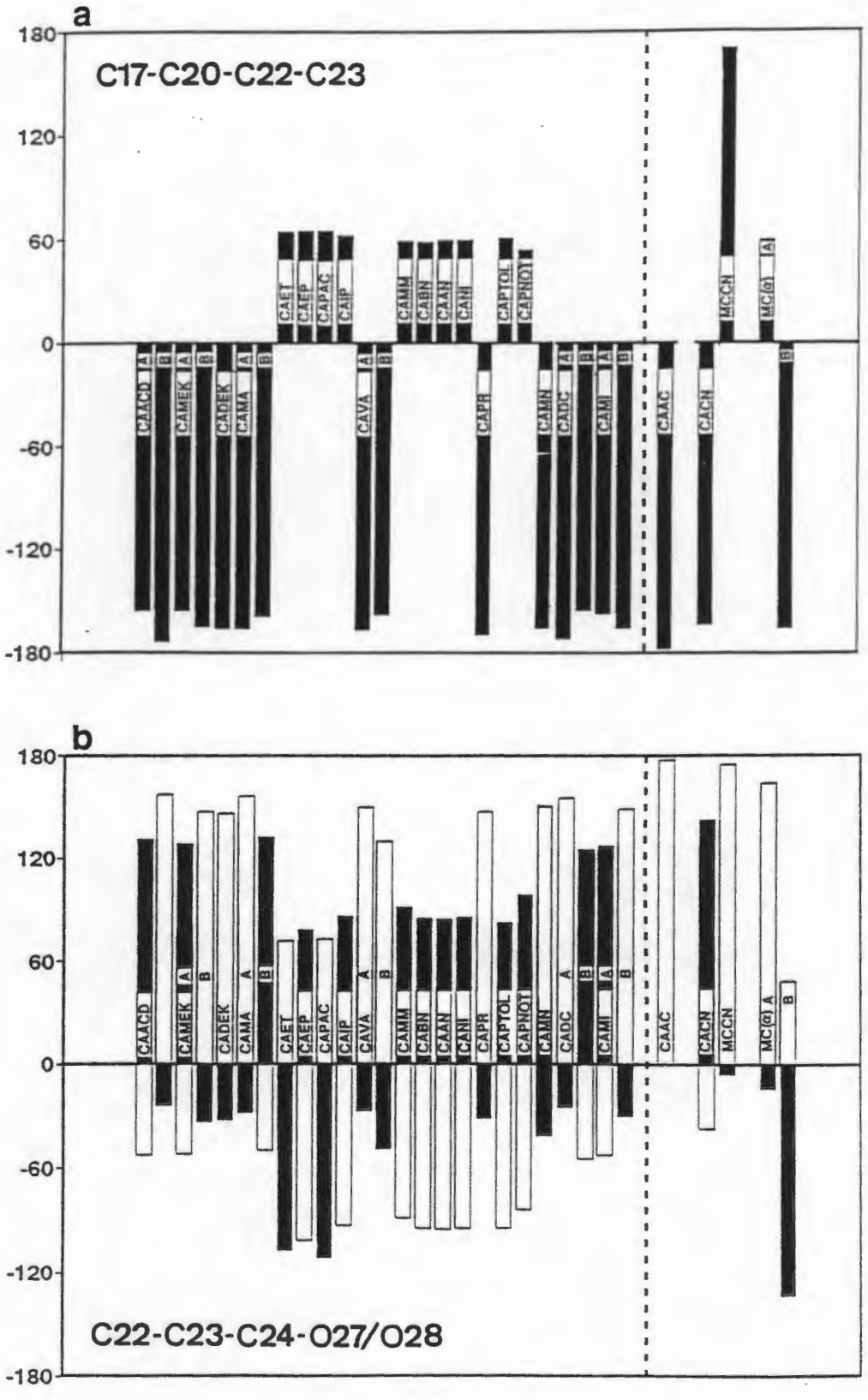

Figure 3.39: Bar charts of the torsion angles a) τ_2, C(17)-C(20)-C(22)-C(23) and b) $\tau_{4/5}$, C(22)-C(23)-C(24)-O(27)/O(28). The dotted line separates the CA tubulate clathrate structures from those of MC and the hydrogen bonded network and cavity clathrate structures. τ_4 and τ_5 are indicated in b as these are not independent of each other: τ_4 is represented by solid bars and τ_5 by unshaded bars.

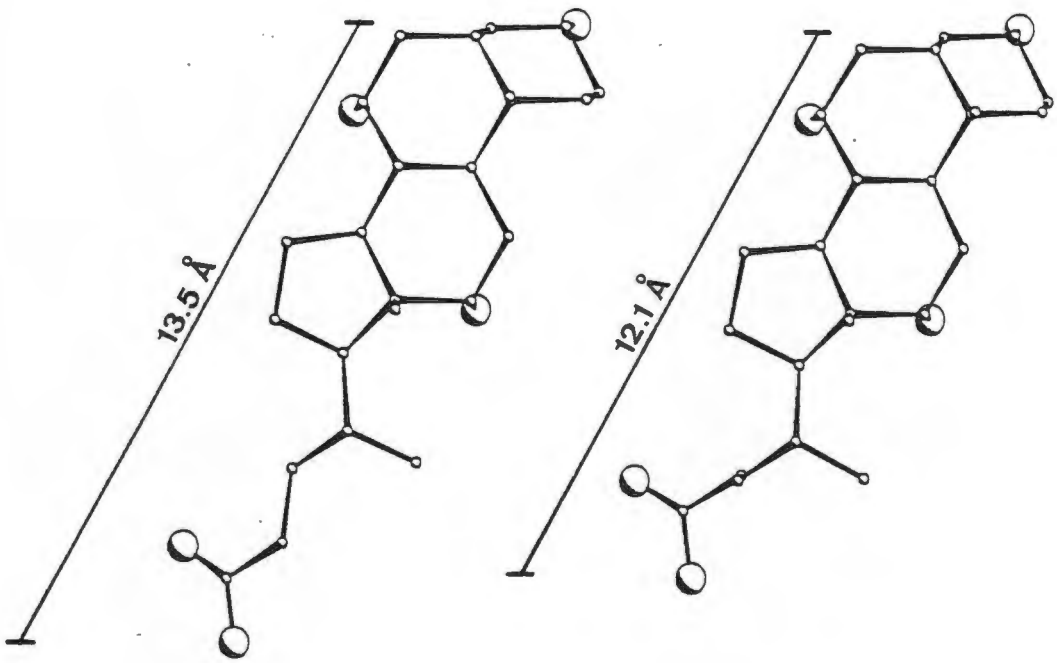

Figure 3.40: Comparison of the 'length' of puckered and extended conformations of the host molecule as found in CAACD(B) and CAPNOT respectively.

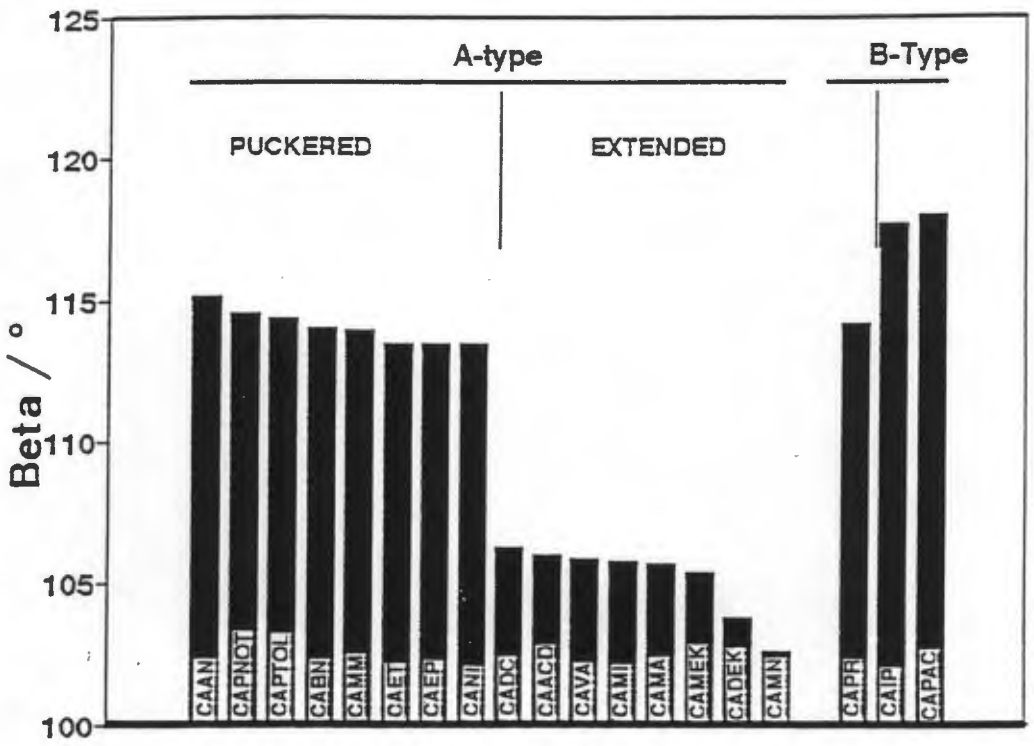

Figure 3.41: Comparison of the β angles of structures consisting of host molecules in either the extended or puckered conformation.

Hydrogen Bonding

Hydrogen bonded distances (and angles where hydroxyl hydrogen atoms were refined) are presented in Table 3.8. The hydrogen bonding of CAAC, CACN, MCCN and MC(α) is discussed above. These data are therefore omitted from these Tables as the former structures are markedly different from the majority of CA inclusion compounds.

Diagrams 3.42a to d indicate O•••O distances for the 4 types of hydrogen bonds occurring. Clearly O(28)•••O(29) and O(29)•••O(25) are on average shorter than O(25)•••O(26) and O(26)•••O(27) and this is reflected in shorter H•••O distances in the structures where hydroxyl hydrogen atoms were refined as illustrated in Figure 3.43. The O-H•••O angles show wide variation over all O•••O distances as shown in Figure 3.44.

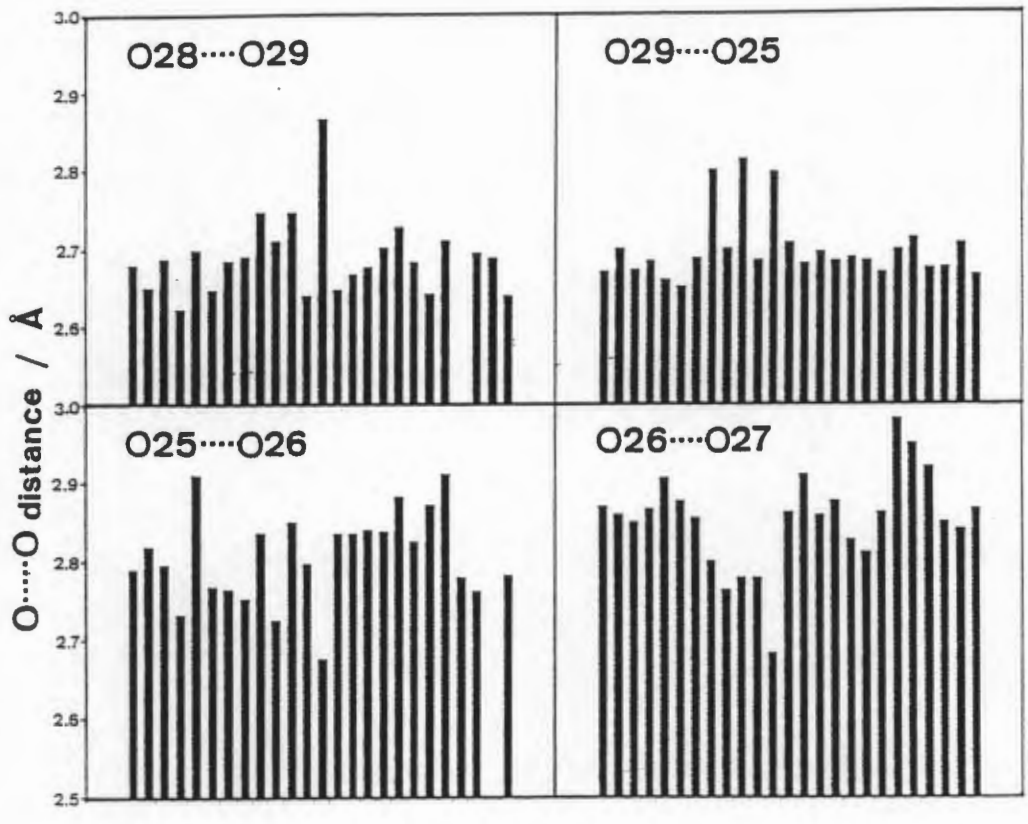

Figure 3.42: O•••O distances for the four host-host hydrogen bonds.

Table 3.8: Hydrogen Bonded distances and Angles.

	O•••O (Å)		H•••O (Å)		O-H•••O (°)	
	28•••29	28•••26	28O•••29	28O•••26	28-28O•••29	28-28O•••26
CAACD	2.68(3)					
	2.65(3)					
CAMEK	2.688(9)					
	2.623(9)					
CADEK	2.700(6)		1.76(9)		160(17)	
CAMA	2.648(7)					
	2.686(6)					
CAET		2.690(9)		1.906(9)		159.8(3)
CAEP	2.748(6)					
CAPAC		2.711(9)				
CAIP	2.747(7)		1.93(1)		172(8)	
CAVA	2.640(9)					
		2.866(8)				
CAMM	2.648(4)		1.69(3)		167(6)	
CABN	2.668(8)					
CAAN	2.678(7)		1.73(3)		162(5)	
CANI	2.702(6)		1.803(4)		147.8(4)	
CAPR	2.728(6)		1.82(6)		153.9(4)	
CAPTOL	2.683(6)					
CAPNOT	2.642(7)		1.72(5)		154(9)	
CAMN	2.713(4)		1.79(2)		158(5)	
CADC	2.700(8)					
		2.695(7)				
CAMI	2.689(13)					
		2.639(13)				

	29•••25	26•••25	29O•••25	26O•••25	29-29O•••25	26-26O•••25
CAACD	2.67(2)					
	2.70(2)					
CAMEK	2.672(9)					
	2.684(10)					
CADEK	2.659(9)		1.85(4)		139(2)	
CAMA	2.650(6)					
	2.687(6)					
CAET		2.800(6)		1.986(9)		172(6)
CAEP	2.700(9)					
CAPAC		2.814(7)				
CAIP	2.685(7)		1.90(3)		161(8)	
CAVA		2.798(10)				
	2.708(9)					
CAMM	2.680(6)		1.71(4)		175(4)	
CABN	2.695(12)					
CAAN	2.684(10)		1.74(6)		162(5)	
CANI	2.688(11)		1.753(8)		158.7(3)	
CAPR	2.683(8)		1.73(6)		172(4)	
CAPTOL	2.669(7)					
CAPNOT	2.698(8)		1.74(3)		164(8)	
CAMN	2.713(6)		1.96(4)		163(3)	
CADC	2.674(7)					
	2.675(10)					
CAMI	2.706(12)					
		2.665(12)				

Table 3.8 (contd.): Hydrogen Bonded distances and Angles.

	O•••O (Å)		H•••O(Å)		O-H•••O(°)	
	25•••26	25•••29	25O•••26	25O•••29	25-25O•••26	25-25O•••29
CAACD	2.79(2)					
	2.82(2)					
CAMEK	2.796(9)					
	2.733(9)					
CADEK	2.910(7)		1.99(5)		157(4)	
CAMA	2.768(6)					
	2.765(7)					
CAET		2.752(7)		2.037(7)		142.2(2)
CAEP	2.837(7)					
CAPAC		2.726(9)				
CAIP	2.851(7)		2.08(5)		156(10)	
CAVA	2.798(8)					
		2.676(10)				
CAMM	2.836(5)		1.89(5)		165(5)	
CABN	2.836(10)					
CAAN	2.840(8)		1.88(7)		174(7)	
CANI	2.839(8)		1.953(5)		150(3)	
CAPR	2.882(6)		1.92(5)		165(5)	
CAPTOL	2.825(6)					
CAPNOT	2.872(7)		2.02(3)		165(4)	
CAMN	2.909(5)		1.96(4)		165(4)	
CADC	2.780(10)					
	2.761(9)					
CAMI	2.781(12)					
	2.782(12)					

	26•••27	29•••27	26O•••27	29O•••27	26-26O•••27	29-29O•••27
CAACD	2.87(3)					
	2.86(3)					
CAMEK	2.850(11)					
	2.866(11)					
CADEK	2.907(8)		1.97(4)		166(4)	
CAMA	2.877(8)					
	2.855(6)					
CAET		2.800(9)		2.044(9)		153.1(2)
CAEP	2.764(9)					
CAPAC	2.779(7)					
CAIP	2.779(8)		2.01(4)		156(10)	
CAVA		2.684(9)				
	2.862(8)					
CAMM	2.911(5)		1.97(4)		163(3)	
CABN	2.858(13)					
CAAN	2.877(10)		2.040(8)		145.3(3)	
CANI	2.828(10)		1.838(8)		166.4(4)	
CAPR	2.812(8)		1.89(7)		155(5)	
CAPTOL	2.862(8)					
CAPNOT	2.982(8)		2.10(5)		151(8)	
CAMN	2.951(5)		2.04(3)		156(3)	
CADC	2.920(11)					
	2.850(10)					
CAMI	2.841(12)					
	2.866(13)					

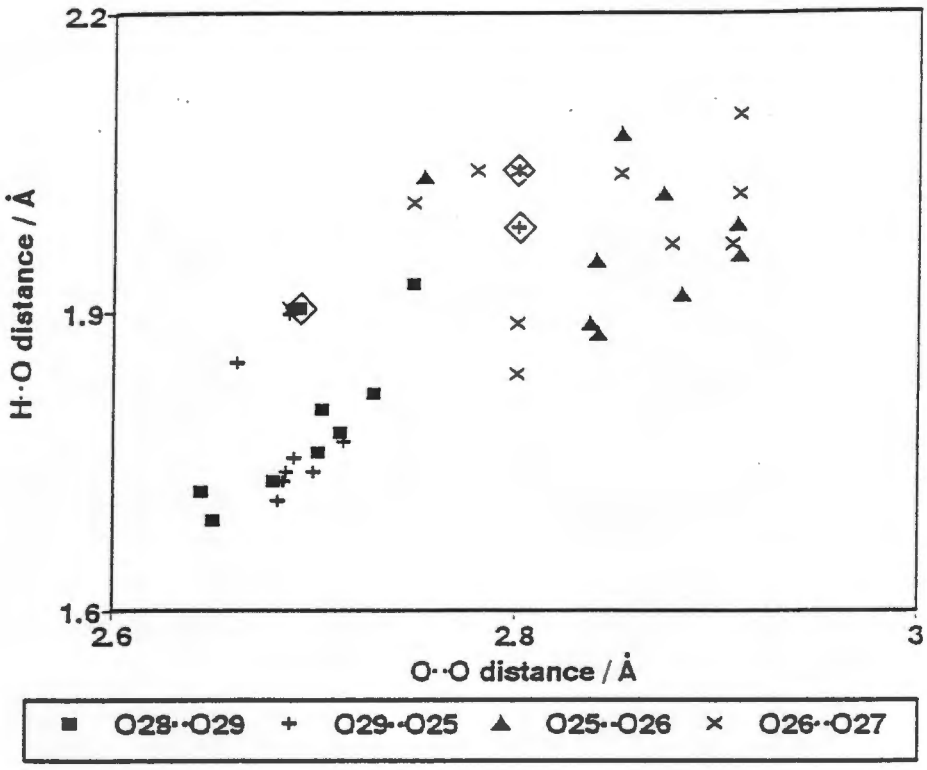

Figure 3.43: H•••O distances versus O•••O distances for all structures in which hydroxyl hydrogen atoms were refined. Points pertaining to the structure of CAET are boxed as this structure shows reversed direction of hydrogen bond donor and acceptor functions and these points are not directly comparable with the others.

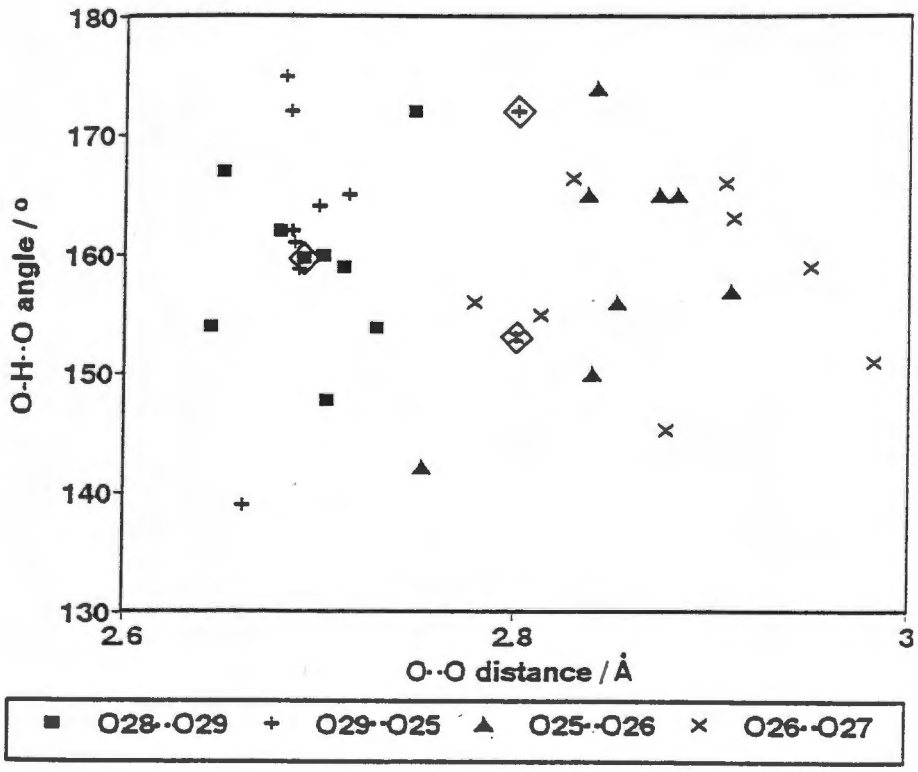

Figure 3.44: O-H•••O angles versus O•••O distances for all structures in which hydroxyl hydrogen atoms were refined. As before points pertaining to CAET are boxed.

Host Bond Lengths and Angles

Bond lengths in the host molecules are in accordance with values found elsewhere for similar steroid structures[13,15]. All carbon and oxygen atoms of the host, except C(24) and O(27) are sp^3 hybridised and exhibit typical C(sp^3)-C(sp^3) or C(sp^3)-O(sp^3) bond lengths. Histograms showing the distribution of C(sp^3)-C(sp^3) and C(sp^3)-O(sp^3) bond lengths in all of the structures studied are presented as Figures 3.45 a and b.

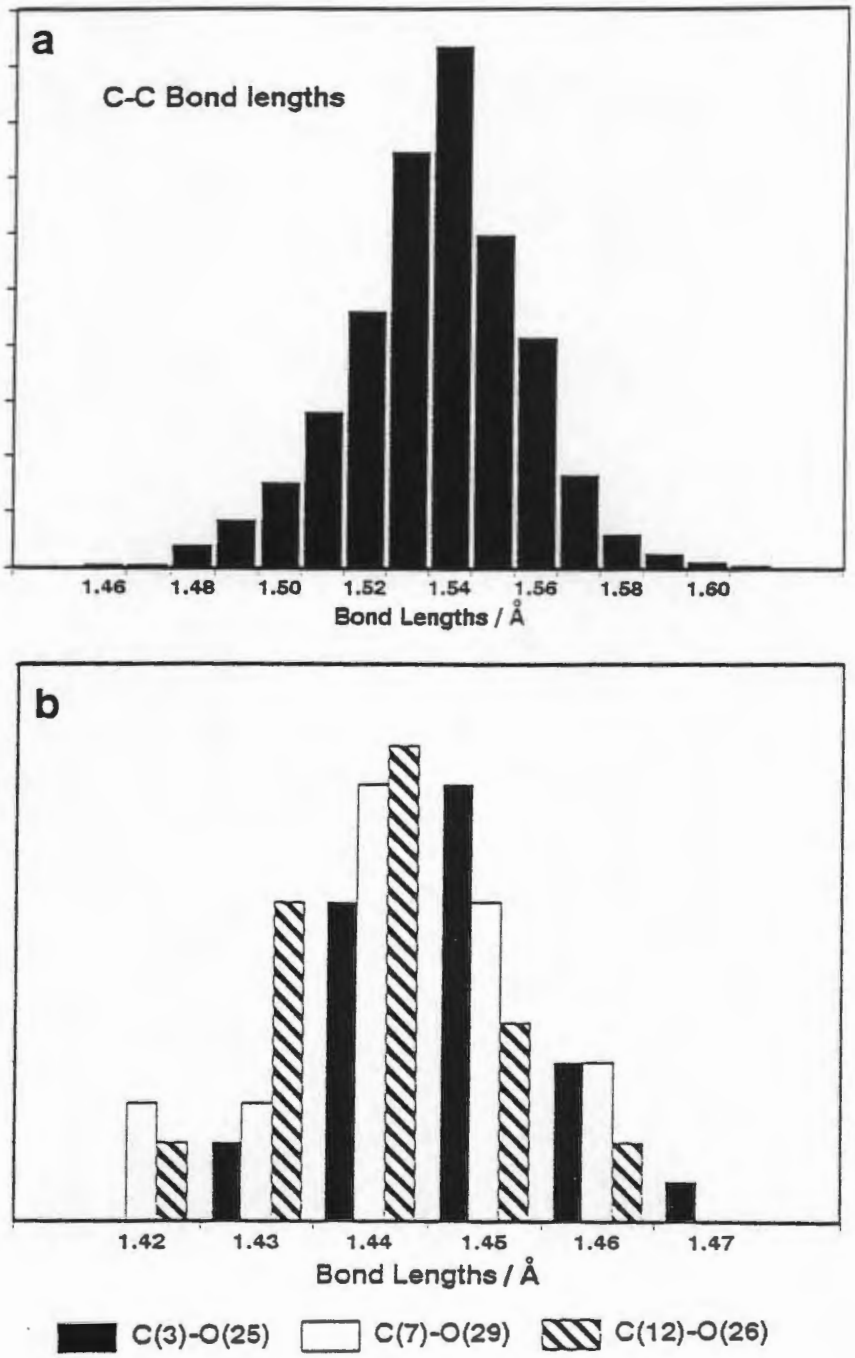

Figure 3.45: Histograms summarising the bond lengths found in the host molecules CA and MC. a) C(sp^3)-C(sp^3) bond lengths and b) C(sp^3)-O(sp^3) bond lengths excluding C(24)-O(28).

The C-O bond lengths of the carboxylic acid end group are presented in Figure 3.46. The occurrence of a significant number of C-O bonds with bond lengths in the range 1.21 to 1.25 Å are indicative of disorder, and resultant bond length averaging, of the COOH group.

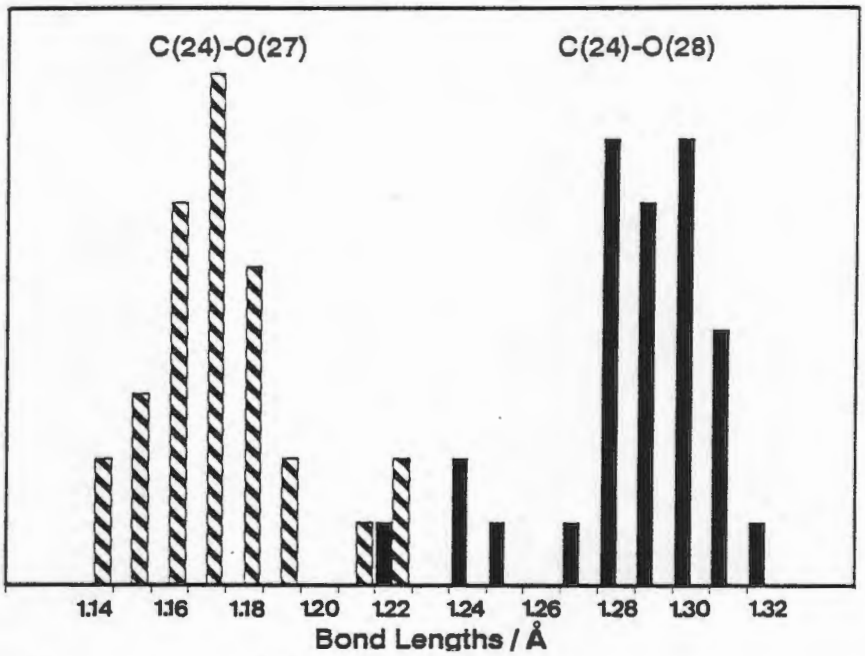

Figure 3.46: Bond lengths of the terminal carbonyl group.

A histogram summarising the bond angles found in the host A, B and C rings and substituents is presented as Figure 3.47. While the three fused cyclohexyl rings of the steroid backbone are not highly strained, a slightly larger spread of bond angles and skewing towards angles >109.5 ° than would be expected in conformationally free systems is noted.

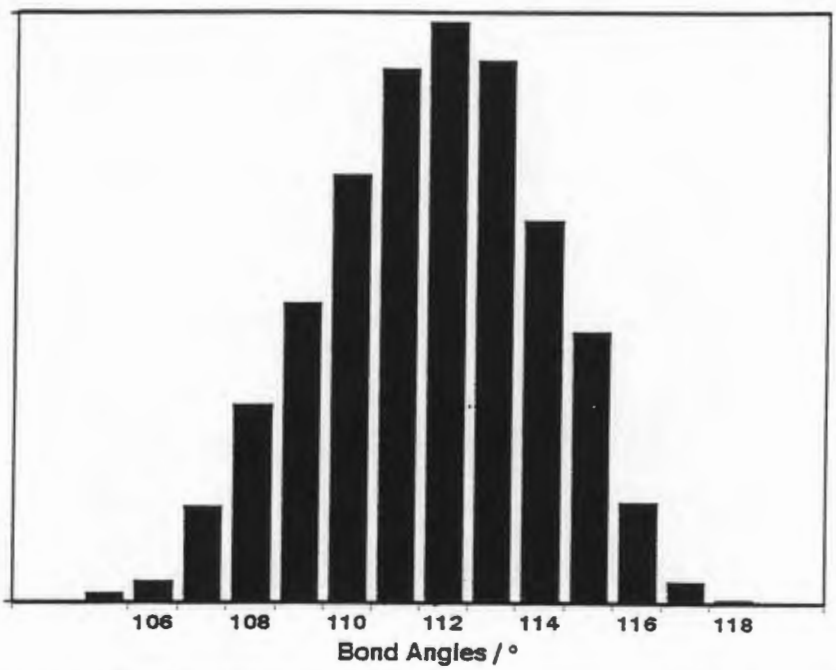

Figure 3.47: Bond angles for all bonded atoms of the A, B and C cyclohexyl fused rings and substituents.

The bond angles of the COOH group are presented in Figure 3.48. The lower distribution of the bond angle C(23)-C(24)-O(28) and high mean indicated for C(23)-C(24)-O(27) is indicative of consistent deformation of the COOH group from idealised geometry.

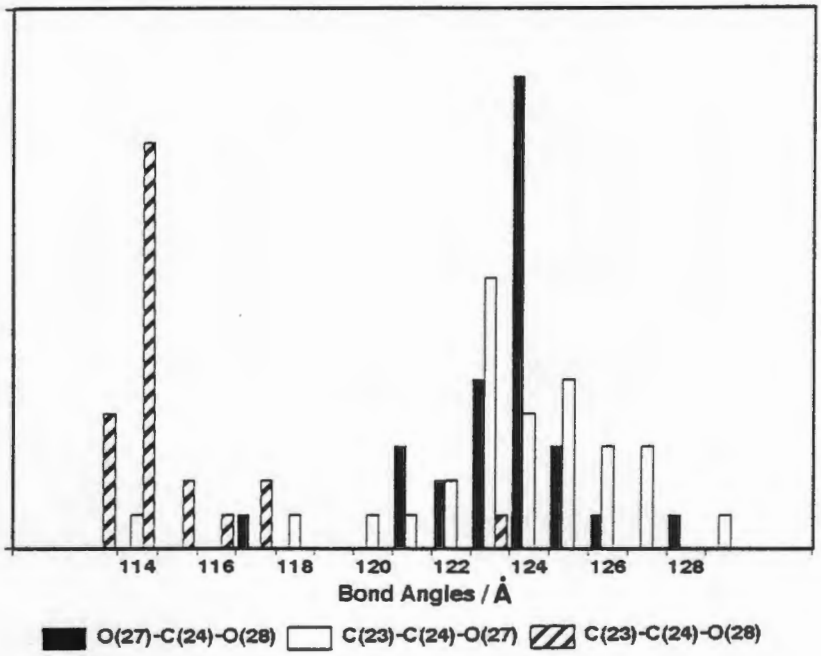

Figure 3.48: Bond angles for the terminal carboxylic acid group.

The cyclopentyl D-ring of CA and derivatives is a strained system and this results in distortion of the bond angles from ideal geometry. The bond angles of ring D are summarised in histogram form as Figure 3.49. All are < 109.5 °: that of C(14)-C(13)-C(17) averages *ca* 100 ° and C(15)-C(16)-C(17) is almost always 107-108 ° while the other three angles approximate 104 °.

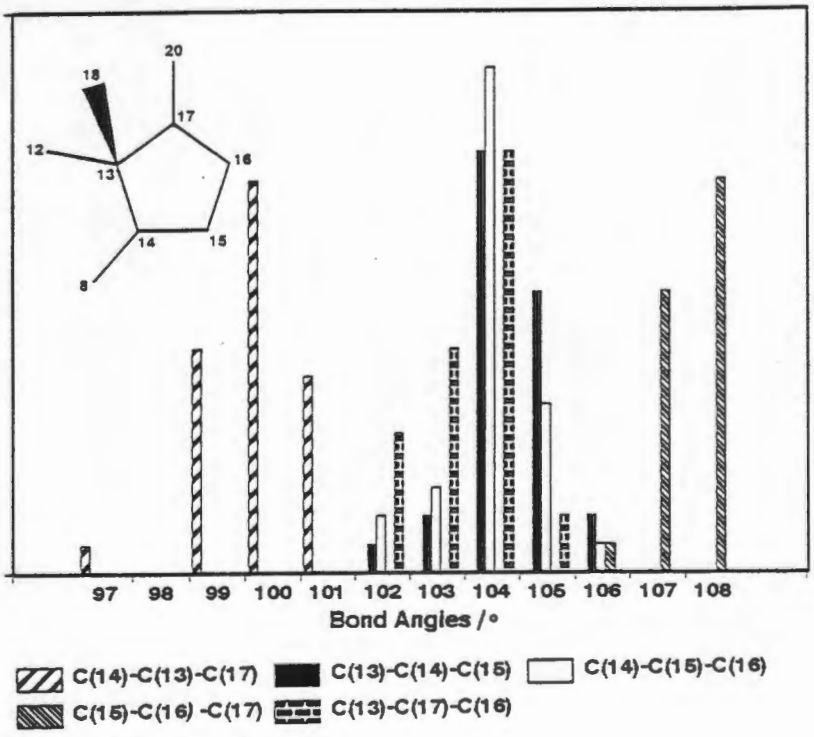

Figure 3.49: Bond angles for the strained D-ring.

1 G.M. Sheldrick, *SHELXS-86 Crystallographic Computing, G.M. Sheldrick*, C. Kruger and R. Goddard, Oxford University Press, Oxford, (1985), Vol. 3, 175.

2 G.M. Sheldrick, *SHELX-76 Program for Crystal Structure Determination*, University of Cambridge, Cambridge, UK, (1976).

3 G.M. Sheldrick, SHELXL-93: *A Program for Crystal Structure Determination, J. Appl. Crystallogr.*, in preparation, 1993.

4 H.D. Flack and D. Schwarzenbach, *Acta Crystallogr. Sect. A*, 1988, **44**, p 499.

5 Olovson and P.- G. Jönson, in "*The Hydrogen Bond, Part II, Structure and Spectroscopy*", eds. P. Schuster, G,. Zundel and C. Sanderfly, 1976, North Holland Publ. Co., Amsterdam.

6 S.K. Kearsley, in "Studies in Organic Chemistry 32, Organic Solid-State Chemistry, Chapter 3", Ed G.R. Desiraju, 1987, p 69.

7 M. Farina, G. Audisio and G. Natta, *J. Am. Chem. Soc.*, 1967, **89**, p 5071.

8 G. Audisio and A. Silvani, *J. Chem. Soc., Chem. Commun.*, 1976, p 481-782.

9 K. Miki, N. Kasai, M. Shibakami, S. Chirachanchai, K. Takemoto and M. Miyata, *Acta Crystallogr. Sect. C*, 1990, **46**, p 2442.

10 D. Cremer and J.A. Pople, *J. Am. Chem. Soc.*, 1975, **97**, 6, p 1354.

11 J.C.A. Boeyens, *J. Cryst. Mol. Struct.*, 1978, **8**(6), p 317.

12 S.A Thomas, *J. Crystallogr. and Spectros. Res.*, 1982, **12**, 2, p 171.

13 W.L. Duax and D.A. Norton, Atlas of Steroid Structure, IFI/Plenum Data Company, 1975, p17.

14 E. Giglio and C. Quagliata, *Acta Crystallogr. Sect. B*, 1975, **31**, p 743.

15 Cambridge Structural Database and Cambridge Structural Database System, Version 5.07 (April 1994), Cambridge Crystallographic Data Centre, University Chemical Laboratory, Cambridge, England.

CHAPTER 4: THERMAL ANALYSIS

Various techniques allowing the measurement of physical properties, or more correctly, changes in physical properties of a substance as a function of temperature exist. Thermal analysis includes methods designed for monitoring changes in mass, mechanical, acoustic, optical, electrical and magnetic properties. Enthalpy values for phase changes may be estimated from measurements of the required power input to maintain a certain sample temperature or heat rate.

In this study thermogravimetry (TG) was used to follow changes in weight upon heating and differential scanning calorimetry (DSC) analysis employed to monitor power flow required to maintain a chosen heating rate respectively. Rising temperature TG was used primarily to determine the host:guest ratio. While a number of studies have been devoted to the determination of ΔH values of the guest release reaction[1] the values thus measured are dependent on heating rates, purge gas flow rates, the geometry and composition of the sample holder and most importantly, on particle size. It must be possible to grind and sieve samples, without loss of guest, to ensure reproducibility. For the purposes of this study DSC was used qualitatively to gain information about the number and approximate temperatures of phase changes (and other processes) occurring during thermal decomposition.

These techniques are well established and described in a series of monographs on the subject[2,3,4] while a number of new developments in the field are detailed in a wide ranging review by Dollimore[5]. Apart from the description of methods and data collection described in the experimental section (chapter 2) only unusual experiments will be described in detail.

THERMAL DECOMPOSITION OF INCLUSION COMPOUNDS

The overall reaction in the decomposition of an inclusion compound without chemical change of either host or guest may be presented as:

$$H \bullet xG_{(s,\beta)} = H_{(s,\alpha)} + xG_{(g)}$$

This reaction however, may be the sum of a number of separate steps each resulting in the existence of discrete identifiable phases. Any reaction occurring in the course of analysis, be it a solid state phase change, guest loss reaction, melt, recrystallisation or guest boil will result in a detectable change in the DSC trace. This might be an endotherm as is usual for guest loss reactions and melts, an exotherm as in the case of recrystallisation reactions or a change in the DSC baseline as occurs in the change from a rigid to a plastic state - the glass transition temperature. Figure 4.1 schematically illustrates some of the more commonly encountered phase changes and resultant solid phases encountered in decomposition of clathrate type inclusion complexes.

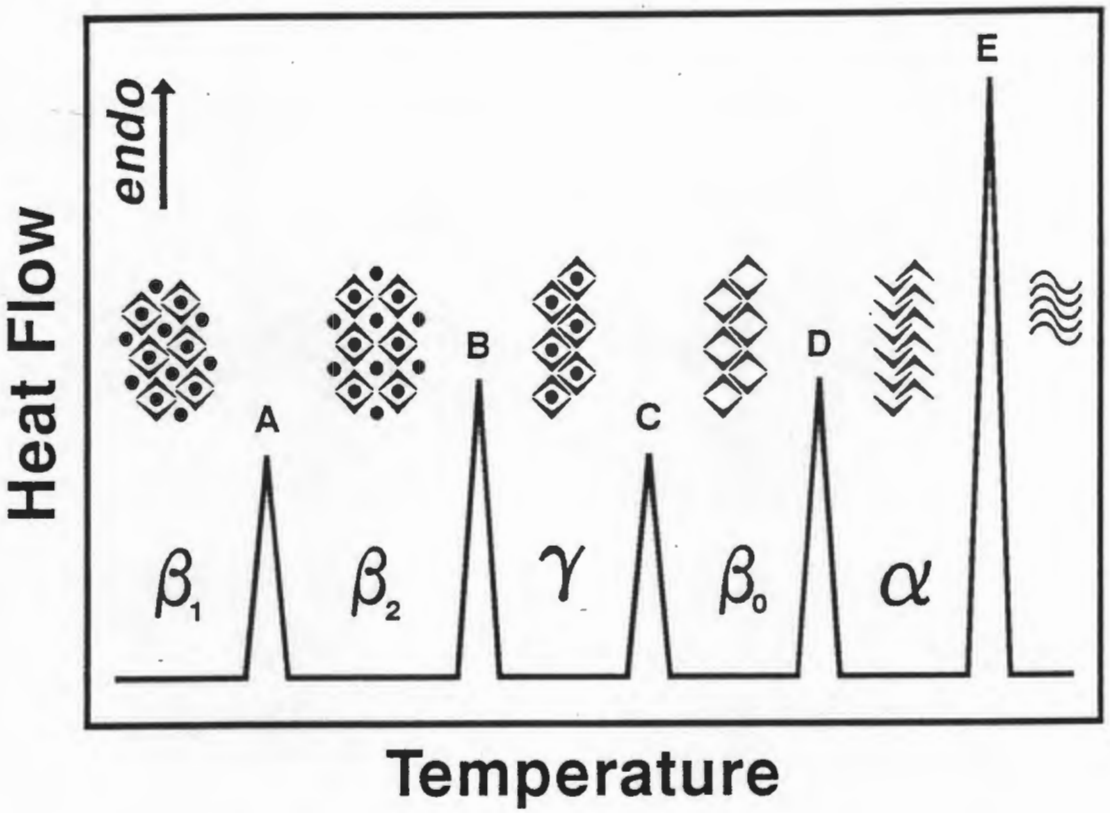

Figure 4.1: Possible thermal decay modes of inclusion compounds.

β_1 is the inclusion compound as grown from solution (or by other methods). This is the phase that is stable (or metastable but kinetically favoured) in mother liquour at room temperature. β_2 is an inclusion compound phase with the same stoichiometry as β_1 but having undergone a solid-solid phase transition with no loss of guest. This phase may lose a portion of the included guest to result in a new inclusion phase (indicated here as the γ phase) with a different host:guest stoichiometry. Should the γ phase lose guest without collapse of the (now porous) host structure the elusive β_0 phase results. Only a small number of inclusion compounds have been shown to decay in this manner[6,7,8]. Collapse of the porous host phase to the stable form (or one of the stable forms of the host) is the transition to the α phase. The α phase is usually defined as the host phase stable at room temperature although other α phases may exist in the form of stable or metastable polymorphs or as high temperature polymorphs. Only peaks B and C will be accompanied by weight loss on TG analysis and this together with techniques such as XRD and hot stage microscopy aids assignment of thermal events. Melting and subsequent recrystallisation of any of the abovementioned phases may occur, as may any number of solid-solid phase changes. Seldom do all such changes occur in the decomposition of one inclusion compound and in the simplest case the inclusion compound will melt congruently[9] and guest loss will not evince a separate thermal event so that only one endotherm will appear in the DSC trace. In the case of clathrate type inclusion compounds the most common scenario is the occurrence of a single endotherm arising from guest loss and β

to α phase change followed by a host melt endotherm, (i.e. B and D combined followed by E.)

Methodology:

In all cases TG and DSC curves were analysed in tandem and wherever possible analysis carried out on the same sample. Other techniques such as hot stage microscopy and XRD analysis were used to elucidate processes occurring, while ^{1}H-NMR analysis was utilised to confirm guest composition in cases where possible ambiguities existed such as when crystals were grown from mixed guest solutions or with the aid of a cosolvent.

The thermal behaviour of a sample is dependent on sample preparation to a greater or lesser degree and thus the history of a sample may be an important factor in thermal analysis[2]. Structural differences in solids (the existence of different phases), density of crystal defects in crystalline solids, sample porosity, particle size and the nature of surfaces all affect thermal behaviour. These are investigated in more detail in chapter 6; suffice to say that particle size and crystal quality proved to have the greatest effect on behaviour of samples of the inclusion compounds of CA and MC under thermal analysis.

To determine the optimum conditions for thermal analysis of these compounds the effects of particle size, heating rate and purge gas flow rate were investigated.

Particle Size

Particle size should properly be considered a subset of the characteristics described under crystal quality as the surface of a crystal is effectively an extensive crystal defect - thus as surface area:volume increases so does the defect density.

A number of experiments were carried out to determine the effect of particle size on *these* systems. Decrease in particle size may be shown to have the following effects:

i) The onset temperature of guest release in TG analysis is (sometimes significantly) reduced as is illustrated for samples of CAET in Figure 4.2.

ii) Better separation of DSC peaks is achieved when small particle sizes are used as is illustrated in Figure 4.3 a and b. This is a function of the sharpness of the resultant endotherms and is almost certainly a kinetic effect due either to the existence of a temperature gradient or to the lag attributable to the finite rate of penetration of the reaction front into the interiors of large particles.

This would appear to militate against the use of whole uncrushed crystals; however, many of the compounds studied were highly labile, beginning to lose guest almost immediately upon removal from mother liquour.

Thus guest loss is greatly accelerated upon crushing of the samples and a balance must be struck between too great a loss of guest and good separation of peaks in DSC traces. Most of the samples were lightly crushed but not sieved in an attempt to keep sample preparation time and thus the extent of guest desorption to a minimum. Even with such relatively cursory sample preparation; drying, crushing, weighing, sealing of the DSC pan in a press and loading of the sample into the analyser result in an appreciable time lapse between removal of the sample from mother liquor and the start of analysis. Although with practice this may be reduced to as little as 1 to 2 minutes, samples of inclusion compounds with such volatile guests as acetone nonetheless exhibit unacceptably high decay, particularly once the surface area of the particles is increased by crushing. It proved possible to obtain accurate TG traces of certain of the more labile compounds only by the use of good quality, *large*, unbroken single crystals. Unfortunately the lack of crushing tends to reduce the definition and reproducibility of the thermal analysis traces.

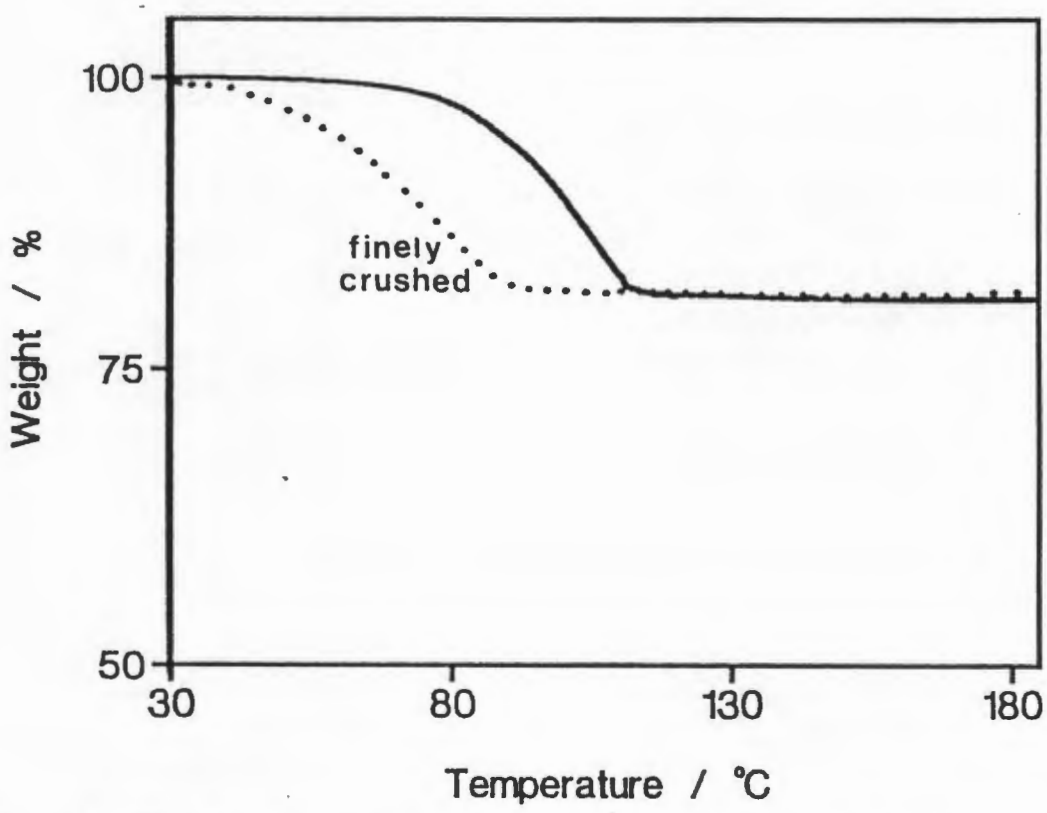

Figure 4.2: Effect of particle size on onset of guest release in TG analysis, illustrated for the compound CAET. Solid line - whole crystals, dotted line - finely crushed crystals.

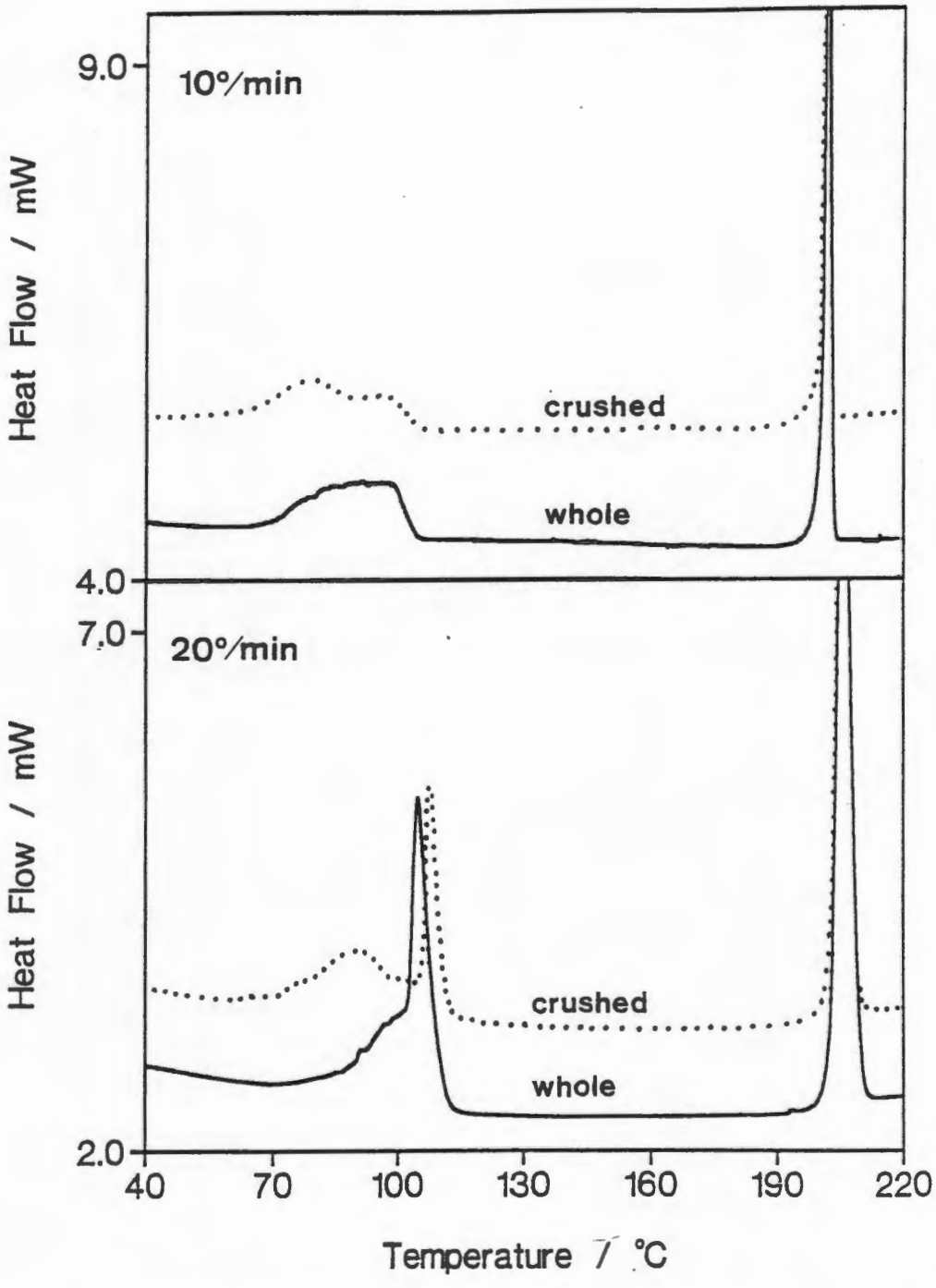

Figure 4.3: Effect of particle size on the shape of the DSC trace, illustrated for the compound CAET at two different heating rates. Solid line - whole crystals, dotted line - finely crushed crystals.

Heat Rate

Although less studied, the rate of sample heating also has a marked effect on the shape of the TG and DSC curves.

Because of problems resulting from non-uniform heating of immobile solid samples[10] resulting in lower temperatures within the sample than measured in the furnace and even in the formation of temperature gradients within the sample, high heating rates are usually avoided. Less attention has been paid to

the effect of lowered heating rates yet it may be shown that operation of the DSC analyser at too low heat rates often results in loss of information. A number of experiments to test the effect of different heating rates were carried out using the CA inclusion compounds with aliphatic ester guests as test samples. These compounds were chosen as they showed relatively complex decomposition paths resulting in a number of peaks on DSC analysis.

Sample sizes in the range 2.0-2.5 mg were analysed at heating rates ranging from 2 °C/min to 40 °C/min. All were blotted dry and lightly crushed as described before. Figure 4.4 shows the DSC traces resulting from analysis of CAEP at 5, 20 and 40 °C/min. As will be described in detail at a later stage, the first diffuse endotherm in the DSC trace of the compound analysed at 40 °C/min is ascribed to the onset of guest loss and the second sharper peak to the resultant β to α phase change while the well defined endotherm at *ca* 200 °C is due to host melt. Clearly the lower heating rate of 5 °C/min results in complete loss of the second sharp endotherm which has become very diffuse and difficult to distinguish from the baseline, while peaks are broader at high heat rates presumably due to the temperature lag mentioned before. This sort of effect is noted in a number of such compounds and 20 °C/min was thus chosen as the most desirable heating rate *for analysis of these compounds*. This is a compromise between lack of definition achieved at lower heat rates and non-uniform heating problems experienced at high heating rates. The instrument was calibrated at this heating rate.

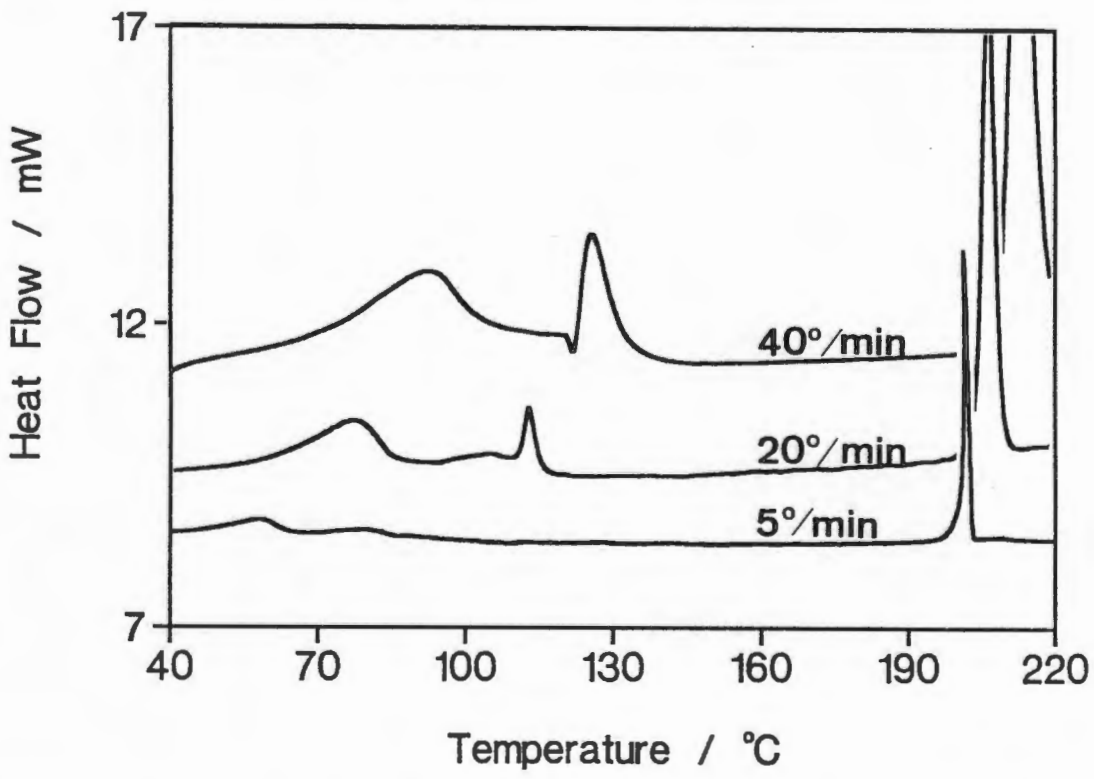

Figure 4.4: Effect of heating rate on the DSC trace, illustrated for the compound CAEP. All traces are normalised and plotted on the same scale.

Purge Gas Flow Rate

The purge gas flow rate is an important factor in DSC analysis of compounds which evolve gases, either by decomposition or reaction, upon heating. A lower purge gas flow rate will allow the formation of a local atmosphere with a significant vapour pressure of, for example, the guest species being released, particularly in the vented, crimped pans used in these experiments. Guest molecules are often released from a crystalline inclusion compound at a temperature lower than that of their boiling point and if the guest vapours are not rapidly swept away these will condense and may on further heating result in dissolution of the remaining material thereby obscuring any phase changes or other thermal events.

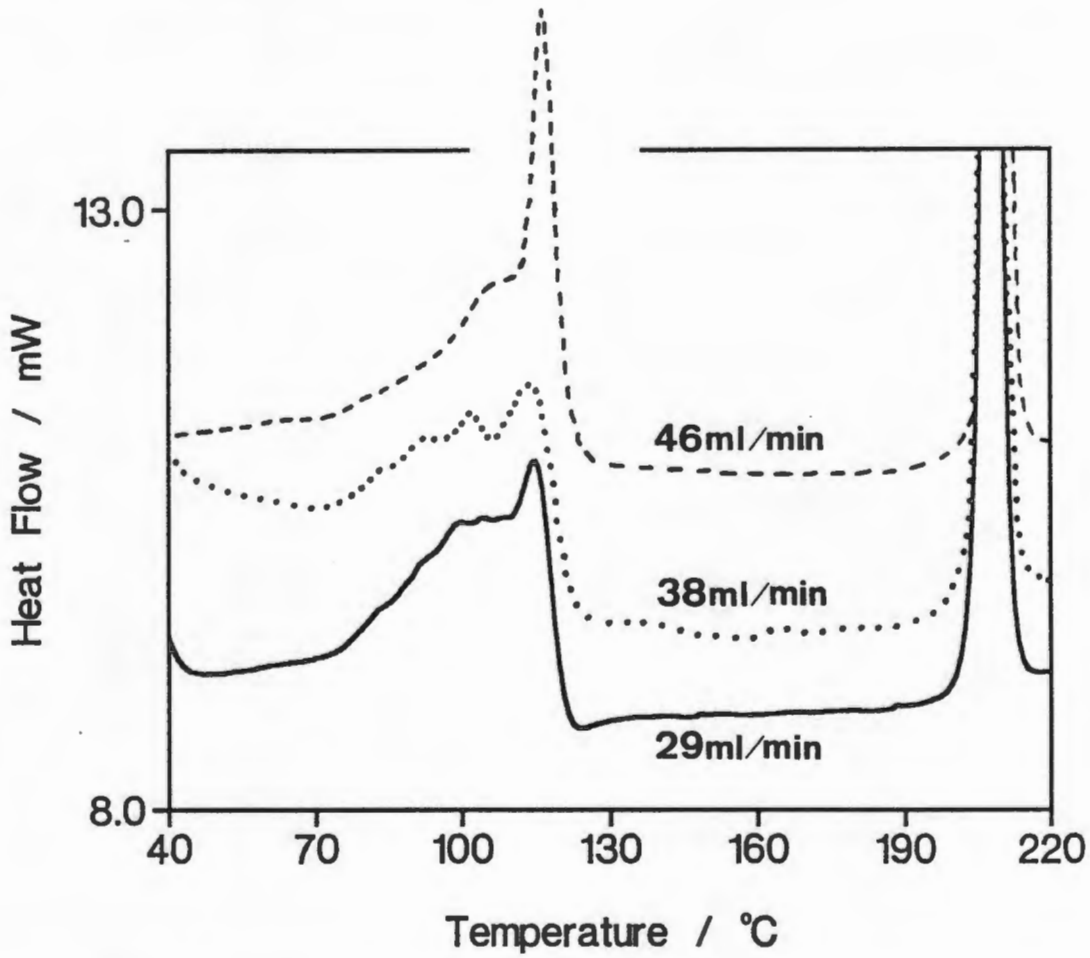

Figure 4.5: Effect of purge gas flow rate on the DSC trace, illustrated here for compound CAET at a heating rate of 40 °C/min. Solid line - 29 ml/min, dotted line - 38 ml/min, dashed line 46 ml/min. Traces are normalised and plotted on the same scale.

Figure 4.5 shows the DSC traces of CAET at a heating rate of 40 °C/min under different purge gas flow rates. Definition of certain peaks appears to be enhanced at higher flow rates but separation of peaks is poor, while at low flow rates neither definition nor separation is good. Interestingly the melt peak appears broadened by use of a higher flow rate, probably due again to differential heating of the sample which may be locally cooled at the surface by high gas flow.

The conditions chosen for analysis of the CA and MC compounds studied were thus:

- lightly crushed crystals (where guest loss was not excessive)
- heating rate of 20 °C/min
- purge gas flow rate of 40 ml/min

All DSC traces were normalised to a sample mass of 1.000 mg for ready comparison.

ANALYSIS OF INCLUSION COMPOUNDS OF CA AND MC:

The thermal analysis results for all CA and MC inclusion compounds studied are summarised as Table 4.1. Details and discussion of features and discrepancies such as the low melt points exhibited by certain compounds will be discussed in detail in later sections. A number of compounds whose crystal structures were not analysed are included for comparison.

Details of the thermal analysis of each compound are presented in groups as in the discussion of the crystal structures.

Table 4.1: Thermal Analysis Results:

	H:G[a]	TG weight loss %			DSC endotherms	
		Calc.	Exp.	Diff	T_{on} (°C)	T_{on}(melt) (°C)
CAACD	2:3	17.6	17.5	-0.1	69 84	202
CAMEK	1:1	15.0	15.2	+0.2	70 99	203
CADEK	1:1	17.4	17.1	-0.3	109	202
CAMA	1:1	15.4	15.5	+0.1	114	203
CAET	1:1	17.7	17.3	-0.4	104	203
CAEP	1:1	20.0	19.2	-0.8	79 113	202
CAPAC	1:1	20.0	19.2	-0.8	47 80[d] 112	202
CAIP	1:1	20.0	19.7	-0.3	45 92[d] 114	202
CANBU	1:1	22.1	20.1	-2.0[b]	67[d] 106	202
CASB	1:1	22.1	22.9	+0.8	60[d] 110	202
CAVA	1:1	17.4	17.5	+0.1	93	201
CAMM	1:1	19.7	18.8	-0.9	98	203
CABN	1:1	20.0	20.0	0.0	144	203
CAAN	1:1	18.6	18.5	-0.1	142[p]	195[l]
CANI	1:1	23.2	22.9	-0.3	160[m]	190[l]
CAACET	1:1	22.7	22.7	0.0	152[e]	200[r]
CAPR	1:1	24.7	24.0	-0.7	126 138[e]	198[r]
CAPTOL	1:1	20.8	19.3	-1.5	146[m]	no melt
CAPNOT	1:1	25.1	23.9	-1.2	133[e,m]	175[c])
CAMN	1:1	25.1	23.2	-1.9	117[e,m]	158(double peak)
CAMI	1:½:½	17.7	16.9	-0.8	103	202
CA•MA/EA	1:½:½	16.6	16.0	-0.6	105	202
CA•MA/n-PA	1:½:½	17.7	17.2	-0.5	112	202
CADC	1:½:½	20.1	18.7	-1.4	80 108	205
CAAC	1:1:3	21.5	20.6	-0.9	38 49 109	194[l]
CACN	1:1	9.1	9.2	+0.1	101	202
MCCN crystals	1:1	8.9	9.0	+0.1	116[m]	no melt
powders	1:1				108	149
MC(α)	-	0	0			149

a - where multiple guest species are included the ratio is indicated H:G_1:G_2, b - crystals are unstable, c - complex peak, d - diffuse peak, e - followed by an endotherm, l - low melt, m - melt associated with guest loss, p - partial melt associated with guest loss, r - melt of recrystallised material

Group 1: Aliphatic Ketones

The TG and DSC curves of CAACD, CAMEK and CADEK are presented as Figure 4.6a to c.

In each case the guest is lost in a single step although there are small changes in the shapes of the curves at high % loss. The DSC traces of CAACD and CAMEK exhibit diffuse endotherms preceding the sharp peak associated with the β to α phase change. Peculiarly, while in CAMEK this appears to be associated with the onset of guest release (which in CADEK begins immediately the sample is removed from mother liquour), this is not the case in CAACD. It should however be noted that the inclusion compounds with aliphatic ketones are extremely labile such that analysis must be done on good quality, whole crystals to avoid inordinately large guest losses during sample preparation and that this may adversely affect the uniformity of samples used in separate analyses.

Figure 4.7 is a series of photographs of the decomposition of CAACD crystals in air at room temperature and under heating immersed in drop of silicone oil. The device of immersion of inclusion compound crystals in a drop of inert, high boiling liquid allows detection of the escape of guest vapours as these result in bubble formation. In both the isothermal and rising temperature decompositions fracturing of the crystal is noted *before* significant guest loss occurs as evidenced by the image in plate 5 of Figure 4.7 where distinct fracturing but no bubble formation is evident. A similar pattern is noted in the decay of CAMEK crystals while CADEK shows no evidence of the fracturing event and crystals gradually decay, becoming opaque slowly at first and then rapidly as the temperature of the β to α phase change is approached.

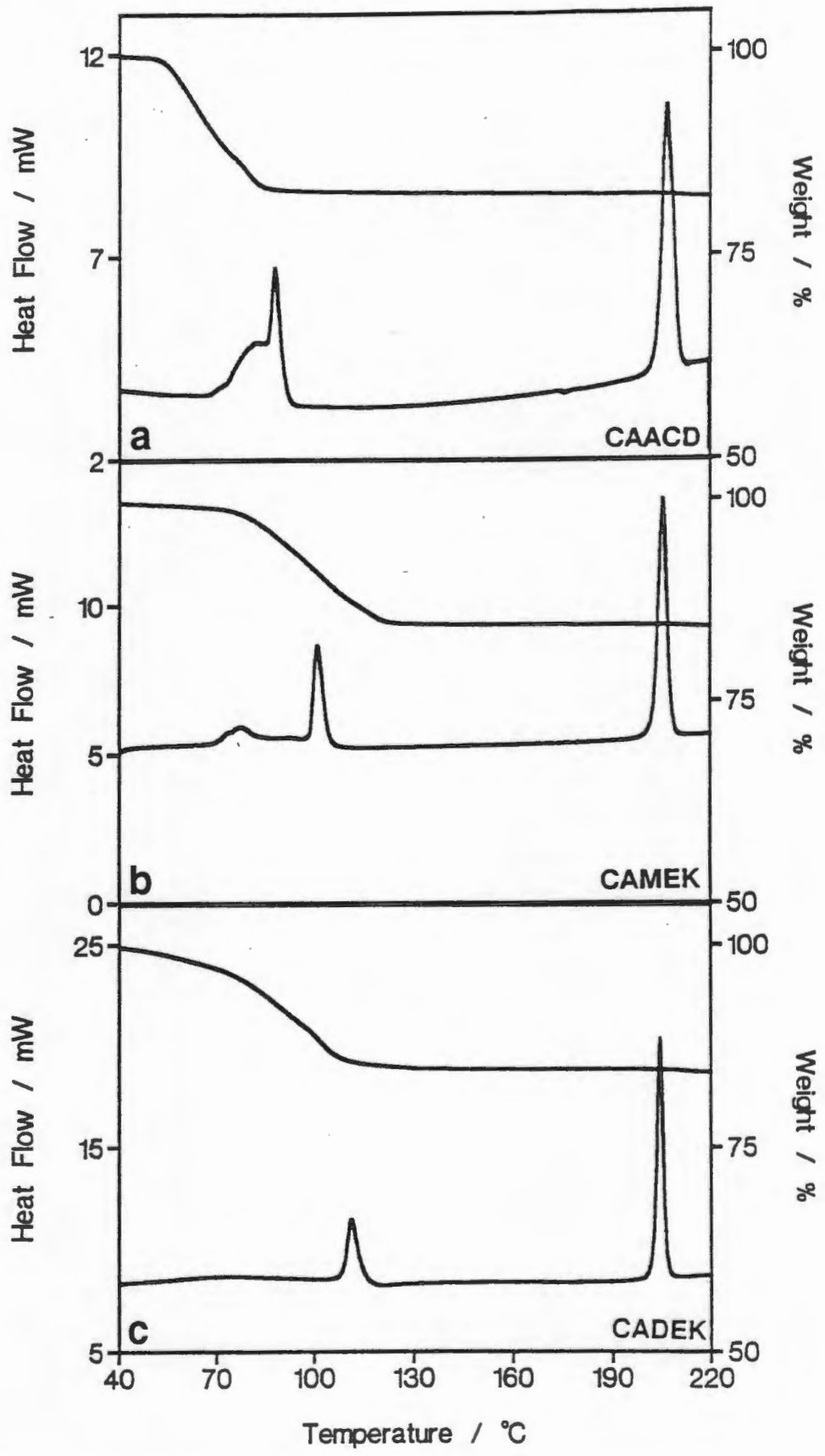

Figure 4.6: TG and DSC traces for a) CAACD, b) CAMEK and c) CADEK at 20 °C/min and purge gas flow rate of 40 ml/min.

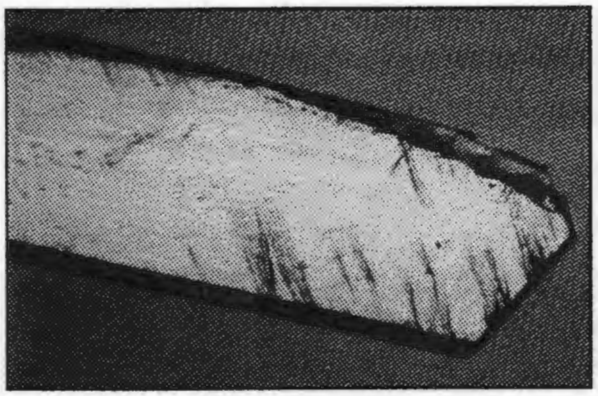

Plate 1

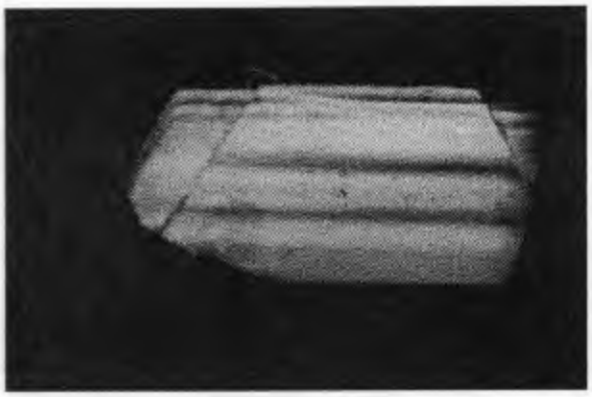

Plate 4

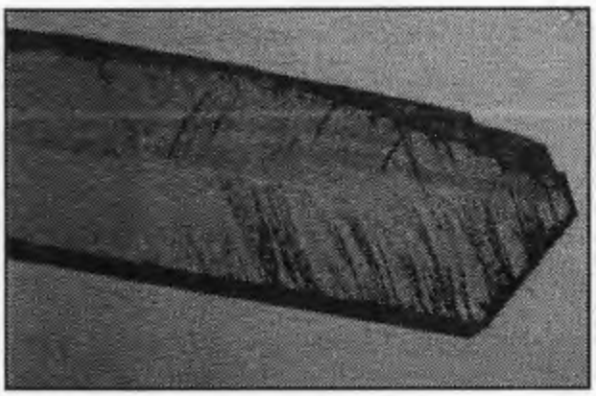

Plate 2

Plate 5

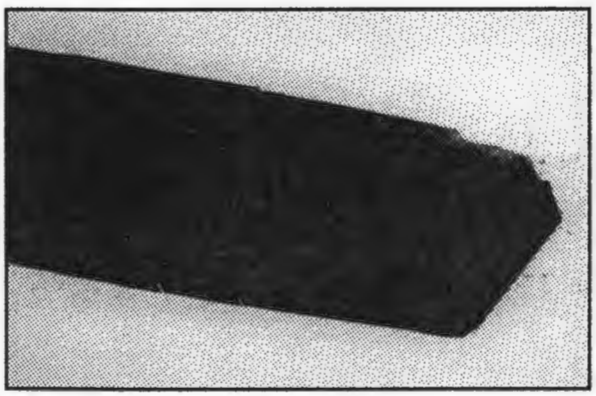

Plate 3

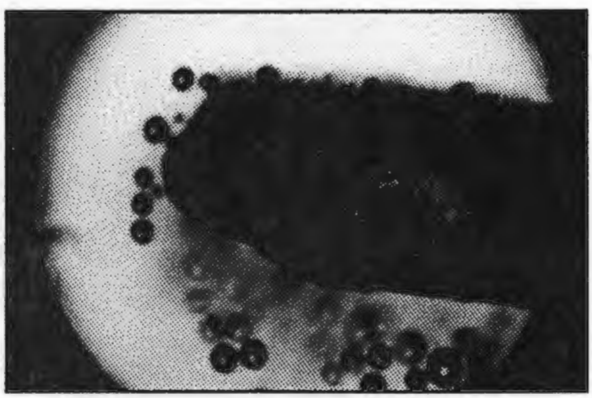

Plate 6

Figure 4.7: Decay of CAACD. Plates 1 to 3: Isothermal decay at room temperature. Plates 4 to 6: Decay under heating with crystal submerged in silicone oil.

Group 2: Aliphatic Esters

TG and DSC traces of CAMA, CAET, CAEP , CAPAC and CAIP are presented as Figure 4.8 a to e.

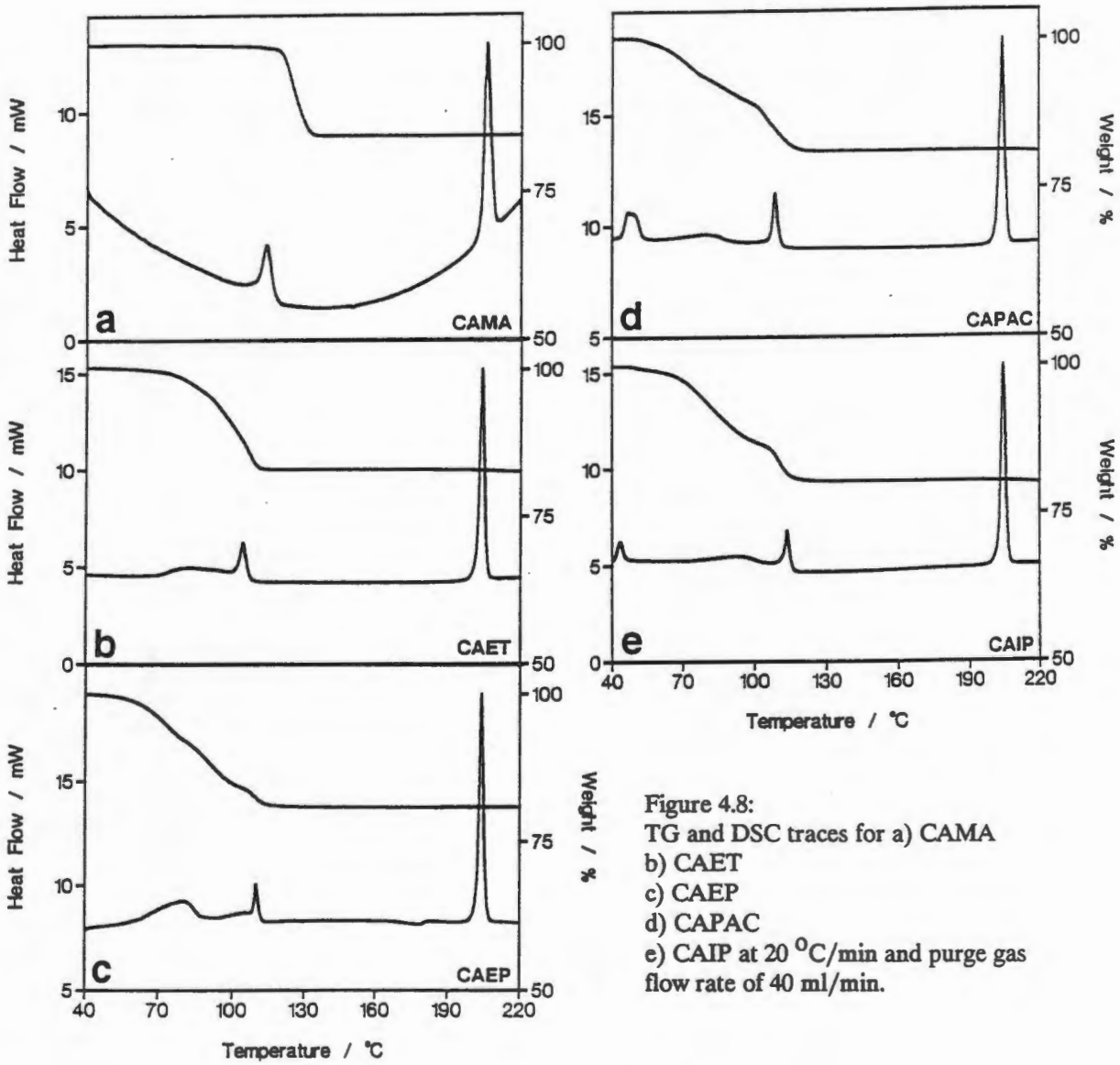

Figure 4.8:
TG and DSC traces for a) CAMA
b) CAET
c) CAEP
d) CAPAC
e) CAIP at 20 °C/min and purge gas flow rate of 40 ml/min.

While CAMA exhibits only one endotherm ascribed to both guest release and concomitant collapse to the α structure, CAET and CAEP both indicate small diffuse peaks before this endotherm, the start of which correlates closely with the beginning of guest loss as indicated by weight loss on TG analysis. CAPAC and CAIP both show small well defined endotherms at low temperature, before any significant guest loss is noted. Microscopic observation of the crystals under heating reveals distinct fracturing of the crystals of CAIP and CAPAC in the temperature range 45-50 °C. Heating of a sample immersed in silicone oil results in almost no bubble formation around the crystal which would indicate

guest loss and the peak is therefore tentatively ascribed to a solid-solid phase change. Thus it appears that the A-type structures (CAMA, CAET and CAEP, see chapter 3) undergo guest loss followed by collapse to the host α form while the B-type structures (CAPAC and CAIP) exhibit a solid-solid phase change *before* guest loss commences followed by guest loss and β to α phase change.

To validate the assertion of a phase change before guest loss in the B-type structures the X-ray powder diffraction patterns of these crystalline adducts under heating were obtained by use of the modified Weissenberg camera and heating mantle described in the experimental section (chapter 2). The resultant X-ray photographs are reproduced as Figures 4.9 a and b and the photometrically measured traces derived from that of CAPAC as Figure 4.9c. While the temperatures at which some phase changes occur appear lower than on DSC analysis it should be noted that the heating rate used in powder photography was slightly lower than 0.3 ^{o}/min. While the A-type structures show a single phase change after significant guest loss, in the B-type structures the existence of an intermediate phase different from that of the β (inclusion compound) phase and the CA(α) phase is indicated. As this appears to occur *before* any significant guest loss this would be designated as a β_1 to β_2 phase change: $H{\bullet}G_{(s,\beta 1)} = H{\bullet}G_{(s,\beta 2)}$.

Since it has been established that CA•*n*-butyl acetate crystallises in a B-type structure (chapter 3) it is interesting to consider the thermal analysis curves of the CA inclusion compounds with isomers of butyl acetate and to examine these for evidence of similar phase changes. The TG and DSC curves of CANBU and CA•(±)sec-butyl acetate (CASB) are presented as Figures 4.10 a and b. The guest loss occurs in a number of overlapping steps with a sudden sharp increase in the rate of guest loss at high % loss. Crystals of these compounds are highly labile and begin to fracture immediately upon removal from mother liquour. This is similar to the fracturing exhibited by the B-type CA inclusion compounds which undergo a β_1 to β_2 phase change; however, no phase change endotherm appears on DSC analysis. It is possible that the expected thermal event occurred before analysis could be begun as sample preparation was, of necessity, carried out at room temperature. In particular, samples for X-ray powder photography must be finely ground and TG analysis of such particles indicated extensive guest loss during this process even when samples were ground under mother liquor and subsequently dried for packing into a capillary. Guest loss almost certainly follows any β_1 to β_2 phase change and this is therefore not detected under the conditions of the experiment.

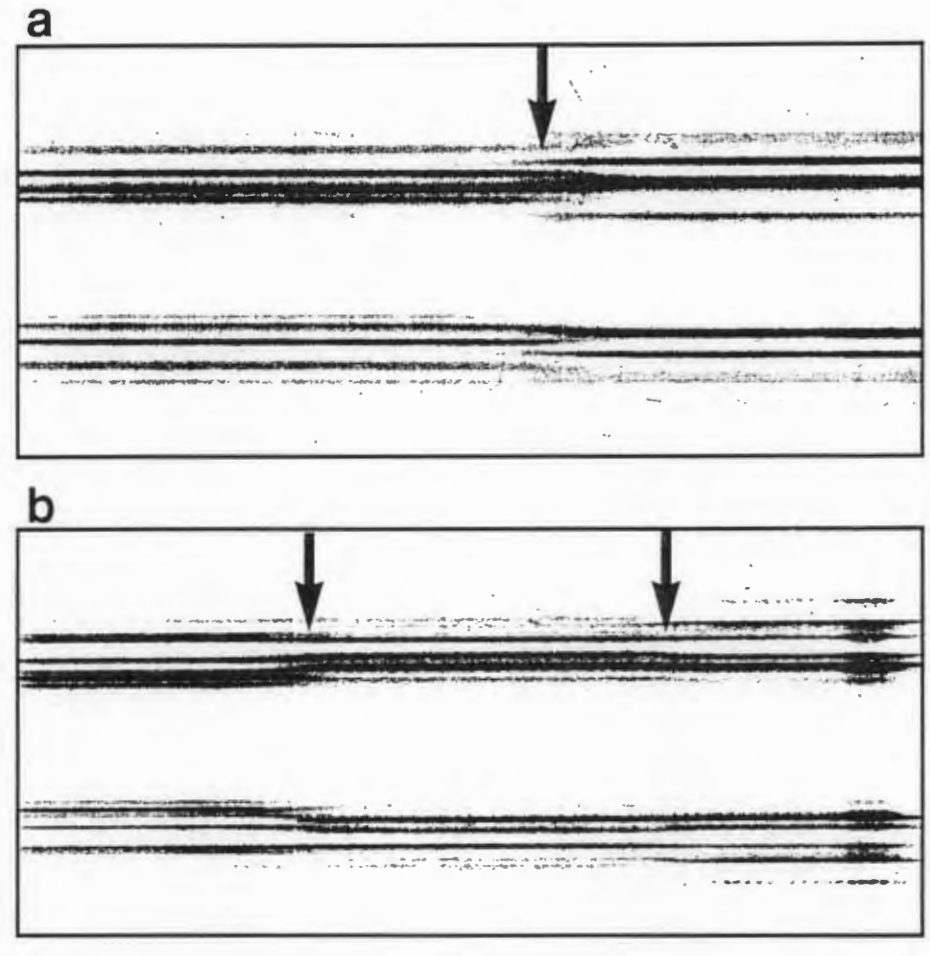

Figure 4.9:
Continuous powder photographs taken under heating for:
a) CAMA and b) CAPAC.
c) Photometrically measured trace of the three phases occurring in the decomposition of CAPAC.
Bottom - Inclusion compound
Middle - Intermediate phase
Top - Desorbed phase (host alone).

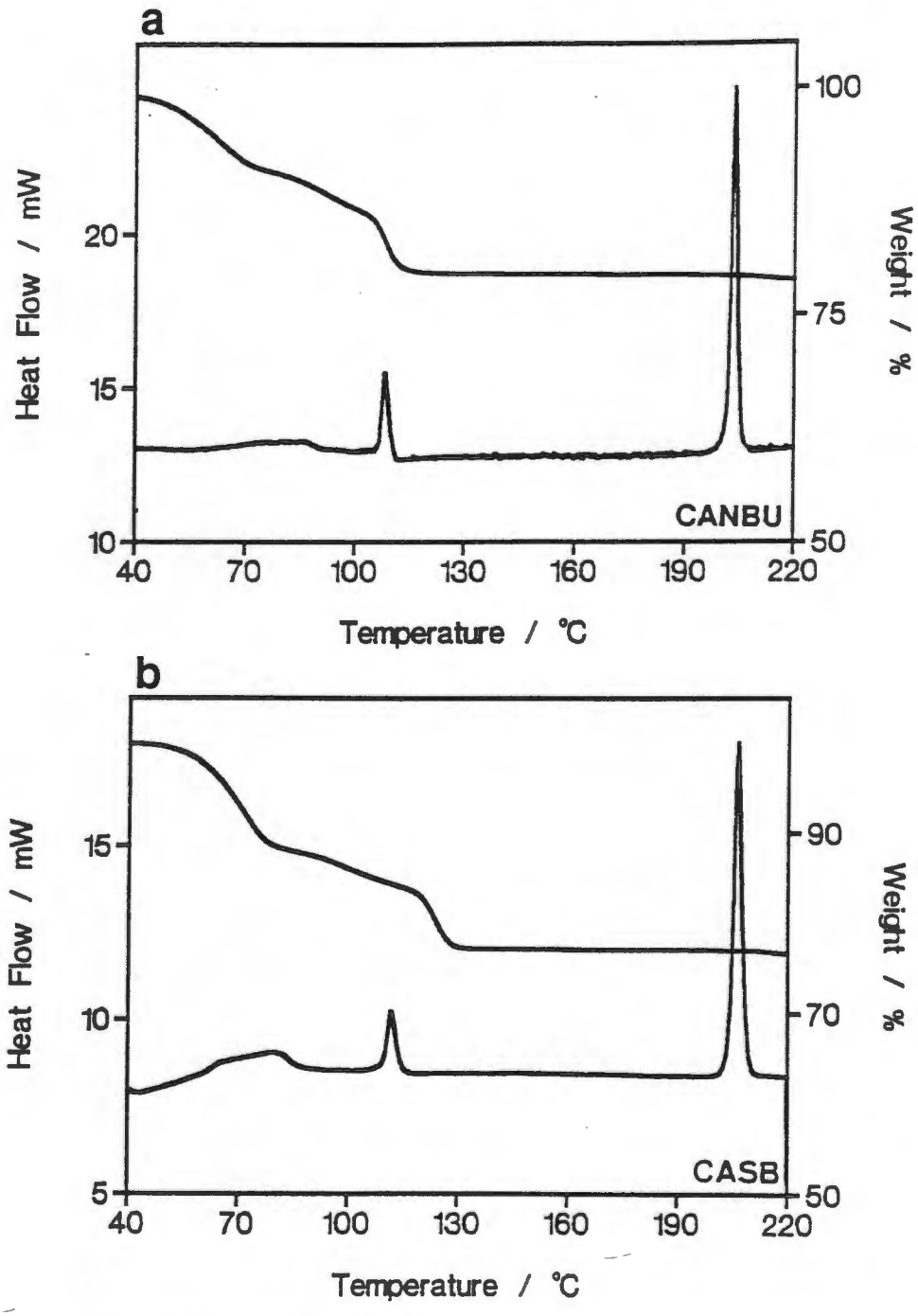

Figure 4.10: TG and DSC traces for: a) CANBU and b) CASB (CA•(±)sec-butyl acetate) at 20 ^{o}C/min and a purge gas flow rate of 40 ml/min.

Group 3: Vinyl Esters

The TG and DSC curves of CAVA and CAMM are presented as Figures 4.11a and b. In both cases the guest loss occurs in a single step and this is reflected in a single guest loss endotherm on DSC analysis. Hot stage microscope observation of samples of these compounds confirms the lack of other thermal events although the loss of guest in CAMM is accompanied by cracking and apparent swelling of the crystals as they become opaque. The guest loss/ β to α phase change peak for CAMM is not simple having shoulders on either side; these could not however be resolved into separate peaks by alteration of heat rates or particle sizes and it appears that the β to α phase change occurs concomitantly with guest loss.

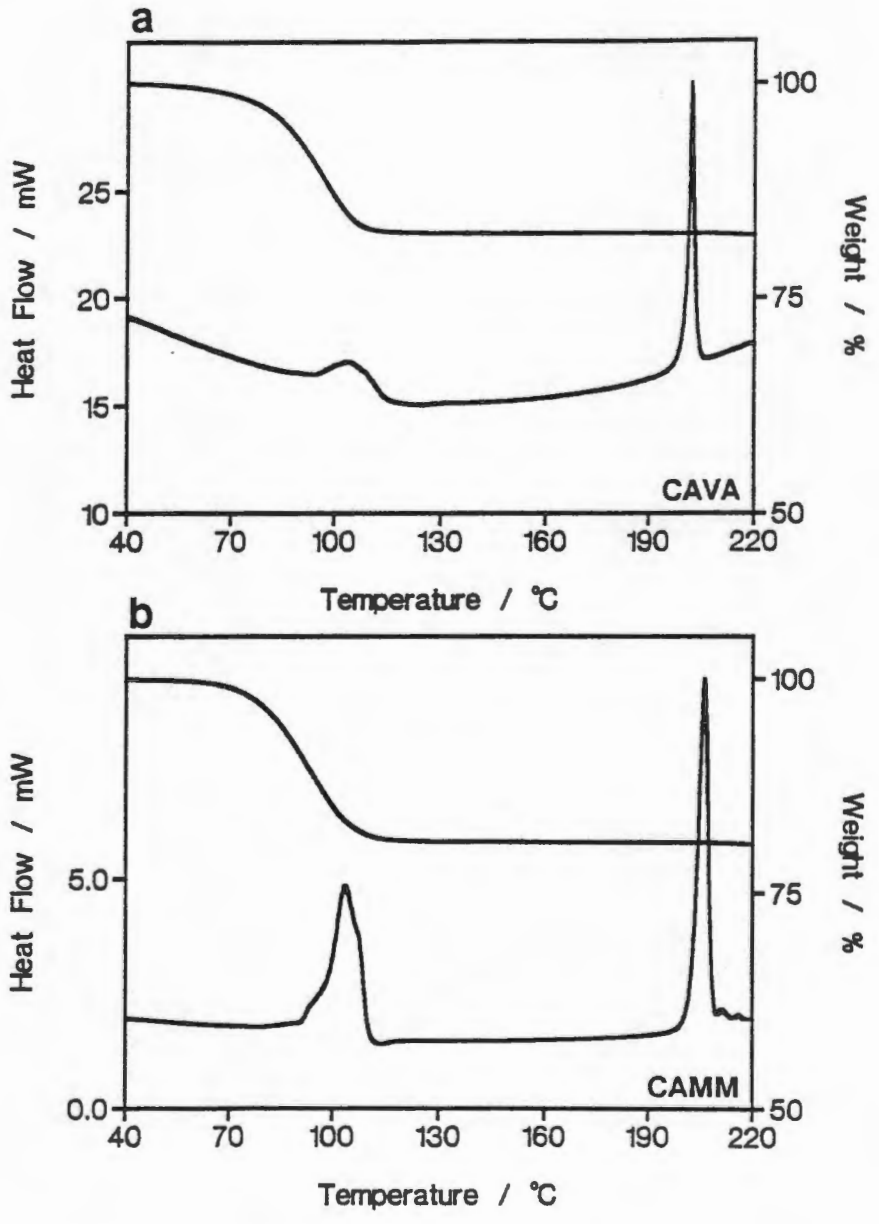

Figure 4.11: TG and DSC traces for a) CAVA and b) CAMM at 20 ^{0}C/min and purge gas flow rate of 40 ml/min.

Group 4: Aromatic Guests

The thermal analysis curves of all of the CA inclusion compounds with aromatic guests including those of CA•acetophenone (the structure of which was analysed by Miki *et al*[11]) are presented as Figures 4.12a to h. That of CAACET is included for comparison with CAPR.

In each case the guest loss occurs in a single step although CABN exhibits minor guest loss at low temperature. This is not uncommon in TG analysis of crystalline inclusion compounds and may indicate loss of guest from crystal surfaces or interstitial spaces. CABN shows a single endotherm associated with guest loss followed by the host melt. In all other cases the host melt endotherm is either significantly reduced (and usually diffuse) or absent. Observation of samples of the crystals under heating reveals that guest loss occurs either upon complete or partial melt of the complex or that the guest appears to "sweat" out of the crystals forming a liquid layer on the surface in which the remaining solid dissolves. Recrystallisation is noted for compounds like CAACET and CAPR and to a lesser extent CAAN, CANI and CAPNOT and this almost certainly accounts for the exotherms following the guest loss peaks in the DSC traces of these compounds. Samples of CAPTOL do not exhibit a host melt endotherm except when the samples are very finely powdered or analysed at a slow heating rate with high purge gas flow rate. Presumably this allows significant reduction of the concentration of guest in the melt and subsequent host recrystallisation.

Figure 4.12 is a series of photographs of crystals of CANI under slow heating; the crystals begin to decay with nuclei of the new phase growing at points of defects. As the guest release temperature is approached the crystal is seen to alter rapidly becoming a mass of small crystallites of the CA(α) phase which melt at the temperature of fusion of the host. If on the other hand these crystals are heated at 20 °C/min they melt congruently at a temperature close to that of guest release (plates 6 and 7, Figure 4.12) and little separation of the CA(α) phase is noted until the concentration of guest in the melt is significantly reduced by volatilisation. Figure 4.13 shows the decomposition of acetophenone crystals at a heating rate of *ca* 20 °C/min. The new phase begins to grow as before but even at a high heating rate congruent melting is never noted and the entire crystal becomes converted to small crystallites of the CA(α) phase. Crystals of CAPTOL (Figure 4.14) decay with initial fracturing of the crystal followed by the start of growth of a new phase and then sudden melt. Little host recrystallisation is noted even after appreciable time at high temperature.

It is probable that both congruent melting and guest release with condensation and subsequent host dissolution give rise to very similar DSC traces. The essential difference between these processes is that in the first case the phase change is : $H{\bullet}G_{(s,\beta)} = H{\bullet}G_{(l)}$ while in the second it is: $H{\bullet}G_{(s,\beta)} = H_{(s,?)} + G_{(l)}$ with subsequent dissolution of the solid host, whose phase is unknown and may be α or β_0.

The DSC trace of CAPR indicates two sharp endotherms followed by a poorly

defined exotherm thought to be due to recrystallisation of the host material. It is notable that CAPR is the only example of a CA inclusion compound with *aromatic* guest exhibiting the B-type packing mode. It is possible that a β_1 to β_2 phase change, analogous to that seen in CAPAC and CAIP decomposition, occurs which would result in a sharp endotherm. However, these endotherms are not easily separated and it proved impossible to detect an intermediate phase. The heating camera used to monitor phase changes on heating does not operate efficiently at temperatures much above 100 °C.

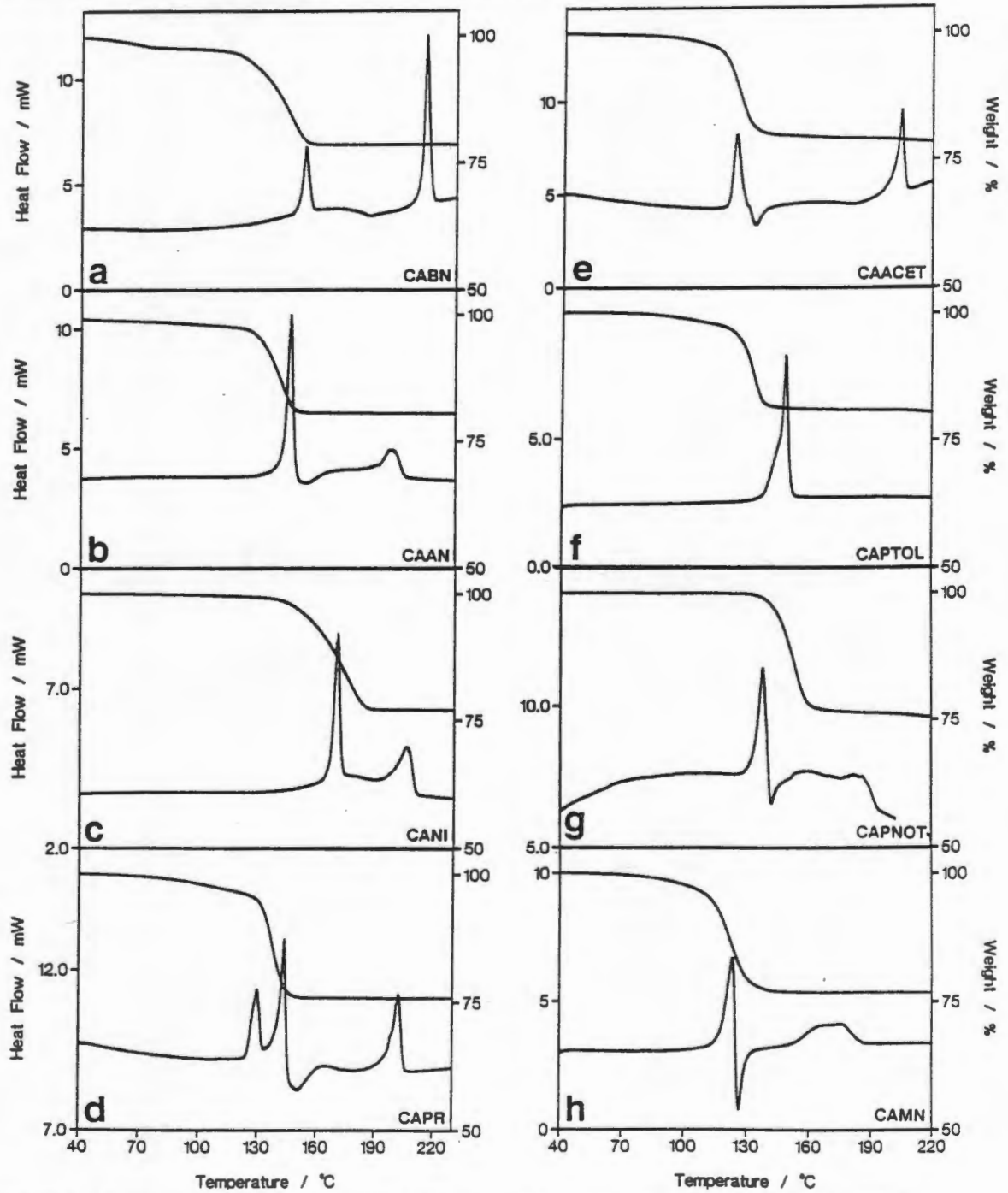

Figure 4.12: TG and DSC traces for a) CABN, b) CAAN, c) CANI, d) CAPR, e) CAACET, f) CAPTOL, g) CAPNOT and h) CAMN at 20 °C/min and purge gas flow rate of 40 ml/min.

Plate 1

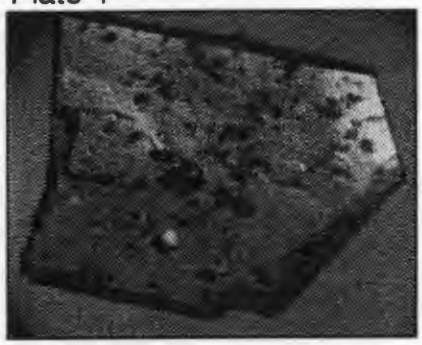

Plate 2

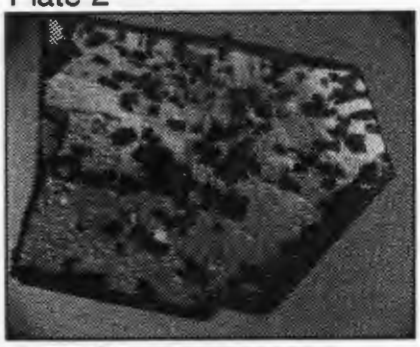

Plate 3

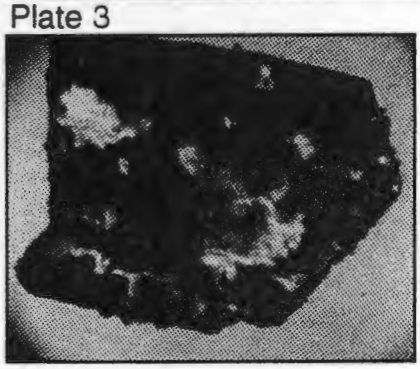

Plate 4

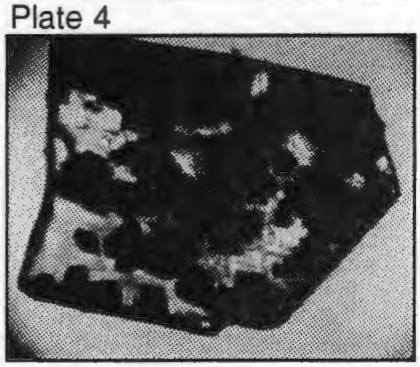

Plate 5

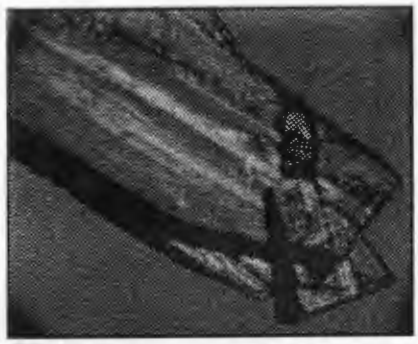

Plate 6

Plate 7

Figure 4.12: Thermal decay of CANI.
Plates 1 to 5, slow heat ing rate;
plate 1 - 33 ^{o}C
plate 2 - 126 ^{o}C
plate 3 - 139 ^{o}C
plate 4 - 154 ^{o}C,
plate 5 - 166 ^{o}C.
Plates 6 and 7, rapid heating .

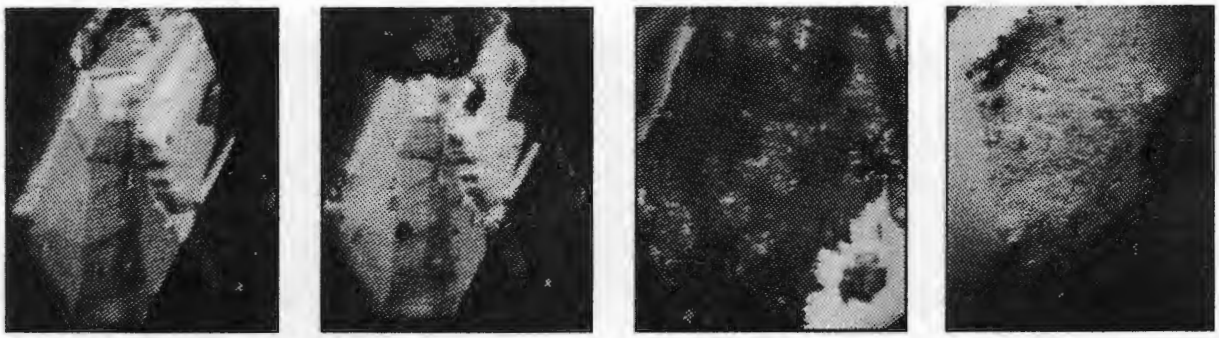

Plate 1 Plate 2 Plate 3 Plate 4

Figure 4.13: Thermal decomposition of CAACET.
Plate 1 - 65 ^{o}C, plate 2 - 102 ^{o}C, plate 3 - 179 ^{o}C, plate 4 - host melt.

Plate 1 Plate 2 Plate 3

Plate 4 Plate 5 Plate 6

Plate 7

Figure 4.14: Thermal decomposition of large single crystals of CAPTOL. Plate 1- room temperature, plate 2 - 108 ^{o}C, plate 3 - 122 ^{o}C, plate 4 - 136 ^{o}C, plate 5 - 148 ^{o}C, plate 6 - 150 ^{o}C, plate 7 - 190 ^{o}C.

Group 5: Mixed Guests

CAMI and other mixed ester compounds

The thermal analysis curves of a number of CA inclusion compounds crystallised from 1:1 mixtures of various aliphatic ketones are presented as Figures 4.16a to c. Interestingly, although there are two guests contained in the same channel, only one guest loss event is noted in each case, the guest loss and β to α phase changes are characterised by a single endotherm which is well defined in CAMI but shows some signs of shoulders or leading tails in the other inclusion compounds grown from solutions of mixed aliphatic esters. Guests in CAMI alternate in the same channels and apparently are lost simultaneously with concomitant β to α phase change.

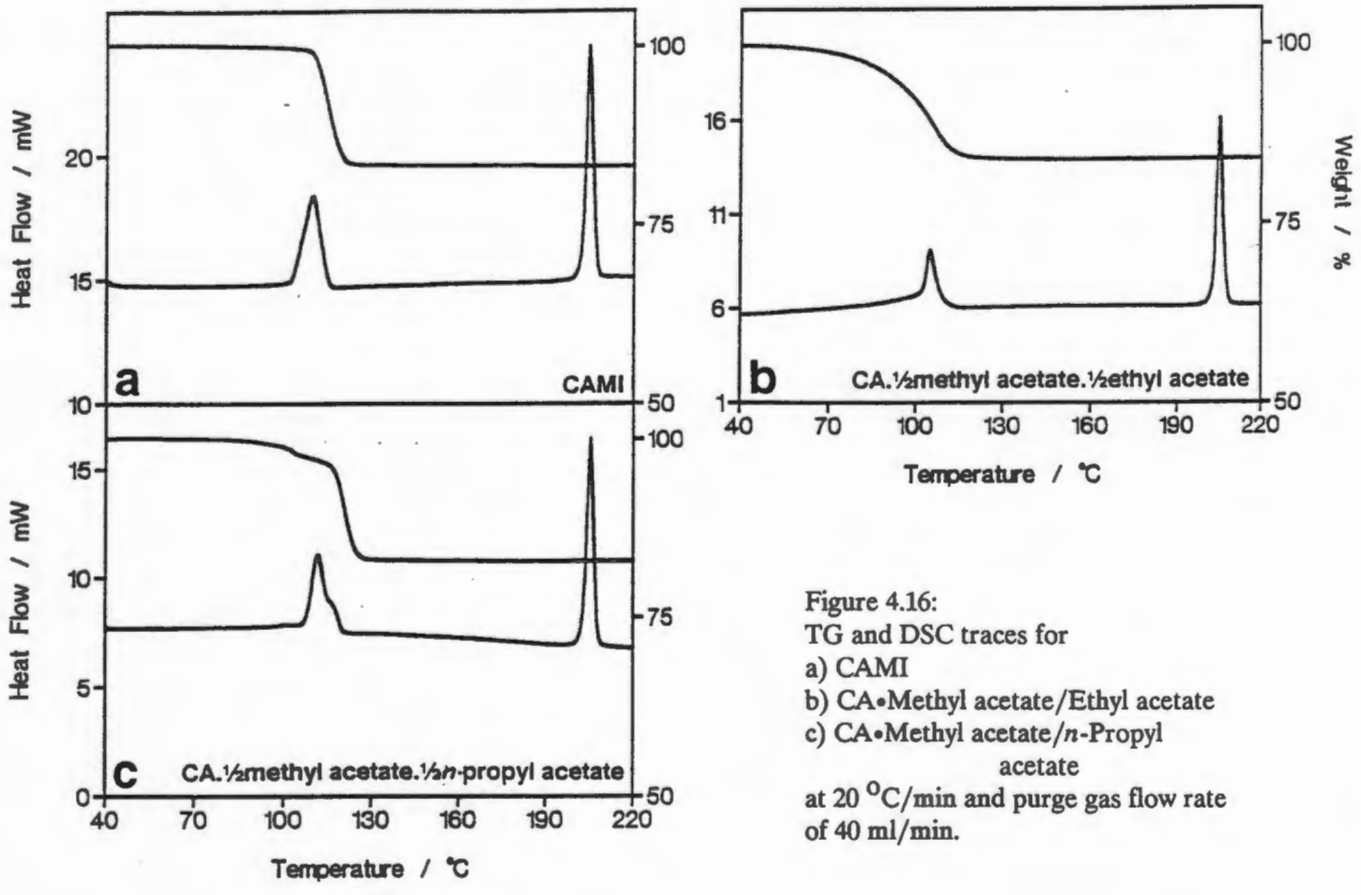

Figure 4.16:
TG and DSC traces for
a) CAMI
b) CA•Methyl acetate/Ethyl acetate
c) CA•Methyl acetate/*n*-Propyl acetate
at 20 °C/min and purge gas flow rate of 40 ml/min.

CADC

The compound CADC also contains different guests alternately in the channels and these are lost in a single but not smooth step (Figure 4.17) which is not separated into two upon alteration of heat rate or particle size. The DSC trace, however is complex with at least two endotherms related to guest loss and β to α phase change. These are ill-defined and diffuse and X-ray powder photographs obtained under heating do not show the existence of a separate phase. Since these endotherms are not associated with discrete guest loss steps

it is possible that the first is the result of mechanical failure of the crystals and indeed the crystals are shown to fracture in spite of the fact that no phase change is observable by rising temperature XRD analysis, strongly implicating such an effect.

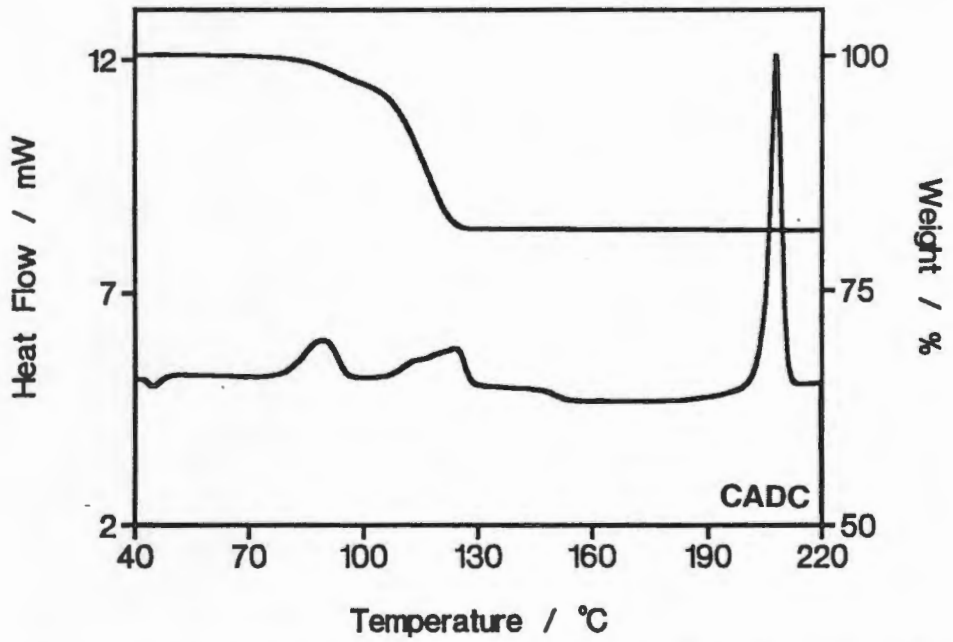

Figure 4.17: TG and DSC traces for CADC at 20 ^{o}C/min and purge gas flow rate of 40 ml/min.

CAAC

The extensively hydrogen bonded compound formed by CA with one acetone and three water guest molecules exhibits complex decomposition behaviour as illustrated in Figure 4.18.

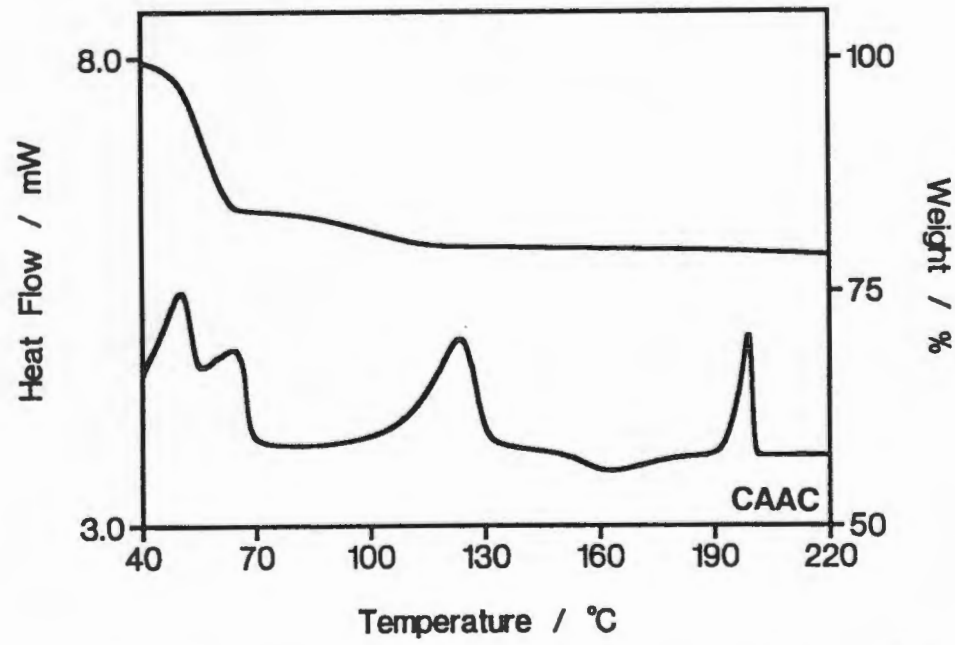

Figure 4.18: TG and DSC traces for CAAC at 20 ^{o}C/min and purge gas flow rate of 40 ml/min.

Changes in the rate of guest loss are indicated by inflection points in the TG curve and these are reflected as a number of diffuse, yet largely discrete, endotherms. In an attempt to separate the events occurring the complex was subjected to programme TG. From a starting temperature of 30 °C the temperature was ramped to 47 °C at 20 °C/min and held at this temperature for 30 mins then ramped to 180 °C at 40 °C/min and held for 10 mins. Separation of two distinct guest loss events was achieved as is illustrated in Figure 4.19. Although the % loss of the first step was difficult to measure as the compound begins to lose guest immediately upon crushing, the % loss in the second step accounts for 1.7 % of the mass of the original compound. This corresponds to the loss of one water molecule per two formula units i.e. per 2(CA•acetone•$3H_2O$). This might be restated as the formation of CA•$\frac{1}{2}H_2O$ units after initial guest loss.

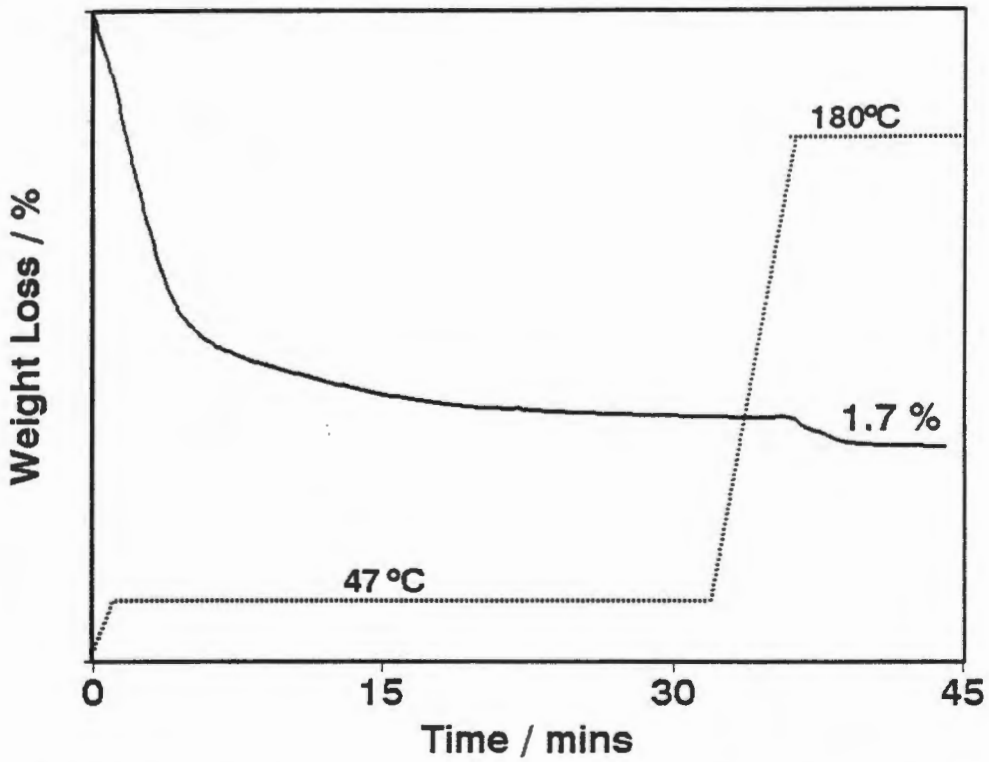

Figure 4.19: TG trace of CAAC under programmed heating: 30 to 47 °C at 20 °C/min, hold for 30 min, 47 to 180 °C at 40 °C/min, hold for 10 min. Solid line - weight loss curve, dotted line - temperature profile.

Analysis of rising temperature XRD photographs of the compound do indeed reveal the existence of at least one stable phase different from that of both the initial inclusion compound phase and the final CA(α) phase. Comparison of XRD patterns of the phase remaining after heating of the inclusion compound to 47 °C for 30 mins and that of the hemihydrate (the structure of which was characterised by Lessinger and Low[12]) reveal that these are analogous and clearly distinguishable from either the inclusion compound or CA(α) phases as illustrated in Figures 4.20a and b. This, combined with the stoichiometry

derived from measured weight loss for this phase, indicates that CA•acetone•$3H_2O$ decomposes with the occurrence of the following solid phases:

$$CA \bullet C_3H_6O \bullet 3H_2O_{(s,\beta)} = CA \bullet \tfrac{1}{2}H_2O_{(s,\gamma)} = CA_{(s,\alpha)}$$

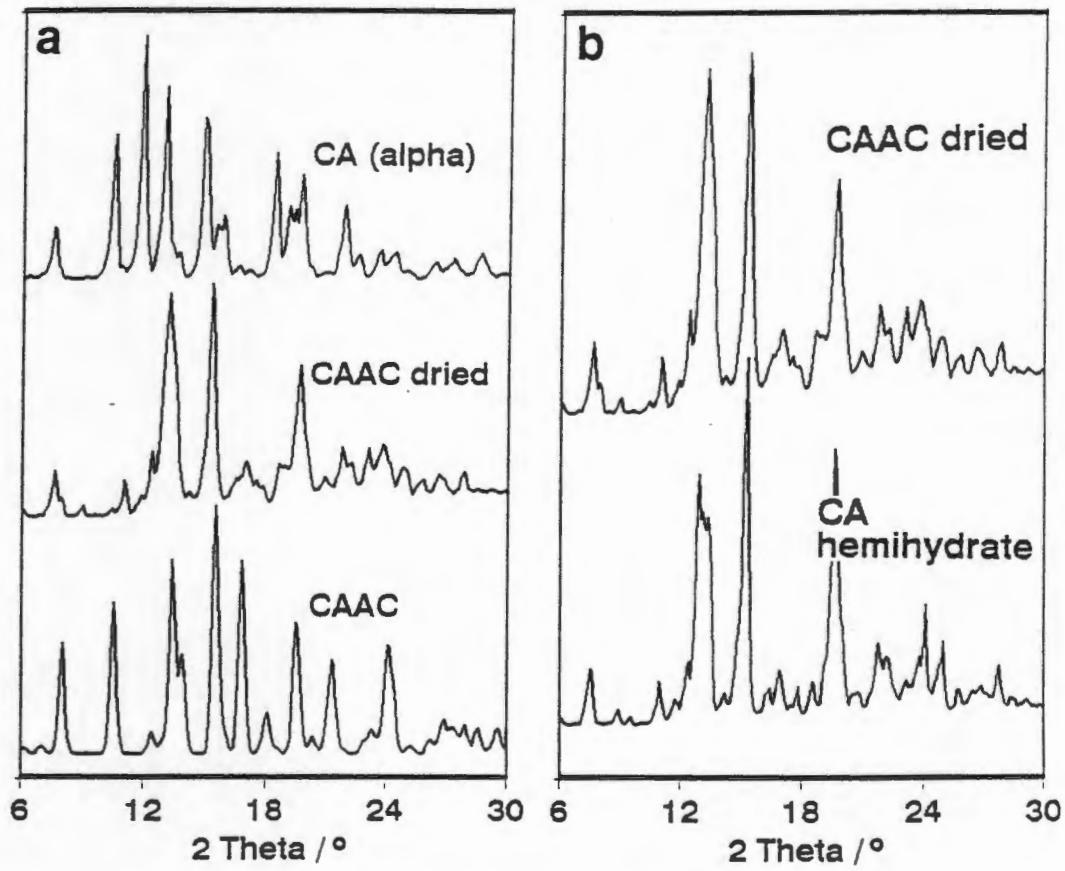

Figure 4.20: a) Comparison of the XRD traces of the CAAC inclusion compound phase (pattern generated from crystal structure data) (bottom), intermediate phase obtained after heating to 47 °C for 30 min (middle) and the CA(α) phase (top) which results upon complete desorption of guest.
b) Comparison of the XRD traces of the intermediate phase obtained on thermal decomposition of CAAC (bottom) and the CA hemihydrate phase (top).

Group 6: Acetonitrile structures

The thermal analysis curves of CACN and MCCN are presented as Figures 4.21a and b. in each case the guest is lost in a single step. CACN shows a single well defined guest loss and concomitant β to α phase change endotherm while MCCN indicates only a single endotherm related to guest loss. No host melt peak is evident in lightly crushed crystalline samples analysed at 20 ^{o}C/min. Observation of samples of MCCN under heating indicates melting of the inclusion compound with associated guest loss and no recrystallisation of host. If the MCCN samples are finely powdered (212-250 μm) the dotted line trace is achieved. The fine powder appears to relinquish the guest without melting and an endotherm at the temperature of fusion of MC is noted. This behaviour would seem to indicate that the melt apparent in the larger crystals is, in fact, a dissolution of the host in the guest such that if the guest is released readily and rapidly swept away, as in the finely powdered sample, no inclusion compound melt ensues.

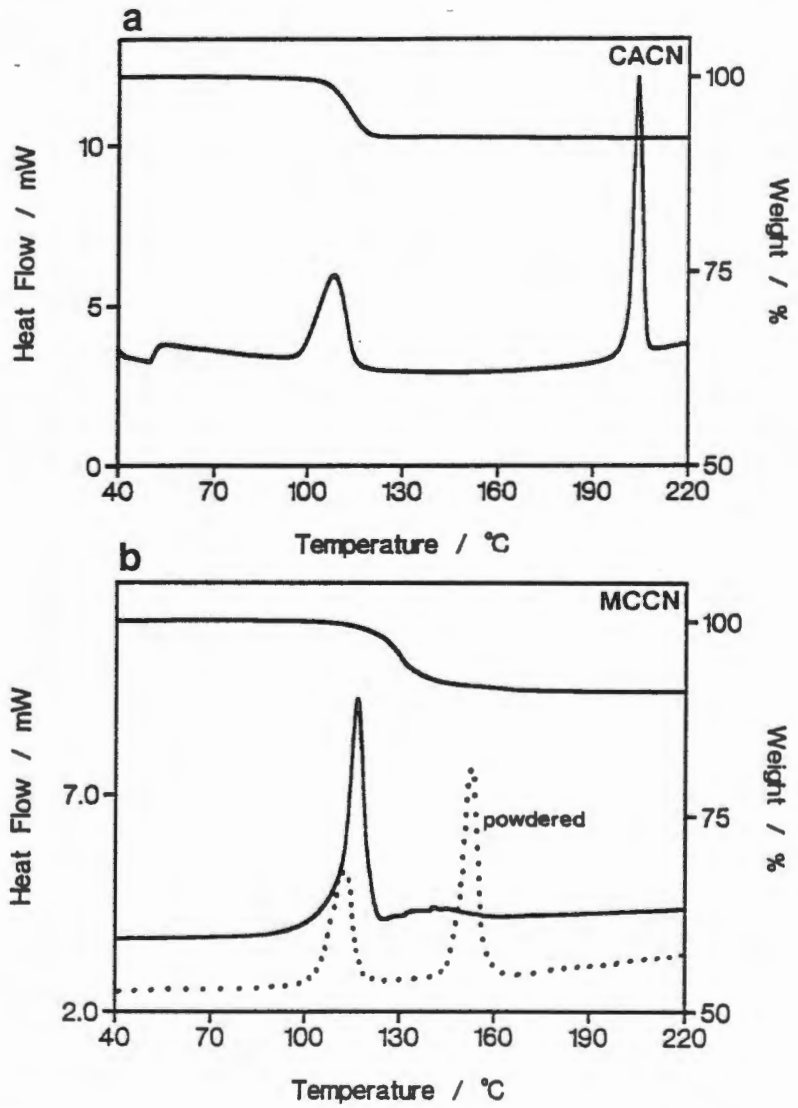

Figure 4.21: TG and DSC traces for a) CACN and b) MCCN at 20 ^{o}C/min and purge gas flow rate of 40 ml/min. Solid line - crushed crystals, dotted line - finely powdered crystals (212-250 μm).

MC(α)

The MC host is difficult to obtain in the crystalline α form and this phase is usually obtained from desorbed samples of readily grown inclusion compound crystals such as those with methanol or acetonitrile. The TG trace of such compounds is identical to that of crushed crystals of MC(α) revealing no guest loss on heating (as required in the α phase) and a single melt endotherm on DSC analysis as seen in Figure 4.22.

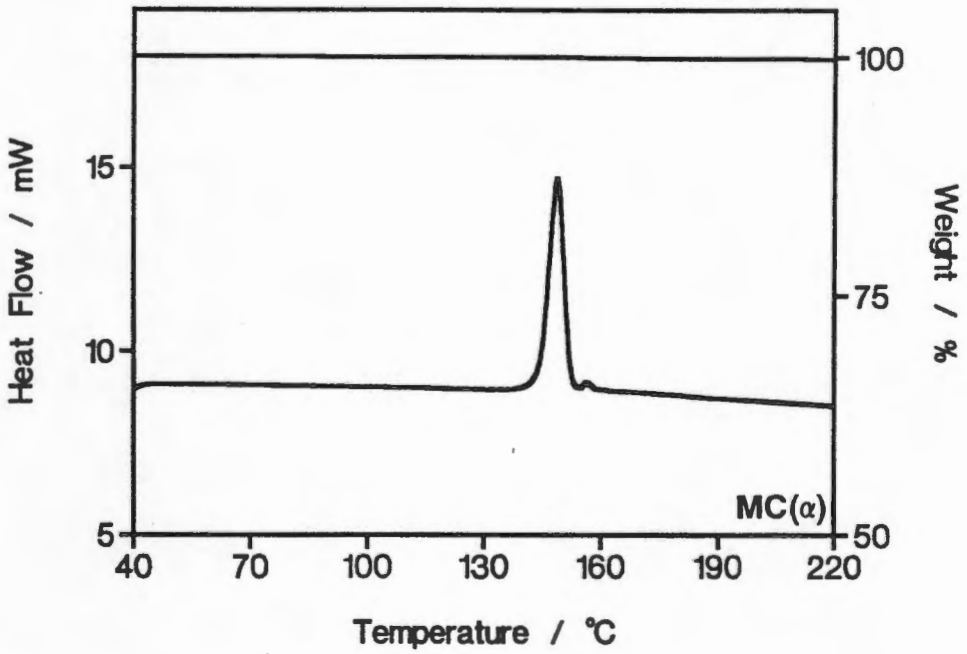

Figure 4.22: TG and DSC traces for MC(α) at 20 °C/min and purge gas flow rate of 40 ml/min.

1 H.G. Mcadie, *Can. J. Chem.*, 1963, **41**, p 2137 / H.G. Mcadie, *Can. J. Chem.*, 1966, **44**, p 1373.

2 M.E. Brown, "Introduction to Thermal Analysis.", Chapman and Hall, 1988.

3 B. Wunderlich, "Thermal Analysis.", Academic Press, 1990.

4 W.W. Wendlandt, "Thermal Analysis, 3rd Edition.", Wiley-Interscience, New York, 1986.

5 D. Dollimore, "Analytical Chemistry", 1992, **64**, p 147R-153R.

6 S.V. Lindeman, V.E. Sulclover and Yu.T. Struchkov , *Cryst. Struc. Commun.*, 1981, p 1173-1179.

7 B.T. Ibragimov, S.A. Talipov, T.F. Aripov, *J. Incl. Phenom. and Mol. Recog. in Chem.*, 1994, **17**, pp 317-324.

8 S.R. Byrn, Solid State Chemistry of Drugs, Academic Press, 1982, p 139 and p 170.

9 M.A. White, R.T. Perry, *Chem. Mater.*, 1994, **6**, p 603-610.

10 C.J. Keattch and D. Dollimore, in "An introduction to Thermogravimetry, 2nd Ed", Chapter 5, 1975, Heydn and Son, London.

11 K. Miki, A. Masui, K. Kasai, M.Miyata, M. Shibakami and K. Takemoto, *J. Am. Chem. Soc.*, 1988, **110**, p 6594.

12 L. Lessinger and B.W. Low, *J. Crystallogr. Spectrosc. Res.*, 1993, **23**, p 85.

CHAPTER 5: SELECTIVITY

Crystallisation has often been used as a mechanism for enriching or separating compounds. Separation may be achieved by spontaneous resolution (for example consider the famous experiment of Pasteur in which ammonium tartrate is resolved into distinguishable crystals of each enantiomer) or may result if crystallisation of one species is kinetically or thermodynamically favoured over another. This is the basis for purification by recrystallisation. Similarly crystallisation of inclusion compounds has been used to separate close isomers or otherwise mixed compounds.

The selective crystallisation of a host material with a particular guest has been investigated by a number of workers. Separation of enantiomers by clathrate formation[1] and isolation and optical resolution of materials[2] have been reviewed and the possibility of asymmetric synthesis in the chiral medium provided by certain types of inclusion complexes investigated[3,4]. Extension of these processes to resolution of racemates by distillation with inclusion compounds[5] or for use as chemical sensors[6,7] is indicative of the potential industrial use of inclusion separation.

CA is a relatively uncostly host compound and reports of separation of optical isomers by inclusion compound formation have appeared in the literature[8] and it was therefore deemed of use to investigate the separating capacity of this host.

NITROBENZENE VERSUS ANILINE

The separation of nitrobenzene and aniline by crystallisation as guest molecules in CA inclusion compounds was attempted. While this is seldom (if ever) a task which could not be better achieved by simple fractional distillation these compounds were amongst the first characterised and were chosen to probe the effectiveness of CA as a potentially "discriminating" host.

A series of crystalline samples of CA inclusion compounds were prepared from solutions made by dissolving dried CA in mixtures of the guest liquids as described in chapter 2. The mole ratios of guest molecules included in the crystals were determined by GC analysis.

The percentage guest composition for each sample as measured by GC analysis are listed in Table 5.1 and the selectivity curve obtained presented as Figure 5.1. Clearly nitrobenzene is preferred over aniline. If the starting solution contains 50% nitrobenzene the inclusion compound crystals produced therefrom will contain 80% nitrobenzene, a significant enrichment of one component over another. To ensure that this apparent selection of the higher boiling component was not an artefact of the method of analysis both the evolved vapours and liquid condensed therefrom were sampled. Percentage composition of guest as measured in the condensate and the vapour were almost identical as is illustrated by the proximity of points from each experiment on the selectivity curve.

Table 5.1: % Composition of Aniline in crystals made from solutions of mixed guest, as measured by GC.

Solution	Head Space Analysis	Condensed Guests	Guest Loss Onset T (°C)
10.38	2.03 2.01	2.05 2.02	160.78
13.44	2.42 2.31	3.14 3.16 3.12	160.75
24.54	4.12 5.58	5.63 5.91	159.55
25.54	6.62 5.05	6.95 6.63	
32.14	9.51 9.73	10.19 10.18	158.53
33.47	8.65 8.58	10.61 10.47 10.42	158.51
54.72	31.89 23.11	29.36 29.21	151.85
56.11	23.72 24.30	27.46 27.49 26.34 26.38	
56.58	28.75 29.26	29.57	
70.34	43.67 40.27	52.05 52.32	145.39
75.74	56.47 58.07	61.49 61.77	
90.90	91.81 91.57	92.33 92.34	134.20
91.76	93.83 93.58	93.96 94.07 94.15	133.62
93.37	95.41 94.61	95.23 95.36	136.62
100.00			135.56
0.00			160.82

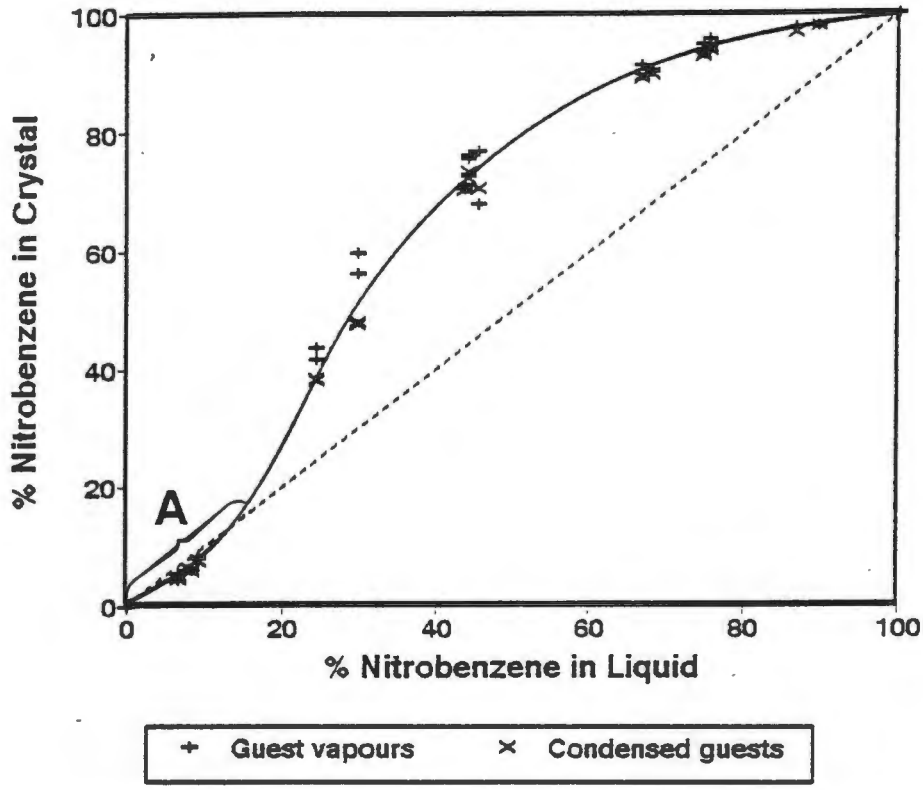

Figure 5.1: Competition curve derived for the crystallisation of CA inclusion crystals from mixed solutions of nitrobenzene and aniline.

While a 30% enrichment of one component over another might seem significant the shape of the curve indicates that complete separation of nitrobenzene or aniline would require numerous crystallisation steps and, in fact, would never be complete because, as the % nitrobenzene drops to *ca* 10%, no enrichment occurs and the crystals contain the same % nitrobenzene as the solution (region A on the graph).

It is often questionable whether separation by inclusion crystallisation is the result of formation of larger number of crystals containing only one guest molecule or of enrichment of one guest molecule in each individual crystal. This is illustrated schematically in Figure 5.2.

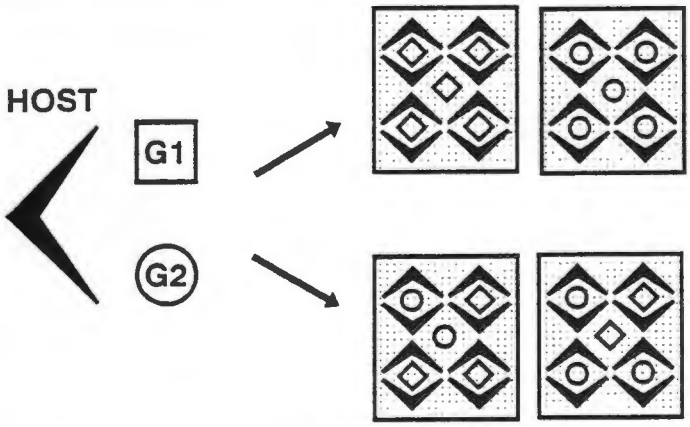

Figure 5.2: Schematic representation of the two possibilities that arise when inclusion compounds are crystallised from mixtures of guest compounds. Top right - mixed crystals containing separate guest species. Bottom right - mixed guest crystals.

A recently published account of a solid state ^{13}C-NMR study of crystals of the inclusion compound of CA with γ-valerolactone raises this point. Miyata *et al*[9] claim 28 to 38 % enrichment of (S)-(-)-γ-valerolactone on absorption by or crystallisation with CA while Miki *et al*[10] publish the structure of CA with (S)-(-)-γ-valerolactone indicating no disorder of the guest molecule which might indicate the existence of more than one type of guest molecule in the CA channels. These results appear mutually exclusive unless there exist two types of crystals: CA•(S)-(-)-γ-valerolactone and CA•(R)-(+)-γ-valerolactone. The existence of two discrete types of crystals is confirmed by a a solid state ^{13}C-NMR study by Imashiro *et al*[11].

To attempt to clarify which type of selectivity (crystals containing mixed guests or crystals containing each guest separately) occurs in the example under study the guest release temperatures of the aniline/nitrobenzene mixed inclusion compounds were measured by DSC. As has been noted in chapter 4 guest release temperatures of the inclusion compounds with pure aniline or nitrobenzene guests are quite different: the endotherms relating to guest release occurring at 135 °C and 162 °C for CAAN and CANI respectively. Interestingly, the crystals produced from solutions of CA in mixtures of nitrobenzene and aniline exhibit only a single guest loss endotherm the temperature of which is related to the guest composition. An example is presented as Figure 5.3 and a plot of guest loss T_{onset} versus % composition as Figure 5.4. The relationship between guest composition and onset temperature is linear over a large range of guest compositions and could be used as an estimate of the % of each guest contained in the crystals.

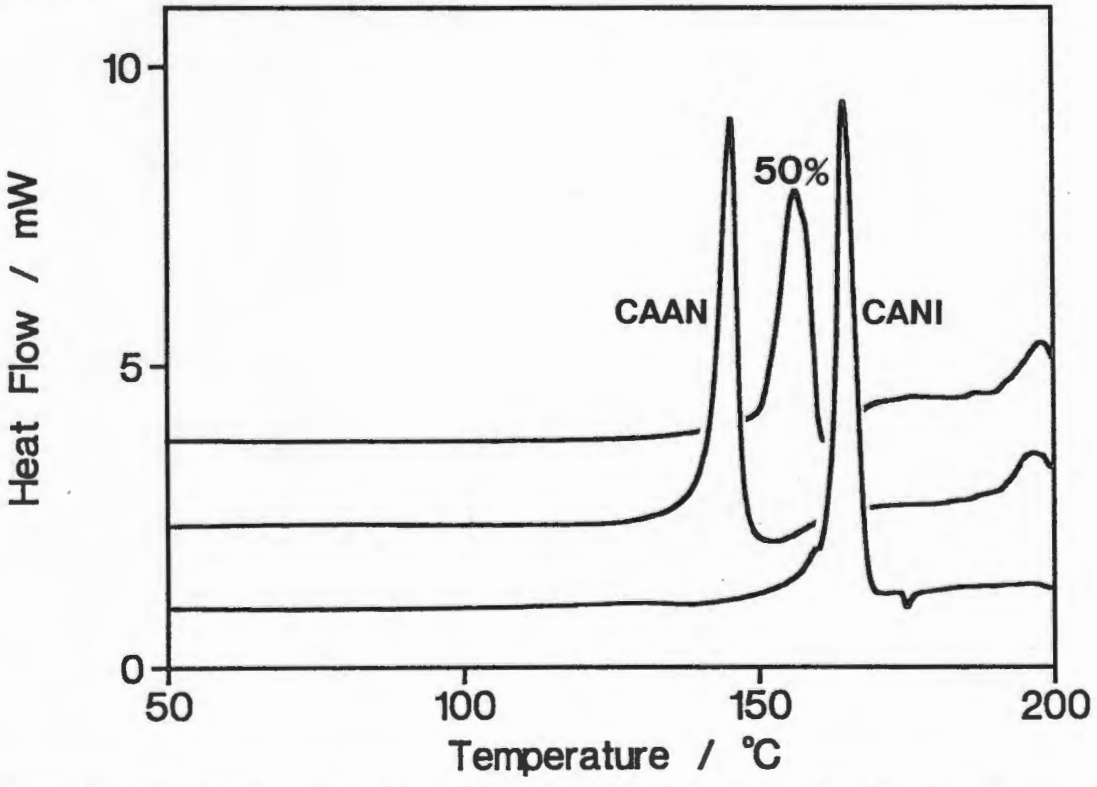

Figure 5.3: Comparison of the position of the guest loss endotherm as a function of guest composition.

The single guest loss endotherm exhibited by these compounds implies that both guests are contained within each single crystal and are released concertedly. This is the first example of the use of DSC as an analytical technique in competition experiments.

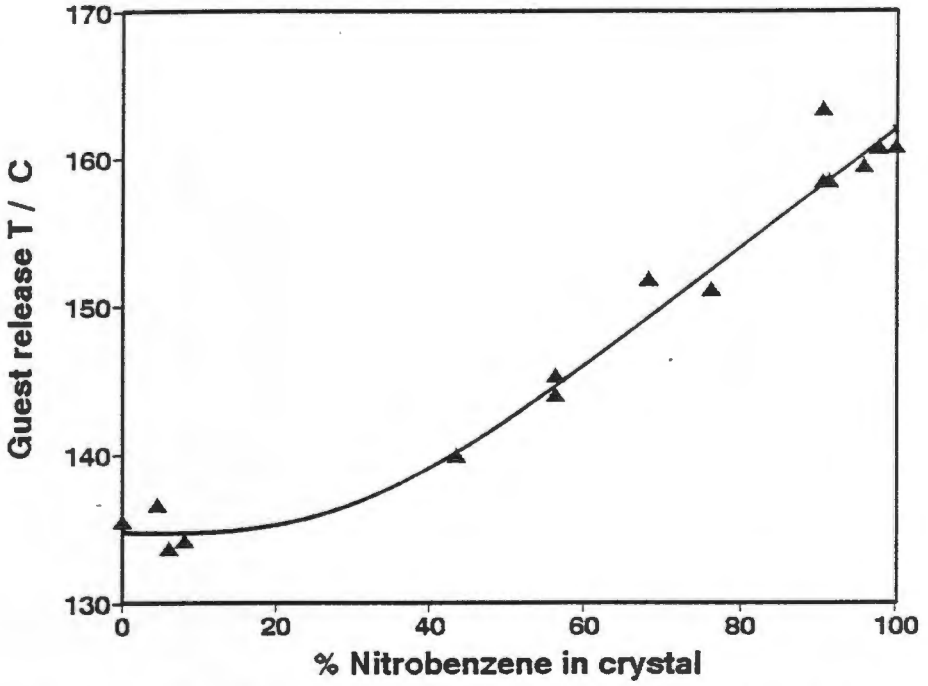

Figure 5.4: Guest loss onset temperature versus % Nitrobenzene contained in the crystals.

It should, in principle, be possible to find a relation between host:guest interactions in the crystal and the results of competition. The program EENY[12] was used to evaluate the van der Waals energy using empirical atom pair potential curves. The coefficients of the atom-atom potentials are of the form:

$$U(r) = a \exp(-br)/r^d - c/r^6$$

where r is the distance between the atom pairs and a, b, c and d are as given by Giglio[13] and recently reviewed by Pertsin and Kitaigorodsky[14].

The potential energies (PE) of single guest molecules surrounded by appropriate host molecules were found to be -20.9 kJ and -15.7 kJ for CANI and CAAN respectively. Thus it appears that the thermodynamically favoured clathrate is the preferred product in crystallisations from solutions containing mixtures of guests nitrobenzene and aniline.

It is interesting to contrast this selective behaviour where one guest is "preferred" to the formation of crystals of inclusion compounds containing mixed guests detailed in chapters 3 and 4. Crystals containing vastly disparate guest molecules such as 1,2-dichlorobenzene and acetone as well as crystals with similar guests methyl acetate and *i*-propyl acetate have been analysed by single crystal diffractometry while evidence for the existence of other 1:½G_1:½G_2 inclusion compounds has been presented.

If mixed guest inclusion compound crystals occur (as is implied by the single guest loss endotherm noted on DSC analysis), a new compound is formed and the potential energy associated with a single guest molecule may be quite different from that determined for the crystals containing pure guests of either type. If the mixed guest crystal is the thermodynamically favoured product a more negative value for the calculated PE per guest molecule would be expected.

To attempt to verify this assertion the PE of single guest molecules in the compounds CAMA, CAIP and CAMI were evaluated using atomic positions derived from the crystal structure analyses. In the structures CAMA and CAMI, which belong to the space group *P*1 with two crystallographically independent host and guest molecules in the asymmetric unit, the PE value for a single guest molecule was determined as the averaged value per guest molecule.

The calculated PE values were found to be: CAMA = -10.74 kJ, CAMI = -18.96 kJ and CAIP = -22.38 kJ. The calculated PE for the mixed guest compound is *not* lower than that of both pure guest compounds and, in fact, falls between the two. In spite of this, the mixed guest compound is formed from solutions of methyl acetate and *i*-propyl acetate.

Two possibilities arise:

i) The formation of mixed crystals containing ordered arrays of both guests indicates formation of the kinetically rather than the thermodynamically preferred product.

OR

ii) The atom-atom potential pair method of calculating the PE of guest molecules in their crystalline environment is inadequate, being oversimplified in that synergistic electronic effects are not accounted for. Guest-guest distances are generally relatively charge and interactions are subtle.

A consideration of close contacts occurring in the mixed guest and pure ester guest inclusion compounds indicates that the second assertion is likely. Close contacts are arbitrarily defined in the program EENY as being any atom-atom pairs for which $U(r) > 0$. These are listed in Table 5.2 and it is immediately clear that there are a number of contacts between guest atoms and host oxygen atoms particularly for the structure CAMI. Using the atom-atom potential method detailed above results in positive values for U(r) for these interactions implying a destabilising effect *although* a consideration of electronic effects might lead to rather different conclusions.

The assertion that the simplified method of determination of PE by consideration of atom-atom potentials results in underestimation of the favourable interaction occurring upon enclathration does not however negate the possibility that the crystallisation reaction (and "choice" of guest) is defined

by kinetic rather than thermodynamic factors. More detailed considerations of the energetic environments of the guests would be required to make such an assertion with any degree of confidence.

Table 5.2: Close contacts between host and guest, and guest and guest, in CAMA, CAMI, CAIP. (Me signifies methyl group)

	Contact			Distance (Å)
CAMA				
	Me1GA	-	H19O	3.162
	Me3GA	-	H1N	3.164
	Me1GA	-	H6N	3.138
	Me1GA	-	H16X	3.176
	Me1GA	-	H23X	2.625
	Me1GA	-	H16M	3.136
	Me1GB	-	H23M	2.765
	Me1GB	-	H6X	2.846
CAMI				
	O2GM	-	H3N	2.738
	O2GM	-	O25A	4.574
	O1GM	-	H25A	4.366
	O2GM	-	O27A	4.469
	O1GM	-	O27A	3.560
	O1GI	-	H5N	3.189
	O1GM	-	O26B	3.754
	O1GI	-	H23X	2.643
	O1GI	-	O27B	4.132
	O1GI	-	O28B	4.343
	O2GI	-	O27B	4.720
	C4GI	-	O28B	3.334
	O2GI	-	O2GM	4.703
	O1GI	-	O2GM	3.920
CAIP				
	O1G	-	H162	2.824
	O1G	-	H221	3.170
	O2G	-	H31	3.095
	O2G	-	H51	3.016

1 D. Worsch and F. Vögtle, *Topics in Current Chemistry, Molecular Inclusion and Molecular Recognition - Clathrates I*, 1987, **140**, p 22.

2 F. Toda, *Topics in Current Chemistry, Molecular Inclusion and Molecular Recognition - Clathrates I,* 1987, **140**, p 140.

3 F. Toda, In "Inclusion Compounds, Vol. 4", Eds: J.L. Atwood, J.E.D. Davies and D.D. MacNicol, Oxford University Press, 1991, p 126.

4 F. Toda, H. Miyamoto, K. Takeda, R. Matsugawa and N. Maruyama, *J. Org. Chem.*, 1993, **58**, p 6208.

5 G. Kaupp, *Angew. Chemie, Int. Ed. Engl.*, 1994, **33**, 7, p 728.

6 E. Weber, C. Wimmer, A.L. Llamas-Saiz and C. Foces-Foces, *J. Chem. Soc, Chem. Commun.*, 1992, p 733.

7 A. Ehlen, C. Wimmer, E. Weber and J. Bargon, *Angew. Chem. Int. Ed. Engl.*, 1993, **32**, 1, p 110.

8 M. Miyata, M. Shibakami and K. Takemoto, *J. Chem. Soc., Chem. Commun.*, 1988, p 655.

9 M. Miyata, M. Shibakami and K. Takemoto, *J. Chem. Soc., Chem. Commun.*, 1988, p 655.

10 K. Miki, N. Kasai, M. Shibakami, K. Takemoto and M. Miyata, *J. Chem. Soc. Chem. Commun.*, 1991, p 1757.

11 F. Imashiro, D. Kuwahara and T. Terao, *J. Chem. Soc. Perkin Trans. 2*, 1993, p 1759.

12 W.D.S. Motherwell, EENY: Potential Energy Program, Cambridge University.

13 E. Giglio, *Nature*, 1969, **222**, p 339.

14 A.J. Pertsin and A.I. Kitaigorodsky, The Atom-Atom Potential Method, Chemical Physics 43, Springer-Verlag, Berlin, 1987, **3**.

CHAPTER 6: REACTIONS IN THE SOLID STATE.

The hosts and host-guest complexes studied undergo a number of reactions in which at least one component exists in the solid state. Desorption and sorption reactions:

$$HG_{(s,\beta)} = H_{(s,\alpha)} + G_{(g)}$$

(the forward and reverse reactions respectively), and solid-solid reactions :

$$H_{(s,\alpha)} + G_{(s)} = HG_{(s,\beta)}$$

will be detailed in separate sections of this chapter.

All of the above-mentioned sorption reactions are effectively heterogeneous reactions involving either solid and gas or two separate solids, each with their own specific crystal structures, which react together to produce a third crystalline material which is an inclusion compound and which exhibits a third, unique structure. In the case of desorption reactions the reactant is in the solid phase while the products are solids and vapours.

GENERAL THEORY OF HETEROGENEOUS KINETICS.

The heterogeneity of reactions is a function both of the occurrence of reactants and products in different phases, as well as of the separation of reactants and products by a "reaction front". This separation is due to the relative immobility of the solid phase and as such the rate of reaction will depend on:

i) displacement of the reactive interface (the reaction front)
ii) diffusion of reactants or products to or from the reaction zone[1,2].

Solid state reactions depend (unlike solution or gas phase reactions), on the relative positions of reactant and/or product *molecules* rather than on concentration or vapour pressure. Not all positions in a crystal are of the same intrinsic potential reactivity and it is generally accepted that proximity to crystalline defects plays a decisive role in defining the points at which reaction will be initiated within the crystal [2]. These defects may be either localised as in the case of point defects or localised non-stoichiometry, or extended defects such as edge or screw dislocations or surfaces including edges and steps [2,3].

Once reaction is initiated strain occurs at the reaction site (the nucleus), due to incompatibility of the crystalline product with the lattice of the crystalline reactant, and the reacted region must either collapse back to the unreacted structure or further reaction must occur and the nucleus propagate. Newly formed nuclei are termed "germ nuclei" while those that have grown to a threshold size and are growing are "growth nuclei". This phenomenon dominates the early phases of reaction in the solid state and often results in the existence of an induction period during which reaction is delayed as is illustrated in Figure 6.1.

The period indicated A often occurs in reactions involving a gaseous reactant or

product such as sorption or desorption reactions. It may be ascribed to the almost instantaneous reaction of finely powdered material or absorption or desorption of gas at the surface of large crystals. Period B is the induction period during which nuclei are formed both at the surface and in the bulk of the crystals and period C the acceleratory period during which the reaction interfaces spread rapidly from nuclei through the crystals. Point D represents the inflection point beyond which the deceleratory period, E, occurs. During this period growth of nuclei is truncated by interception with other burgeoning nuclei resulting in decrease of the overall rate of reaction.

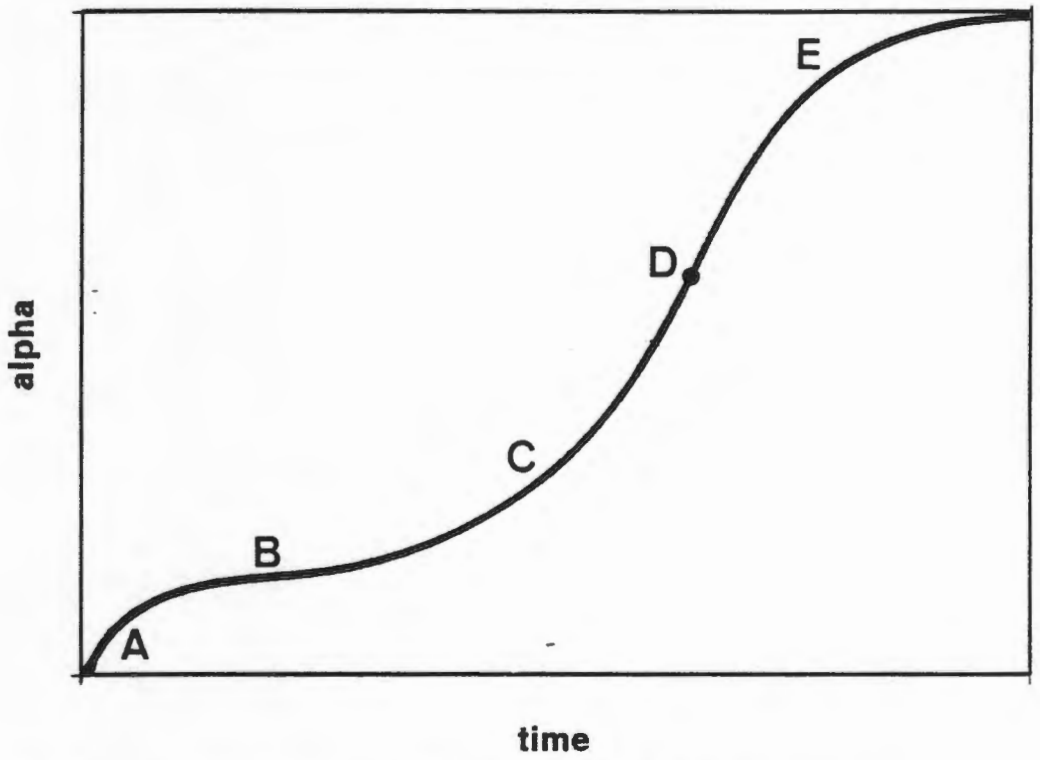

Figure 6.1: Typical α vs time curve. A: Initial rapid reaction, B: Induction period, C: Acceleratory period, D: Inflection point, E: Deceleratory period.

Since the concept of concentration, generally employed in the study of homogeneous reaction kinetics, clearly has no meaning in the solid state, the progress of reaction must be followed through monitoring of another parameter. We define the extent of reaction, α, which in the case of a guest release, or desorption, reaction may be related to amount of gas evolved as measured by weight loss of an accurately weighed sample at time t:

$$\alpha_t = (m_0 - m_t)/(m_0 - m_f)$$

where m_0 is the initial mass, m_t the mass at time t, and m_f the mass at the completion of reaction. By analogy α for a sorption reaction would be:

$$\alpha_t = (m_t - m_0)/(m_f - m_0).$$

A kinetic study therefore involves measurement of α with time at constant temperature.

Various kinetic equations of the form: $f(\alpha) = kt$ (where k is the rate of reaction and t time) have been derived to account quantitatively for the kinetics of solid state reactions. The most commonly encountered kinetic equations are listed in Table 6.1.

Table 6.1: Theoretical rate equations for solid-state reactions (integral form). (Modified from Brown[4].)

		$f(\alpha) = kt$
Sigmoid α-time curves:		
A2	Avrami-Erofe'ev	$[-\ln(1-\alpha)]^{1/2}$
A3	Avrami-Erofe'ev	$[-\ln(1-\alpha)]^{1/3}$
A4	Avrami-Erofe'ev	$[-\ln(1-\alpha)]^{1/4}$
B1	Prout-Tompkins	$\ln[\alpha/(1-\alpha)]$
Deceleratory α-time curves:		
Based on geometrical models		
R2	contracting area	$1-(1-\alpha)^{1/2}$
R3	contracting volume	$1-(1-\alpha)^{1/3}$
Based on diffusion mechanisms		
D1	one-dimensional	α^2
D2	two-dimensional	$(1-\alpha)\ln(1-\alpha)+\alpha$
D3	three-dimensional	$[1-(1-\alpha)^{1/3}]^2$
D4	Ginstling-Brounshtein	$(1-2\alpha/3)-(1-\alpha)^{2/3}$
Based on 'order of reaction'		
F1	first order	$-\ln(1-\alpha)$
F2	second order	$1/(1-a)$
F3	third order	$[1/(1-\alpha)]^2$
Acceleratory α-time curves:		
P1	power law	$\alpha^{1/n}$
E1	exponential law	$\ln \alpha$

The Avrami-Erofe'ev and the Prout-Tompkins equations, which are derived from considerations of the geometry of nucleation and growth of the product phase within crystals of the reactant phase, are usually invoked to describe decomposition reactions which result in evolution of gas. The Avrami-Erofe'ev mechanisms describe reactions which begin with random and rapid evolution of nuclei which grow in two, (A2), or three, (A3), dimensions or which proceed with two stages of nucleation, (A4). The Prout-Tompkins expression which occurs in two forms (that presented above and $k \ln t = \ln[\alpha/(1-\alpha)]$), is derived to account for reactions that proceed by a chain branching mechanism of nuclei growth. Thus it comprises an initial acceleratory phase which is terminated at $\alpha_t = ½$ as the reaction fronts proceeding from the separate nuclei begin to

impinge on each other resulting in cessation of growth; the deceleratory phase.

Rate laws describing deceleratory α-time curves are divided into those based on geometrical models of advancement of the phase boundary towards the centre of particles, (the 'R' rate laws), and the 'D' rate laws describing diffusion controlled mechanisms. These result in reaction fronts that propagate towards the centre of the particle either in one dimension i.e. as a flat sheet (D1), in two dimensions i.e. towards the centre of a cylinder (D2) or in three dimensions where the reacting particle is envisaged as a sphere completely covered by a uniformly thick layer of product (D3). The D4 mechanism is a modification which is invoked where the molar volumes of solid reactant and product are unequal.

While 'order' of reaction in its usual sense as a measure of the molecularity of the collision leading to the 'activated complex' clearly has no significance in the solid state, certain reactions such as those between two separate crystalline solid phases, often appear best described by these formulae. In particular, apparent first order behaviour is often observed. This probably indicates that the rate of reaction is directly dependent on the availability of one reactant and is thus dependant on, for example, the rate of diffusion of this species towards the reaction zone. This is analogous to the concept of concentration in solution phase or of vapour pressure in gas phase reactions.

DECOMPOSITION REACTIONS:

The type of decomposition reaction pertinent here involves the loss of gaseous guest with concomitant or subsequent collapse to the host α-phase. No *chemical* change occurs in that no covalent bonds are broken or formed; the guest vapour and host molecules are chemically unchanged while the solid undergoes a complete rearrangement: a phase change accompanied by a large decrease in "molecular volume" as well as significant conformational changes occur. Thus this sort of decomposition is significantly different from the desorption of adsorbed species from zeolites, (where the phase change is merely a shrinking of the lattice[5]) and indeed even more different from the decomposition of inorganic materials[6] so oft studied in that the only interactions between host and guest are weak van der Waals interactions (or at most hydrogen-bonded interactions). The dehydration reactions of various inorganic salts have been extensively studied[7,8,9] and certain of these are similar to the decompositions of the tubulate clathrates formed by CA, particularly where water molecules form part of the *outer* coordination sphere of the metal (for example).

The reaction: $HG_{(s,\beta)} = H_{(s,\alpha)} + G_{(g)}$ is usually reversible, particularly at low α values and it is thus imperative that experimental conditions are chosen such that the guest absorption reaction is minimised. Fortunately in the case of MC and CA inclusion compounds the absorption of guest is slow and it is relatively simple to ensure that the vapour pressure of guest above the decomposing sample is so low that the desorption reaction occurs effectively

irreversibly even at quite low α values. A constant flow of inert gas (N_2) over the sample is maintained so that all evolved gases are rapidly diluted and swept away.

Apart from the requirement that the experimental conditions approximate irreversibility of reaction it is important that the inclusion compound to be studied be stable for extended periods of time after removal from mother liquour. This series of experiments was therefore confined to the inclusion compounds of CA and MC which were stable enough to be filtered, washed, ground (mortar and pestle) and sieved and then maintained under guest vapour for a period of days without significant guest loss. These inclusion compounds may be separated into two groups:

i) Group 1: the inclusion compounds of CA with aromatic guests
  Group 1a: CAAN, CABN, CANI, CAPNOT, CAPTOL
  Group 1b: CAACET, CAPR
ii) Group 2: the acetonitrile inclusion compounds of CA and MC.

The experiment

The extraction of kinetic data from isothermal decomposition data has been discussed at length[10] and a flow chart indicating the strategy adopted is presented as Figure 6.2.

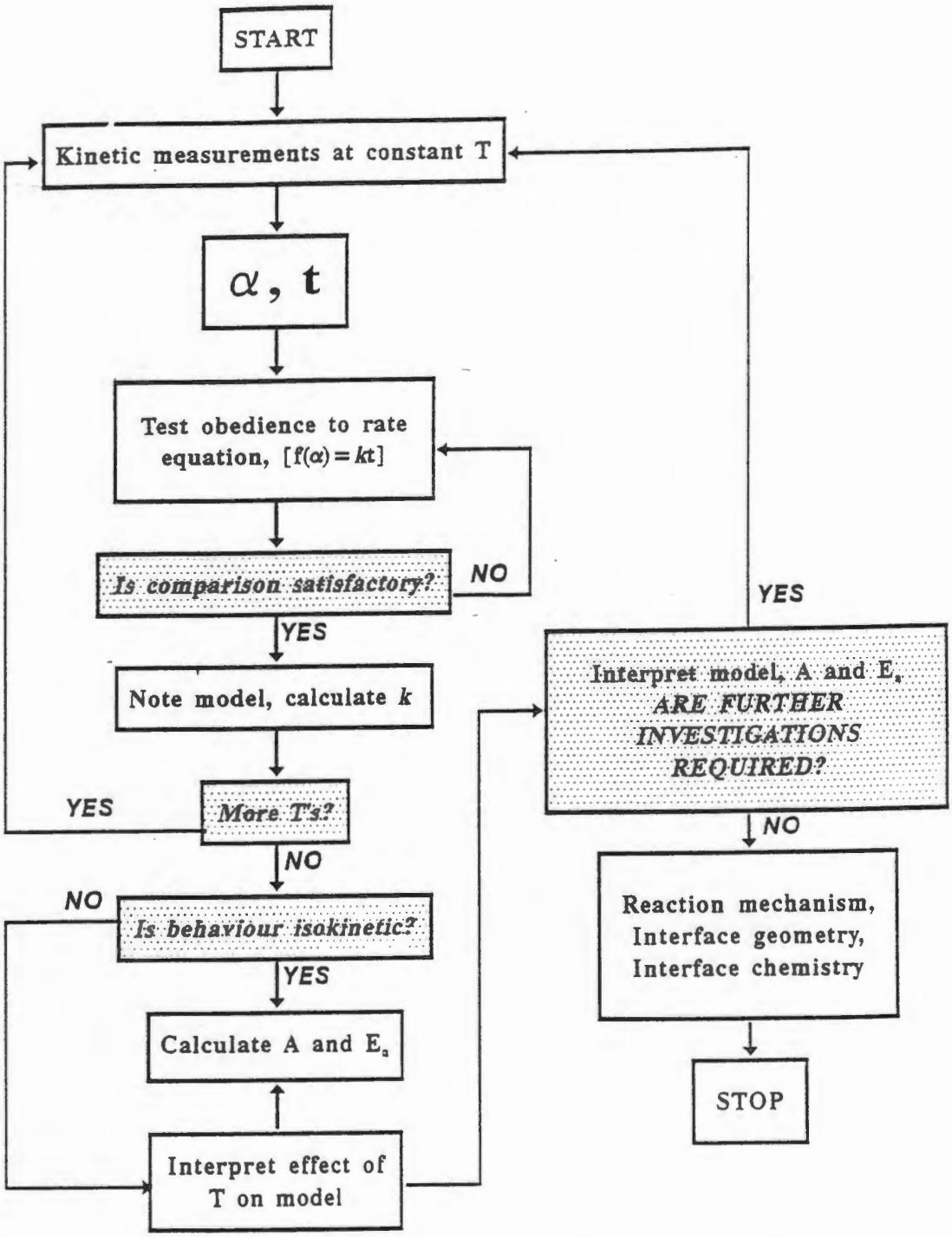

Figure 6.2: Flow chart summarising the strategy adopted for the extraction of kinetic parameters from measurements of velocity of reaction at constant temperature.

Data collection

Samples were prepared as described in the experimental section under isothermal thermogravimetry. The bulk of the experiments for derivation of kinetic parameters for comparison were carried out on samples with particle size of 212-250 μm although the effect of decreased particle size and sample pretreatment were also investigated. All data were collected as described in the experimental section.

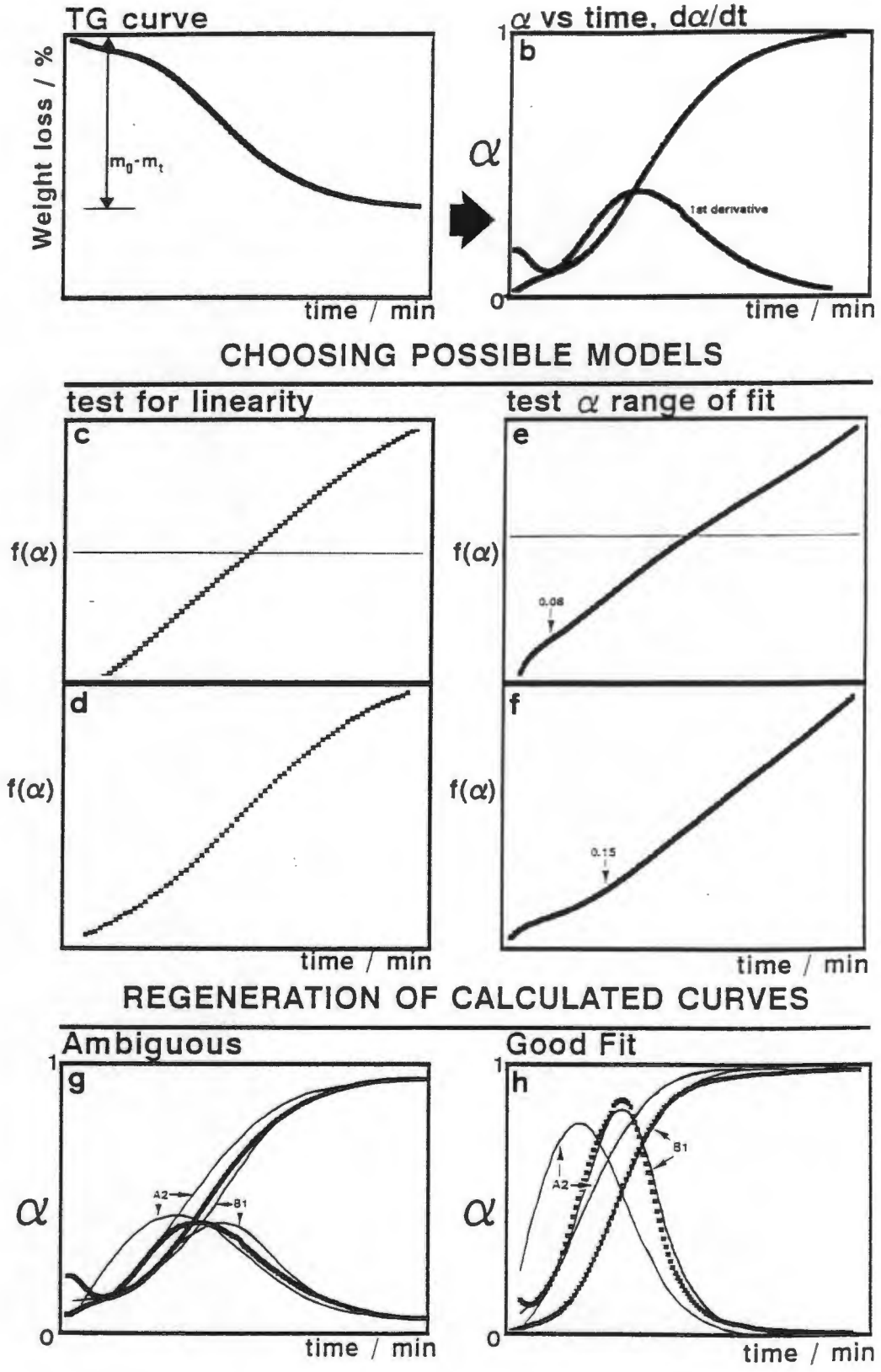

Figure 6.3: Steps involved in curve fitting: a) TG curve, b) α vs time and dα/dt curves, c) and d) application of rate law functions resulting in either a linear plot i.e. a good fit or a non-linear plot i.e. a poor fit, e) and f) application of rate law functions resulting in linear fit over a large α range and a shorter α range, g) and h) comparison of experimental and calculated curves where the rate law assignment is ambiguous and where one rate law clearly describes the data.

Data conversion and manipulation

The steps involved in data fitting are illustrated in Figures 6.3a to h. The weight loss versus time curve (TG curve), is converted to an α vs time curve and reduced time plots produced for each data set. Rescaling is achieved by choosing $t_{0.99} = 1$ for all data sets.

Comparison of the shapes of these plots at this point indicate the acceptability of the temperature range chosen. The *shapes* of all curves for a particular system should be similar if the same reaction mechanism dominates throughout. In other words the reduced time curves provide a check that the reaction is, in fact, isokinetic over the chosen temperature range. (*"For a given substance and crystal habit there is an isokinetic range of temperatures and concentrations in which the characteristic kinetics of phase change remain the same."* Avrami[11], 1939).

The data points at the beginning of an isothermal decomposition run carried out in the TG furnace described suffer from large errors in the *temperature* and are thus notoriously unreliable. This temperature instability is unavoidable at the beginning of any relatively high temperature isothermal TG experiment and results from the need to steeply ramp the temperature to rapidly approach the reaction temperature to avoid unmonitored weight loss. Unfortunately this often leads to "overshooting" where the furnace temperature rises to a few degrees higher than the desired reaction temperature for a short while. These initial data points were discounted in determination of the model and no claims are made for data up to $\alpha = 0.05$. In some cases rapid weight loss persists up to quite a high α-value and this must be taken into account when attempting to fit a rate equation to the body of the curve. It is not sufficient to merely ignore data up to $\alpha = 0.05$ in this case and instead data are rescaled for purposes of curve fitting and then reduced to the original range for comparison.

The first derivative of the α vs t curve is calculated using the Savitsky-Goulay approximation as illustrated in Figure 6.3b. Changes of shape of the curve are more easily seen in the first derivative curve and these proved invaluable in comparing fits of experimental and calculated curves.

Data fitting

Attempts are made to fit the α vs t data to one of the common rate law equations given in Table 6.1. The best fit is deemed to be that in which the function, $f(\alpha)$, is linear over the largest possible α range as illustrated in Figures 6.3c to f.

While it is clear that certain rate equations provide a better fit than others it frequently occurs that more than one (although usually closely related), function results in reasonable fit.

For example the data used to produce the diagrams in Figure 6.3c and e appear to fit either an A2 or B1 model, the functions $f(\alpha)$ being linear over large α ranges. In this case the model that shows the greater degree of linearity over the greatest α range, such as that illustrated in Figures 6.3d and f, and the

largest temperature range is chosen. Data from other experiments or related systems may be invoked to aid choice.

Comparison of Experimental and Fitted Data

To test the model chosen by consideration of linearity of the derived function, calculated α data are regenerated from the chosen function and plotted for comparison with the experimental data. The comparison of derivatives allows critical analysis of the applicability of a particular function in describing the reaction mechanism operating. Figures 6.3g and h illustrate comparison of regenerated curves with experimental data for a reaction that appears well described by either an A2 or B1 model (Figure 6.3g) and for one that is clearly better described by the Prout-Tompkins, (B1), model (Figure 6.3h).

Derivation of kinetic parameters

Once isokinetic behaviour is established and a rate law assigned, rate constants, k, for each reaction are extracted and a plot of $\ln k$ vs T^{-1} produced. If the data are truly isokinetic over the temperature range chosen this should result in a straight line Arrhenius plot, $\ln k = e^{(-E_a/RT)} + \ln A$. The intercept is ln A and the gradient $-E_a/R$ and thus the pre-exponential factor A and the "Energy of activation" (E_a) for the reaction may be calculated. The significance of these factors will be discussed at a later stage.

Verification of chosen model

Once a model has been chosen and shown to fit the experimental data supporting experimental evidence should be sought to validate (or not), the proposed mechanism[12]. The mechanism should be in accord with known characteristics for the reactant and product materials. As both reactant and solid product phases are well characterised and the crystal structures known (see chapter 3), it should be possible to relate the mechanism of decomposition to structure and to verify the choice of rate limiting step.

Apart from analysis of crystal structures, optical microscopy was employed to check the proposed processes dominating at various degrees of desorption. Experimental conditions under which desorption isotherms were measured were duplicated as closely as possible with respect to particle size, N_2 flow rate and temperature and the decomposition followed photographically.

DECOMPOSITION OF CA INCLUSION COMPOUNDS

In each case the solid product of decomposition was the α-phase of the relevant host. This was confirmed by comparison of powder XRD patterns. Only one host polymorph was encountered in the experiments.

The results of the experiments on the two separate classes of inclusion compounds studied will be presented separately.

CA.aromatic guest inclusion compounds

Analysis of the reduced time curves of the decompositions of CA with aromatic guests revealed the existence of two main curve types. While the shapes of the reduced time curves for most of the inclusion compounds of CA with aromatic guests were very similar as illustrated in Figure 6.4, those for the decomposition of CAACET and CAPR were significantly different and rather more complex than the main group comprising: CAAN, CABN, CANI, CAPNOT and CAPTOL. These will therefore be dealt with separately as groups 1a and 1b.

Group 1a: (CAAN, CABN, CANI, CAPNOT, CAPTOL)

Results

Reduced time plots for a selected range of temperatures for each compound are presented as Figure 6.4. It is clear that these are similar in overall shape and it is therefore suggested that the mechanism of decomposition is likely to follow the same (or very similar), rate laws. It would have been a startling result were this not so, given the similarity in stoichiometry and structure of all of these inclusion compounds.

All curves indicate an initial rapid evolution of gas followed by a sigmoidal curve characterised by an acceleratory region followed by a deceleratory region. Microscopic observations of crystallites under heating and nitrogen flow indicated that the initial rapid evolution of gas resulted from finely powdered material clinging to the surfaces of the sieved crystallites. Such particles are clearly visible in the first frame of Figure 6.8. These small particles were observed to become rapidly opaque as the reaction temperature was approached and this, perhaps aided by the rapid evolution of vapours from the surfaces of large particles, would account for the rapid initial weight loss. The extent of weight loss appeared to show some correlation with the amount of powder visibly clinging to the surfaces of different samples.

The sigmoidal nature of the α vs t curves indicate either Avrami-Erofe'ev or Prout-Tompkins rate laws and $f(\alpha)$ vs t plots were produced for each of these four possible rate laws, illustrated for one data set in Figure 6.5. The sigmoidal regions of the curves were best fitted to either a B1 or an A2 rate law. In some cases one of these rate laws appeared to better describe the reaction at lower temperatures while the other provided a better fit at higher temperatures. Since both functions are derived from models describing rates of nucleation and growth this is not surprising and in fact k values derived from either model result in parallel Arrhenius plots and similar values of E_a.

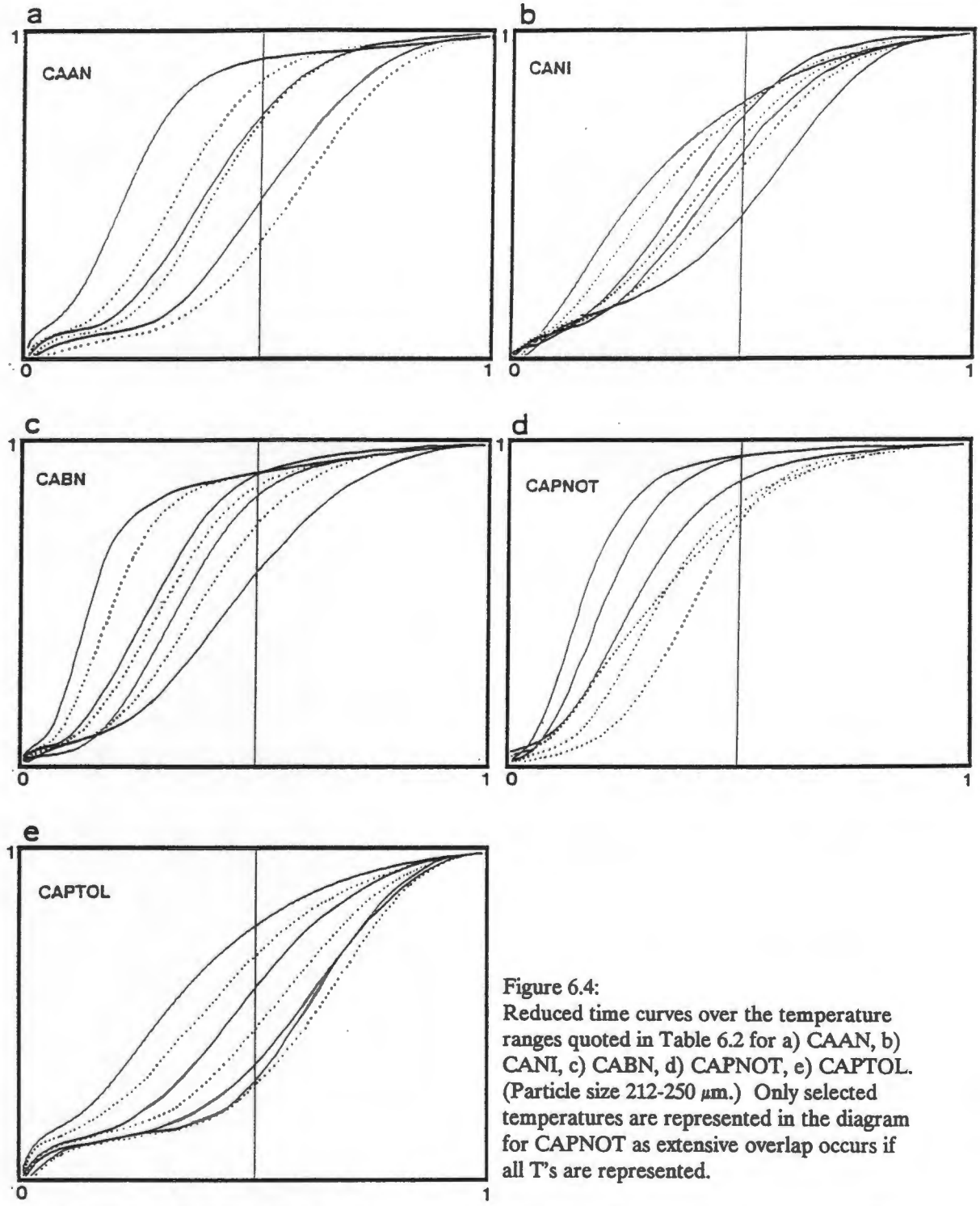

Figure 6.4:
Reduced time curves over the temperature ranges quoted in Table 6.2 for a) CAAN, b) CANI, c) CABN, d) CAPNOT, e) CAPTOL. (Particle size 212-250 μm.) Only selected temperatures are represented in the diagram for CAPNOT as extensive overlap occurs if all T's are represented.

Although it is possible to obtain similar values for the kinetic parameters from either model, as illustrated in Figure 6.7 it is desirable to attempt to differentiate between models in an attempt to ascribe reaction mechanisms. Careful comparison of ranges of fit with respect to both α and temperature ranges and the fit of regenerated curves led to the choice of the B1 (Prout-Tomkins) model as the most accurate descriptor of the decomposition of the aromatic guest inclusion compounds of CA. Figures 6.6a and b illustrate the experimental and regenerated α vs time curves for the situation where the assignment of the rate law is ambiguous and where only one of the possible rate laws describes the experimental data.

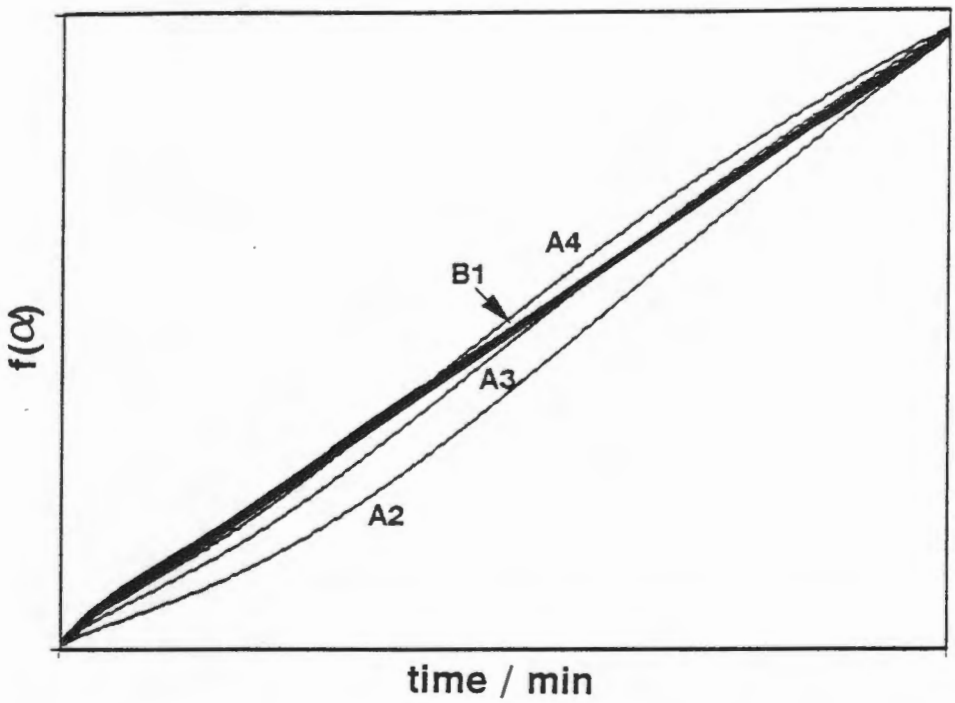

Figure 6.5: Comparison of fit of all sigmoidal rate law functions to the α vs time data for the isothermal decomposition of CABN 212-250 μm at 120 ^{o}C.

Values of the rate constants, *k*, and the alpha range over which the decay curves fitted the rate law are presented in Table 6.2 and the Arrhenius plots resulting as Figures 6.7a to e.

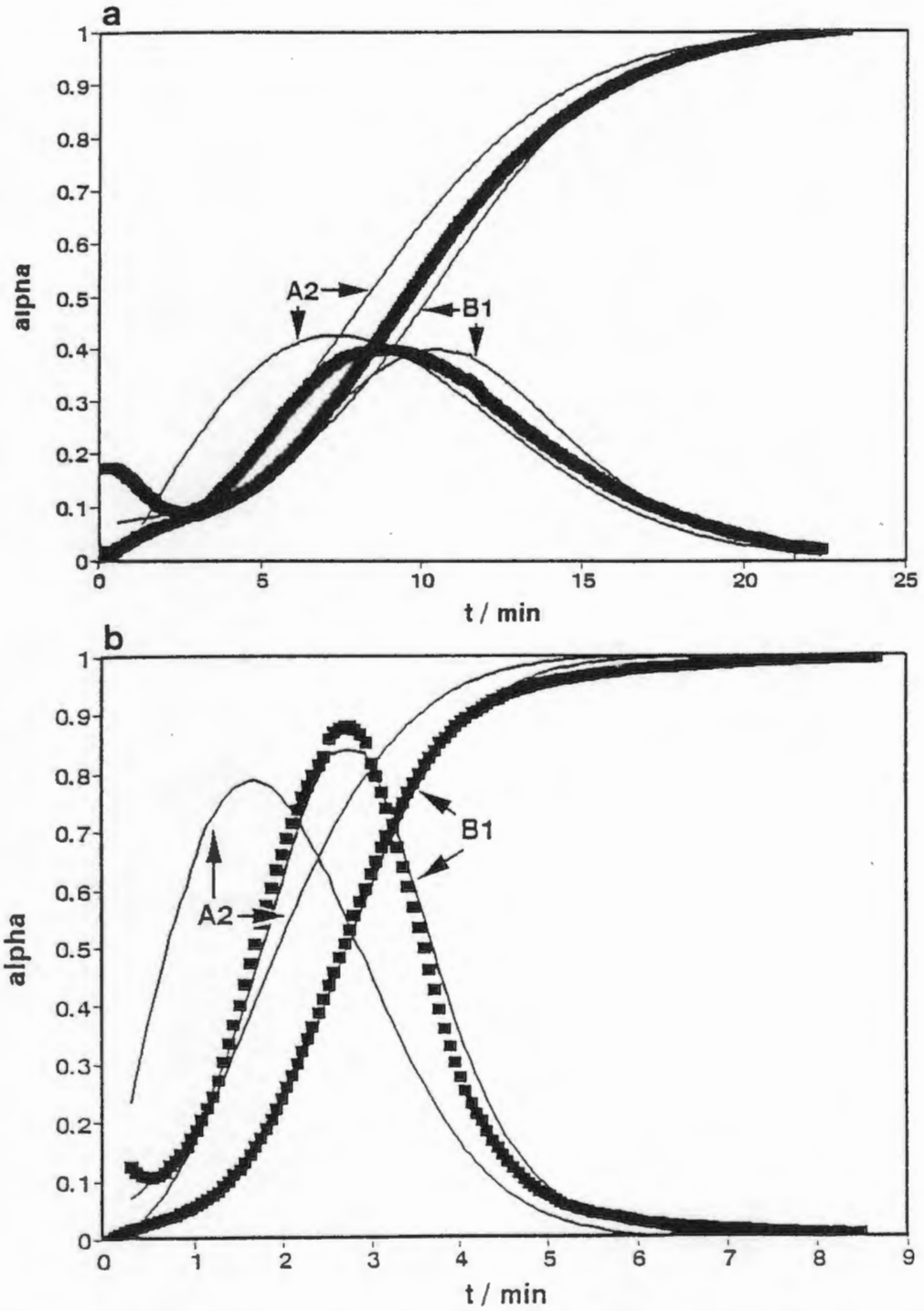

Figure 6.6: Experimental α vs time and $d\alpha/dt$ curves compared with those generated using either A2 or B1 rate laws, a) where the choice of rate law is ambiguous (CABN 212-250 μm at 125 ^{o}C and b) where the B1 rate law clearly best describes the experimental data (CAPNOT 212-250 μm at 130 ^{o}C).

Table 6.2: Data for analysis of decomposition isotherms for CA inclusion compounds with aromatic guests.

	T(°C)	α-range	k (min^{-1})	r
CAAN (212-250 μm crystals)				
	90	0.1 - 0.85	0.0455(1)	0.997
	100	0.1 - 0.85	0.1735(5)	0.995
	105	0.1 - 0.95	0.328(2)	0.994
	110	0.1 - 0.95	0.626(2)	0.999
	115	0.12 - 0.95	1.160(2)	0.999
	120	0.1 - 0.95	1.80(1)	0.998
	125	0.1 - 0.95	2.35(2)	0.996
CAAN (212-250 μm conglomerate)				
	90	0.15 - 0.95	0.06427(4)	0.997
	95	0.1 - 0.95	0.1946(6)	0.999
	100	0.1 - 0.95	0.3621(3)	1.000
	110	0.1 - 0.95	1.222(9)	0.996
		0.1 - 0.95	1.192(4)	0.999
	115	0.1 - 0.95	2.10(2)	0.996
	120	0.1 - 0.95	3.14(4)	0.994
CAPNOT (212-250 μm crystals)				
	98	0.05 - 0.95	0.00120(6)	0.982
	101	0.10 - 0.95	0.0170(1)	0.980
	105	0.15 - 0.95	0.0257(2)	0.989
	107	0.05 - 0.90	0.291(3)	0.978
	108	0.10 - 0.90	0.0353(4)	0.977
	110	0.15 - 0.95	0.0406(3)	0.983
	111	0.24 - 0.95	0.0422(4)	0.966
	115	0.15 - 0.95	0.0621(8)	0.989
	117	0.2 - 0.95	0.0941(4)	0.982
	120	0.15 - 0.95	0.172(2)	0.973
	122	0.10 - 0.95	0.237(2)	0.977
	125	0.05 - 0.95	0.537(7)	0.968
	130	0.05 - 0.95	1.58(1)	0.997
	132	0.05 - 0.95	1.838(8)	0.999
CABN (212-250 μm crystals)				
B1	95	0.1 - 0.8	0.0228(2)	0.994
	100	0.1 - 0.8	0.0426(6)	0.986
		0.1 - 0.9	0.0409(4)	0.984
	105	0.07 - 0.9	0.0734(6)	0.991
	110	0.07 - 0.9	0.1142(9)	0.989
	115	0.05 - 0.9	0.181(2)	0.989
	120	0.07 - 0.95	0.242(2)	0.996
	125	0.08 - 0.95	0.376(1)	0.997
	130	0.1 - 0.95	0.552(4)	0.998
A2	95	0.1 - 0.8	0.00623(2)	0.999
	100	0.08 - 0.8	0.01183(7)	0.997
		0.1 - 0.85	0.01304(4)	0.999
	105	0.1 - 0.9	0.02088(7)	0.999
	110	0.1 - 0.85	0.03343(7)	0.999
	115	0.05 - 0.9	0.0491(2)	0.998
	120	0.1 - 0.95	0.0691(4)	0.998
	125	0.15 - 0.95	0.1075(1)	1.000
	130	0.2 - 0.95	0.1625(9)	0.999

Table 6.2 continued.

T(°C)	α-range	k (min^{-1})	r
CANB (212-250 μm crystals)			
110	0.15 - 0.98	0.0148(1)	0.949
115	0.1 - 0.98	0.02262(6)	0.994
120	0.04 - 0.93	0.04298(6)	0.998
125	0.06 - 0.98	0.06734(2)	1.000
130	0.08 - 0.96	0.12666(8)	1.000
135	0.08 - 0.99	0.2064(6)	0.997
140	0.15 - 0.95	0.350(3)	0.978
145	0.15 - 0.95	0.652(9)	0.954
CAPTOL (212-250 μm crystals)			
95	0.12 - 0.95	0.02587(7)	0.996
100	0.1 - 0.95	0.06492(4)	1.000
105	0.2 - 0.95	0.1201(2)	0.999
110	0.2 - 0.95	0.272(2)	0.994
115	0.2 - 0.95	0.395(4)	0.986
120	0.2 - 0.95	0.79(1)	0.987
125	0.2 - 0.95	1.053(7)	0.993

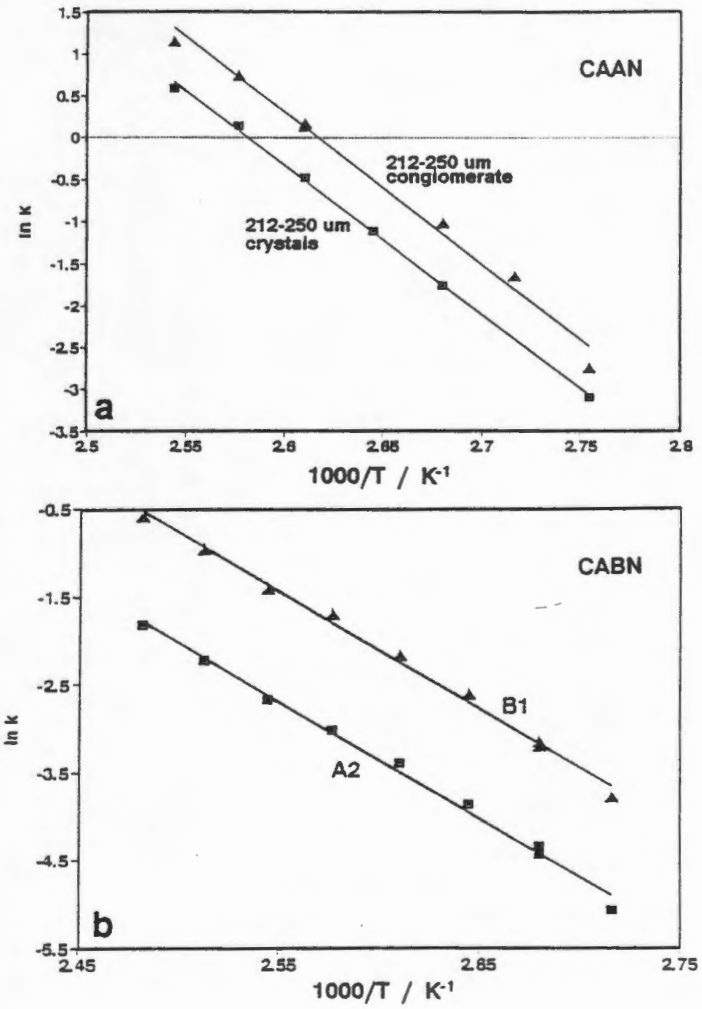

Figure 6.7: Arrhenius plots over the isokinetic ranges for a) CAAN, b) CABN.

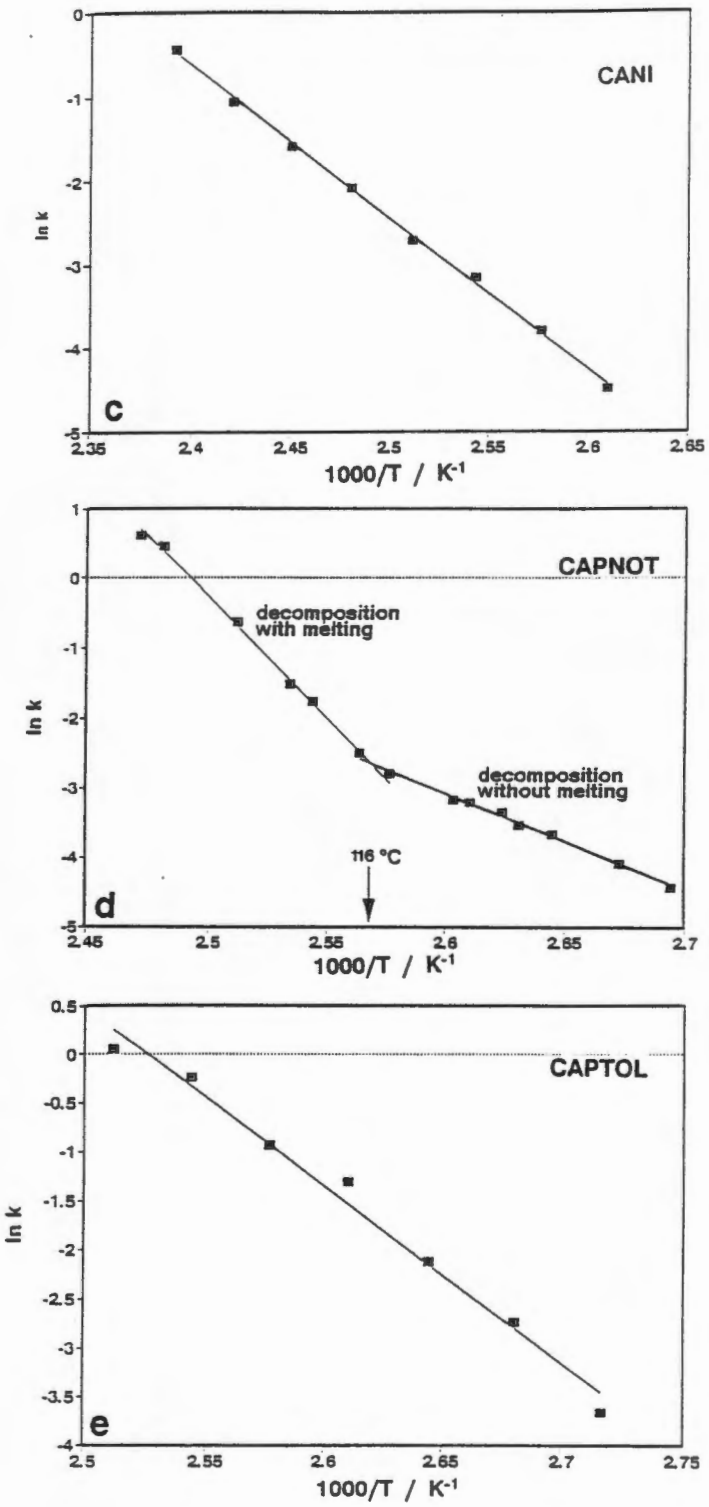

Figure 6.7 (contd.): Arrhenius plots over the isokinetic ranges for c) CANI, d) CAPNOT, e) CAPTOL.

Isokinetic behaviour over the temperature ranges chosen is confirmed by the linearity of the plots of ln *k* vs 1/T. The Arrhenius plot for the compound CAPNOT shows the existence of two distinct lines with quite different slopes intersecting at a temperature of *ca* 116 °C. This was initially puzzling as the fit of the α time curves to the B1 rate law was good over the entire temperature range. However microscopic examination of the material under heating and nitrogen flow indicated that above 116 °C partial melting of the crystallites occurred. Figure 6.8 is a series of photographic plates illustrating this phenomenon. Interestingly, the activation energy for decomposition with melting is significantly greater than that without. It is, of course, impossible to attempt to describe the mechanism of decomposition when partial melting occurs unless one is able to distinguish between vapour evolved from the liquid or vapour evolved from the solid. Presumably when the solid is covered with a layer of liquid (due to the formation of a eutectic) evolution of vapour occurs from the liquid/atmosphere interface and one might expect a rate law based on diffusion mechanisms to operate. However a more complex mechanism can also be envisaged in which vapour is evolved from the liquid/atmosphere interface at a rate determined by the concentration of the guest species in the melt which may in turn be determined by the rate of movement of guest from the solid to the melt. In other words the rate of vapour evolution measured is still dependent on the rate of decomposition of the solid (which may not melt if the concentration of guest species in the solid is below a certain threshold value). Clearly the rate of vapour evolution measured is the net rate, which is the sum of the rates of the separate processes operating. It is thus impossible to draw any mechanistic conclusions based on the measurement of the rate law in such cases although it is interesting to note that the activation energy for the desorption reaction with melting is higher than that for the desorption reaction without melting.

While a number of the inclusion compounds, other than CAPNOT, were observed to undergo partial or complete melting concomitant with guest release on rising temperature thermal analysis (see chapter 4), the temperature range for decomposition was carefully chosen to ensure that the reaction monitored was the loss of gaseous guest from the *crystalline* complex rather than from the *melt* containing both host and guest.

Activation energy and pre-exponential factors derived from the above Arrhenius plots are presented as Table 6.3. It is interesting to note that the values for the activation energy E_a derived for CABN, modelling the reaction either as following an A2 or B1 rate law, are indistinguishable from each other although the pre-exponential factor is slightly smaller in the A2 case.

Table 6.3: Kinetic parameters for CAAN, CABN, CANI, CAPNOT and CAPTOL.

	E_a (kJmol^{-1})	ln A	*r*
CAAN			
(212-250 μm crystals)	148(3)	45.90(6)	0.996
(212-250 μm conglomerate)	151(8)	47.35(18)	0.991
CABN			
Prout-Tomkins (B1)	110(3)	32.28(8)	0.995
Avrami-Erofe'ev (A2)	110(3)	31.09(9)	0.994
CANI	151(2)	42.85(6)	0.999
CAPNOT			
Decomposition without melt	117(5)	33.41(4)	0.993
Decomposition with melt	277(5)	82.29(6)	0.998
CAPTOL	151(8)	45.87()	0.987

Discussion

Both the A2 and B1 rate laws are derived to account for mechanisms dominated by growth of nuclei of the product phase[13,14] implying that the reaction :

$$HG_{(s,\beta)} = H_{(s,\beta^0)} + G_{(g)}$$

is faster than the reaction:

$$H_{(s,\beta^0)} = H_{(s,\alpha)}$$

where β_0 denotes the host framework remaining after guest desorption but before collapse to the α-phase. This is therefore the rate determining step.

The derivation of either of these rate laws begins with the assumption that germ nuclei are already present and randomly distributed throughout the reactant phase and that the length of the induction period is determined by the rate of transformation of germ nuclei to growth nuclei. Germ nuclei will transform to growth nuclei when the cluster of the new phase attains a certain critical size such that the free energy change associated with the creation of a reaction interface is less than the difference between the internal free energy of the old (reactant) phase and the lower internal free energy of the new (product) phase[15]. The acceleratory period is dominated by the rate of unimpeded expansion of the growth nuclei and the decelerator period by the decrease in rate of expansion of nuclei caused by cessation of growth in certain directions due to impingement of growing nuclei upon each other.

Figure 6.9 plates 1 to 6 show decay of CAPTOL as viewed on a hot stage microscope at a temperature of 120 °C under constant nitrogen flow (to simulate conditions in the TG experiment).

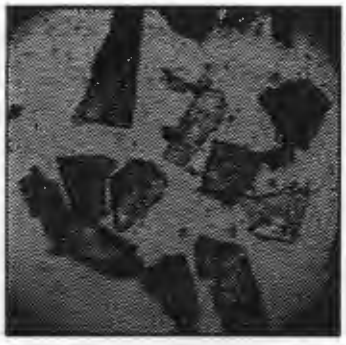

Plate 1

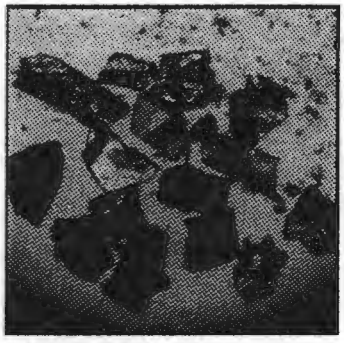

Plate 5

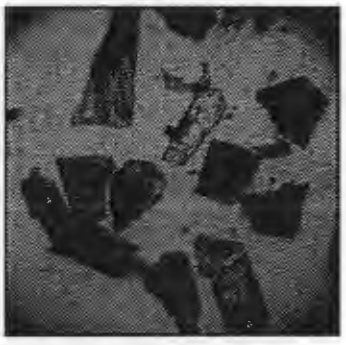

Plate 2

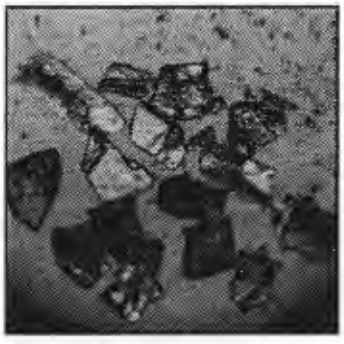

Plate 6

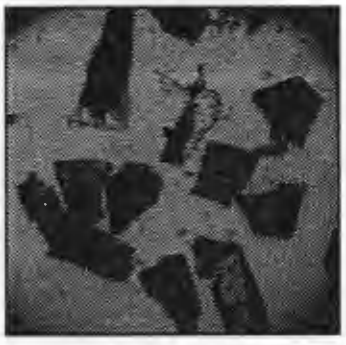

Plate 3

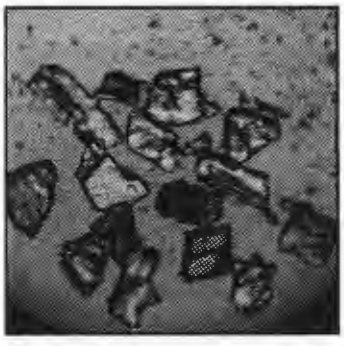

Plate 7

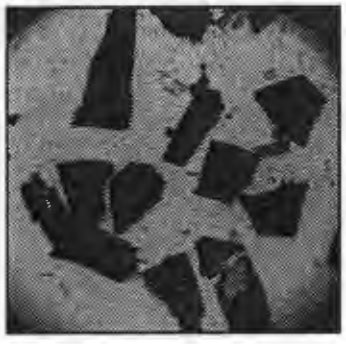

Plate 4

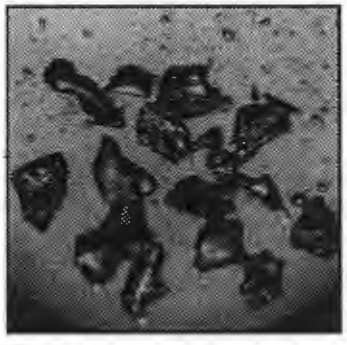

Plate 8

Figure 6.8 : Isothermal decomposition of CAPNOT , plates 1 to 4 at 115 ^{o}C, plates 5 to 8 at 140 ^{o}C.

Plate 1

Plate 4

Plate 2

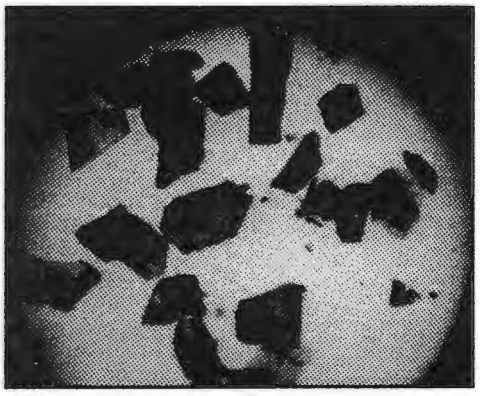

Plate 5

Plate 3

Plate 6

Figure 6.9: Isothermal decomposition of CAPTOL at 120 ^{o}C under N_2 flow.
Plate 1 - room temp, plate 2 - 2 min, plate 3 - 4 min, plate 4 - 6 min, plate 5 - 8 min, plate 6 - 11 min.

Initially the crystallites are transparent and rotate plane polarised light. Imperfections are clearly visible and there are small particles of powder clinging to the surfaces of the particles. Upon heating to 120 °C fine cracks appear probably due to thermal shock although these may add to the rapid evolution of vapour in the initial phases of the reaction. By plate 3 and 4 nuclei of the new phase are clearly visible as dark regions. These are growing rapidly through the plate-like crystals. The spread and subsequent intersection of growing nuclei are evident in later plates.

The difference between the two rate laws arises from the different modes of nuclear growth posited. The A2 rate law describes the circular growth of nuclei while the B1 rate law is derived for branching growth. The branching mode (originally derived for the decomposition of $KMnO_4$ crystals[14]), arises from the stresses resulting from the formation of a new phase with significantly different molecular volume (and in this case different crystal structure with new molecular orientations and hydrogen bonds). Fine cracks perpendicular to the layer of the new phase penetrate the crystal resulting in enhanced reaction at the crack "mouth", since the new cracks formed will be perpendicular to the new product layer, the nucleus will grow in a branching fashion into the body of unreacted material. As branching becomes widespread, cracks will terminate as they impinge upon other similar cracks and the deceleratory phase will commence[14].

The implication is that for decay to occur a molecule or molecular aggregate must be adjacent either to a product molecule *or* a germ nucleus (dislocation etc.). The density of germ nuclei in the reactant crystal will therefore have a direct effect on the measured rate of reaction, not only in the initial stages but throughout the time period of the reaction, as a larger number of growing nuclei implies more rapid conversion to product and shorter path lengths for growing branches before intersection. It has been shown by a number of authors that pretreatment [10] of samples for kinetic analysis results in changes in the rate of reaction. Irradiation by X-rays or γ-rays, bombardment by particles such as neutrons or protons, ageing and mechanical grinding as well as particle size[1,2,14,16] have all been cited as influences on the rate and even on the rate law exhibited by decomposing systems. Changes in the rate (and even the rate law) are presumably due to the introduction of a greater number of germ nuclei in the form of crystal defects, including the large discontinuity represented by the surface of the crystal. Thus smaller crystallites or crystallites with significantly enhanced numbers of germ nuclei, should show an enhanced rate of reaction.

The decomposition reactions of smaller particles (63-125 μm) were analysed for a number of compounds and the α vs time curves compared with those obtained for the 212-250 μm particles at the same temperature. Two examples are illustrated in Figures 6.10a and b. Although the induction time for the smaller crystallites of CAAN appear to have a shorter induction period, the rate of reaction is not significantly altered and in other systems such as CAPNOT (Figure 6.10b) the curves are indistinguishable. Conglomerates of very small

crystals of CAAN were produced in one of the crystallisation experiments and these had a particle size (for individual crystals) of *ca* 100 times smaller than the 212-250 μm particles produced by grinding. The relative sizes of the particle are illustrated in Figure 6.12.

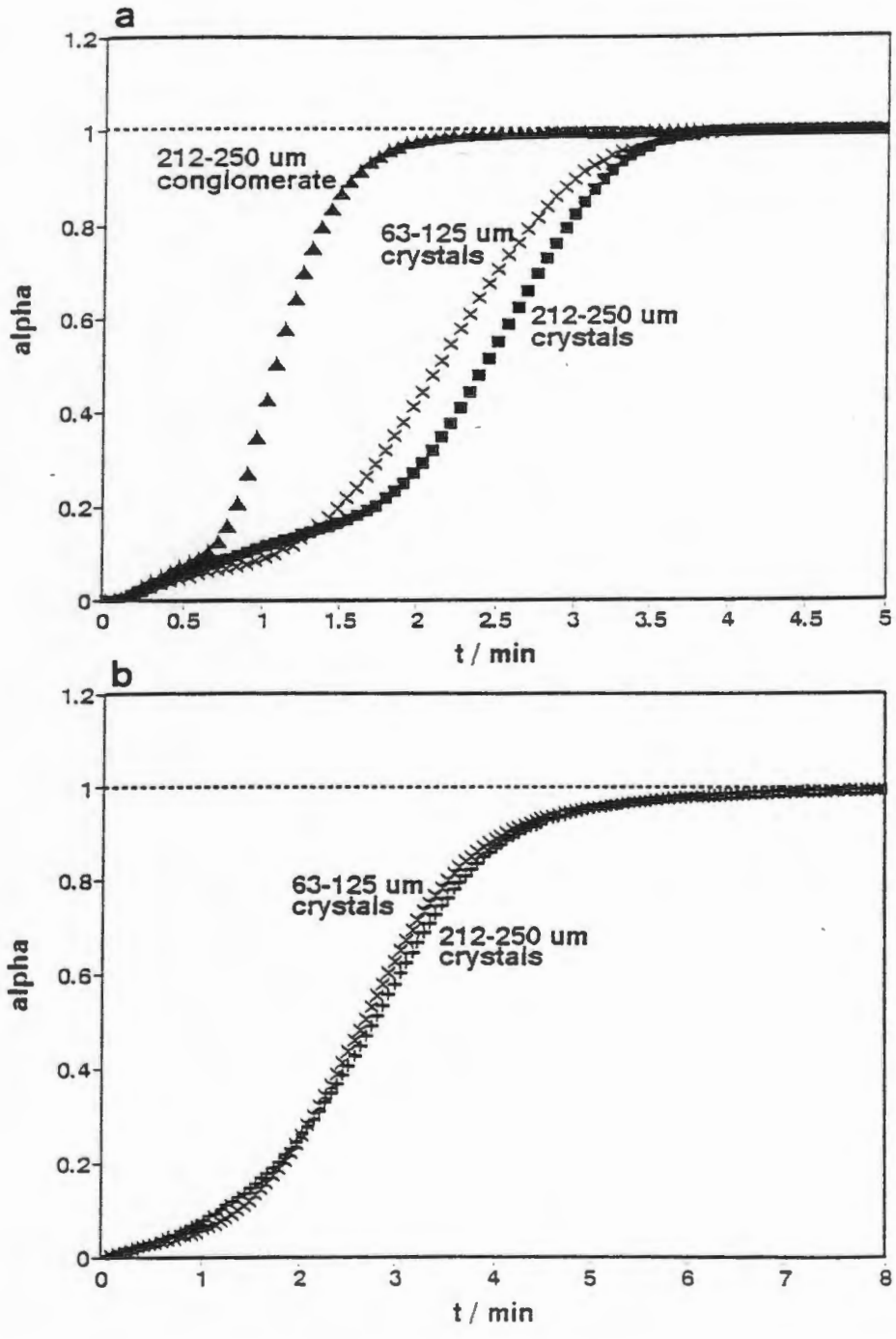

Figure 6.10: Effect of particle size on rate of reaction. a) CAAN 212-250 μm crystals. 63-125 μm crystals and 212-250 μm conglomerates of tiny crystals compared at 125 °C. b) CAPNOT 212-250 μm and 63-125 μm at 130 °C.

The rate of reaction of these much smaller particles was significantly enhanced at 120 °C as illustrated in Figure 6.10b. α vs time curves for these 212-250 μm conglomerates of tiny crystallites were obtained for the same temperature

range as the larger particles and analysed as described before. While the rate of reaction at any particular temperature is enhanced the value for the activation energy is almost identical to that obtained for the larger particles as is illustrated in Figure 6.7a. This result lends credence to the argument that it is the collapse of the host crystal structure to the α-form that is the rate determining step.

To investigate the role of crystal defects samples of 212-250 μm were subjected to cycles of freezing in liquid nitrogen followed by rapid warming to room temperature. After five freeze/warm cycles the TG and thence α vs time curves were obtained and compared to those of untreated samples. An example of the resultant curves is presented in Figure 6.11. The curves of the treated samples are almost indistinguishable from those of the untreated crystals over a range of temperatures. There is no effect on the rate of reaction or the relative length of the induction period and this may be interpreted in two ways:

i) either the increase in the density of crystal defects has no effect on the rate of desorption

OR

ii) the density of crystal defects is so high in the untreated sample that the increased density of defects due to the effects of cooling and heating is insignificant by comparison.

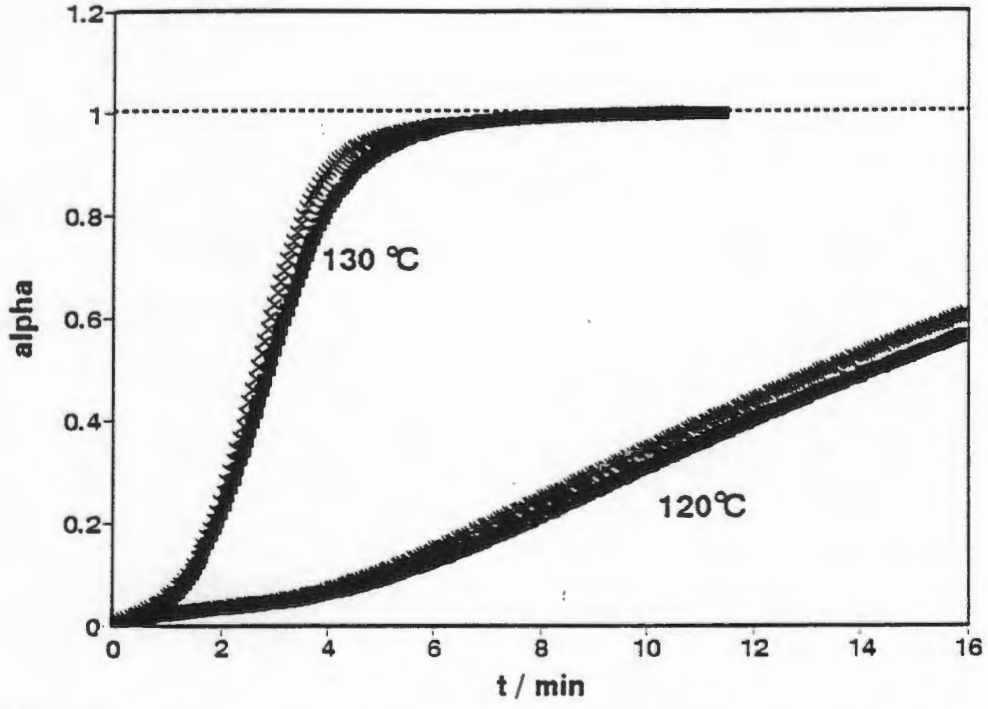

Figure 6.11: Comparison of α vs time curves for a sample subjected to alternate freeze/warm cycles and an untreated sample of CAPNOT 212-250 μm crystallites at 120 °C and 130 °C.

Given that the particles used in the experiment were ground to create the small particles used, the second option is a distinct possibility.

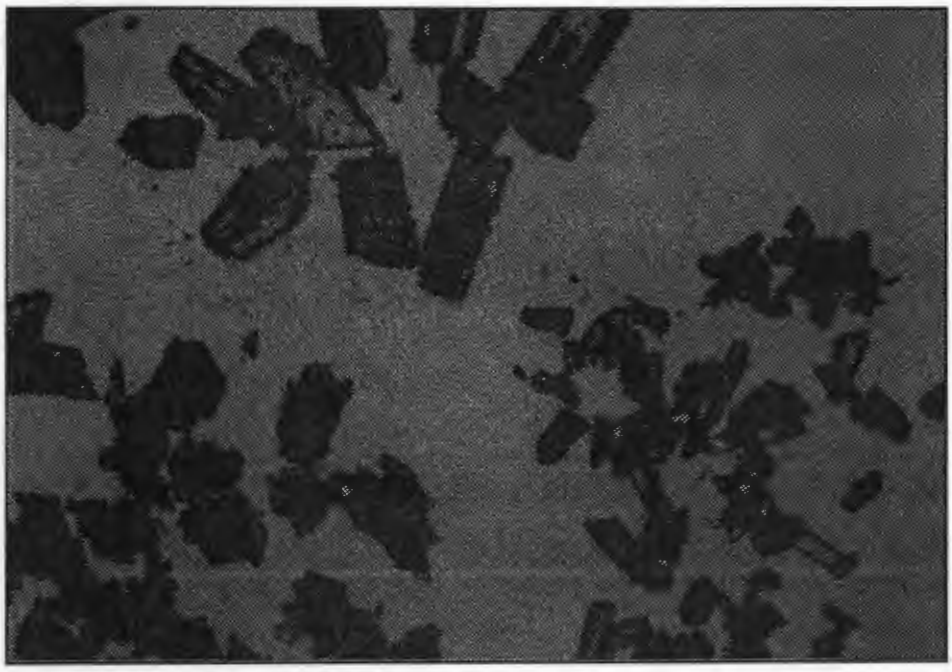

Plate 1

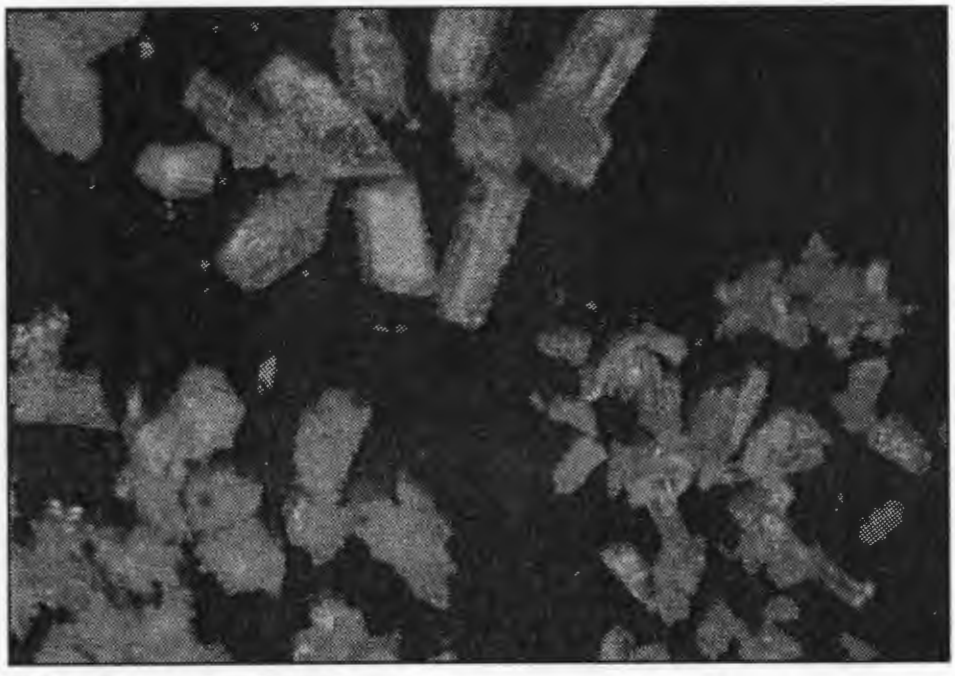

Plate 2

Figure 6.12: Particle sizes of samples used in investigation of the isothermal decomposition of CAAN. Plate 1 - polarised light, Plate 2 - overhead light only.
Top left: 63-125 *u*m, top right: 212-250 *u*m conglomerate and bottom: 212-250 *u*m crystallites.

Group 1b (CAACET, CAPR)

Results

Reduced time plots for CAACET and CAPR are reproduced as Figures 6.13a and b. Clearly the shape of the curves is complex, apparently representing the sum of overlapping or succeeding curves.

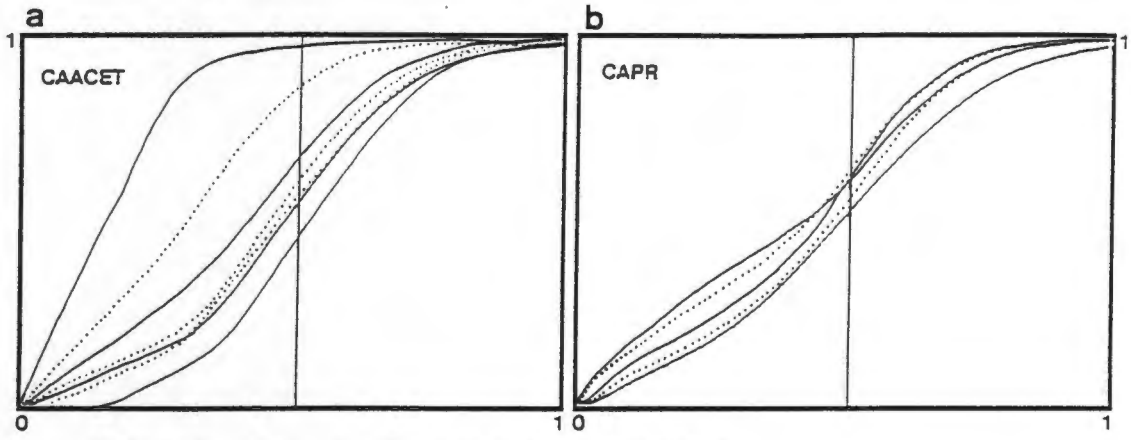

Figure 6.13: Reduced time plots for a) CAACET and b) CAPR.

Careful analysis of the α vs time curves for CAACET reveal an initial linear region, which persists to higher α values at lower temperatures. This is followed by a truncated sigmoidal curve. The truncated nature of the sigmoidal part of the curve indicates overlapping of two separate processes. A number of different possible rate laws were fitted to the second region of the curve after rescaling as described earlier but regeneration of the α vs time curve over the shorter alpha region indicated that the experimental data are best described by a linear region (i.e. a zero order rate law) followed by a region conforming to a B1 rate law. The fit of the calculated curve with the experimental data for decomposition at one temperature is indicated in Figure 6.14. Each curve was analysed in this fashion and the rate constants extracted for the first and second processes are presented in Table 6.4.

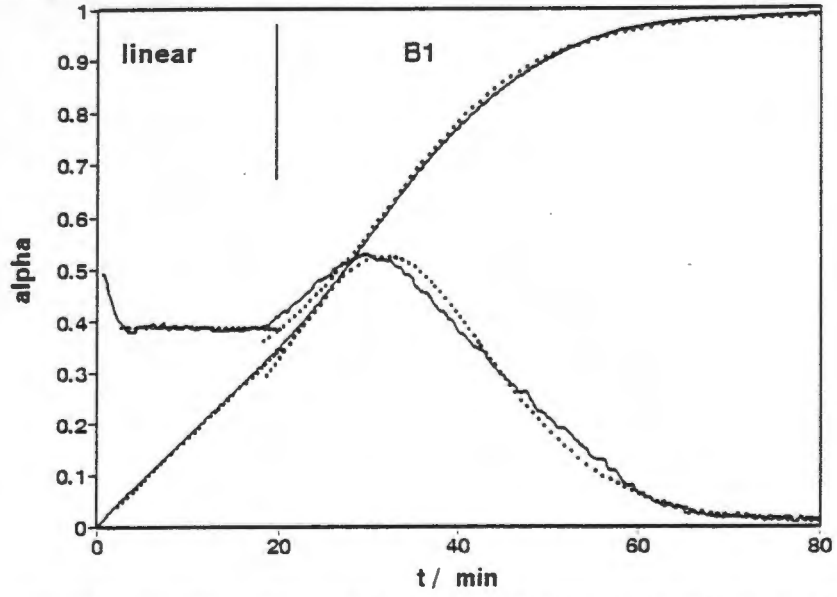

Figure 6.14: Comparison of experimental (solid line) and calculated (dotted line) α vs time and dα/dt curves for CAACET 212-250 μm at 85 °C.

Table 6.4: Data for analysis of decomposition isotherms for CAACET and CAPR.

T(°C)	α-range	k (min^{-1})	r	α-range	k (min^{-1})	r
CA.Acetophenone (Miki *et al*[17])						
(linear)				(B1)		
80	0.02 - 0.7	0.0101(2)	0.999			
85	0.005 - 0.45	0.01753(2)	1.000			
90	0.001 - 0.36	0.0310(4)	0.999	0.3 -0.95	0.2302(6)	0.997
95	0.001 - 0.2	0.03994(8)	1.000	0.2 -0.95	0.4458(9)	0.999
100	0.002 - 0.20	0.0668(2)	0.999	0.35-0.95	0.0825(2)	0.999
105	0.005 - 0.18	0.0925(6)	0.998	0.13-0.95	1.114(3)	0.999
110	0.007 - 0.16	0.118(3)	0.995	0.1 -0.95	1.382(6)	0.999
CAPR						
(R3)				(B1)		
100	0.05 - 0.4	0.00750(1)	0.999	0.45-0.95	0.1213(6)	0.995
105	0.05 - 0.42	0.01195(2)	0.999	0.45-0.95	0.251(1)	0.997
110	0.05 - 0.4	0.0187(2)	0.994	0.4 -0.95	0.477(3)	0.998
115	0.05 - 0.25	0.0292(1)	0.998	0.3 -0.95	0.790(5)	0.994
120	0.05 - 0.2	0.0413(3)	0.998	0.4 -0.95	0.477(3)	0.998

The isothermal decomposition curves for CAPR proved even more complex yet with three different regions indicated. The initial region, terminated at low α, appears either linear or deceleratory but was not modelled due to uncertainty in temperature at the beginning of the isothermal run. This region is followed by a second, distinctly different, deceleratory region extending to α *ca* 0.4 and in turn superseded by a sigmoidal region. Unlike the CAACET case the second deceleratory region does not vary in α-range with variations in temperature. The best fit of successive rate laws was achieved by modelling an R3 (contracting volume) followed by a B1 (Prout-Tompkins) rate law. The fit of the calculated and experimental data is illustrated in Figure 6.15 and the rate constants extracted for particular α ranges quoted in Table 6.4.

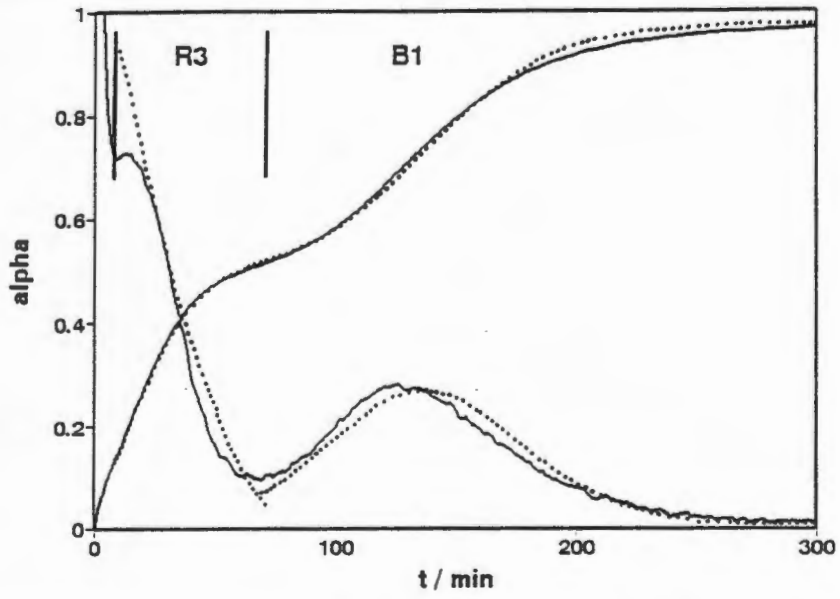

Figure 6.15: Comparison of experimental (solid line) and calculated (dotted line) α vs time and dα/dt curves for CAPR 212-250 μm at 90 °C. The first region is not modelled.

Arrhenius plots for the various parts of the curves modelled are presented in Figure 6.16a and b and the kinetic parameters resulting in Table 6.5.

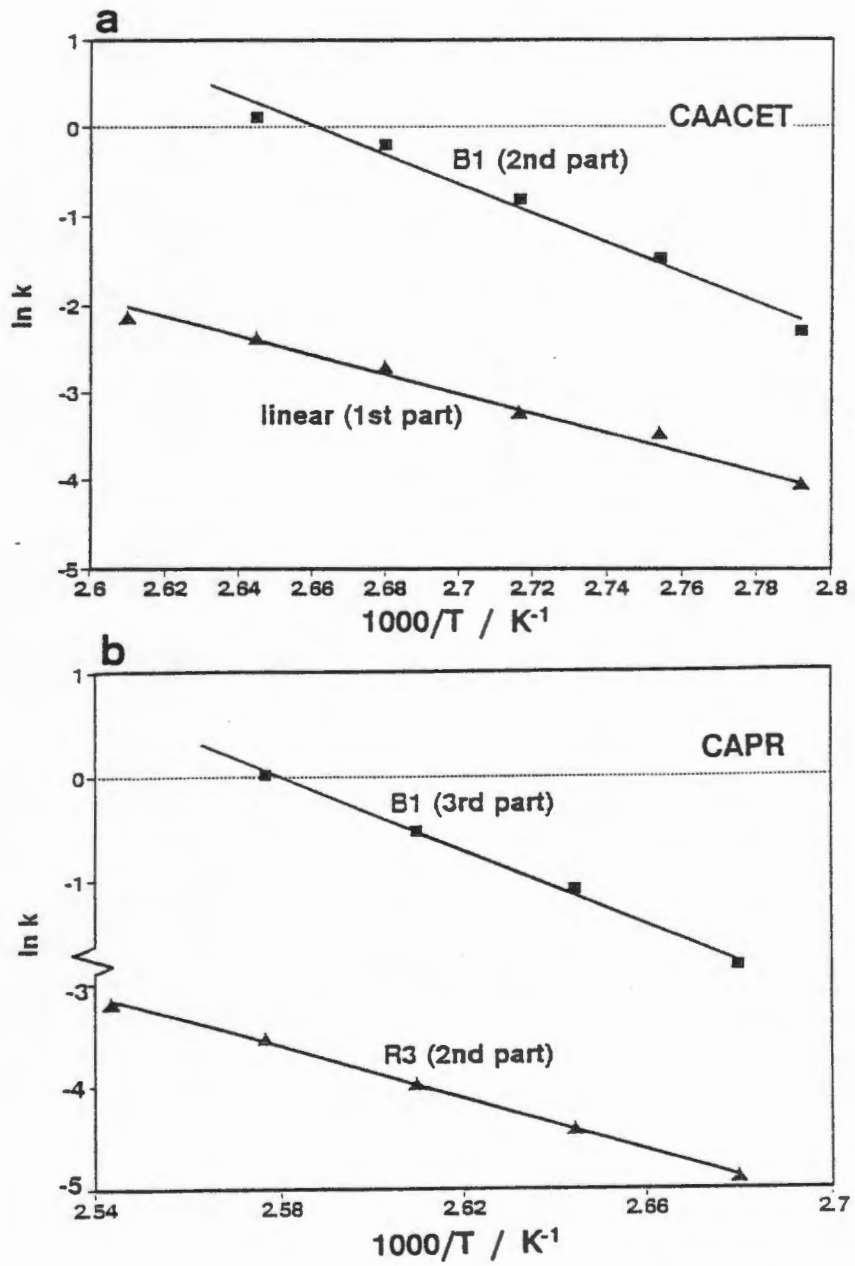

Figure 6.16: Arrhenius plots for CAACET and CAPR over the isokinetic ranges. The two regions of the CAACET curves and the second and third region of the CAPR curves are plotted separately and values of E_a and ln A determined for each.

Table 6.5: Kinetic parameters for CAACET, CAPR

	E_a (kJmol^{-1})	ln A	*r*
CAACET			
linear region	93(5)	27.01(11)	0.988
Prout Tomkins (B1)	138(11)	44.15(16)	0.980
CAPR			
Contracting volume (R3)	105(2)	29.02(3)	0.999
Prout tomkins (B1)	151(7)	46.60(7)	0.995

Discussion:

While it is difficult to validate possible processes which might account for such multi-step behaviour it is interesting to note that the E_a derived for the linear and R3 regions of the decomposition curves of CAACET and CAPR are similar and lower than those derived for the B1 sections. A possible mechanism involves loss of guest from channels and surfaces with no significant growth of the CA(α) phase followed by the formation and subsequent growth of growth nuclei of the product CA(α) phase. It should however be noted that during programmed thermal analysis both compounds melt/dissolve with subsequent recrystallisation of CA(α) from the liquid. Localised melting can thus not be ruled out although no gross melting is observable by hot stage microscopy under conditions similar to those prevailing in isothermal TG.

Group 2: CACN and MCCN desorption kinetics

The inclusion compounds of CA and MC with acetonitrile form a class of their own, being very similar to each other in structure yet rather different from the bulk of other CA inclusion compounds (MC forms a very limited number of inclusion compounds). These compounds represent cavity rather than channel enclathration of guest molecules and are remarkably stable to guest desorption in spite of the relatively volatile nature of the acetonitrile guest.

Differences in their behaviour under rising temperature thermal analysis are described in chapter 4. Large single crystals of MCCN melt at the temperature of guest release but if the size of the particles is sufficiently reduced the guest is lost without melting of the inclusion compound. This behaviour is indicated by the appearance of two discrete thermal events in rising temperature DSC (chapter 4) and confirmed by hot stage microscopy. No sign of melting is evident and if a sample is removed after the guest loss event it is shown to consist of small highly porous particles such as those one might expect to result from mechanical disruption of the particles upon guest release. If partial melting occurred, this should be reflected in the texture of the resultant particles.

Reduced time plots for CACN and MCCN are presented in Figures 6.17a and b. The α vs time curves for MCCN show no induction period and are deceleratory throughout while those of CACN are sigmoidal in shape.

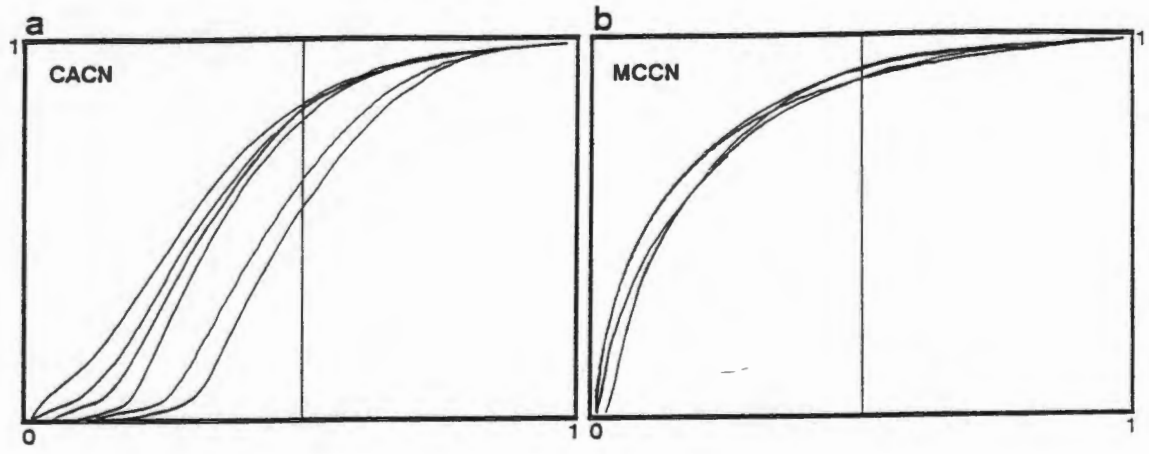

Figure 6.17: Reduced time plots for the decomposition of a) CACN and b) MCCN over the ranges indicated in Table 6.6. (Only a few representative curves are presented.)

The best descriptor of the shape of the MCCN curves appears to be the D3 rate law describing a continually decreasing rate of evolution of guest vapour. This rate law is derived for reactions in which the reactant is represented by a cube of continuously decreasing volume presenting an ever decreasing surface area or reaction front for reaction. This implies that the rate of diffusion of the desorbed guest vapour from the reaction front is the rate limiting step. It should be remembered that following a decomposition reaction by isothermal

TG means that only the rate at which vapour is removed from the bulk sample is monitored and this might vary significantly from the rate of appearance of the new phase, particularly if the new phase formed presents an ever thickening barrier of product which the escaping gas must traverse.

The decomposition of CACN to produce CA(α) and acetonitrile vapour is best described by an A2 rate law describing the 2-dimensional growth of nuclei of the new phase. This is similar to the rate law cited for the decomposition of CAAN, CABN, CANI, CAPNOT and CAPTOL and probably implies that the phase change to CA(α) is the rate determining step.

Values of *k* and the alpha ranges over which these are derived are presented in Table 6.6 and the resulting Arrhenius plots as Figures 6.18a and b.

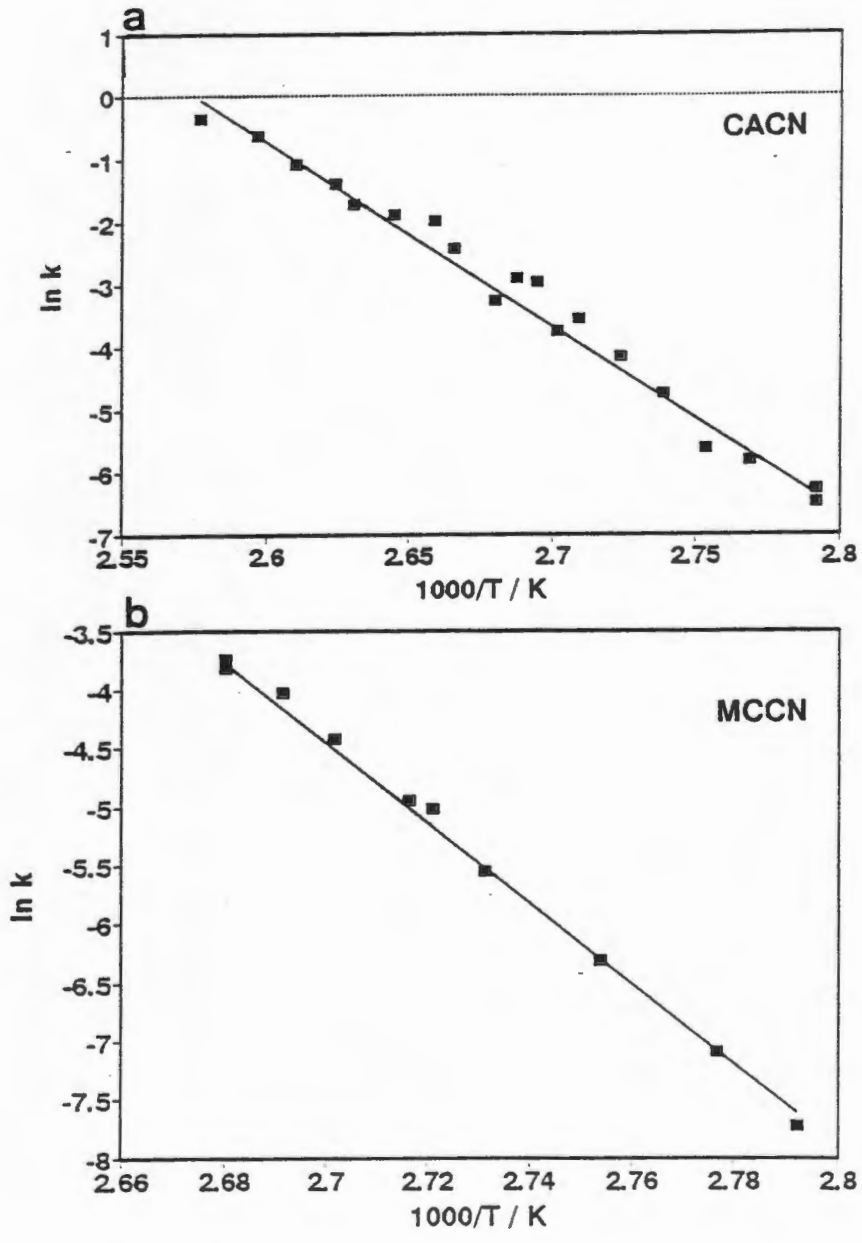

Figure 6.18: Arrhenius plots for a) CACN and b) MCCN over the isokinetic ranges.

Table 6.6: Rate constants for isothermal decompositions of CACN and MCCN.

	T (°C)	k (min^{-1})	r
CACN (A2)			
	85	0.001507(2)	0.999
	85	0.001869(5)	0.995
	88	0.002939(7)	0.995
	90	0.00363(1)	0.992
	92	0.00881(2)	0.995
	94	0.01551(6)	0.994
	96	0.0289(1)	0.995
	97	0.02357(8)	0.994
	98	0.05121(2)	0.995
	99	0.05522(2)	0.982
	100	0.0380(2)	0.989
	102	0.0881(9)	0.985
	103	0.138(1)	0.990
	105	0.152(1)	0.991
	107	0.181(2)	0.989
	108	0.249(3)	0.989
	110	0.337(4)	0.990
	112	0.529(3)	0.998
	115	0.711(6)	0.998
MCCN (D3)			
	85	0.000444(1)	1.000
	87	0.000829(1)	1.000
	90	0.00183(1)	0.997
	93	0.00386(3)	0.990
	94	0.00659(11)	0.877
	95	0.00711(2)	0.995
	97	0.01202(3)	0.998
	98	0.01781(4)	0.998
	100	0.0219(1)	0.996
	100	0.0237(1)	0.996

The straight line nature of these plots indicates Isokinetic behaviour over the temperature range chosen. Values of the kinetic parameters derived are presented as Table 6.7.

Table 6.7: Kinetic data derived for desorption reactions of CACN and MCCN.

	CACN	MCCN
Rate law	A2	D3
α range	0.05-0.95	0.05-0.95
ln A	75.5(3)	88.6(1)
E_a ($kJ.mol^{-1}$)	244(9)	287(8)
r	0.9788	0.9935

The E_a for MCCN appears significantly higher than that for CACN suggesting that there is a larger energy barrier to desorption of acetonitrile from the MC compound than the CA inclusion compound. This is in spite of the fact that CACN has one more hydrogen bond per molecular unit than MCCN (that of O(28)-H(28)). The host-host hydrogen bonds of the inclusion compounds must be overcome to allow rearrangement of the host molecules into the α-phase, which has a different hydrogen-bonding arrangement. The implications of this will be discussed later, suffice to note that this result is contrary to that expected from cursory consideration of the relative strengths of the intermolecular forces operating in each compound as detailed in chapter 3.

SOLID / VAPOUR REACTIONS (SORPTION REACTIONS):

Many inclusion compounds may be formed by exposing the solid host to vapours of the guest[18,19]. This reaction may be summarised:

$$H_{(s,\alpha)} + G_{(g)} = HG_{(s,\beta)}$$

Analogously to the desorption reaction just discussed, no chemical change occurs and host and guest molecules remain chemically unaltered; however the solid undergoes complete rearrangement to incorporate the guest molecules and a large increase in effective molecular volume results. The initial and final solid phases are quite different in both packing and hydrogen-bonding motifs. Although the sorption reaction is also reversible the reaction conditions are again chosen such that the equilibrium position is shifted towards the products to such an extent that the reaction may be considered irreversible under the conditions of the experiment. These are: temperatures in the region of ambient temperatures (20 to 25 °C; far lower than those chosen for investigation of the desorption reaction) and an atmosphere saturated with guest vapour.

The experiment

The experimental procedures are similar to those followed for desorption reactions: sample preparation is described in the experimental section. In all experiments particles in the range 212-250 μm were used. It is however important to note that although the gross particle size was within these dimensions the CA(α) and MC(α) used was produced by desorption of volatile guests (such as acetone, ethyl acetate or acetonitrile) and the host particles were thus highly porous. The surface area available for reaction was thus vastly larger than implied by consideration of the particle size. Sample preparation was identical for all samples used and the powder XRD trace of the host α-phase used indicated that only one α form resulted from desolvation of different solvents.. The temperature of the experiment with aromatic guest molecules was maintained at 31 °C: chosen to be slightly higher than ambient temperatures to minimise temperature fluctuations over the *months* of the experiment.

For the rapid reactions (CACN and MCCN) α vs time curves were obtained directly from the levitatory balance equipment described in the experimental section and all fitting procedures are as before.

For the slow reactions (the reactions were not complete after 90 days) between CA and aromatic guests the experimental setup was modified and the reactions were carried out under normal air pressure using the simplified experimental setup described (chapter 2). Since many months were required for complete reaction any other experimental setup proved unfeasible.

Results

CA aromatic guests

Surprisingly, while some of the substituted aromatic guests were absorbed by CA(α) resulting in formation of the inclusion compounds, other aromatic guests proved unreactive under the conditions of the experiment. Details of the aromatic guests absorbed are summarised in Table 6.8.

Table 6. 8: Absorption of aromatic guests to form CA inclusion compounds.

Guest	m.p. (°C)	b.p. (°C)	$t_{½}$ @31 °C (days)
Aniline 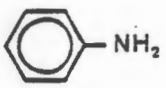	-6.2	184.4	44
Benzonitrile 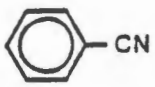	-12.9	189.6	27
Nitrobenzene 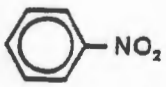	5.7	210.6	110
o-Nitrotoluene* 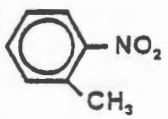	-4.1	222.3	not absorbed
m-Nitrotoluene 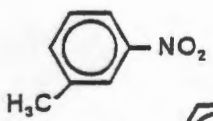	5.7	231.9	not absorbed
p-Nitrotoluene 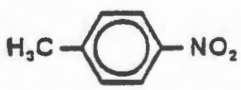	51.9	238.3	not absorbed
p-Toluidine 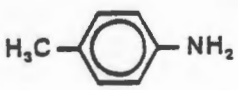	44.5	200.4	47
p-Bromo-phenol* 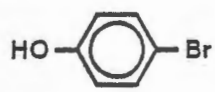	64.0	238	>120
Acetophenone 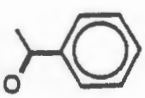	20.5	202.5	not absorbed
Propiophenone 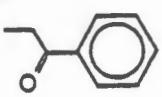	21.0	218.0	not absorbed

* Inclusion compounds not formed from solution.

Adsorption isotherms for those guests which showed appreciable reaction at 31 °C are presented as Figures 6.19. There are distinct differences in the rate of reaction of the different guests as illustrated by comparison of the reaction half-lives given in Table 6.8.

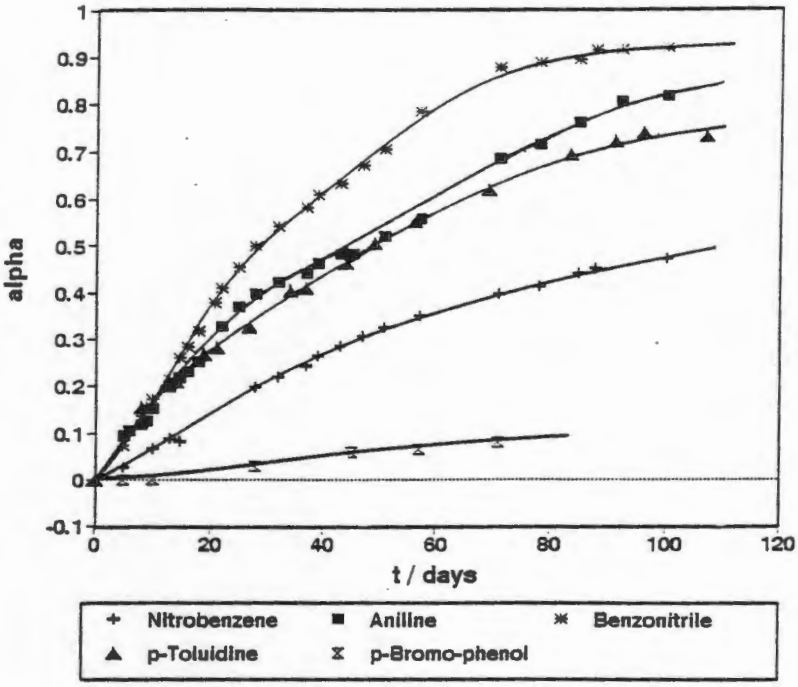

Figure 6.19: Absorption isotherms for aromatic guests which react with CA(α) at 31 °C to form 1:1 inclusion compounds.

Figure 6.20 illustrates the vapour pressure curves for each of the guests, all except aniline have vapour pressures less than 1 mmHg at 31 °C. While all of these guest compounds have very low vapour pressures under the conditions of the experiment these *do* differ and the order of volatility is:

benzonitrile > aniline > *p*-toluidine > nitrobenzene > *m*-nitrotoluene > *p*-nitrotoluene.

Note that this is reflected in the order of reactivity and thus it is possible that the vast differences in reactivity are due to differences in vapour pressure. This would imply that *m*- and *p*-nitrotoluene have vapour pressures less than some threshold value below which reaction does not proceed.

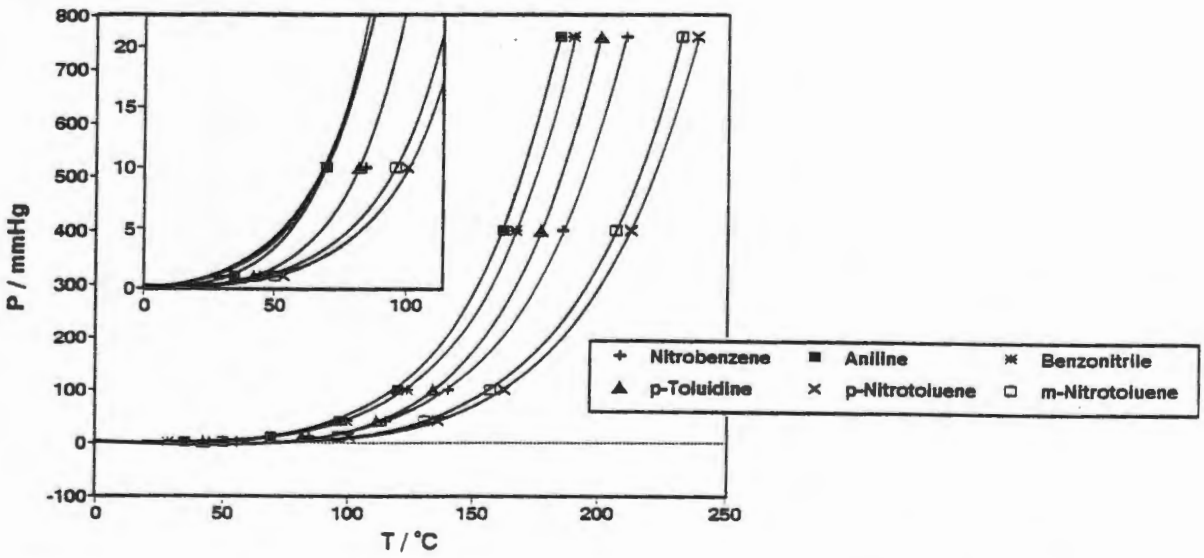

Figure 6.20: Vapour pressure curves for various aromatic compounds investigated for reaction with CA(α).

CACN and MCCN

Both CA and its O(28) methyl ester absorb acetonitrile at temperatures close to ambient temperatures to form the inclusion compounds CACN and MCCN. As in the cases mentioned above the product is the same as that formed by crystallisation from solution both with respect to stoichiometry (as confirmed by TG) and structure, as illustrated in Figure 6.21a and b which shows the powder XRD traces of each. The structures of the inclusion compounds CACN and MCCN are very similar but it is important to note that the structure of MC(α) is quite different both in packing motif and hydrogen bonding patterns from CA(α) (as detailed in chapter 3).

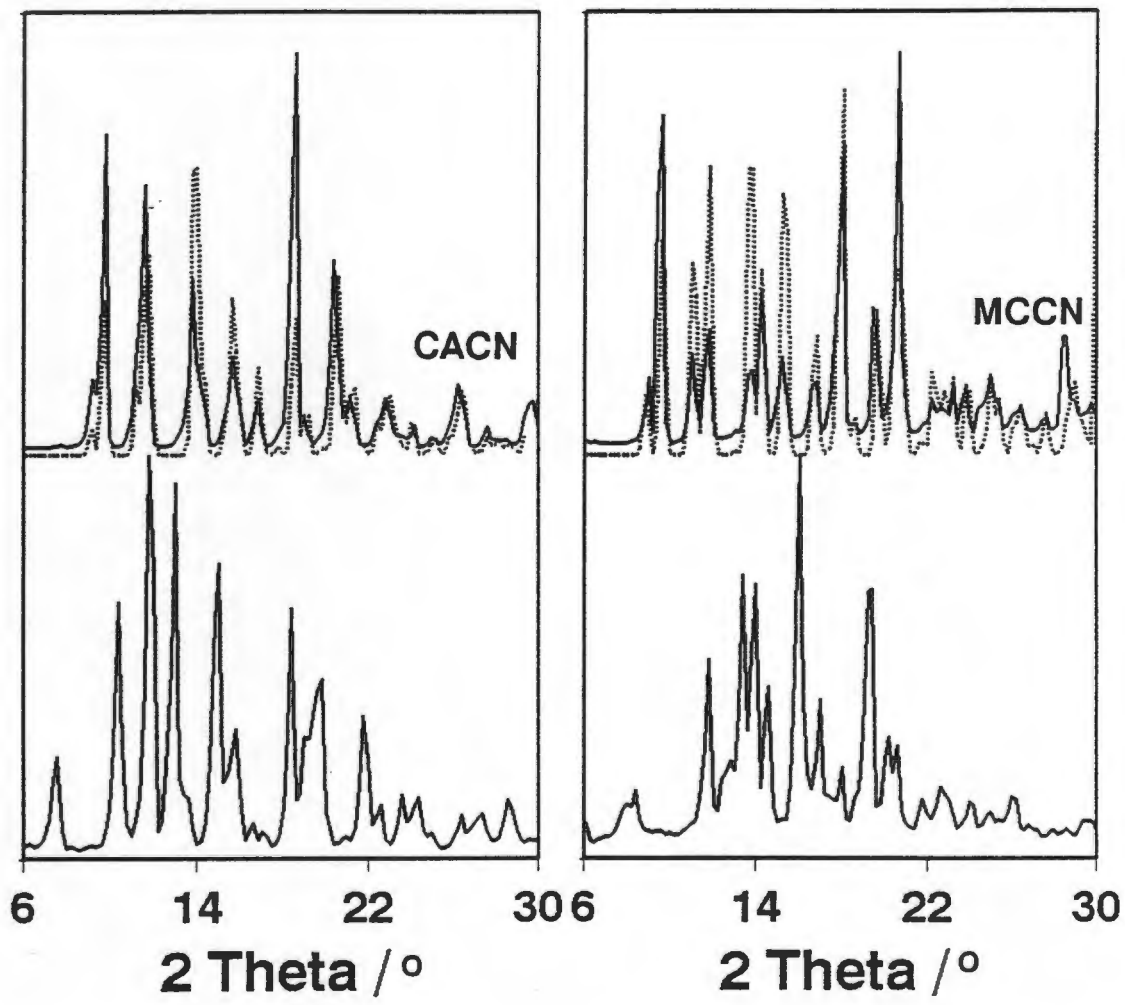

Figure 6.21: Powder XRD traces of α phases (bottom) and complexes made by absorption of guest vapours compared with traces generated from crystal structure data (dotted line). a) CACN and b) MCCN.

The absorption of acetonitrile and subsequent reaction to form the inclusion compounds occur far more rapidly than for the aromatic guests absorbed by CA as might be expected given the far higher vapour pressure of acetonitrile (*ca* 78 mm Hg at 20 °C). Absorption isotherms for both the CA and MC compounds are presented as Figure 6.22. The reaction with MC proceeds far more rapidly

than that with CA with a half life of 8.5 min compared to that of CA for which $t_{½}$ = 26 min. Thus the ester MC reacts with acetonitrile more rapidly than the free acid CA and MCCN shows a higher energy barrier to desorption of the guest than CACN as detailed in the previous section on desorption reactions. This is initially surprising as the structures are virtually isostructural except that that of CACN has the added stabilisation of one extra hydrogen bond per host molecule. One might expect the packing energy of MCCN to be lower than that of CACN allowing ready collapse of the structure resulting in a lower E_a value. In an attempt to reconcile the kinetic data with structure, similarities and differences in the structures of phases involved in the reaction:

$$HOST{\cdot}CH_3CN_{(s,\beta)} = HOST_{(s,\alpha)} + CH_3CN_{(g)}$$

were considered in the hope that this might supply the reason for the apparently anomalous fact that the inclusion compound less stabilised by hydrogen-bonding compound is *more* readily formed and *less* readily decays. It is immediately obvious that the α structure of the MC host allows for fewer and weaker hydrogen-bonds than that of CA. In fact the potential of certain of the hydroxyl and ester groups to participate in hydrogen-bonds remains unfulfilled.

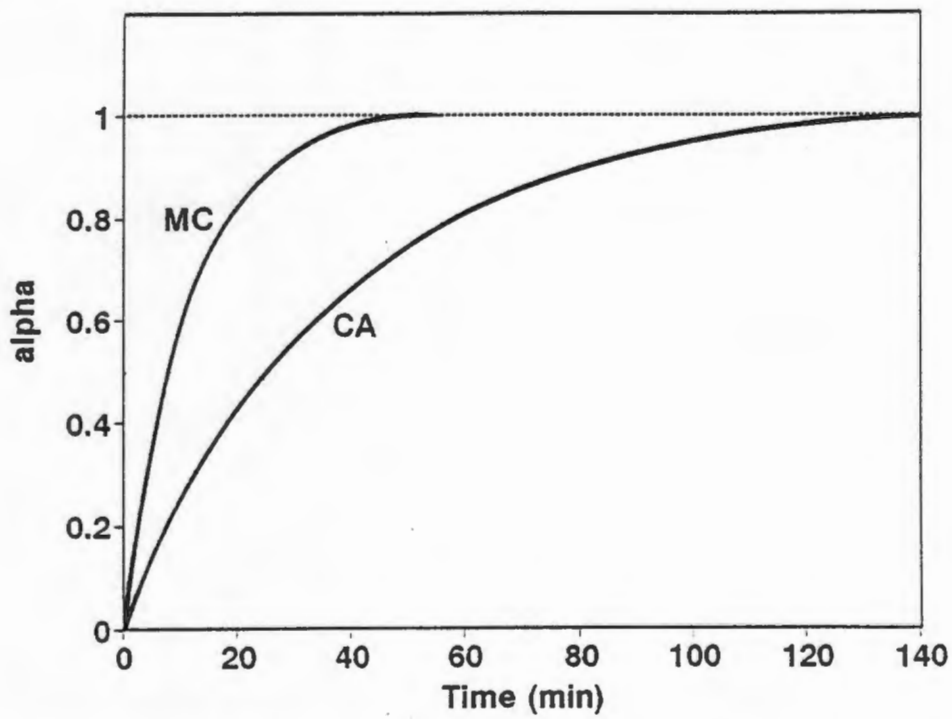

Figure 6.22: Absorption isotherms for the reaction of MC(α) 212-250 μm and CA(α) 212-250 μm with acetonitrile at 20 °C.

In an attempt to quantify the *difference* in hydrogen bond stabilisation between the two α phases, values of the atom-atom potential functions for all hydrogen bonds in each structure were calculated and expressed these per host molecule. (Data for calculation of CA(α) atom-atom potentials were derived from the structure by Miki *et. al.*[20]). We used a modified form of the Lennard-Jones potential function for non-bonded interactions between pairs of atoms:

$$E_{hb} = (A/r^{12}_{H\cdot\cdot O} - C/r^{10}_{H\cdot\cdot O}) \cos^2(\theta_{O\text{-}H\cdot\cdot O}) \cos^2(\chi_{H\cdot\cdot O\text{-}C} - \chi_0)$$

where the coefficients A and C are as modified by Vedani and Dunitz[21], r is the distance between the donor hydrogen atom and the acceptor oxygen atom and θ and χ are the angles between donor O, donor H and acceptor O and between donor H, acceptor O and acceptor C respectively. These angles are quoted in Table 6.9 and describe the geometry of the hydrogen bond as is illustrated schematically in Figure 6.23. In the "best case" one would expect the angle O-H•••O to approach 180° (a linear H-bond), while the angle H•••O-C will depend on the hybridisation at the C atom and will thus ideally be either 109.5° or 120°, (the quantity χ_0 accounts for this ideality). The modification to take into account the geometry of the lone pair orbitals at the *acceptor* atom, (the third term) is as suggested by Vedani and Dunitz[21] and is important in correctly weighting the approach to ideal geometry of the hydrogen bond.

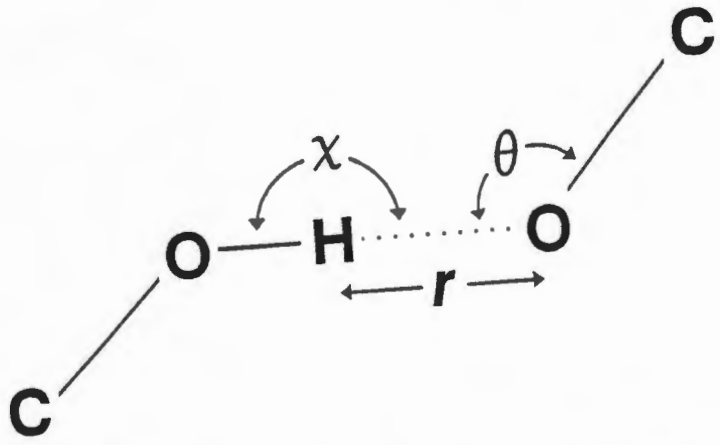

Figure 6.23: Schematic diagram of parameters used to describe the geometry of a hydrogen bond.

Values for the hydrogen bond potentials are quoted in Table 6.9. It becomes clear from the total hydrogen-bonded potential per host molecule that formation of CA(α) is a far more favourable reaction than formation of MC(α). If the differences in hydrogen-bonded potentials between reactant and product species are computed instead, the same trend is noted. While the favourable interactions occurring upon formation of hydrogen bonds are by no means the only energy considerations it is to be expected that all other terms will be of similar magnitude in the inclusion compounds given that these are isostructural, exhibit the same stoichiometry and lack of host:guest interactions. The structures of CA(α) and MC(α) are not isostructural and the hydrogen bonded potential of CA(α) is larger than that of MC(α). Consideration of the relative melting points of the host compounds (MC melt onset = 150 °C, CA melt onset = 200°C), reveals that the sum of all factors such as dispersion forces, packing efficiency and hydrogen bonding, reflect the trend in hydrogen bonding potential.

Table 6.9: Hydrogen Bonding Schemes and atom-atom potentials for CACN and MCCN

	O···O (Å)	H···O (Å)	O-H···O (°)	H···O-C (°)		$U_{hb}(r)$ (kJ.mol^{-1})
CACN						
O(28)-H(28O)···O(29)[a]	2.629(5)	1.70(6)	156(3)	139(2)		-8.81
O(29)-H(29O)···O(25)[b]	2.714(7)	1.77(4)	162(5)	124(2)		-14.42
O(25)-H(25O)···O(26)[b]	2.750(6)	1.83(4)	157(3)	115(2)		-14.49
O(26)-H(26O)···O(27)[c]	3.015(7)	2.14(4)	149(2)	138(1)		-4.81*
						-42.53
MCCN						
O(26)-H(26O)···O(25)[d]	2.794(7)	1.83(4)	174(4)	122(2)		-16.36
O(25)-H(25O)···O(29)[d]	2.857(9)	1.93(4)	157(4)	124(3)		-11.18
O(29)-H(29O)···O(27)[e]	2.918(6)	1.99(6)	156(4)	147(2)		-7.94*
						-35.48
MC(α)						
O(25A)-H(5AO)···O(29A)[f]	3.028(10)	2.10(4)	160(9)	129(3)		-6.69
O(29A)-H(9AO)···O(25B)[g]	2.830(9)	1.90(2)	160(4)	112(1)		-13.49
O(25B)-H(5BO)···O(26A)[f]	2.730(9)	1.78(3)	174(10)	119(4)		-17.08
O(26A)-H(6AO)···O(25A)[f]	2.884(9)	1.93(2)	178(9)	135(3)		-11.58
O(26B)-H(6BO)···O(27B)[h]	2.945(11)	2.05(5)	155(9)	146(3)		-6.65*
O(29B)-H(9BO)···O(26B)[i]	3.254(10)	2.82(7)	141(8)	114(2)		-1.30
O(29B)-H(9BO)···O(28A)[j]	3.612(10)	2.50(8)	136(8)	134(3)		-0.32
					(2 hosts)	-57.11
					(1 host)	-28.56
CA(α) (Miki *et al* [?])						
O(28)-H(28)···O(26)	2.634	1.68	173	149		-8.81
O(26)-H(26)···O(25)	2.723	1.80	174	122		-14.42
O(25)-H(25)···O(29)	2.774	1.88	171	126		-14.97
O(29)-H(29)···O(27)	2.857	1.98	169	150		-4.81*
						-43.01

* carbonyl oxygen atom, expect sp^2 hybridisation; $\chi_0 = 120°$

a -x-1, y-½, -z-2 b -x-1, y+½, -z-1 c -x-1, y+½, -z-2 d -x-2, y-½, -z-2 e -x-2, y+½, -z-1

f -x+2, -y, z g -x-2, -y, z+1 h -x+1½, y-½, -z+1 i -x+2, -y, z-1 j x, y, -1+z

SOLID / SOLID REACTIONS:

A number of the aromatic guests that form inclusion compounds with CA are solids at ambient temperatures and the possibility for solid/solid reaction exists. The type of reaction expected would be :

$$CA_{(s,\alpha)} + G_{(s)} = CA \bullet G_{(s,\beta)}$$

Clearly if both reactants are in the solid phase the absolute and relative particle sizes, the phases and density of crystal defects of both constituents as well as the degree of compaction and mixing must be considered.

The experiment

Ground samples of potential guests were mixed with ground, sieved CA as described in the experimental section. After 10 days samples were washed to remove excess guest and subjected to TG and NMR analysis to determine whether any reaction had occurred. As all of the guests considered were aromatic in nature the ^{1}H-NMR signals of the guests were easily distinguishable from those of CA. Guests were chosen to test a number of different functional groups common to other CA inclusion compounds.

Results

Table 6.10 lists the compounds tested for solid/solid reactivity with CA and gives details of their melting and boiling points.

Table 6.10: Solid Guests

Guest	m.p. (°C)	b.p. (°C)
p-Br-Nitrobenzene 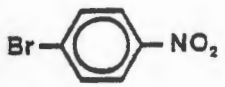	125-127	255-256
p-Nitrotoluene 	53-54	238
p-Toluidine 	44-45	200-201
p-Amino-phenol 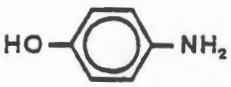	189.6-190.2	284
p-Br-phenol 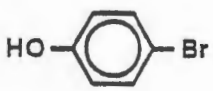	64	238
Benzoic acid 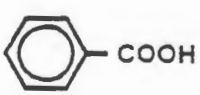	122.4	249.2
o-Vanillin 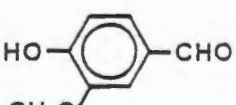	80-81	285
Resorcinol 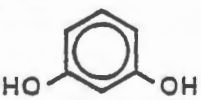	109-111	280

Of the potential guest compounds listed above only *p*-Br-phenol and *p*-Toluidine showed significant reactivity with CA. Both produced 1:1 complexes with CA as determined by extent of weight loss on TG analysis and confirmed by ^{1}H-NMR.

The complex with *p*-toluidine so formed has the same structure as that crystallised from solution and the powder XRD traces are presented as Figure 6.24a. Unfortunately, it proved impossible to grow single crystals of *p*-Br-phenol in spite of attempting a number of crystallisations using different co-solvents and conditions. Nonetheless both TG and ^{1}H-NMR analysis of washed samples of the solid/solid reaction product indicate the existence of a 1:1 host:guest complex. The powder XRD trace of the 1:1 complex obtained by solid/solid reaction is presented in Figure 6.24b for comparison with the traces of the host and guest alone.

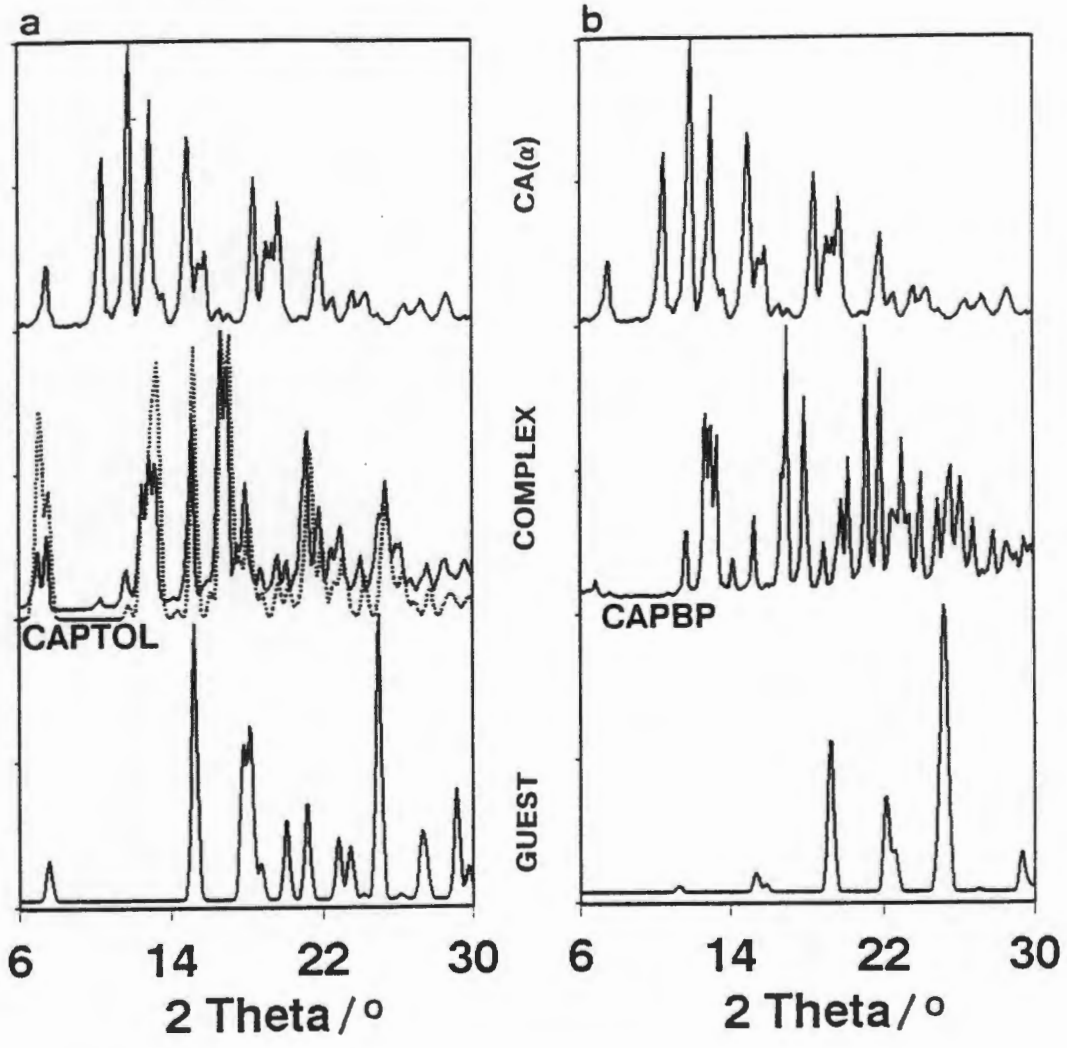

Figure 6.24: Comparison of powder XRD traces of pure host (top, pure solid guest; bottom, pure solid host) and the 1:1 complexes formed by solid/solid reaction (solid line - centre) for: a) CAPTOL (dotted line represents the powder XRD pattern calculated from crystal structure data) and b) CAPBP.

Given the great degree of isostructurality seen in the inclusion compounds of CA with aromatic guests one would predict the existence of a structure held together by host:host hydrogen bonding with guests accommodated in channels and exhibiting no strong host:guest interactions. Indeed the powder XRD trace of CAPBP is very similar to that of CAPTOL.

Reaction isotherms for the reactions between solid *p*-toluidine and CA and solid *p*-Br-phenol and CA are presented in Figure 6.25. As with the solid/vapour reactions the absorption of *p*-Br-phenol proceeds more slowly than that of *p*-toluidine at the same temperature, with half lives of 180 and 45 min respectively. While at first glance the α vs time curves appear deceleratory throughout, closer scrutiny reveals a distinctly acceleratory region below α = 0.5. It is probable that the shape of the curves is in fact sigmoidal but with a very long deceleratory period which masks this. Any attempt to model a possible reaction mechanism may be simplified by the observation that the guest species (either *p*-toluidine or *p*-Br-phenol) migrates into the host structure rather than a mutual diffusion of one into the other. This may be inferred from the observation of vapour/solid reactions where there cannot be any migration of the CA solid into the guest structure.

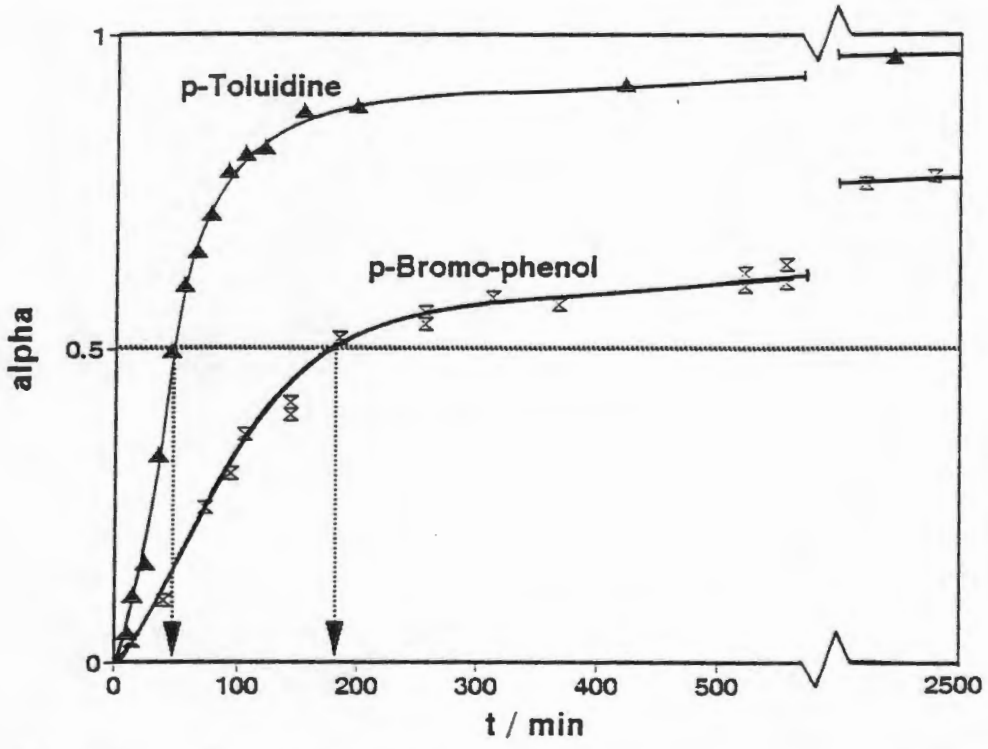

Figure 6.25: Reaction isotherms for *p*-toluidine and *p*-Br-phenol with CA(α) particle size 212-250 μm at 21-23 ^{o}C.

Surprisingly, no reaction with *p*-nitro-toluene (either in the vapour or solid phase) is observed even after prolonged periods of contact with CA(α). This is in spite of the fact that the 1:1 inclusion complex is formed from solution.

The molecular structures of a few *p*-substituted aromatic molecules which might be expected to react with CA (because of their similarities with reactive

compounds) are indicated in Figure 6.26. Note the similar substituent groups and the relative polarity of each. The molecular volumes of the compounds are similar and none is so large that it might be excluded from the CA channel on the basis of bulk. The guests included in the solid phase are not simply those with the lowest melting point or highest vapour pressure. In particular it is surprising that *p*-nitro-toluene shows no reactivity with CA in the solid phase although the inclusion compound is formed from solution.

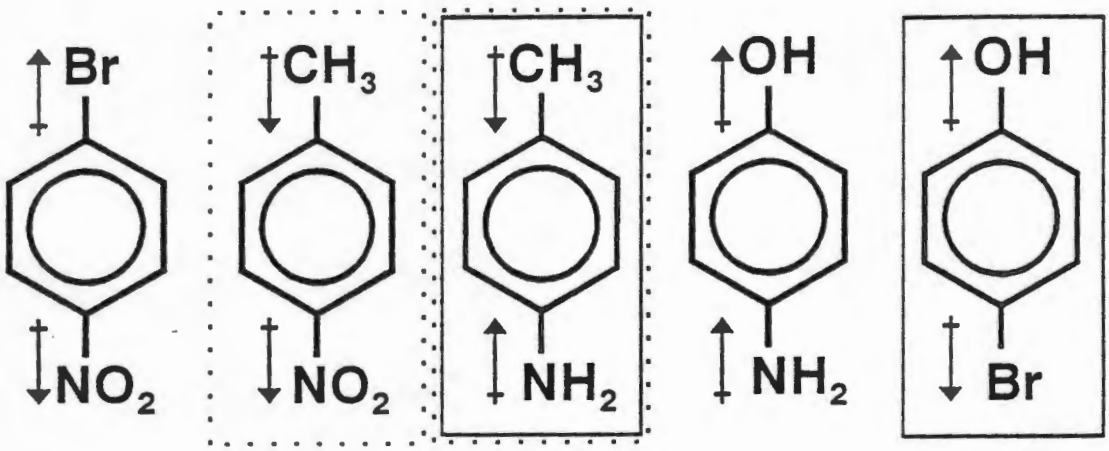

Figure 6.26: Potential solid guest molecules. Those that react with CA(α) in the vapour or solid state are enclosed in a solid box while those that form inclusion compounds from solution and for which inclusion compounds crystal structures have been determined are enclosed with a broken line.

In an attempt to further probe the solid phase reactivity of CA and its inclusion compounds with aromatic guests a number of guest exchange experiments were attempted. The inclusion compound of CA with *p*-toluidine was formed by grinding CA with excess *p*-toluidine and allowing to stand until the 1:1 inclusion compound formed. This material was washed with ether to remove all excess, unclathrated *p*-toluidine and weight loss on TG analysis used to confirm formation of the complex. Samples of this powder were then ground with large excesses of various of the other potential solid guest compounds and allowed to stand for 10 days with occasional grinding. Guest exchange was monitored by ^{1}H-NMR spectroscopy of washed samples as the signals due to these aromatic guests are well removed from those of CA and may be used to quantify the relative amounts of each guest in the powders.

Such exchange experiments were attempted with all guests in Figure 6.26 and yet only *p*-Br-phenol exhibited exchange with *p*-toluidine: forming the CA•*p*-Br-phenol inclusion compound within 2 hours. Thus even once the inclusion compound structure is formed by solid state reaction with *p*-toluidine the other solid guests do not displace the *p*-toluidine guest although present in vast excess.

One is tempted to note that both compounds that react with CA in the solid

state have either two electron donating or two electron withdrawing substituents on the aromatic ring or that these have lower melting points than the other guests; however the lack of reaction with *p*-Br-nitro-toluene contradicts the first statement and the lack of reaction with *p*-nitro-toluene the second. It appears that the interactions in the solid phase are complex and may be dependent on both electronic interactions between CA and the guest molecule as well as guest:guest interactions in the unreacted guest solid. A study of the relevant entropic and enthalpic effects and hence estimations for the values of the Gibbs free energy changes are needed to predict CA solid phase reactivity accurately .

1 G. Pannetier and P. Souchay, "Chemical Kinetics", Elsevier Publishing Co., Amsterdam, London, New York, 1967.

2 C.H. Bamford and C.F.H. Tipper, in "Chemical Kinetics, Volume 22, Reactions in the Solid State", Elsevier Publishing Co., Amsterdam, London, New York, 1980

3 F.C. Tompkins, in "Decomposition Reactions, Chapter 4, Treatise on Solid State Chemistry, Volume 4 - Reactivity of Solids", Ed. N.B. Hannay, Plenum Press, New York, London, 1976.

4 M.E. Brown, "Introduction to Thermal Analysis - Techniques and Applications.", Chapman and Hall, London and New York, 1988.

5 R.M. Barrer, "Zeolites and Clay Minerals as Sorbents and Molecular Sieves.", Academic Press, London, New York and San Francisco, 1978.

6 D. Dollimore, *Therochim. Acta*, 1991, **177**, p 59.

7 A.K. Galway, N. Koga and H. Tanaka, *J. Chem. Soc., Faraday Trans.*, 1990, **86**(3), p 531.

8 G.G.T. Guarini and S. Piccini, *J. Chem. Soc., Faraday Trans.*, 1988, **84**(1), p 331.

9 D. Dollimore and D.L. Griffiths, *J. Therm. Anal.*, 1970 ,**2** , p 229.

10 M.E. Brown, A.K. Galway and A. Li Win Po, *Thermochim. Acta*, 1992, **203**, p 221 and refs therein.

11 M. Avrami, *J. Chem. Phys.*, 1939, **7**, p 1103.

12 C. J. Keatch and D. Dollimore, in "Interpretation of Data, Chapter 4, Introduction to Thermochemistry.", Heyden and Son Ltd, London, 1975.

13 A.M. Avrami, *J. Chem. Phys.*, 1939, **7**, p 1103.

14 E.G. Prout and F.C. Tompkins, *Trans. Faraday Soc.*, 1944, **40**, p 488.

15 M.A. Avrami, *J. Chem. Phys.*, 1941, **9**, p 177.

16 E.G. Prout and F.C. Tompkins, *Trans. Faraday. Soc.*, 1945, p 468.

17 K. Miki, A. Masui, N. Kasai, M. Miyata, M. Shibakami and K. Takemoto, *J. Am. Chem. Soc.*, 1988, **110**, p 6594.

18 Leonard J. Barbour, Mino R. Caira and Luigi R. Nassimbeni, *J. Chem. Soc. Perkin Trans 2.*, 1993, p 2321.

19 D.R. Bond, L. Johnson. L.R. Nassimbeni and F. Toda, *J. Solid State Chemistry*, 1991, **92**, p 68.

20 K. Miki, N. Kasai, M. Shibakami, S. Chirachanchai, K. Takemoto and M.

Miyata, *Acta. Crystallogr. Sect. C,* 1990, **46**, p 2442.

21 Angelo Vedani and Jack D. Dunitz, *J. Am. Chem. Soc.*, 1985, **107**, p 7653.

CHAPTER 7: GENERAL DISCUSSION AND CONCLUSION

CA shows remarkable predictability with respect to the packing of host and guest in the crystals of the inclusion compounds formed. In most cases extensively hydrogen bonded host bilayers are formed with the hydrophilic α face of the CA host steroid "buried" in the centre of the bilayer while the hydrophobic β face remains exposed. These bilayers, which are puckered due to the curved shape of the steroid ABCD cis/trans/trans fused ring system, pack together leaving channels into which guest molecules pack. In this study none of the guest molecules in the tubulate clathrate type compounds exhibits short range host-guest interactions in spite of the fact that all guests included contain at least one potential hydrogen bond donor or acceptor group. Nonetheless the orientations of the guests within the channels appear to be affected by the overall direction of the guest dipole(s) and it is likely that long range electrostatic host-guest and guest-guest interactions play a role.

While the overall packing mode in the crystal structures of the tubulate clathrates appears to be predictable it should be noted that a number of subtle guest responsive variations do occur. Side chain conformations may be either extended or puckered and subtle alterations in the D-ring conformation result in greater or lesser curvature of the steroid host. Both of these effects result in variation in the shape and size of the channel allowing efficient packing in spite of inclusion of guests with different spatial demands. Similarly, guest conformations often differ from the lowest energy conformation (as calculated by Giglio and Quagliata, reference 14, chapter 3) which would be expected to dominate in the vapour or liquid phase. With only one exception (host A of CAMI) the side chain conformation of the host does *not* exhibit the lowest energy conformation. One may conclude therefore that the energy gain achieved by guest inclusion and hydrogen bond formation more than compensates for the loss due the to adoption of higher energy conformations of host and/or guest.

In addition to variation of host conformation the cross sectional shapes and areas and hence the channel volumes may be altered by the adoption of either the A- or B-type packing modes. Two of the three B-type structures studied show firm evidence of solid-solid phase changes of the inclusion compound (i.e. β_1 to β_2 phase changes) while that of CAPR exhibits an unassigned endotherm on DSC analysis which appears not to correspond to guest release and may be indicative of a similar change. It would be interesting to compare the packing energies of each mode explicitly and to attempt to probe the nature of the β_2 phase by modelling and minimisation procedures followed by comparison of generated with experimental powder diffraction patterns. Unfortunately both the poor quality of the powder patterns obtained and the lack of access to the highly sophisticated computer programs required for minimisation of postulated structures militated against the use of such procedures in this study.

Kinetic studies result in the assignment of a B1 (Prout-Tompkins) rate law to the desorption reactions of CABN, CAAN, CANI, CAPTOL and CAPNOT

implying that the mechanism of desorption is the same in each case. The rate of reaction appears to depend upon the rate of formation of the new phase (CA(α)) rather than on the rate of desorption of the guest although these are almost certainly intrinsically related as evidenced by the non-occurrence of a detectable β_0 phase in the thermal decomposition of any of the inclusion compounds studied. Similar values for the activation energy (E_a) and the pre-exponential factor reinforce the assertion that these structurally similar compounds decay by similar pathways. Activation energy is possibly a misnomer when applied to reactions in the solid state (and to heterogeneous reactions) as no state analogous to the "activated complex" can be readily imagined. A number of authors have attempted to describe this term in terms of vibrational energy, lowered energy barrier to conversion at defect sites or the "excess energy" required by a molecule for reaction to occur[1] and most agree that the values thus determined are useful as indicators of the *relative* ease of transformation or reaction. Thus these are presented for comparison within a a group of compounds where much else (crystal structure, lack of short range interactions and the nature of reactants and products of desorption) is similar.

Surprisingly the compounds CAACET and CAPR exhibit decomposition pathways significantly different (and rather more complicated) from any of the other CA clathrates with aromatic guests. The complexity of shape of the decomposition isotherms, which appear to be the sum of a number of separate but overlapping curves, indicate the dominance of different rate laws at different stages of the reaction. This may be the result of competing or successive processes occurring in the bulk sample.

For example:

> A particular rate law dominates up to some threshold α value after which it is superseded by a rate law which is indicative of another reaction mechanism. This might occur if the decomposition followed a pathway which included formation of a short lived metastable inclusion phase different to the β phase with a different host:guest stoichiometry. The overall rate of weight loss might then initially depend upon the rate of formation of such a phase and at a later stage (after the threshold α value is passed) upon the rate of decomposition of this intermediate.
>
> Alternately the rate of evolution of vapour from the bulk sample (measured as the rate of weight loss) might initially be dependent on the mechanism of decomposition at a molecular level and later on the rate of diffusion of the guest vapours through a layer of reacted (desorbed) material. In this latter case the rate law inferred from the shape of the desorption isotherms is *not* a measure of the mechanism of the desorption reaction at a molecular level but of the size of the *physical* diffusion barrier that must be overcome. A similar isotherm shape results if

partial or localised melting of the compounds occurs and the rate of guest vapour evolution is dependent on the rate of evaporation from the melt.

It is important to note therefore that rate laws derived, and mechanistic relationships inferred from, such complicated curves may reflect only the *rate of evolution of vapour from the bulk sample* and not the mechanism of decomposition at a molecular level.

While the existence of transient, metastable phases occurring during thermal decomposition are notoriously difficult to measure, detection of such might be facilitated by the use of an electron microscope in alternately scanning and diffraction mode. If the rate of evolution of vapour were simultaneously monitored then appearance of different phases at different α values could be recorded. Such a technique of direct measurement might also prove useful in assignment of thermal events measured by rising temperature DSC analysis. Unfortunately even quite "stable" inclusion compounds tend to decay rapidly under the high vacuum required in such an instrument.

CA is shown to undergo a number of gas/solid and solid/solid reactions resulting in formation of inclusion compounds with the same stoichiometry and structure as the inclusion compounds made by crystallisation. Rates of absorption of guest vapours appear to reflect the vapour pressures of the guest compounds involved and thus are similar to reactions in solution or the gas phase which are dependent on the concentration of one reactant. The absorption isotherms appear first order overall as might be expected if the rate of reaction is dependent on the vapour pressure of guest. Certain of the guest compounds included from solution do not react with CA in the vapour phase and it is possible that there exists some threshold vapour pressure, which may be different for each compound, below which the sorption reaction does not occur.

The solid vapour reactivity shown by CA is reflected in the reaction of MC with acetonitrile resulting in the formation of the only MC inclusion compound studied. Both CACN and MCCN may be formed either by crystallisation from solution or by reaction of dried host with acetonitrile vapour either of which results in the same 1:1 host:guest inclusion compound with the guests enclosed in cavities. Kinetic investigations reveal that MC absorbs acetonitrile more rapidly than CA and has a higher E_a for the desorption reaction. This has been ascribed to the lower stability of the MC(α) phase as compared to the CA(α) phase. Although CACN is stabilised by one more hydrogen bond per host than occurs in MCCN (that of O(28)-H(28O)), the MC(α) phase exhibits six hydrogen bonds per host pair (or an average of three per host) compared to four hydrogen bonds per host in CA(α). The geometry of the hydrogen bonds in the CA(a) structure indicates strong interactions (with short O•••O distances) for all four bonds. Computation of the strength of hydrogen bonded interactions indicate a greater gain in the formation of MCCN from MC(α) than in the formation of CACN from CA(α). The converse is true for the

desorption reactions. Thus reactivity is directly related to the structures of the reactant and product phases.

Solid-solid reactions in which solid powdered CA reacts with solid powdered guest to form the inclusion compound appear to be restricted to a small number of compounds. In this study only *p*-toluidine and *p*-Br-phenol were found to react with CA in the solid state. Both of these guest species also react with CA in solid/vapour reactions although the rate of reaction is greatly reduced. Other solid guests, such as *p*-nitro-toluene react neither in the solid nor in the vapour phases and attempts to stimulate solid-solid reaction by guest exchange also proved fruitless.

The occurrence of CA inclusion compounds as tubulate clathrates with guests stacked in channels separated from each other by host bilayers combined with the predictability of these structures provide a number of interesting further directions of study. The centre to centre distances between guest atoms in monomolecular stacks are *ca* 4 Å and the stacks are well separated from each other by intervening host bilayers. Reaction between included monomers would, if successful, result in the formation of long polymer chains with no cross linking or branching. While neither of the monomers included in this study showed such reactivity it is possible that guests with different geometry or with more than one potentially reactive site might be induced to react. Given the restricted cross section of the channels in the inclusion compounds, topotactic control of reaction is a possibility, as is stereocontrol.

1 C.H. Bamford and C.F.H. Tipper, in "Chemical Kinetics, Volume 22, Reactions in the Solid State.", Elsevier Publishing Co., Amsterdam, London, New York, 1980.

APPENDIX A

The diskette attached inside the back cover contains tables of atomic co-ordinates, anisotropic displacement parameters, bond lengths, bond angles and hydrogen atom positions for all of the structures elucidated in this study.

These are grouped by structure and stored in a series of self-extracting MS-DOS formatted EXE files in the A subdirectory.

To access the data for any structure, copy the relevant EXE file to the hard drive of an IBM-compatible PC and type the structure name. All files pertaining to that structure will self extract and may be viewed by any text editing program.

ATERNATIVELY:

All of the above data is also supplied on microfische grouped in the same manner as described above and also attached on the inside back cover.

APPENDIX B

The diskette attached inside the back cover contains tables calculated and observed structure factors for all of the structures elucidated in this study.

These are stored in a series of self-extracting MS-DOS formatted EXE files in the A subdirectory.

To access the data for any structure, copy the relevant EXE file to the hard drive of an IBM-compatible PC and type the structure name with the suffix SF. For example to view the structure factors for the structure CAMA type: CAMASF. The file pertaining to that structure will self extract and may be viewed by any text editing program.

ATERNATIVELY:

All of the above data is also supplied on microfische attached on the inside back cover.

Inclusion Compounds of Cholic Acid and Methyl Cholate

Janet L. Scott - PhD thesis

CABN	Benzonitrile 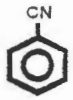
CAAN	Aniline 
CANI	Nitrobenzene 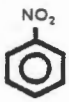
CAPR	Propiophenone 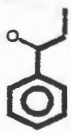
CAPTOL	*p*-Toluidine 
CAPNOT	*p*-Nitro toluene 
CAMN	*m*-Nitro toluene 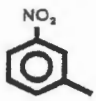
CAPBP	*p*-Bromo phenol 
CAACET	Acetophenone 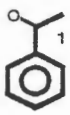
CADC	Acetone 1,2 Dichlorobenzene 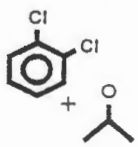
CAMI	Methyl acetate *i*-Propyl acetate 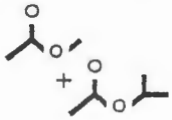
CAAC	Acetone 3 water 

1 K. Miki, A. Masui, K. Kasai, M. Miyata, M. Shibakami and K. Takemoto, *J. Am. Chem. Soc.*, 1988, 110

Inclusion Compounds of Cholic Acid and Methyl Cholate

Janet L. Scott - PhD thesis

CAACD	Acetone 
CAMEK	Methyl ethyl ketone 
CADEK	Diethyl ketone 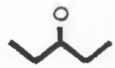
CAMA	Methyl acetate 
CAET	Ethyl Acetate 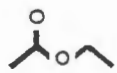
CAPAC	*n*-Propyl acetate 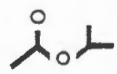
CAIP	*i*-Propyl acetate 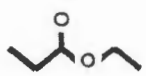
CAEP	Ethyl propionate 
CANBU	*n*-Butyl acetate 
CAVA	Vinyl acetate 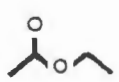
CAMM	Methyl methacrylate 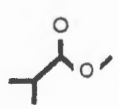
CACN	Acetonitrile CH_3CN
MCCN	Acetonitrile CH_3CN
MC(α)	No guest
CA(α)	No guest